

University of Nebraska - Lincoln

DigitalCommons@University of Nebraska - Lincoln

Civil Engineering Theses, Dissertations, and
Student Research

Civil Engineering

Winter 12-2011

EXPANDING THE LENGTH OF JOINTLESS BRIDGES BY PROVIDING ROTATIONAL CAPACITY OVER THE PILE HEAD

Ardalan Sherafati

University of Nebraska-Lincoln, ardalansherafati@gmail.com

Follow this and additional works at: <http://digitalcommons.unl.edu/civilengdiss>



Part of the [Civil Engineering Commons](#), and the [Structural Engineering Commons](#)

Sherafati, Ardalan, "EXPANDING THE LENGTH OF JOINTLESS BRIDGES BY PROVIDING ROTATIONAL CAPACITY OVER THE PILE HEAD" (2011). *Civil Engineering Theses, Dissertations, and Student Research*. 40.

<http://digitalcommons.unl.edu/civilengdiss/40>

This Article is brought to you for free and open access by the Civil Engineering at DigitalCommons@University of Nebraska - Lincoln. It has been accepted for inclusion in Civil Engineering Theses, Dissertations, and Student Research by an authorized administrator of DigitalCommons@University of Nebraska - Lincoln.

EXPANDING THE LENGTH OF JOINTLESS BRIDGES BY PROVIDING
ROTATIONAL CAPACITY OVER THE PILE HEAD

by

Ardalan Sherafati

A DISSERTATION

Presented to the Faculty of

The Graduate College at the University of Nebraska

In Partial Fulfillment of Requirements

For the Degree of Doctor of Philosophy

Major: Interdepartmental Area of Engineering

(Civil Engineering)

Under the Supervision of Professors Elizabeth G. Jones and Atorod Azizinamini

Lincoln, Nebraska

December, 2011

EXPANDING THE LENGTH OF JOINTLESS BRIDGES BY PROVIDING
ROTATIONAL CAPACITY OVER THE PILE HEAD

Ardalan Sherafati, Ph.D.

University of Nebraska, 2011

Advisors: Elizabeth G. Jones and Atorod Azizinamini

Jointless bridges have been in service for more than 50 years. Since no expansion joint is utilized in these structures, they have longer service life, reduced maintenance and construction costs, improved riding quality, and added redundancy. Because of integrity of the superstructure with the substructure, the thermal movements as well as other longitudinal movements are transferred to substructure. These lateral movements can induce relatively large forces and moments in the substructure elements including the abutment and the piles. Typically, flexible foundations which include single row of piles are preferred in jointless bridges to reduce the stiffness of the system against longitudinal movements of the superstructure.

The main objective of this dissertation is to improve and expand the application of jointless bridges to longer bridge lengths. As the imposed movements at the pile head level due to superstructure's displacements are linearly proportional to the length of the jointless bridge, by increasing the pile head displacement capacity the length of jointless bridges can be expanded. A parametric study has been conducted using nonlinear pushover analysis. The results of this study show that the pile head displacement capacity can be increased up to four times if rotational capacity is provided at the pile-cap connection. Further, it is shown that strong axis bending results in more displacement

capacity as compared to weak axis bending, although the lateral stiffness would be smaller in the latter case. Experimental study has been carried out on the proposed connection of CFT piles to the concrete cap. It is shown that this detail can effectively reduce the moment-rotation stiffness of the connection and increase the displacement capacity up to four times.

New design procedure is proposed for HP piles supporting jointless bridges. In this approach, only compact sections are recommended in order to prevent local buckling prior to reaching full plastic moment capacity of the cross section. Further, fatigue and strength criteria are combined and displacement capacity is estimated based on the boundary conditions, axial load, soil type, and orientation of the pile.

DEDICATION

To my wife, Elham Forouzes, and my parents.

ACKNOWLEDGEMENT

This study was conducted at the National Bridge Research Organization (NaBRO) under the supervision of Dr. Atorod Azizinmaini. I am deeply grateful for his guidance, advice, and valuable suggestions throughout the duration of the research. Thank you to Dr. Jones for stepping in as Graduate Chair to serve as chair of my committee so that our main supervisory professor, Dr. Azizinamini could continue to serve as our main supervisory professor and at least remain as co-chair of my committee after leaving the University of Nebraska-Lincoln for his current position as Department Chair of Civil and Environmental Engineering at Florida International University.

I offer my thanks to Dr. Andrzej S. Nowak, Dr. Mehrdad Negahban, and Dr. Fred Choobineh who served on my committee and evaluated my work. I am especially grateful to Dr. Mehrdad Negahban for his thorough review of the manuscript and his words of encouragement over the years. I wish to thank my colleagues in NaBRO, Saeed Javidi Niroumand, Nima Ala, Paulo Marchon, Marcelo Da Silva, Saeed Eghtedar Doust, Dr Ashwani Goel, and Dr. Aaron Yakel for their friendship and support. I also thank Peter Hillsabeck for his assistance with the experimental portion of this research.

I would especially like to thank my wife, Elham Forouzesh, for her understanding and patience. Her love and support kept me going through all of the years.

Finally, I offer my sincere thanks and love to my parents, Mohtaram Salehi and Abdolhamid Sherafati, who raised and supported me, and installed in me the value of an education.

Table of Contents

TABLE OF CONTENTS	VI
LIST OF FIGURES.....	XVII
LIST OF TABLES.....	XXIX
CHAPTER 1 INTRODUCTION.....	1
1.1. BACKGROUND AND PROBLEM STATEMENT	1
<i>1.1.1. PROBLEM STATEMENT.....</i>	<i>2</i>
1.2. BACKGROUND	3
1.3. OBJECTIVES OF THE RESEARCH	4
1.4. RESEARCH APPROACH.....	4
CHAPTER 2 ANALYSIS OF THE AVAILABLE DATA.....	7
2.1. INTRODUCTION	7
2.2. SYNOPSIS OF PUBLISHED LITERATURE	8
2.2.1. <i>AASHTO PROVISIONS</i>	<i>8</i>
2.2.1.1. ARTICLE 11.6.1.3 (INTEGRAL ABUTMENTS).....	8
2.2.1.2. ARTICLE 3.12.2 (UNIFORM TEMPERATURE CHANGE).....	9
2.2.1.3. ARTICLE 3.12.3 (TEMPERATURE GRADIENT)	10
2.2.1.4. ARTICLE 5.4.2.3.2 (CREEP)	14
2.2.1.5. ARTICLE 5.4.2.3.3 (SHRINKAGE)	15
2.2.1.6. ARTICLE 10.7.2.4 (HORIZONTAL PILE FOUNDATION MOVEMENT).....	16
2.2.2. <i>DOT PRACTICES.....</i>	<i>17</i>
2.2.2.1. 1999 SURVEY (NYSDOT)	17
2.2.2.2. 2002 SURVEY (UNIVERSITY OF MARYLAND)	18
2.2.2.3. 2004 SURVEY (FHWA).....	20
2.2.2.4. DOT DESIGN GUIDES REGARDING INTEGRAL ABUTMENT BRIDGES	21
2.2.3. <i>CTL REPORT</i>	<i>23</i>

2.2.3.1.	DESIGN RECOMMENDATION	24
2.2.3.1.1.	MAXIMUM LONGITUDINAL MOVEMENT.....	24
2.2.3.1.2.	ABUTMENT PILES.....	25
2.2.3.1.3.	LOAD TRANSFER TO SOIL.....	29
2.2.3.1.4.	PILE-TO-PILE CAP CONNECTION.....	30
2.2.3.1.5.	ABUTMENT WALL.....	30
2.2.3.1.6.	ABUTMENT SUPPORTED ON SPREAD FOOTING.....	31
2.2.3.1.7.	FULL-HEIGHT ABUTMENTS	31
2.3.	SYNOPSIS OF OTHER RESEARCH ACTIVITIES.....	32
2.3.1.	<i>SOIL-STRUCTURE INTERACTION.....</i>	32
2.3.1.1.	SOIL-ABUTMENT INTERACTION	32
2.3.1.2.	SOIL-PILE INTERACTION.....	35
2.3.1.2.1.	LIMIT-EQUILIBRIUM METHOD	35
2.3.1.2.2.	LINEAR ELASTIC METHOD.....	35
2.3.1.2.3.	EQUIVALENT CANTILEVER METHOD.....	35
2.3.1.2.4.	P-Y METHOD.....	36
2.3.1.2.5.	FEM METHOD	37
2.3.2.	<i>FIELD TESTS ON JOINTLESS BRIDGES.....</i>	37
2.3.3.	<i>FIELD TESTS ON SINGLE PILES</i>	49
2.3.4.	<i>CREEP AND SHRINKAGE</i>	53
2.3.4.1.	CREEP.....	54
2.3.4.2.	SHRINKAGE.....	56
2.3.5.	<i>CURVED AND SKEWED BRIDGES</i>	56
CHAPTER 3	SOIL-STRUCTURE INTERACTION.....	58
3.1.	SOIL-PILE INTERACTION.....	58
3.1.1.	<i>GOVERNING DIFFERENTIAL EQUATION OF PILE.....</i>	58
3.1.2.	<i>GOVERNING DIFFERENTIAL EQUATION OF FRICTION PILES.....</i>	62
3.1.3.	<i>P-Y METHOD.....</i>	64

3.1.3.1.	LOADING.....	64
3.1.3.2.	SOFT CLAYS BELOW THE WATER TABLE.....	64
3.1.3.2.1.	STATIC LOADING	64
3.1.3.2.2.	CYCLIC LOADING.....	66
3.1.3.3.	STIFF CLAY BELOW THE WATER TABLE.....	67
3.1.3.3.1.	STATIC LOADING	67
3.2.	SOIL-ABUTMENT INTERACTION.....	70
CHAPTER 4	EXPERIMENTAL PROGRAM.....	74
4.1.	INTRODUCTION.....	74
4.2.	TEST SETUP.....	74
4.2.1.	<i>INSTRUMENTATION.....</i>	<i>76</i>
4.2.1.1.	ARAMIS (OPTICAL 3-D DEFORMATION ANALYSIS SYSTEM).....	79
4.2.2.	<i>BUILDING SPECIMENS.....</i>	<i>80</i>
4.2.2.1.	FIRST POUR (MARCH 7TH 2011).....	83
4.2.2.2.	SECOND POUR (MARCH 10TH 2011).....	86
4.2.2.3.	THIRD POUR (MARCH 15TH 2011).....	87
4.2.3.	<i>PREPARING THE TEST SETUP.....</i>	<i>88</i>
4.2.4.	<i>TEST PROCEDURE ON SPECIMEN #1.....</i>	<i>91</i>
4.2.4.1.	LOADING SCHEDULE.....	91
4.2.4.1.1.	INCREASING CYCLIC LOADING UP TO 1 INCH.....	91
4.2.4.1.2.	CONSTANT CYCLIC LOADING (± 0.5 INCH).....	92
4.2.4.1.3.	INCREASING CYCLIC LOADING UP TO FAILURE.....	92
4.2.4.2.	CONDUCTING THE TEST.....	93
4.2.4.2.1.	LOAD STAGE 1.....	93
4.2.4.2.2.	LOAD STAGE 2.....	94
4.2.4.2.3.	LOAD STAGE 3.....	94
4.2.5.	<i>TEST PROCEDURE ON SPECIMEN #2.....</i>	<i>97</i>
4.2.5.1.	LOADING SCHEDULE.....	97
4.2.5.1.1.	INCREASING CYCLIC LOADING UP TO 4.5 INCH.....	98

4.2.5.1.2.	CONSTANT CYCLIC LOADING (± 0.5 INCH)	99
4.2.5.1.3.	ULTIMATE LOADING	99
4.2.5.2.	CONDUCTING THE TEST	100
4.2.5.2.1.	LOAD STAGE 1	100
4.2.5.2.2.	LOAD STAGE 2	102
4.2.5.2.3.	LOAD STAGE 3	103
4.3.	ANALYSIS OF TEST RESULTS	107
4.3.1.	<i>SPECIMEN #1 (FIXED)</i>	107
4.3.1.1.	LOAD STAGE 1	108
4.3.1.2.	LOAD STAGE 2	110
4.3.1.3.	LOAD STAGE 3	112
4.3.2.	<i>SPECIMEN #2 (PINNED)</i>	117
4.3.2.1.	LOAD STAGE 1	117
4.3.2.2.	LOAD STAGE 2	122
4.3.2.3.	LOAD STAGE 3	124
4.3.3.	<i>ROTATIONAL STIFFNESS IN SAP2000</i>	126
4.4.	MATERIAL PROPERTY TESTS	131
4.4.1.	<i>STEEL TENSIONS TESTS</i>	131
4.4.2.	<i>CONCRETE COMPRESSION TESTS</i>	133
4.4.2.1.	COMPRESSION TEST ON FIRST POUR SPECIMEN	133
4.4.2.2.	COMPRESSION TEST ON SECOND POUR SPECIMEN	134
4.4.2.3.	COMPRESSION TEST ON THIRD POUR SPECIMEN	134
4.4.3.	<i>SOFT MATERIAL COMPRESSION TESTS</i>	134
4.4.3.1.	DELPATCH ELASTOMERIC CONCRETE	134
4.4.3.1.1.	WOODEN MOLD	136
4.4.3.1.2.	PLEXIGLASS MOLD	136
4.4.3.1.3.	CYCLIC TEST	137
4.4.3.2.	FIBERLAST (ELASTOMERIC MATERIAL)	140
4.5.	CONCLUSIONS OF EXPERIMENTAL STUDY	144

CHAPTER 5	ANALYTICAL STUDY	146
5.1.	ELASTIC BUCKLING OF EMBEDDED STEEL PILES.....	147
5.1.1.	<i>PILE DESIGN FOR JOINTLESS BRIDGES.....</i>	<i>148</i>
5.1.2.	<i>NUMERICAL STUDY.....</i>	<i>150</i>
5.1.2.1.	P-Y CURVES FOR SOFT CLAY	151
5.1.2.2.	ENERGY METHOD	152
5.1.2.3.	VERIFICATION OF BUCKLING CALCULATIONS	153
5.1.2.3.1.	SIMPLE UNSUPPORTED COLUMN.....	153
5.1.2.3.2.	PILE BUCKLING TEST	154
5.1.2.4.	ANOTHER COMPARISON WITH CURRENT METHOD	156
5.1.3.	<i>RESULTS AND DISCUSSION</i>	<i>158</i>
5.1.3.1.	EFFECT OF PILE HEAD DEFLECTION.....	159
5.1.3.2.	EFFECT OF PILE'S FLEXURAL STIFFNESS	160
5.1.3.3.	EFFECT OF EMBEDDED LENGTH.....	161
5.1.3.4.	EFFECT OF SOIL SHEAR RESISTANCE	162
5.1.4.	<i>CONCLUSIONS</i>	<i>163</i>
5.2.	PILE HEAD DETAIL	164
5.2.1.	<i>FEM MODELING OF AN EMBEDDED PILE.....</i>	<i>166</i>
5.2.2.	<i>FEM MODELING OF THE SPECIMENS</i>	<i>170</i>
5.2.2.1.	DESCRIPTION OF THE MODEL.....	171
5.2.2.1.1.	SPECIMEN #1.....	171
5.2.2.1.2.	SPECIMEN #2.....	171
5.2.2.2.	RESULTS OF ANALYSIS.....	172
5.3.	DESIGN OF PILES FOR FATIGUE.....	173
5.3.1.	<i>ESTIMATION OF MAXIMUM ALLOWABLE STRAIN</i>	<i>173</i>
5.3.2.	<i>PUSHOVER ANALYSES.....</i>	<i>177</i>
5.3.3.	<i>SOIL-PILE INTERACTION MODEL</i>	<i>177</i>
5.3.3.1.	PILE DRIVEN IN CLAY	178

5.3.4.	<i>DESCRIPTION OF THE MODEL</i>	178
5.3.5.	<i>RESULTS OF THE ANALYSES</i>	180
5.3.5.1.	EXAMPLE PROBLEM	181
5.3.5.1.1.	STRONG AXIS BENDING	181
5.3.5.1.2.	WEAK AXIS BENDING	182
5.4.	DEVELOPMENT OF THE DESIGN PROVISIONS FOR PILES	184
5.4.1.	<i>GLOBAL STABILITY</i>	185
5.4.2.	<i>DUCTILITY</i>	186
5.4.3.	<i>FATIGUE</i>	186
5.5.	FINDINGS	188
CHAPTER 6	CONCLUSIONS AND RECOMMENDATIONS	189
6.1.	CONCLUSIONS	189
6.2.	FUTURE RESEARCH	191
REFERENCES	193	
APPENDIX A.	DESIGN OF SPECIMENS	201
A1.	DESIGN OF PILE CAP	201
A2.	CAP REINFORCEMENT DESIGN	204
A3.	DESIGN OF SPREADER BEAM	205
APPENDIX B.	MOMENT-CURVATURE ANALYSIS	207
B1.	CONSTITUTIVE MODELS	209
B1.1.	STEEL MODEL	209
B1.2.	CONCRETE MODEL	209
B1.2.1.	<i>MODIFIED HOGNESTAD MODEL (HOGNESTAD, 1951)</i>	210
B1.2.2.	<i>KENT AND PARK MODEL (KENT AND PARK, 1971)</i>	211
APPENDIX C.	DESIGN GUIDE FOR JOINTLESS BRIDGES	212

C1.	INTRODUCTION.....	212
C2.	HISTORY OF JOINTLESS BRIDGES.....	212
C3.	TYPES OF JOINTLESS BRIDGES.....	214
C3.1.	INTEGRAL BRIDGES.....	215
C3.2.	SEMI-INTEGRAL BRIDGES.....	216
C3.3.	SEAMLESS BRIDGES.....	216
C3.4.	ADVANTAGES OF JOINTLESS BRIDGES.....	217
C3.5.	COST EFFECTIVENESS OF JOINTLESS BRIDGES.....	218
C4.	FACTORS AFFECTING PERFORMANCE OF JOINTLESS BRIDGES...222	
C4.1.	CURVATURE.....	222
C4.2.	SKEW.....	222
C4.3.	BEARING.....	222
C4.4.	CONNECTION BETWEEN SUPERSTRUCTURE AND SUBSTRUCTURE.....	223
C4.5.	OTHER CONSIDERATIONS.....	224
C4.5.1.	SITE CONDITION.....	224
C4.5.2.	DETERIORATION OF PILING.....	227
C4.5.3.	JOINTLESS BRIDGE ABUTMENTS WITH MSE WALLS.....	227
C5.	STRATEGY SELECTION PROCESS.....	230
C6.	DESIGN PROVISIONS FOR JOINTLESS BRIDGES.....	233
C6.1.	METHOD A.....	234
C6.2.	METHOD B.....	234
C6.2.1.	LOADS.....	234
C6.2.1.1.	DEAD LOADS.....	234
C6.2.1.2.	LIVE LOADS.....	235
C6.2.1.3.	SOIL LOADS.....	236

C6.2.1.3.1.	SOIL LOAD ON ABUTMENT.....	236
C6.2.1.3.2.	SOIL LOAD ON PILES.....	238
C6.2.1.4.	THERMAL LOADS.....	239
C6.2.1.4.1.	UNIFORM TEMPERATURE CHANGE.....	239
C6.2.1.4.2.	TEMPERATURE GRADIENT	242
C6.2.1.5.	CREEP	246
C6.2.1.6.	SHRINKAGE	248
C6.2.1.7.	SETTLEMENT	248
C6.2.1.8.	WIND	249
C6.2.1.9.	OTHER LOADS	250
C6.2.2.	<i>LOAD COMBINATIONS AND LIMIT STATES</i>	250
C6.2.2.1.	LOAD COMBINATIONS.....	250
C6.2.2.1.1.	LOAD COMBINATIONS ARE PRESCRIBED PER AASHTO PROCEDURES.....	250
C6.2.2.1.2.	LOADS AND LOAD DESIGNATIONS	250
C6.2.2.1.3.	LOAD FACTORS AND COMBINATIONS.....	251
C6.2.3.	<i>BRIDGE MOVEMENT</i>	252
C6.2.3.1.	DISPLACEMENT OF STRAIGHT BRIDGES (NON-SKEW).....	252
C6.2.3.1.1.	PRESTRESSED CONCRETE BRIDGES	254
C6.2.3.1.2.	REINFORCED CONCRETE BRIDGES	257
C6.2.3.1.3.	COMPOSITE STEEL BRIDGES	257
C6.2.3.2.	DISPLACEMENT OF SKEWED BRIDGES	258
C6.2.3.2.1.	BACKGROUND	258
C6.2.3.2.2.	DESIGN RECOMMENDATIONS FOR TRANSVERSE RESPONSE OF SKEWED BRIDGES	260
C6.2.3.3.	DISPLACEMENT OF CURVED BRIDGES	268
C6.2.4.	<i>RESTRAINT MOMENTS</i>	272
C6.2.4.1.	BACKGROUND	273
C6.2.4.2.	DESIGN RECOMMENDATIONS	282
C6.2.4.2.1.	RESTRAINT MOMENTS IN PRESTRESSED CONCRETE GIRDERS	282
C6.2.4.2.2.	RESTRAINT MOMENTS IN COMPOSITE STEEL BRIDGE BEAMS	289
C6.2.5.	<i>DESIGN OF PILE FOUNDATION</i>	290

C6.2.5.1.	PILE ORIENTATION	292
C6.2.5.1.1.	STRAIGHT BRIDGES	292
C6.2.5.1.2.	CURVED BRIDGES.....	292
C6.2.5.2.	PILE DESIGN.....	294
C6.2.5.2.1.	DUCTILITY	295
C6.2.5.2.2.	FATIGUE.....	296
C6.2.5.2.3.	PILE GROUP INTERACTION.....	297
C6.2.5.3.	ANALYSIS TOOLS.....	300
C6.2.5.3.1.	SIMPLIFIED ANALYSIS (P-Y METHOD).....	301
C6.2.5.3.2.	FINITE ELEMENT ANALYSIS	301
C6.2.6.	<i>DESIGN OF OTHER FOUNDATION TYPES</i>	302
C6.2.6.1.	DRILLED SHAFTS	303
C6.2.6.2.	SPREAD FOOTINGS.....	303
C6.2.6.3.	MICRO-PILES	303
C6.2.7.	<i>DESIGN OF PILE CAP</i>	303
C6.2.7.1.	INTEGRAL PILE CAP DESIGN	304
C6.2.7.1.1.	ENCASED PILES (FIXED CONDITION)	304
C6.2.7.1.2.	PIN HEAD PILES (FLEXIBLE CONDITION)	306
C6.2.7.2.	SEMI INTEGRAL PILE CAP DESIGN.....	308
C6.2.7.3.	SEAMLESS DETAILS	309
C6.2.8.	<i>END-DIAPHRAGM (BACKWALL) DESIGN</i>	309
C6.2.8.1.	INTEGRAL.....	310
C6.2.8.2.	SEMI-INTEGRAL.....	312
C6.2.8.3.	SEAMLESS	312
C6.2.9.	<i>APPROACH SLAB DESIGN</i>	312
C6.2.9.1.	INTEGRAL AND SEMI-INTEGRAL	312
C6.2.9.2.	SEAMLESS DECK TRANSITION ZONE	314
C6.2.10.	<i>DESIGN OF SUPERSTRUCTURE-PIER CONNECTION</i>	316
C6.2.10.1.	INTEGRAL PIER CAP.....	318
C6.2.10.2.	FIXED (PINNED) AND EXPANSION PIER CAPS	319

C6.2.10.3.	LINK SLAB EXPANSION PIER CAP.....	321
<i>C6.2.11.</i>	<i>DESIGN OF INTEGRAL PIERS.....</i>	<i>323</i>
C6.2.11.1.	FOUNDATION ROTATION.....	323
C6.2.11.2.	PIER DISPLACEMENT.....	324
<i>C6.2.12.</i>	<i>DESIGN OF WING WALLS.....</i>	<i>325</i>
C7.	DETAILS.....	326
C7.1.	GENERAL ABUTMENT DETAILS FOR JOINTLESS BRIDGES.....	326
<i>C7.1.1.</i>	<i>INTEGRAL ABUTMENTS.....</i>	<i>327</i>
<i>C7.1.2.</i>	<i>SEMI-INTEGRAL ABUTMENTS.....</i>	<i>332</i>
<i>C7.1.3.</i>	<i>SEAMLESS ABUTMENTS.....</i>	<i>335</i>
C7.2.	PILE CAP AND BACKWALL.....	335
C7.3.	SLEEPER SLAB.....	336
C7.4.	DETAILS FOR SKEWED AND CURVED BRIDGE.....	338
C8.	CONSTRUCTION.....	339
C8.1.	CONSTRUCTION STABILITY.....	339
C8.2.	UTILITIES.....	339
C8.3.	CRACKING CONTROL.....	340
C8.4.	CONSTRUCTION SEQUENCING.....	340
C8.5.	FILL COMPACTION.....	342
C9.	MAINTENANCE AND REPAIR.....	342
C9.1.	PROBLEMS WITH JOINTLESS CONSTRUCTION.....	342
<i>C9.1.1.</i>	<i>DECK CRACKING.....</i>	<i>343</i>
<i>C9.1.2.</i>	<i>LATERAL ROTATION OF SEMI-INTEGRAL BRIDGES.....</i>	<i>343</i>
<i>C9.1.3.</i>	<i>APPROACH SLABS.....</i>	<i>344</i>
<i>C9.1.4.</i>	<i>DRAINAGE.....</i>	<i>344</i>
<i>C9.1.5.</i>	<i>CYCLE-CONTROL JOINTS.....</i>	<i>345</i>

C9.2. DECK REPLACEMENT345

C9.3. BEARING REPLACEMENT FOR SEMI-INTEGRAL.....346

C10. RETROFITS.....347

C10.1. DETAILS OVER THE PIER.....348

C10.1.1. RETROFIT WITH GIRDER CONTINUITY348

C10.1.2. LINK SLAB.....348

C10.2. DETAILS OVER THE ABUTMENT349

C10.3. CONVERSION351

List of Figures

FIGURE 2-1- CONTOUR MAPS FOR $T_{MaxDesign}$ FOR CONCRETE GIRDER BRIDGES WITH CONCRETE DECKS (FIGURE 3.12.2.2-1 FROM AASHTO).....	10
FIGURE 2-2- SOLAR RADIATION ZONES FOR THE UNITED STATES. (FIGURE 3.12.3-1 FROM AASHTO)	11
FIGURE 2-3- POSITIVE VERTICAL TEMPERATURE GRADIENT IN CONCRETE AND STEEL SUPERSTRUCTURES (FIGURE 3.12.3-2 FROM AASHTO).....	12
FIGURE 2-4- ANNUAL AVERAGE AMBIENT RELATIVE HUMIDITY IN PERCENT. (FIGURE 5.4.2.3.3-1 FROM AASHTO).....	16
FIGURE 2-5- DEFINITION OF LOADING DIRECTION AND SPACING FOR GROUP EFFECTS (FIGURE 10.7.2.4-1 FROM AASHTO).....	17
FIGURE 2-6- STATES WITH DESIGN RECOMMENDATIONS FOR JOINTLESS BRIDGES (GRAY)	22
FIGURE 2-7- RELATIONSHIP BETWEEN WALL MOVEMENT AND EARTH PRESSURE. (CLOUGH AND DUNCAN, 1991).....	33
FIGURE 2-8- RELATIONSHIP BETWEEN WALL MOVEMENT AND EARTH PRESSURE FOR A WALL WITH COMPACTED BACKFILL (CLOUGH AND DUNCAN, 1991).....	34
FIGURE 2-9- CANTILEVER IDEALIZATION OF THE PILE (A) FIXED HEAD (B) FREE HEAD (ABENDROTH, GREIMANN AND EBNER, 1989)	36
FIGURE 2-10- SR-18 END BENT INSTRUMENTATION (FROSCH, WENNING AND CHIVIVHIEN, 2005)	40
FIGURE 2-11- SR-249 END BENT DETAIL (FROSCH, WENNING AND CHIVIVHIEN, 2005).....	40
FIGURE 2-12- BOONE RIVER BRIDGE (A) ABUTMENT CROSS SECTION (B) INITIAL STIFFNESS VS. DEPTH (GIRTON, HAWKINSON AND GREIMANN, 1991)	42
FIGURE 2-13- MAPLE RIVER BRIDGE (A) ABUTMENT CROSS SECTION (B) INITIAL STIFFNESS VS. DEPTH (GIRTON, HAWKINSON AND GREIMANN, 1991)	42

FIGURE 2-14- TYPICAL LONGITUDINAL CROSS SECTION NEAR ABUTMENT AND BENCHMARK POST INSTALLATION FOR STORY COUNTY BRIDGE AND GUTHRIE COUNTY BRIDGE (ABENDROTH AND GREIMANN, 2005)	44
FIGURE 2-15- INSTRUMENTATION AT MID-WIDTH OF EAST ABUTMENT FOR THE TAMA COUNTY BRIDGE (ABENDROTH, GREIMANN AND LAVIOLETTE, 2007)	45
FIGURE 2-16- END ABUTMENT DETAIL AT ROCHESTER BRIDGE (LAWVER, FRENCH AND SHIELD, 2000).....	47
FIGURE 2-17- INSTRUMENTATION AT SCOTCH ROAD BRIDGE (HASSIOTIS, LOPEZ AND BERMUDEZ, 2005) ...	48
FIGURE 2-18- PORT MATILDA BRIDGE ABUTMENT SECTION AND INSTRUMENTATION PLAN (FENNEMA, LAMAN AND LINZELL, 2005)	49
FIGURE 3-1- BEAM-COLUMN SEGMENT FORCES	59
FIGURE 3-2- FINITE DIFFERENCE ANALYSIS OF LATERALLY LOADED PILES.....	61
FIGURE 3-3- CHARACTERISTIC SHAPES OF P-Y CURVES FOR SOFT CLAY BELOW WATER TABLE (A) STATIC LOADING (B) CYCLIC LOADING (MATLOCK, 1970).....	66
FIGURE 3-4- VALUES OF A_s , AND A_c (REESE, COX AND KOOP, 1975)	68
FIGURE 3-5- CHARACTERISTIC SHAPE OF P-Y CURVE FOR STIFF CLAY (REESE, COX AND KOOP, 1975).....	70
FIGURE 3-6- RELATIONSHIP BETWEEN WALL MOVEMENT AND EARTH PRESSURE (CLOUGH AND DUNCAN, 1991).....	72
FIGURE 3-7- RELATIONSHIP BETWEEN WALL MOVEMENT AND EARTH PRESSURE FOR A WALL WITH COMPACTED BACKFILL (CLOUGH AND DUNCAN, 1991).....	72
FIGURE 4-1- TEST SETUP	75
FIGURE 4-2- PILE CAP REINFORCEMENT	76
FIGURE 4-3- INSTRUMENTATION PLAN AROUND THE CONNECTION (SPECIMEN #2)	77
FIGURE 4-4- DETAILS OF MOUNTING THE SPRING POTS	78
FIGURE 4-5- INSTRUMENTATION PLAN AROUND THE CONNECTION (SPECIMEN #2)	78

FIGURE 4-6- ARAMIS SETUP.....	80
FIGURE 4-7- PIPES BEFORE CASTING	81
FIGURE 4-8- EMBEDDED PLATE.....	81
FIGURE 4-9- CASTS FOR THE CAPS	82
FIGURE 4-10- HOLDING THE EMBEDDED PLATE AT THE MIDDLE OF THE CAP.....	83
FIGURE 4-11- PREPARING THE PIPES FOR THE POUR	84
FIGURE 4-12- POURING CONCRETE INTO THE PIPE.....	84
FIGURE 4-13- FIRST POUR INTO SPECIMEN #2	85
FIGURE 4-14- SPECIMEN #2 AFTER FIRST POUR (EMBEDDED PLATE AT THE MIDDLE)	85
FIGURE 4-15- SPECIMEN #1 BEFORE THE POUR	86
FIGURE 4-16- SPECIMEN #1 AFTER THE POUR.....	87
FIGURE 4-17- PREPARING SPECIMEN #2	88
FIGURE 4-18- PREPARING SPECIMEN #2	88
FIGURE 4-19- PLACING SPECIMEN #1 ON TOP OF SUPPORT BLOCKS	89
FIGURE 4-20- (A) PREPARING FRESH HYDROSTONE (B) PUMPING THE HYDROSTONE INTO THE GAPS	90
FIGURE 4-21- LOAD POINT CONFIGURATION	90
FIGURE 4-22- TYPICAL PATTERN OF LATERAL LOADING FOR STAGE 1 (SPECIMEN #1).....	92
FIGURE 4-23- CONDITION OF THE CONNECTION AT LOAD STAGE 3-8 (± 2.00 IN).....	94
FIGURE 4-24- WELDING THE SPREADER BEAM'S BOTTOM FLANGE TO THICK PLATE	95
FIGURE 4-25- (A) EXCESSIVE DEFORMATION NEAR THE FIRST GAGES AT LOAD STAGE 3-16 (± 3.00 IN) (B) LARGE DEFORMATION AROUND THE ROD HOLDING PT1	96
FIGURE 4-26- CONDITION OF CONNECTION AT LOAD STAGE 3-18 (± 4.50 IN) (A) HUGE CRACK AT THE BOTTOM (B) LARGE DEFORMATION AT THE TOP	96

FIGURE 4-27- CRACK COMPLETELY OPENED AT LOAD STAGE 3-19 (± 4.75 IN).....	97
FIGURE 4-28- TYPICAL PATTERN OF LATERAL LOADING FOR STAGE 1 (SPECIMEN #2).....	99
FIGURE 4-29- CONDITION OF THE CONNECTION AT STAGE 1-9 (± 2.00 IN)	100
FIGURE 4-30- CONDITION OF THE CONNECTION AROUND PEAK MOVEMENT AT STAGE 1-11D (± 2.50 IN)	101
FIGURE 4-31- CONDITION OF THE TOP OF THE CONNECTION AFTER STAGE 1-18H (± 4.25 IN).....	102
FIGURE 4-32- SPECIMEN #2 AFTER LUBRICATION AT PEAK DISPLACEMENT IN LOAD STAGE 2 (± 4.25 IN)	103
FIGURE 4-33- SPACERS USED FOR ADDITIONAL STROKE.....	104
FIGURE 4-34- ULTIMATE TEST (SPECIMEN #2)	104
FIGURE 4-35- FAILURE OF THE DYWIDAG.....	105
FIGURE 4-36- FAILURE OF THE DYWIDAG.....	106
FIGURE 4-37- SETUP USED TO REMOVE CFT.....	106
FIGURE 4-38- PIPE CONDITION AFTER THE TEST	107
FIGURE 4-39- LOAD DEFLECTION CURVE FOR LOAD STAGE 1-1.....	108
FIGURE 4-40- LOAD DEFLECTION CURVE FOR LOAD STAGE 1-2.....	109
FIGURE 4-41- ENVELOPE OF LOAD-DEFLECTION CURVE FOR STAGE 1	110
FIGURE 4-42- APPLIED FORCES IN LOAD STAGE 2-1 (A) MAXIMUM APPLIED LATERAL LOAD BY ACTUATORS (B) APPLIED AXIAL LOAD	111
FIGURE 4-43- MAXIMUM STRAINS ACCORDING TO INSTALLED GAGES	112
FIGURE 4-44- LOAD-DEFLECTION CURVE FOR SPECIMEN #1 AT STAGE 3.....	113
FIGURE 4-45- ENVELOPE OF LOAD-DEFLECTION CURVE.....	114
FIGURE 4-46- MOMENT-CURVATURE CURVE FOR SPECIMEN #1 UP TO STAGE 3-10 (± 2.5 IN).....	115
FIGURE 4-47- MOMENT-CURVATURE CURVE FOR SPECIMEN #1 UP TO STAGE 3-10 (± 2.5 IN).....	116
FIGURE 4-48- MOMENT-ROTATION CURVE FOR SPECIMEN #1	117

FIGURE 4-49- LOAD-DEFLECTION POINTS FOR STAGE 1 (SPECIMEN #2).....	118
FIGURE 4-50- LOAD-DEFLECTION CURVE FOR STAGE 1 (SPECIMEN #2).....	119
FIGURE 4-51- MOMENT-ROTATION CURVE FOR STAGE 1 (SPECIMEN #2).....	120
FIGURE 4-52- ENVELOPE OF MOMENT-ROTATION CURVE FOR STAGE 1 (SPECIMEN #2).....	121
FIGURE 4-53- MAXIMUM STRAINS IN STAGE 1 (SPECIMEN #2) (A) GB1 (B) GT1	121
FIGURE 4-54- CALIBRATED MOMENT-ROTATION CURVES	122
FIGURE 4-55- AXIAL AND LATERAL LOAD DURING LOAD STAGE 2 (SPECIMEN #2).....	123
FIGURE 4-56- READINGS FROM FIRST ROW POTS (SPECIMEN #2)	124
FIGURE 4-57- LOAD-DEFLECTION CURVE FOR LOAD STAGE 3 (SPECIMEN #2).....	125
FIGURE 4-58- LOAD-DEFLECTION CURVE FOR LOAD STAGE 3 (SPECIMEN #2).....	126
FIGURE 4-59- CALIBRATED MOMENT-ROTATION CURVES	127
FIGURE 4-60- LOAD-DEFLECTION CURVES FROM TESTS AND SAP2000	128
FIGURE 4-61- SCHEMATIC MODELS USED IN SAP2000 ANALYSIS	129
FIGURE 4-62- PUSHOVER ANALYSIS RESULTS IN MEDIUM CLAY FOR CFT PILES TESTED.....	130
FIGURE 4-63- TENSILE TEST DIMENSIONS	131
FIGURE 4-64- STRESS-STRAIN CURVES FOR SAMPLES FROM SPECIMEN #1.....	132
FIGURE 4-65- STRESS-STRAIN CURVES FOR SAMPLES FROM SPECIMEN #2.....	133
FIGURE 4-66- DELPATCH MIXING PROCEDURE	135
FIGURE 4-67- SAMPLES MADE IN WOODEN MOLDS.....	136
FIGURE 4-68- (A) POURING THE MIX (B) LEVELED TOP SURFACE.....	137
FIGURE 4-69- MTS LOAD FRAME FOR CYCLIC LOAD TEST	138
FIGURE 4-70- STRESS-STRAIN CURVES FOR (A) STATIC LOADING UP TO 5% STRAIN (B) CYCLIC LOADING ...	139

FIGURE 4-71- (A) CRACKS FORMING ON THE OPPOSITE SIDE OF THE SPECIMEN (B) DISLOCATION OF THE SPECIMEN AND CRACKS AFTER ABOUT 8000 CYCLES	139
FIGURE 4-72- STRESS-STRAIN CURVES FOR (A) INITIAL STATIC LOADING UP TO 10% STRAIN (B) CYCLIC LOADING (C) MAX LOAD CHANGE DURING THE CYCLIC LOADING.....	140
FIGURE 4-73- STRESS-STRAIN CURVES FOR TEST F-C-1 (A) STATIC LOADING UP TO 10% STRAIN (B) CYCLIC LOADING.....	141
FIGURE 4-74- STRESS-STRAIN CURVES FOR TEST F-C-2 (A) STATIC LOADING UP TO 10% STRAIN (B) CYCLIC LOADING (C) MAX LOAD CHANGE DURING THE CYCLIC LOADING.....	142
FIGURE 4-75- STRESS-STRAIN CURVES FOR TEST F-C-3 (A) STATIC LOADING UP TO 10% STRAIN (B) CYCLIC LOADING.....	142
FIGURE 4-76- STRESS-STRAIN CURVES FOR TEST F-C-4 (A) STATIC LOADING UP TO 30% STRAIN (B) CYCLIC LOADING.....	143
FIGURE 4-77- STRESS-STRAIN CURVES FOR TEST F-C-5 (A) STATIC LOADING UP TO 5% STRAIN (B) CYCLIC LOADING.....	143
FIGURE 4-78- STRESS-STRAIN CURVES FOR TEST F-C-6 (A) INITIAL STATIC LOADING UP TO 15% STRAIN (B) CYCLIC LOADING	144
FIGURE 5-1- EQUIVALENT CANTILEVERS IN UNIFORM SOILS FOR (A) PINNED HEAD PILES (B) FIXED HEAD PILES (ABENDROTH, GREIMANN AND EBNER, 1989).....	150
FIGURE 5-2- BUCKLING LOAD ESTIMATION FOR A PIPE COLUMN USING ENERGY METHOD (A) PIN-PIN (B) FIX-FIX.....	154
FIGURE 5-3- (A) TEST SETUP (B) BUCKLING LOAD ESTIMATION FOR THE PILE TESTED BY VOGT ET AL. (2009).	155
FIGURE 5-4- BUCKLING LOAD ESTIMATION FOR A PILE USING ENERGY METHOD ($\Delta=2.0$ CM).....	158

FIGURE 5-5- EFFECT OF PILE HEAD MOVEMENT ON CRITICAL BUCKLING LOAD (A) PINNED HEAD (B) FIXED HEAD.	160
FIGURE 5-6- EFFECT OF PILE FLEXURAL STIFFNESS ON CRITICAL BUCKLING LOAD (A) PINNED HEAD (B) FIXED HEAD ($\Delta=2.0$ CM)	161
FIGURE 5-7- EFFECT OF PILE LENGTH ON CRITICAL BUCKLING LOAD (A) PINNED HEAD (B) FIXED HEAD ($\Delta=2.0$ CM).....	162
FIGURE 5-8- EFFECT OF SOIL SHEAR RESISTANCE ON CRITICAL BUCKLING LOAD (A) PINNED HEAD (B) FIXED HEAD ($\Delta=2.0$ CM)	163
FIGURE 5-9- TEST SETUP BY BURDETTE ET AL.	167
FIGURE 5-10- FEM MODEL OF THE TEST BY BURDETTE ET AL.	168
FIGURE 5-11- STRESSES IN PINNED SYSTEM AT 1.84 IN GROUND DEFLECTION.....	169
FIGURE 5-12- PRINCIPAL MAXIMUM PLASTIC STRAIN (A) FIXED HEAD AT 1.0 IN GROUND LEVEL DEFLECTION (B) PINNED HEAD AT 1.84 IN GROUND LEVEL DEFLECTION.....	170
FIGURE 5-13- LOAD DEFLECTION CURVE (A) COMPARISON OF TEST RESULT WITH FEM MODEL (B) COMPARISON OF FEM RESULTS FOR FULL FIXITY, 1 IN RUBBER, AND 4 IN RUBBER.....	170
FIGURE 5-14- LOAD DEFLECTION CURVES COMPARING THE TEST RESULTS WITH FEM MODELS	172
FIGURE 5-15- MAXIMUM PRINCIPAL PLASTIC STRAINS AT 4.0 IN DEFLECTION (A) SPECIMEN #1 (B) SPECIMEN #2	173
FIGURE 5-16- PILE STRAIN AS A FUNCTION OF TIME (DICLELI AND ALBHAISI, 2004)	174
FIGURE 5-17- ACTUAL AND MODELED P-Y CURVES FOR CLAY (DICLELI AND ALBHAISI, 2004)	178
FIGURE 5-18- SCHEMATIC MODEL USED IN SAP2000	179
FIGURE 5-19- DISPLACEMENT CAPACITY OF COMPACT HP SECTIONS IN SOFT CLAY ($C_u = 2.9$ PSI) (A) HP10x57 (B) HP12x84	180

FIGURE 5-20- DISPLACEMENT CAPACITY OF COMPACT HP SECTIONS IN MEDIUM CLAY ($C_u = 5.8$ PSI) (A)	
HP10x57 (B) HP12x84	180
FIGURE 5-21- MOMENT-CURVATURE FOR HP12x84 BENDING ALONG STRONG AXIS WITH NO AXIAL LOAD.	181
FIGURE 5-22- MOMENT-CURVATURE FOR HP12x84 BENDING ALONG STRONG AXIS WITH NO AXIAL LOAD.	182
FIGURE 5-23- MOMENT-CURVATURE FOR HP12x84 BENDING ALONG STRONG AXIS WITH NO AXIAL LOAD.	183
FIGURE 5-24- MOMENT-CURVATURE FOR HP12x84 BENDING ALONG STRONG AXIS WITH NO AXIAL LOAD.	184
FIGURE 5-25- DISPLACEMENT CAPACITY OF COMPACT HP SECTIONS IN SOFT CLAY ($C_u = 2.9$ PSI) (A)	
HP10x57 (B) HP12x84	187
FIGURE 5-26- DISPLACEMENT CAPACITY OF COMPACT HP SECTIONS IN MEDIUM CLAY ($C_u = 5.8$ PSI) (A)	
HP10x57 (B) HP12x84	187
FIGURE A1- TRANSFER OF PILE MOMENTS TO PILE CAP (WASSERMAN AND WALKER, 1996).....	201
FIGURE A2- MOMENT-CURVATURE ANALYSIS OF THE CROSS SECTION OF THE PILE.....	202
FIGURE B1- DISCRETIZATION OF THE CROSS SECTION FOR MOMENT-CURVATURE ANALYSIS.....	207
FIGURE B2- BILINEAR STRESS-STRAIN CURVE FOR STEEL	209
FIGURE B3- MODIFIED HOGNESTAD MODEL (HOGNESTAD, 1951)	211
FIGURE B4- KENT AND PARK MODEL (KENT AND PARK, 1971)	211
FIGURE C1- ELEMENTS OF JOINTLESS INTEGRAL BRIDGES	215
FIGURE C2- SEAMLESS BRIDGE SYSTEM.....	217
FIGURE C3- LIFE-TIME COST ANALYSIS OF JOINTED VS. JOINTLESS BRIDGE OVER TIME	221
FIGURE C4- LIFE-TIME COST DIFFERENTIAL ANALYSIS OF JOINTED VS. JOINTLESS BRIDGE.....	222
FIGURE C5- ALTERNATIVES TO INTEGRAL FULL-HEIGHT WALL ABUTMENTS USING REINFORCED SOIL RETAINING STRUCTURE (NICHOLSON, BARR, COOKE, HICKMAN, JONES AND TAYLOR, 1997)	230
FIGURE C6- RELATIONSHIP BETWEEN WALL MOVEMENT AND EARTH PRESSURE (CLOUGH AND DUNCAN, 1991).....	237
FIGURE C7- RELATIONSHIP BETWEEN WALL MOVEMENT AND EARTH PRESSURE FOR A WALL WITH COMPACTED BACKFILL (CLOUGH AND DUNCAN, 1991).....	238

FIGURE C8- MAXIMUM DESIGN TEMPERATURE FOR CONCRETE GIRDER BRIDGES. (FIGURE 3.12.2.2-1 FROM AASHTO).....	240
FIGURE C9- MINIMUM DESIGN TEMPERATURE FOR CONCRETE GIRDER BRIDGES. (FIGURE 3.12.2.2-2 FROM AASHTO).....	241
FIGURE C10- MAXIMUM DESIGN TEMPERATURE FOR STEEL GIRDER BRIDGES. (FIGURE 3.12.2.2-3 FROM AASHTO).....	241
FIGURE C11- MINIMUM DESIGN TEMPERATURE FOR STEEL GIRDER BRIDGES. (FIGURE 3.12.2.2-4 FROM AASHTO).....	242
FIGURE C12- SOLAR RADIATION ZONES FOR THE UNITED STATES. (FIGURE 3.12.3-1 FROM AASHTO)	243
FIGURE C13- POSITIVE VERTICAL TEMPERATURE GRADIENT IN CONCRETE AND STEEL SUPERSTRUCTURES (FIGURE 3.12.3-2 FROM AASHTO)	244
FIGURE C14- ANNUAL AVERAGE AMBIENT RELATIVE HUMIDITY IN PERCENT. (FIGURE 5.4.2.3.3-1 FROM AASHTO).....	247
FIGURE C15- ILLUSTRATION COMPARING OF SETTLEMENT EFFECTS ON THE SUPERSTRUCTURE.....	249
FIGURE C16- COMPONENTS OF ABUTMENT SOIL PASSIVE PRESSURE RESPONSE TO THERMAL ELONGATION IN SKEWED INTEGRAL ABUTMENT BRIDGES.	259
FIGURE C17- TWO-SPAN SEMI-INTEGRAL ABUTMENT BRIDGE WITH AN OVERALL LENGTH OF 89 M, WIDTH OF 11.6 M, AND A SKEW ANGLE OF 45° (NICHOLSON, BARR, COOKE, HICKMAN, JONES AND TAYLOR, 1997).....	259
FIGURE C18- CRACKING IN THE ABUTMENT WALL NEAR AN ACUTE CORNER OF THE SUPERSTRUCTURE FOR THE BRIDGE SHOWN IN FIGURE C17 (NICHOLSON, BARR, COOKE, HICKMAN, JONES AND TAYLOR, 1997).....	260
FIGURE C19- ASPHALT OVERLAY DISTRESS (WEST END) (TABATABAI, OESTERLE AND LAWSON, 2005).....	261
FIGURE C20- BARRIER DISTRESS AT WEST ABUTMENT (TABATABAI, OESTERLE AND LAWSON, 2005).....	262
FIGURE C21- SOIL PRESSURE LOAD, P_p , AND SOIL ABUTMENT INTERFACE FRICTION, F_{AF}	263
FIGURE C22- RELATIONSHIP BETWEEN FORCE REQUIRED FOR ABUTMENT LATERAL RESISTANCE, F_A , AND PASSIVE PRESSURE RESPONSE, P_p , TO RESTRAIN LATERAL MOVEMENT.	264

FIGURE C23- RELATIONSHIP BETWEEN END NORMAL MOVEMENT, $\Delta\ell_n$, AND END THERMAL EXPANSION, $\Delta\ell$	265
FIGURE C24- RELATIONSHIP BETWEEN TRANSVERSE MOVEMENT AT THE ACUTE CORNER, Δ_{T1} , AND THERMAL EXPANSION, $\Delta\ell$, FOR AN EXPANSION OF 1 INCH WITH CONSTANT LENGTH BRIDGE, $L = 415.92$ FT, AND VARYING L/W	267
FIGURE C25- RELATIONSHIP BETWEEN RESULTANT LONGITUDINAL RESTRAINT FORCE AND SKEW ANGLE FOR THERMAL EXPANSION, $\Delta\ell$, OF 1 INCH WITH CONSTANT LENGTH BRIDGE, $L = 415.92$ FT, AND VARYING L/W	268
FIGURE C26- MODIFICATION FACTOR FOR BRIDGE CONTRACTION.....	270
FIGURE C27- MODIFICATION FACTOR FOR BRIDGE SHRINKAGE	271
FIGURE C28- A TYPICAL PRECAST PRESTRESSED BRIDGE SIMPLY SUPPORTED FOR DEAD LOAD AND MADE CONTINUOUS FOR LIVE LOAD.	273
FIGURE C29- RESTRAINT AGAINST UPWARD MOVEMENT, POSITIVE SECONDARY MOMENT.....	274
FIGURE C30- CRACKS NEAR GIRDER SUPPORTS	286
FIGURE C31- CRACK AND SPALL AT DIAPHRAGM OVER PIER SUPPORT.....	286
FIGURE C32- CONTROLLING TYPE OF LOAD COMBINATION.....	293
FIGURE C33- DIRECTION OF BRIDGE END DISPLACEMENT	293
FIGURE C34- ANGLE OF DIRECTION OF BRIDGE END DISPLACEMENT	294
FIGURE C35- DISPLACEMENT CAPACITY OF COMPACT HP SECTIONS IN SOFT CLAY ($C_u = 2.9$ PSI) (A) HP10x57 (B) HP12x84	296
FIGURE C36- DISPLACEMENT CAPACITY OF COMPACT HP SECTIONS IN MEDIUM CLAY ($C_u = 5.8$ PSI) (A) HP10x57 (B) HP12x84	296
FIGURE C37- DEFINITION OF LOADING DIRECTION AND SPACING FOR GROUP EFFECTS (FIGURE 10.7.2.4-1 FROM AASHTO).....	298
FIGURE C38- MOMENT TRANSFER FROM PILE TO CAP	305
FIGURE C39- MOMENT TRANSFER FROM PILE TO CAP	306

FIGURE C40- PROPOSED DETAIL	307
FIGURE C41- PREFABRICATED PILE CAP.....	308
FIGURE C42- LATERAL PRESSURE RESTRAINT BY SUPERSTRUCTURE (OESTERLE, TABATABAI, LAWSON, REFAI, VOLZ AND SCANLON, 2005).....	310
FIGURE C43- LATERAL PRESSURE RESTRAINT BY SUPERSTRUCTURE (OESTERLE, TABATABAI, LAWSON, REFAI, VOLZ AND SCANLON, 2005).....	311
FIGURE C44- DETERMINATION OF APPROACH SLAB LENGTH.....	314
FIGURE C45- SEAMLESS PAVING OVER BRIDGE TRANSITIONING TO JOINTED PAVEMENT	315
FIGURE C46- CONTINUOUSLY REINFORCED TO JOINTED PAVEMENT (JUNG, ZOLLINGER AND TAYABJI, 2007)	316
FIGURE C47- INTEGRAL, PINNED, AND EXPANSION TYPE BEARINGS FOR JOINTLESS BRIDGES	316
FIGURE C48- SIMPLE FOR DEAD AND CONTINUOUS FOR LIVE PIER DETAIL AFTER THE PLACING OF GIRDERS (B), AND AFTER THE CLOSURE POUR (C).....	318
FIGURE C49- INTEGRAL CAP AS COMPLETED	319
FIGURE C50- PRECAST, PRESTRESSED GIRDERS CONNECTED WITH LIVE LOAD CONTINUITY	320
FIGURE C51- CONCEPTUAL DETAIL FOR LINK SLAB	322
FIGURE C52- GENERAL INTEGRAL ABUTMENT CONCEPT.....	328
FIGURE C53- INTEGRAL ABUTMENT DETAILS.....	329
FIGURE C54- INTEGRAL ABUTMENT ROTATION DETAIL	330
FIGURE C55- INTEGRAL ABUTMENT DETAILS (NYSDOT).....	332
FIGURE C56- GENERAL SEMI-INTEGRAL ABUTMENT CONCEPT.....	333
FIGURE C57- SEMI-INTEGRAL DETAILS	334
FIGURE C58- SEMI-INTEGRAL DETAILS WITH EXTENDED DIAPHRAGM	335
FIGURE C59- SUGGESTED HELPER (SLEEPER) SLAB DETAILS (WASSERMAN AND WALKER, 1996).....	337
FIGURE C60- SLEEPER SLAB WITH CONCRETE PAVEMENT APPROACH (NYSDOT).....	338
FIGURE C61- SLEEPER SLAB WITH ASPHALT PAVEMENT APPROACH (NYSDOT).....	338
FIGURE C62- IMPROPER DECK REMOVAL	346

FIGURE C63- INTEGRAL CONVERSION AT PIERS (LEATHERS, 1990).....	349
FIGURE C64- CONVERSION OF A BRIDGE WITH MOVEABLE DECK JOINTS AT THE SUPERSTRUCTURE-ABUTMENT INTERFACE WITH INTEGRAL ABUTMENT (A) BEFORE CONVERSION (B) AFTER CONVERSION	350
FIGURE C65- CONVERSION OF A VERY SHORT SPAN BRIDGE WITH MOVEABLE DECK JOINTS AT THE SUPERSTRUCTURE-ABUTMENT INTERFACE WITH INTEGRAL ABUTMENT (A) BEFORE CONVERSION (B) AFTER CONVERSION	351

List of Tables

TABLE 2-1- PROCEDURE A TEMPERATURE RANGES (TABLE 3.12.2.1-1 FROM AASHTO).....	9
TABLE 2-2- BASIS FOR TEMPERATURE GRADIENTS (TABLE 3.12.3-1 FROM AASHTO).....	11
TABLE 2-3- PILE P-MULTIPLIERS, P_m FOR MULTIPLE ROW SHADING (TABLE 10.7.2.4-1 FROM AASHTO) .	16
TABLE 2-4- SUMMARY OF DESIGN LIMITATIONS FOR JOINTLESS BRIDGES	22
TABLE 2-5- THE MODULUS OF SUB-GRADE REACTION FOR DIFFERENT SOIL TYPES	25
TABLE 2-6- APPROXIMATE MAGNITUDES OF MOVEMENTS REQUIRED TO REACH EXTREME SOIL PRESSURE CONDITION (CLOUGH AND DUNCAN, 1991)	34
TABLE 2-7- LIST OF FIELD INSTRUMENTED JOINTLESS BRIDGES IN THE US.....	37
TABLE 2-8- LIST OF ALL AVAILABLE LITERATURE ON TESTS OF Laterally LOADED SINGLE PILES	50
TABLE 3-1- REPRESENTATIVE VALUES OF E_{50}	65
TABLE 3-2- REPRESENTATIVE VALUES OF K AND E_{50} FOR STIFF CLAY	68
TABLE 3-3- APPROXIMATE MAGNITUDES OF MOVEMENTS REQUIRED TO REACH EXTREME SOIL PRESSURE CONDITION (CLOUGH AND DUNCAN, 1991)	73
TABLE 4-1- LOCATION OF POTS (INCH)	79
TABLE 4-2- LOAD STAGES AT WHICH ARAMIS SYSTEM WAS USED.....	80
TABLE 4-3- LOAD STAGE 1 (SPECIMEN #1).....	91
TABLE 4-4- LOAD STAGE 2 (SPECIMEN #1).....	92
TABLE 4-5- LOAD STAGE 3 (SPECIMEN #1).....	93
TABLE 4-6- LOAD STAGE 1.....	98
TABLE 4-7- LOAD STAGE 2 (SPECIMEN #2).....	99
TABLE 4-8- NONLINEAR PROPERTIES OF LINK ELEMENT REPRESENTING CONNECTION STIFFNESS.....	127

TABLE 4-9- COMPARISON OF DIFFERENT BOUNDARY CONDITIONS FOR CFT PILE IN MEDIUM CLAY	130
TABLE 4-10- COMPRESSION TESTS ON FIRST POUR SPECIMENS (MARCH 7 TH 2011).....	131
TABLE 4-11- COMPRESSION TESTS ON FIRST POUR SPECIMENS (MARCH 7 TH 2011).....	133
TABLE 4-12- COMPRESSION TESTS ON SECOND POUR SPECIMENS (MARCH 10 TH 2011).....	134
TABLE 4-13- COMPRESSION TESTS ON THIRD POUR SPECIMENS (MARCH 15 TH 2011).....	134
TABLE 4-14- MIX RATIOS FOR 2” CUBE SPECIMENS.....	135
TABLE 4-15- COMPRESSION TESTS ON ELASTOMERIC CONCRETE SPECIMENS.....	137
TABLE 4-16- COMPRESSION TESTS CONDUCTED ON FIBERLAST SPECIMEN	141
TABLE 5-1- RANGE OF PARAMETERS IN THE PARAMETRIC STUDY	159
TABLE 5-2- MAXIMUM PRINCIPAL PLASTIC STRAIN IN DIFFERENT ELEMENTS	173
TABLE 5-3- REPRESENTATIVE VALUES OF C_U AND E_{50}	178
TABLE 5-4- COMPACTNESS OF HP SECTIONS	186
TABLE A1- ASSUMED INFORMATION IN THE MOMENT-CURVATURE ANALYSIS	203
TABLE C1- STRATEGY TABLE FOR ABUTMENT IN JOINTLESS BRIDGES- STRAIGHT BRIDGES	231
TABLE C2- STRATEGY TABLE FOR FOUNDATION AT ABUTMENT IN JOINTLESS BRIDGES- STRAIGHT BRIDGES	232
TABLE C3- STRATEGY TABLE FOR CONNECTION BETWEEN PIERS AND SUPERSTRUCTURE IN JOINTLESS BRIDGES- STRAIGHT BRIDGES.....	233
TABLE C4- REQUIREMENTS FOR USING METHOD A.....	234
TABLE C5- APPROXIMATE MAGNITUDES OF MOVEMENTS REQUIRED TO REACH EXTREME SOIL PRESSURE CONDITION (CLOUGH AND DUNCAN, 1991).....	238
TABLE C6- PROCEDURE A TEMPERATURE CHANGES (TABLE 3.12.2.1-1 OF AASHTO).....	239
TABLE C7- BASIS FOR TEMPERATURE GRADIENTS (TABLE 3.12.3-1 FROM AASHTO).....	243
TABLE C8 - LOAD COMBINATIONS AND LOAD FACTORS (FROM TABLE 3.4.1-1 IN AASHTO LRFD)	251

TABLE C9- LOAD FACTORS FOR PERMANENT LOADS, γ_p (FROM TABLE 3.4.1-2 IN AASHTO LRFD)	251
TABLE C10- CONCRETE PARAMETERS (OESTERLE, TABATABAI, LAWSON, REFAL, VOLZ AND SCANLON, 2005).....	255
TABLE C11- SUMMARY OF RECOMMENDED MAGNIFICATION FACTORS.....	257
TABLE C12- RECOMMENDED STEEL PARAMETERS (OESTERLE, TABATABAI, LAWSON, REFAL, VOLZ AND SCANLON, 2005).....	258
TABLE C13- SUMMARY OF STRENGTH AND SERVICEABILITY LIMIT STATES THAT MUST BE CONSIDERED IN THE DESIGN OF PILE FOUNDATIONS (BARKER, ET AL. 1991).....	291
TABLE C14- COMPACTNESS OF HP SECTIONS	295
TABLE C15- PILE P-MULTIPLIERS, P_m FOR MULTIPLE ROW SHADING (TABLE 10.7.2.4-1 FROM AASHTO).298	

Chapter 1

Introduction

1.1. Background and Problem Statement

Jointless bridges have been used for more than 50 years and have been proven to have several advantages over regular jointed bridges including lower initial and maintenance costs, longer service life, improved riding quality, easier and faster construction, and added redundancy.

Jointless bridges have significant cost savings compared to regular jointed bridges, which includes construction costs as well as maintenance costs. The important differences between an integral abutment and a standard jointed deck include a lack of expansion joint, no bearings, reducing the number of required piles, reducing the number of concrete pours, and inclusion of a sleeper slab. Taking these into consideration, the cost savings are readily apparent.

Typically, expansion joints have shorter service life compared to other components of a bridge. Live loads (traffic load), environmental loads (sunshine, temperature changes), and incorrect installation are the main causes of expansion joint deterioration. All of these factors affect the main role of an expansion joint, which is sealing of the deck. As a result, deteriorated joint leaks and lets water and deicers to pass through the deck and reach the girders, and substructure elements. This problem has been the source of major deterioration of some bridge elements and can easily reduce the service life a bridge. Because of all the problems with the use of expansion joints, jointless

construction is becoming more popular. Despite all these great advantages, there is discrepancy in the design of jointless bridges. Technically, the design of jointless bridges has been the matter of engineering judgment and intuition rather than a scientific approach.

1.1.1. Problem Statement

The maximum length of jointless bridges is limited because of uncertainties in the soil-structure interaction problem as well as the limited capacity of piles to accommodate the lateral displacement. The maximum length of jointless bridges is completely based on DOT's level of practice rather than a scientific approach. Different agencies have pushed their limits based on their success with their previous projects. This fact is confirmed by different surveys conducted on jointless bridges. The responses of different agencies to these surveys revealed that each state has its own limitations.

On the other hands, there have always been controversies about the orientation of piling system supporting jointless bridges. The discrepancy in the pile design among different agencies is obvious from different surveys. Most of the respondents have been orienting their pile to bend along the weak axis, while the rest allow for strong axis bending.

Another problem in design of piles supporting jointless bridges is the calculations related to global buckling of the embedded piles. The lateral support provided by the surrounding soil, complicates the estimation of buckling capacity of the embedded piles.

In current design method, the buckling capacity is estimated by assuming linear soil response (Abendroth, Greimann and Ebner, 1989).

1.2. Background

As the movements of the superstructure are directly transferred to substructure in jointless bridges, the foundation supporting these structures should be flexible to reduce the induced forces and moments due to soil-structure interaction. Three methods are generally used to reduce the stiffness of piling system in jointless bridges.

In the first method, piles are oriented for weak axis bending. Although relatively lower stiffness is provided with this strategy, however it is shown that the pile's displacement capacity will be reduced.

Another method is using pre-drilled holes. While the top 10-20 ft portion of the surrounding soil plays the most important role in the behavior of the embedded pile, this portion of the soil can be replaced by softer soil. In this method, holes are drilled at pile locations to the depth of 10-15 ft. Then the piles are driven, and finally the hole is filled with non-compact granular soil.

The best method, that is much more effective than all of the above strategies, is to let pile/cap connection to act as pinned. In this method the pile deflects in single curvature rather than double, and can effectively reduce the stiffness of piling system. Further, the displacement capacity of the pile can be increased up to four times.

1.3. Objectives of the Research

The main objective of this research was to expand the application of jointless construction to longer bridge lengths. After extensive literature search on jointless bridges it was concluded that the best strategy in expanding the length of jointless bridges is to increase the displacement capacity of their supporting piles.

The other objective in this study was to provide a robust design method for the piles supporting jointless bridges, as there are controversies on available design methods. Some states design the piles in jointless bridges just for axial load and completely ignore their lateral movement, while the rest attempt to consider the lateral response from the soil using simplified assumptions; and important criteria, including local stability and fatigue are often ignored.

1.4. Research Approach

After solving the governing differential equation of the pile, it was observed that boundary conditions play an important role in the response of the embedded pile to lateral movement. Further, finite element modeling of the prestressed pile tested in Tennessee showed that pinned pile/cap connection can increase the pile's lateral displacement capacity.

To provide rotational capacity at the pile/cap connection, a detail was proposed, which includes encasing the embedded portion of the pile with elastomeric material. Compression tests on two different soft materials were conducted and an elastomeric material was chosen because of its great behavior at relatively larger strains.

Experimental study was conducted on two specimens representing two different pile/cap connections. The first specimen included the current practice of using a relatively fixed condition. The second specimen, however, included a relatively pinned condition provided by encasing the pile head with elastomeric material. Test results show that the proposed concept is valid and much larger displacement capacity can be obtained.

In parallel, the design of piles was conducted using the nonlinear pushover analyses in SAP2000. A parametric study was carried out on important parameters involved in the problem including orientation of the pile, soil properties, boundary conditions, and axial load level.

Chapter 2 summarizes the available data related to design of jointless bridges. First, AASHTO design provision related to jointless bridges are presented, followed by the summary of different surveys on jointless bridges. Then the design provisions proposed by CTL are summarized. Finally, the field tests on jointless bridges and single piles are presented.

Soil-pile and soil-abutment interaction is discussed in Chapter 3. First, the derivation of the governing differential equation of the pile is presented, followed by a description of the p-y method.

Experimental studies including the tests on CFT piles and material tests are discussed in Chapter 4.

Chapter 5 presents the analytical studies carried out. First, the calculation of buckling load for embedded piles is discussed, followed by finite element modeling of the

proposed detail. Design of piles for fatigue and strength is also presented in this chapter. Further, the comprehensive design method for piles is discussed.

Conclusions of this study as well as recommendations for further research are presented in Chapter 6.

A comprehensive design guide for jointless bridges is also developed that partially includes the results of this study as well as other ongoing researches from the SHRP2-R19A project. This guide can be found in Appendix C.

Chapter 2

Analysis of the Available Data

2.1. Introduction

Use of expansion joints will continue for some forcible time. However, there is an agreement that there is a need to provide designers with complete guidelines needed to design and construct jointless bridges. The objective of this research topic is two folded; first to provide the state of the art with respect to design and construction of the jointless bridges and second, to identify the knowledge gap that currently exists to efficiently utilize jointless bridges. The knowledge gap includes finding ways of using jointless bridges for longer span bridges. Additionally, one of the objectives of this research topic is to develop a design guide, which could provide the designers with complete design and construction steps for effective use of jointless bridges in practice.

Sections 2.2.1 and 2.2.2 provide the summary of the design and construction provisions practiced by various DOTs and stated in the AASHTO LRFD Bridge Design Specification (2010). The information related to DOT practices are collected from DOTs web sites and four different published surveys conducted by different research projects.

Section 2.2.3 provides summary of research studies conducted by Construction Technologies (CTL) in early 2000s on jointless bridges. The CTL study is the most comprehensive investigation reported. The major shortcoming of the CTL research study appears to be the use of simple numerical models to develop the suggested design

provisions and further, there is a lack of comparison between some of the suggested design provisions and experimental data.

Section 2.3 provides a summary of other recent research studies in the area of jointless bridges. Extensive literature search is summarized in this chapter for field tests on jointless bridges as well as single pile tests.

2.2. Synopsis of Published Literature

2.2.1. AASHTO Provisions

Following articles are listed in AASHTO LRFD Bridge Design specification and related to jointless bridges.

2.2.1.1. Article 11.6.1.3 (*Integral Abutments*)

“Integral abutments shall be designed to resist and/or absorb creep, shrinkage and thermal deformations of the superstructure. Deformations are discussed in Article 3.12. Movement calculations shall consider temperature, creep, and long-term prestress shortening in determining potential movements of abutments. Maximum span lengths, design considerations, details should comply with recommendations outlined in FHWA Technical Advisory T 5140.13 (1980), except where substantial local experience indicates otherwise. To avoid water intrusion behind the abutment, the approach slab should be connected directly to the abutment (not to wingwalls), and appropriate provisions should be made to provide for drainage of any entrapped water.”

This article only mentions that superimposed deformations such as creep, shrinkage, thermal deformations ... should be considered.

2.2.1.2. Article 3.12.2 (Uniform Temperature Change)

In this article, two procedures, to calculate longitudinal bridge movements, by uniform temperature changes, are presented.

The first procedure which is applicable to all types of bridges recommends using maximum and minimum design temperature values from the following table. In this method, if the number of freezing days is less than 14 days per year, the climate is considered moderate; otherwise it is cold. Freezing day is defined as a day in which the average temperature is less than 32°F.

Table 2-1- Procedure A Temperature Ranges (Table 3.12.2.1-1 from AASHTO)

Climate	Steel / Aluminum	Concrete	Wood
Moderate	0° to 120°F	10° to 80°F	10° to 75°F
Cold	-30° to 120°F	0° to 80°F	0° to 75°F

In the second procedure which is a calibrated method for concrete and steel girder bridges with concrete decks, the corresponding maximum and minimum design temperatures are extracted from the contour maps provided for steel and concrete girder bridges (Figures 3.12.2.2-1 to 3.12.2.2-4). As an example, Figure 2-1 depicts the contour map for maximum design temperature for concrete girder bridge with concrete deck.

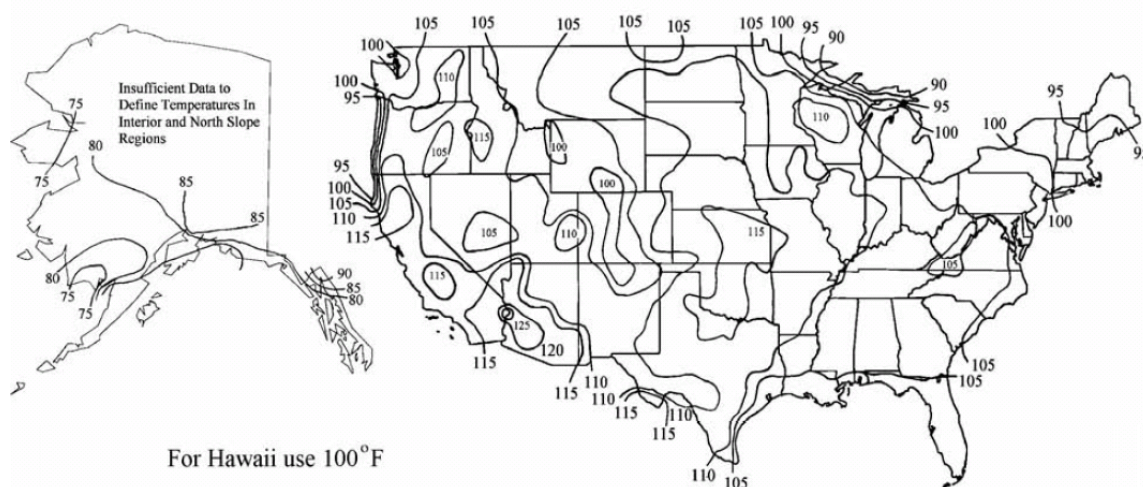


Figure 2-1- Contour Maps for $T_{MaxDesign}$ for Concrete Girder Bridges with Concrete Decks (Figure 3.12.2.2-1 from AASHTO)

After the maximum and minimum design temperatures are defined, the design thermal movement is calculated in equation 3.12.2.3-1 as follows:

$$\Delta_T = \alpha L (T_{MaxDesign} - T_{MinDesign}) \quad \text{Eq. 1}$$

Where,

L = expansion length (in.)

α = coefficient of thermal expansion (in./in./°F)

2.2.1.3. Article 3.12.3 (Temperature Gradient)

In this article the effect of temperature gradient in the cross section is considered. For this purpose, the country is divided into 4 zones as illustrated in Figure 2-2. Positive temperature values shall be taken from Table 2-2. Negative temperature values shall be obtained by multiplying the values from the same table by -0.3 for plain concrete decks and by -0.2 for decks with asphalt overlay.



Figure 2-2- Solar Radiation Zones for the United States. (Figure 3.12.3-1 from AASHTO)

Table 2-2- Basis for Temperature Gradients (Table 3.12.3-1 from AASHTO)

Zone	T_1 (°F)	T_2 (°F)
1	54	14
2	46	12
3	41	11
4	38	9

The profile of the temperature in steel and concrete girder bridges may be taken as shown in Figure 2-3. Dimension A in this figure shall be taken as:

- (12.0) in for concrete superstructures deeper than 16 in.
- (Depth-4.0) for concrete superstructures shallower than 16 in.
- (12.0) in. for steel superstructures. Also, t is equal to concrete deck.

This article also specifies that the value T_3 shall be taken zero, unless a specific field study is carried out to determine this value. In this case T_3 should not exceed 5°F.

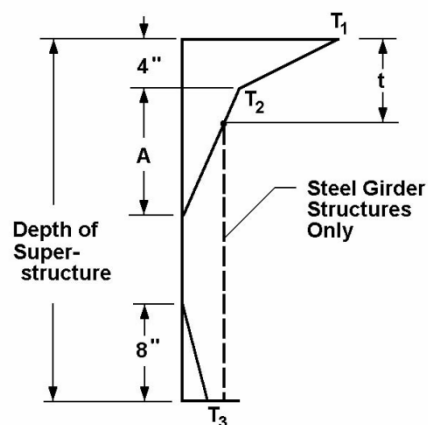


Figure 2-3- Positive Vertical Temperature Gradient in Concrete and Steel Superstructures (Figure 3.12.3-2 from AASHTO)

Article 4.6.6 specifies that when considering temperature gradient in the section profile, the analysis should consider axial extension, flexural deformation, and internal stresses. The response of the structure to temperature gradient can be divided into three parts as follows:

Axial Expansion: This component is due to the uniform part of the temperature gradient and can be calculated as (equation C4.6.6-1 from AASHTO):

$$T_{UG} = \frac{1}{A_c} \iint T_G dw.dz \quad \text{Eq. 2}$$

Where,

T_G = temperature gradient ($\Delta^\circ\text{F}$)

T_{UG} = temperature averaged across the cross-section ($^\circ\text{F}$)

A_c = cross-section area—transformed for steel beams (in^2)

w = width of element in cross-section (in)

z = vertical distance from center of gravity of cross-section (in)

Then the corresponding uniform axial strain shall be taken as (equation C4.6.6-2 from AASHTO):

$$\varepsilon_u = \alpha(T_{UG} + T_U) \quad \text{Eq. 3}$$

Where,

α = coefficient of thermal expansion (in./in./°F)

T_U = uniform specified temperature (°F)

Flexural Deformation: Assuming that plane sections remain plane, a curvature is imposed to the section to accommodate the temperature gradient. The rotation per unit length corresponding to this curvature may be determined as

$$\phi = \frac{\alpha}{I_c} \iint T_G z dw \cdot dz = \frac{1}{R} \quad \text{Eq. 4}$$

Where,

I_c = inertia of cross-section—transformed for steel beams (in⁴)

R = radius of curvature (ft)

If the structure is structurally unrestrained, no external force is imposed due to this deformation.

Internal Stresses: stresses in addition to those corresponding to the restrained axial expansion and/or rotation may be calculated as:

$$\sigma_E = E[\alpha T_G - \alpha T_{UG} - \phi z] \quad \text{Eq. 5}$$

Where,

$E =$ modulus of elasticity (ksi)

2.2.1.4. Article 5.4.2.3.2 (Creep)

Based on this article creep coefficient may be taken as (equation 5.4.2.3.2-1 from AASHTO)

$$\Psi(t, t_i) = 1.9k_s k_{hc} k_f k_{td} t_i^{-0.118} \quad \text{Eq. 6}$$

In which,

$$k_s = 1.45 - 0.13 \frac{V}{S} \quad \text{Eq. 7}$$

$$k_{hc} = 1.56 - 0.008H \quad \text{Eq. 8}$$

$$k_f = \frac{5}{1 + f'_{ci}} \quad \text{Eq. 9}$$

$$k_{td} = \left(\frac{t}{61 - 4f'_{ci} + t} \right) \quad \text{Eq. 10}$$

Where,

$H =$ relative humidity (%). In the absence of better information, H may be taken from Figure 2-4.

$k_s =$ factor for the effect of the volume-to-surface ratio of the component

$k_f =$ factor for the effect of concrete strength

$k_{hc} =$ humidity factor for creep

$k_{td} =$ time development factor

$t =$ maturity of concrete (day), defined as age of concrete between time of loading for creep calculations, or end of curing for shrinkage calculations, and time being considered for analysis of creep or shrinkage effects

$t_i =$ age of concrete at time of load application (day)

$V/S =$ volume-to-surface ratio (in.)

$f'_{ci} =$ specified compressive strength of concrete at time of pre-stressing for pre-tensioned members and at time of initial loading for non-prestressed members. If concrete age at time of initial loading is unknown at design time, f'_{ci} may be taken as 0.80 f'_c (ksi).

2.2.1.5. Article 5.4.2.3.3 (Shrinkage)

For concrete elements shrinkage strain ϵ_{sh} may be calculated as (equation 5.4.2.3.3-1 from AASHTO)

$$\epsilon_{sh} = k_s k_{hs} k_f k_{td} 0.48 \times 10^{-3} \quad \text{Eq. 11}$$

In which,

$$k_{hs} = (2.00 - 0.014H) \quad \text{Eq. 12}$$

Where,

$k_{hs} =$ Humidity factor for Shrinkage

This article states that if the concrete is exposed to drying before 5 days of curing have elapsed, the shrinkage as determined in Eq. 11 should be increased by 20 percent.

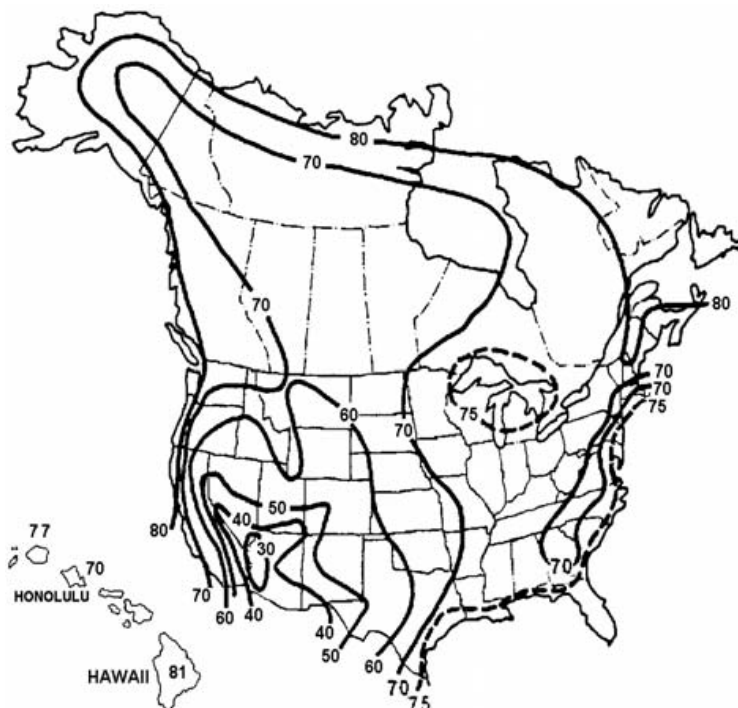


Figure 2-4- Annual Average Ambient Relative Humidity in Percent. (Figure 5.4.2.3.3-1 from AASHTO)

2.2.1.6. Article 10.7.2.4 (Horizontal Pile Foundation Movement)

This article specifies that if p-y method of analysis is used when evaluating pile group horizontal movement, the values of p should be multiplied by p-multiplier values, P_m from Table 2-3 to account for group effect.

Table 2-3- Pile P-Multipliers, P_m for Multiple Row Shading (Table 10.7.2.4-1 from AASHTO)

Pile CTC spacing (in the direction of loading)	p-Multiplier, p_m		
	Row 1	Row 2	Row 3 and higher
3B	0.7	0.5	0.35
5B	1.0	0.85	0.7

Figure 2-5 defines the loading direction and spacing. As In jointless bridges usually the bottom detail in the figure is the case of loading, a group reduction factor of less than 1.0 should only be used if the pile spacing is 5B or less.

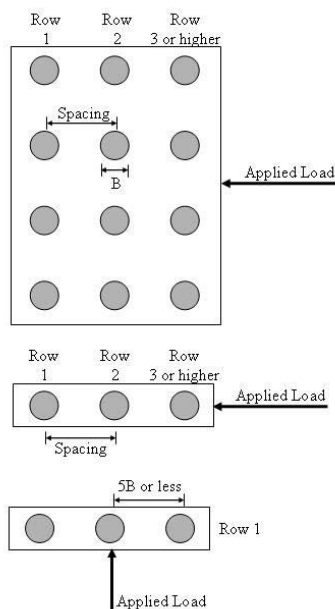


Figure 2-5- Definition of Loading Direction and Spacing for Group Effects (Figure 10.7.2.4-1 from AASHTO)

2.2.2. DOT Practices

Several surveys have been conducted to investigate the state of the practice of DOT's in the case of jointless bridges (Kunin and Alampalli, 1999, Haj-Najib, 2002, Maruri and Petro, 2005)

2.2.2.1. 1999 Survey (NYSDOT)

In the survey supported by New York State Department of Transportation the following conclusions were made: (Kunin and Alampalli, 1999)

- At least 30 agencies are building integral bridges.
- The performance of these bridges is rated as “good” or “excellent”.
- Design practices and assumptions made regarding thermal limits, soil-structure interaction, and pile design vary significantly among the responding agencies.

Basically, most of these assumptions are based on previous local experience of the agencies with respect to integral bridges and are empirical in nature.

- The major difference regarding integral abutment bridge design is related to the method of resisting soil pressure.
- Although most agencies use passive soil pressure, but the distribution of this load varies.
- Steel HP Piles are frequently used, but other types of pile have also been used (cast-in-place and pipe piles)
- Two methods are used for design of approach slabs. In the first one, approach slab lies on a lip or corbel over the abutment, and in the other one it is either connected to the abutment or floats on the corbel. Flaws have been reported for both design methods. Approach slab has cracked at the far end when it is rigidly connected to the abutment. On the other hand, deterioration of the abutment concrete has been reported due to runoff coming through the joint, when the approach slab floats on the corbel.
- The differences between integral structures having steel or concrete girders are minor. The main differences are shrinkage happening in concrete and larger movement in steel girders.

2.2.2.2. 2002 Survey (University of Maryland)

In another survey conducted by University of Maryland, College Park (Haj-Najib, 2002) questionnaires have been sent to highway departments of all fifty states as well as many foreign agencies. Forty three departments of transportation and six foreign agencies

have responded to this survey. The followings are the summary of the responses and conclusions made:

- Of the responding agencies, only Alabama, Delaware, Florida, Mississippi, and Texas indicated that they were not using integral abutment bridges. On the other hand, Arizona had stopped using this system due to some problems.
- A high percentage of the respondents (about 40%) indicated that they don't calculate the pile stresses due to lateral movement.
- Most of the states assume the pile head is fixed (about 70%), while some assume a pinned condition (about 20%). Only one state assumes partial restraint for the pile head.
- Most of the respondents use the piles in the weak axis of bending (about 60%). On the other hand only few states orient the piles about their strong axis (about 10%) and the rest leave it to the designer.
- Some agencies indicated that integral abutment bridges outperform the conventional bridges in terms of durability, maintenance, and design efficiency.
- Tennessee and California have noted that integral abutment system provides redundancy and substantial reserve capacity to resist extreme loading.
- Integral abutments result in rapid, efficient, and economic construction, since fewer piles are placed in one single row and the entire diaphragm/backwall can be cast simultaneously.

- In spite of great success with integral abutment bridges for most of the respondents, two major issues were observed; Settlement of approach slab, and damage to the approach embankment and backfill as a result of water intrusion between the abutment and approach slab.

2.2.2.3. 2004 Survey (FHWA)

In 1995 and 1996 a survey and a workshop on integral abutment bridges was conducted by FHWA in conjunction with the Constructed Facilities Center (CFC) at West Virginia University (WVU). A similar questionnaire was sent to highway departments of all fifty states in 2004 (Maruri and Petro, 2005). Thirty nine states responded to this survey by 2005. The results of this survey revealed that the design practices and details vary significantly from state to state. The fields with non-uniformity in design and detailing were identified as

- Criteria used for selection of integral abutments
- Forces and pressures used to design integral abutment and integral abutment piles
- Orientation of integral abutment piles
- Design of integral abutments with curved bridges
- Detailing of approach slab at bridge interface and approach fill interface

As a result, development of guidelines and additional information for design and detailing of the abovementioned criteria was recommended.

2.2.2.4. DOT Design Guides Regarding Integral Abutment Bridges

Results of past surveys clearly revealed that there is inconsistency in the design philosophy and detailing of integral abutment bridges. The main reason for this variation is the experience of agencies with the performance of this system in practice. Most of the states have changed their details and limits based on their previous experience. If a good performance has been observed the limits have been pushed a little. As a result, the design of these systems is basically an empirical approach rather than a rational procedure. One of the main problems regarding the design of jointless bridges is the soil structure interaction which makes the analysis a little different than conventional bridges. Besides, creep and shrinkage affect the structure due to its integrity and continuity with the substructure. On the other hand, lack of an analysis tool which can incorporate all mentioned parameters is another issue. All these have led to the complexity of the analysis of the integral abutment bridges.

As a part on this study, the status of DOT's design guides with respect to integral abutment bridges has been studied. Online search conducted to find bridge design manual or any specific guide for design of jointless bridges in website of highway departments of all fifty states. 21 states found to have at least minimal consideration or limitations about jointless bridges (Figure 2-6). As shown in the figure, except for South Carolina, all other states with design recommendations for jointless bridges are in the cold region. The summary of the findings is presented in Table 2-4.

2.2.3. CTL Report

An extensive research project has been performed by Construction Technology Laboratories (CTL) on Jointless Bridges (Oesterlie, Tabatabai, Lawson, Refai, Volz and Scanlon, 2002). The main objectives of this research project included:

- Determination of the criteria that limit the length of jointless bridges
- Identifying the effect of longitudinal length change on stresses developed in the superstructure elements.
- Determination of the significance of continuity moments from temperature gradient, creep, and shrinkage
- Development of the design criteria for pier
- Determination of the effects of different construction sequences
- Identifying the limitations and special considerations for skewed and curved bridges
- Development of more uniform design criteria and methods for new and retrofitted jointless bridges

The CTL study focuses on investigating following six areas:

- Abutment Soil-Structure Interaction
- Pier Behavior
- Longitudinal Bridge Movement
- Secondary Continuity Forces

- Skewed Bridge Behavior
- Construction Sequences

2.2.3.1. Design Recommendation

The following major conclusions and design recommendations were made from this research.

2.2.3.1.1. Maximum Longitudinal Movement

The major step in the design of jointless bridges involves calculating longitudinal movement due to temperature changes. CTL report states that the design temperatures proposed by AASHTO LRFD are too conservative for steel bridges and not conservative for concrete bridges. AASHTO LRFD indicates that the setting temperature should be taken as the actual air temperature averaged over the 24-hour period immediately preceding the setting event. For jointless bridges, the setting event occurs when the longitudinal continuity is established by tying the bridge deck to the integral abutments. A procedure is recommended to determine end movements in the longitudinal direction while accounting for the uncertainty of calculations (Monte Carlo study)

$$\varepsilon_{th} = \alpha \Delta T \quad \text{Eq. 13}$$

Coefficient of thermal expansion for concrete can be calculated base on Emmanuel and Hulsey model. If prestressed concrete girders are used, Eq. 14 and Eq. 15 shall be used to calculate strains related to shrinkage and creep.

$$\varepsilon_{sh} = \varepsilon_{sh,girder} + \frac{\varepsilon_{sh,deck} - \varepsilon_{sh,girder}}{1 + \frac{(EA)_{girder}}{(EA)_{deck}}} \quad \text{Eq. 14}$$

$$\varepsilon_{cr} = \varepsilon_{cr,girder} \left[\frac{1}{1 + \frac{(EA)_{girder}}{(EA)_{deck}}} \right] \quad \text{Eq. 15}$$

$$\Delta l = \Gamma \varepsilon_{total} l$$

$$\text{Expansion: } \varepsilon_{total} = \varepsilon_{th} - \varepsilon_{sh} - \varepsilon_{cr} \quad \text{Eq. 16}$$

$$\text{Contraction: } \varepsilon_{total} = -\varepsilon_{th} - \varepsilon_{sh} - \varepsilon_{cr}$$

2.2.3.1.2. Abutment Piles

In the design procedure presented by Abendroth et al. (1989) the soil-pile interaction problem is simplified by replacing the soil-pile system with an equivalent cantilever in the air. l_c is a critical depth below which lateral displacements and bending moments are considered to be insignificant.

$$l_c = 4.4 \sqrt{\frac{EI}{k_h}} \quad \text{Eq. 17}$$

Where,

EI : flexural stiffness of the pile

k_h : lateral stiffness of the soil (force/length squared)

Table 2-5- The Modulus of Sub-grade Reaction for Different Soil Types

Soil Type		K_h (kips/ft ²)
Clay	Soft	Min(72 or 58x*)
	Stiff	Min(580 or 190+41x)
	Very Stiff	Min(2200 or 750+610x)
Sand	Loose	8.0 x
	Medium	27x
	Dense	72x

*x = soil depth (ft)

Once the equivalent lengths have been established, the pile can be checked as a structural member using either elastic analysis (Alternative 1) or inelastic analysis (Alternative 2).

Three limit states are provided for design piles. These are Strength, Ductility and Stability limit states.

2.2.3.1.2.1. Elastic Analysis (Alternative 1)

The moment developed at the top of the pile because of displacement Δ is given by:

$$M = \frac{D_i \cdot EI \cdot \Delta}{L^2} \quad \text{Eq. 18}$$

Where,

$$D_i = 6 \text{ for fixed end}$$

$$D_i = 3 \text{ for pinned end}$$

$$L = \text{total length of equivalent cantilever for moment} = l_e + l_u$$

The pile can be checked for combined axial load and moment using the following interaction equations and the appropriate equivalent cantilever length for buckling:

$$\frac{P}{P_{cr}} + \frac{C_m M}{M_p \left(1 - \frac{P}{P_e}\right)} \leq 1 \quad \text{Eq. 19}$$

$$\frac{P}{P_y} + \frac{M}{M_p} \leq 1 \quad \text{Eq. 20}$$

Where,

$P =$ vertical load applied to pile head

$P_{cr} =$ critical buckling load

$P_e =$ Euler elastic buckling load

$P_y =$ yield load

$C_m =$ moment gradient coefficient = 0.85

$M =$ bending moment applied to pile head

$M_p =$ plastic moment strength of pile

$A =$ pile area

For elastic analysis, the critical buckling load P_{cr} is equal to the Euler buckling load given as:

$$P_{cr} = P_e = \frac{\pi^2 EA}{\left(\frac{kl}{r}\right)^2} \quad \text{Eq. 21}$$

2.2.3.1.2.2. *Inelastic Analysis (Alternative 2)*

In this approach, yielding is permitted and a check is made on the ductility capacity of the pile. This method is only recommended for steel H-piles or CFT piles. For inelastic analysis, the critical buckling load P_{cr} is given as:

$$P_{cr} = F_y A \left[1 - \frac{F_y}{4\pi^2 E} \left(\frac{kl}{r}\right)^2 \right] \quad \text{Eq. 22}$$

Where,

$F_y =$ yield stress of the pile

The ductility is satisfied if:

$$\Delta \leq \Delta_p (D_3 + 2.25C_i) \quad \text{Eq. 23}$$

Where,

$$\Delta_p = \text{displacement corresponding to formation of plastic hinge} = \frac{M_p L^2}{D_i EI}$$

$D_3 =$ 0.6 for fixed end, 1.0 for pinned end

$D_i =$ 6 for fixed end, 3 for pinned end

$C_i =$ rotation capacity reduction factor as defined below

$$M_p = F_y Z$$

$Z =$ plastic section modulus

$EI =$ flexural rigidity

For the H-piles:

$$C_i = \begin{cases} 1 & \text{for compact section} \left(\frac{b_f}{2t_f} \leq \frac{65}{\sqrt{F_y}} \right) \\ \frac{19}{6} - \frac{b_f \sqrt{F_y}}{60t_f} & \text{for} \left(\frac{65}{\sqrt{F_y}} < \frac{b_f}{2t_f} < \frac{95}{\sqrt{F_y}} \right) \end{cases}$$

$$= 0 \text{ for non-compact section } \left(\frac{b_f}{2t_f} \geq \frac{95}{\sqrt{F_y}} \right)$$

Where b_f and t_f are the width and the thickness of the flange, respectively.

For concrete-filled pipe pile:

$$C_i = 1.0 \text{ with } \frac{h}{t} \leq 39$$

Where,

$h =$ outside diameter of the pipe

$t =$ wall thickness

Tests show that, when $\frac{h}{t}$ was larger than 39 the maximum load was determined by local buckling of the steel tube. No recommendations are provided for this case because of lack of test data.

To provide a margin of safety against reaching the ductility limit, M_p is replaced by $M_b = F_b S$ in which F_b is the allowable stress in the pile and S is the elastic section modulus.

2.2.3.1.3. Load Transfer to Soil

In addition to structural capacity, the pile should be checked for its capacity to transfer load to the supporting soil.

2.2.3.1.4. Pile-to-Pile Cap Connection

The pile-to-pile-cap connection should develop the moment capacity of the pile and shear associated with the longitudinal displacement of the pile cap.

2.2.3.1.5. Abutment Wall

Passive soil pressure is developed in the soil behind the wall and moment and shear are developed at the top of the pile because of the bending of the pile. The maximum passive pressure force, P_p is calculated as

$$P_p = \frac{1}{2} K_p \gamma H^2 \quad \text{Eq. 24}$$

Where,

K_p = the passive pressure coefficient

It should be noted that K_p is not necessarily the maximum K_p associated with full passive pressure. It is recommended that K_p be determined based on the results of research by Clough and Duncan (1991).

Literature review on current practice on the backfill revealed that there are two philosophies for the degree of compaction for the backfill soil adjacent to the abutment. The first approach recommends using loose granular backfill to minimize passive pressure while the other approach recommends using highly compacted backfill to minimize the settlement of the approach slab. Tests on large scale abutments indicated that even with 97% relative compaction voids would still develop under the approach slab. Therefore, compaction of the backfill does not appear to be an advantage.

2.2.3.1.6. Abutment Supported on Spread Footing

Although integral abutment bridges are generally supported on a single row of flexible piles, there are situations where spread footing is used such as when rock or competent soil is close to the surface. Two approaches to design spread footing are proposed

Use relatively shallow abutment for use when rock is very close to the surface or when spread footings are used on competent soil close to the surface. In this approach the end movements caused by thermal, creep, and shrinkage strains are accommodated by sliding of the footing.

When possible, use deeper abutment walls to accommodate end movement by bending in the abutment wall.

2.2.3.1.7. Full-Height Abutments

This type of abutment is used when setting the abutment on the embankment is either impractical or not economical. The design recommendations for full-height abutment are similar to those proposed for deep abutment on spread footing; however in this case full-height retaining walls are required on the sides of the abutment. U-type wingwalls can't be cast integrally with the full-height abutment since they increase the stiffness of the abutment. One option in this case would be use of semi-integral abutment in which the bridge superstructure is built integrally with an end diaphragm and approach slab. However, the end diaphragm rests on elastomeric bearings on top of the abutment.

2.3. Synopsis of other Research Activities

2.3.1. Soil-Structure Interaction

One of the major uncertainties in the analysis of jointless bridges is the reaction of soil adjacent to the stub abutment backwall and piles (Faraji, Ting, Crovo and Ernst, 2001). The magnitude of forces generated during expansion and contraction of the bridge structure can become substantial and directly affect the overall behavior of the structure. Technically, soil-structure interaction in jointless bridges is of great importance and still there is not a unified method to handle this problem. For instance, to account for the effect of soil-pile interaction Abendroth et al. (1989) recommended an equivalent length of the pile while ignoring the soil surrounding it, but another approach is to model the soil around the pile with winker springs using p-y curves. Even in the latter case, there are different approaches for calculation of the spring stiffnesses.

2.3.1.1. Soil-Abutment Interaction

The amount of pressure of the soil behind the abutment wall and its distribution is nonlinear and depends on wall displacement, soil type, depth, piles stiffness, and also direction of the displacement (Faraji, Ting, Crovo and Ernst, 2001).

As a wall moves toward the backfill passive pressure, and when it moves away from that active pressure is generated. Studies show that a minimum movement is required to reach these extremes. Clough and Duncan (1991) Investigated this effect and concluded that these values are proportional to the height of the wall. They also concluded that the movement required to reach the maximum passive pressure is of the order of ten times as

large as the movement required to reach the minimum soil pressure. The results of analyses also revealed that the movement required to reach the extreme pressures are larger for loose soils than for dense soils (Figure 2-7 and Figure 2-8).

NCHRP Report 343 (Barker, Duncan, Rojiani, Ooi and Tan, 1991) design manual recommends force-deflection design curves based on the abovementioned research by Clough and Duncan (1991). Many researchers have incorporated this approach to model soil-abutment interaction using Winkler springs behind the abutment. The stiffnesses of the springs behind the abutment wall are nonlinear depending on the type of the soil (Faraji, Ting, Crovo and Ernst, 2001) (Pugasap, Kim and Laman, 2009) (Basu and Knickerbocker, 2005).

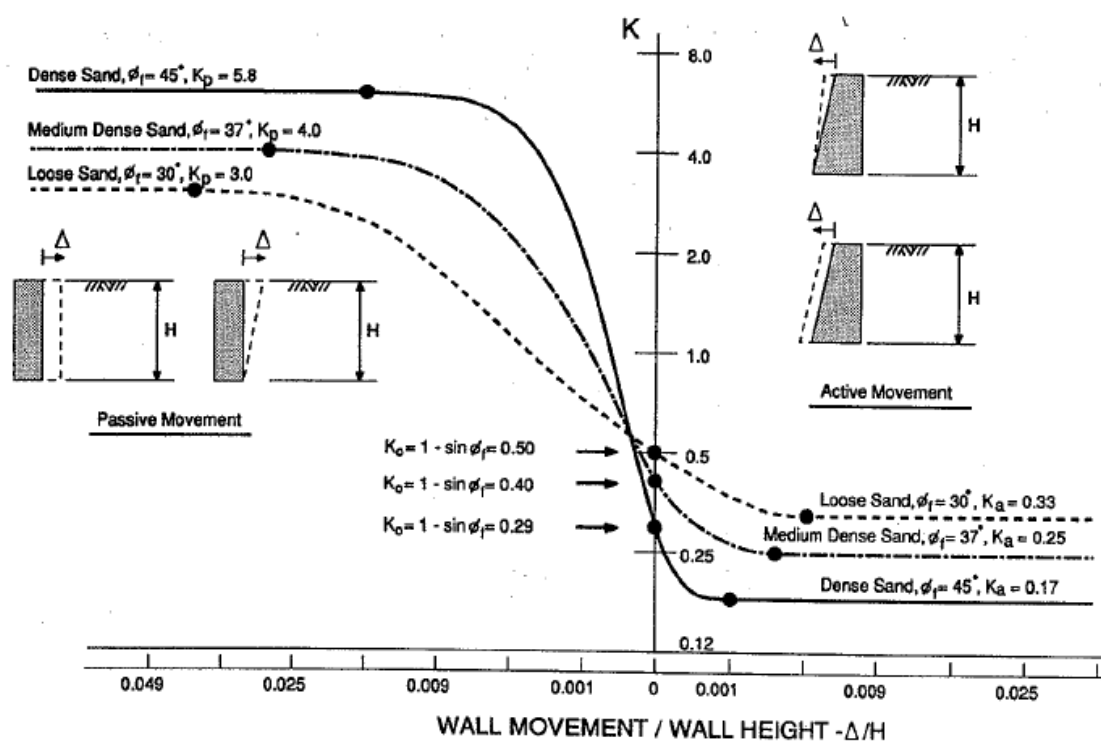


Figure 2-7- Relationship between wall movement and earth pressure. (Clough and Duncan, 1991)

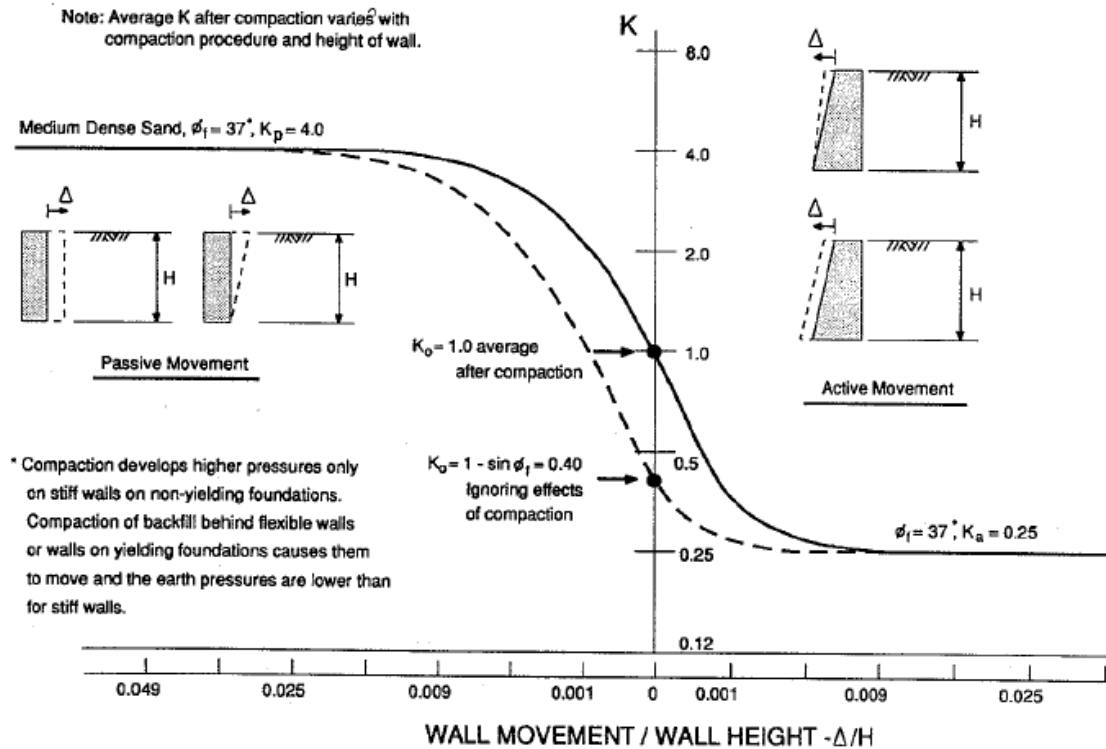


Figure 2-8- Relationship between wall movement and earth pressure for a wall with compacted backfill (Clough and Duncan, 1991)

Table 2-6- approximate magnitudes of movements required to reach extreme soil pressure condition (Clough and Duncan, 1991)

Type of Backfill	Values of $\Delta/H^{(a)}$	
	Active	Passive
Dense Sand	0.001	0.01
Medium-Dense Sand	0.002	0.02
Loose Sand	0.004	0.04
Compacted Silt	0.002	0.02
Compacted lean clay	0.01 ^(b)	0.05 ^(b)
Compacted fat clay	0.01 ^(b)	0.05 ^(b)

(a) Δ = movement of top of the wall required to reach extreme soil pressure, by tilting or lateral translation, H = height of the wall

(b) Under stress conditions close to the minimum active or maximum passive pressures, cohesive soils creep continually. The movement shown would produce temporary passive pressures. If pressures remain constant with time, the movements shown will increase. If movement remains constant, active pressures will increase time while passive pressures will decrease.

2.3.1.2. Soil-Pile Interaction

Soil-Pile interaction is generally more complex compared to soil-abutment interaction. Several methods have been used in the analysis and design of laterally loaded piles.

2.3.1.2.1. Limit-Equilibrium Method

This method was proposed by Broms (1956) and can be applied to find the ultimate lateral capacity of the pile, but soil-structure interaction at lesser loads is not addressed in this method.

2.3.1.2.2. Linear Elastic Method

Poulos and Davis (1980) presented the linear elastic model for the soil although the soil can't be categorized as linear elastic material.

2.3.1.2.3. Equivalent Cantilever Method

Equivalent cantilever method is proposed by Abendroth et al. (1989) and is a simple way to handle soil-structure interaction, however there is dispute on accuracy of this model. In this method the pile in the soil is replaced by a cantilever beam, fixed against rotation but free of soil. For a relatively large embedded pile, the equivalent length of the cantilever beam below which the lateral displacements are relatively small compared to head displacement is defined as:

$$l_c = 4\sqrt{\frac{EI}{k_h}} \quad \text{Eq. 25}$$

In the design method proposed by Abendroth et al. (1989) three design criteria are considered: (1) Horizontal stiffness of the soil and pile system; (2) maximum moment in the pile; and (3) elastic buckling load of the pile.

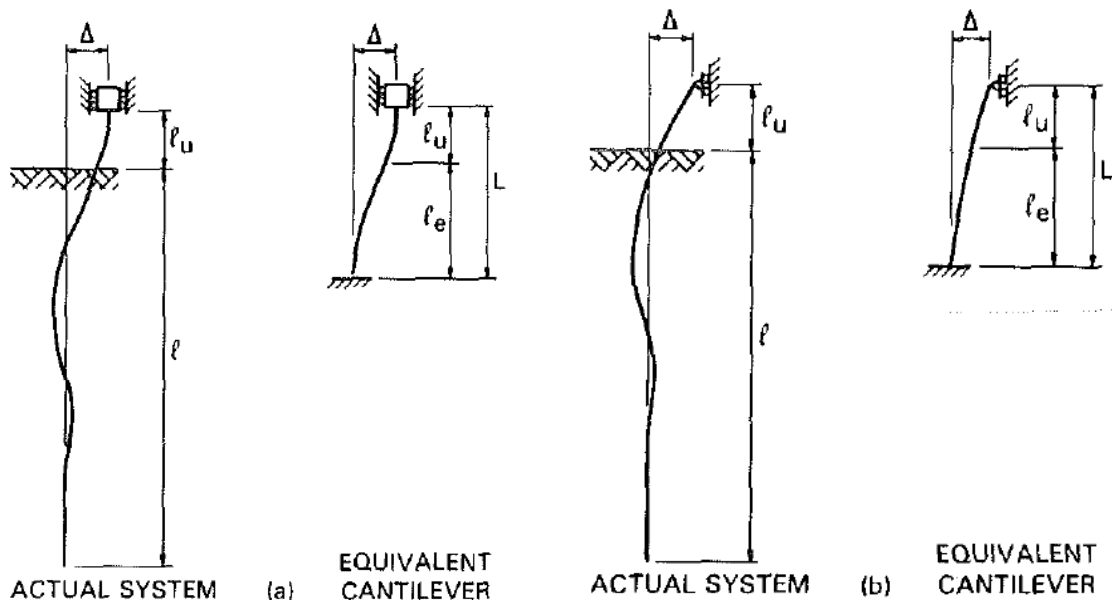


Figure 2-9- Cantilever Idealization of the Pile (a) Fixed Head (b) Free Head (Abendroth, Greimann and Ebner, 1989)

2.3.1.2.4. P-y Method

Starting 1950's extensive research studies were conducted on soil-pile interaction in which full scale tests on piles were carried out in different soil types (Matlock and Ripperger, 1958, Matlock, 1970, Reese, 1971, Reese, Cox and Koop, 1974, Reese, Cox and Koop, 1975). These studies were initially aimed to develop a rational method for the design of laterally loaded piles supporting offshore platforms. The main outcome of these research studies were development of p-y method representing the response of soil to lateral loading. This method is being used extensively and is included in publications of the Federal Highway Administration (FHWA) and also American Petroleum Institute (API, 1993).

Several software programs currently being used for the analysis of laterally loaded piles (such as LPILE, COM624P, FB-MultiPier) utilize this approach.

2.3.1.2.5. FEM Method

By rapid progress in computational capabilities of computers, FEM methods are being more widely used. In this method instead of using Winkler springs, the soil medium is modeled around the pile and failure models such as Mohr-Coulomb or Drucker-Prager ... are used to model nonlinear behavior of the soil (Trochanis, Bielak and Christiano, 1991, Khodair and Hassiotis, 2005, Miao, Goh, Wong and Teh, 2006).

2.3.2. Field Tests on Jointless Bridges

Thermal loading is probably the most evident loading on jointless bridges. Bridges expand and contract due to changes of temperature. Jointless bridges are directly affected by thermal changes and if not well designed large forces can be generated in the structure due to the integrity of the structure.

Table 2-7 summarizes the list of field studies in which the behavior of jointless bridges has been monitored during a period of time. In most of these studies the major loading addressed is thermal changes.

Table 2-7- List of Field Instrumented Jointless Bridges in the US

Bridge	Reference	State	Length (ft)	Skew (d)	Span Length (ft)	Girders	Abutment Pile, Orientation
SR18 over Mississinewa River	(Frosch, Wenning and Chivivhien, 2005)	IN	367	8	5 (62-3@81-62)	4 (PC)	10 x CFT
SR249 over US12	(Chovichien, 2004)	IN	990	13	10 (86.6-3@98.4-114.8-4@101.7-86.6)	4 (PC)	5 x HP 14x89 (Strong Axis)
165 over SR25	(Chovichien, 2004)	IN	152	25	2 (2@76)	7 (Steel)	6 x HP 12x53 plus 4 x CFT (Weak Axis)
Boone River Bridge	(Girton, Hawkinson and Greimann, 1991)	IA	324.5	45	4 (80-2@82.25-80)	(PC)	HP 10x42 (Weak Axis)
Maple River Bridge	(Girton, Hawkinson and Greimann, 1991)	IA	320	30	3 (98-124-98)	(Steel)	HP 10x42 (Weak Axis)

Bridge	Reference	State	Length (ft)	Skew (d)	Span Length (ft)	Girders	Abutment Pile, Orientation
Guthrie County Bridge	(Abendroth and Greimann, 2005)	IA	318	30	3 (105.75-106.5-105.75)	(PC)	12 x HP 10x42 (Weak Axis)
Story County Bridge	(Abendroth and Greimann, 2005)	IA	201.3	15	3 (64.08-73.17-64.08)	(PC)	7 x HP 10x42 (Weak Axis)
Tama County Bridge	(Abendroth, Greimann and LaViolette, 2007)	IA	110	20	1 (110)	5 (PC)	7 x 12"x12" Prestressed Concrete Piles
Nash Stream Bridge	(Hartt, Sanford and Davis, 2006)	ME	98	35	1 (98)		4 x HP 14x89 (Strong Axis)
Forks Bridge	(Sanford and Elgaaly, 1993)	ME		20	1		N/A(Shallow Foundation)
Mills River Bridge	(DeJong, Howey, Civjan, Brena, Butler, Crovo, Hourani and Connors, 2004)	MA	270	0	3 (80-110-80)	4 (Steel)	8 x HP 10x57 (Weak Axis)
Rochester Bridge	(Lawver, French and Shield, 2000)	MN	216	0	3 (3@72)	4 (PC)	HP 12x53 (Weak Axis)
Southwest Omaha Bridge	(Kamel, Benak, Tadros and Jamshidi, 1996)	NE	324	0	2 (160-164)		HP 10 and Prestressed Concrete Pile
Scotch Road Bridge	(Hassiotis, Lopez and Bermudez, 2005)	NJ	298	15	2 (149-149)	(Steel)	19 x HP 14x102 (Weak Axis)
Cass County Bridge	(Jorgenson, 1983)	ND	450	0	6 (6@75)	(PC)	HP 10x42 (Weak Axis)
Port Matilda Bridge (Rout 322)	(Fennema, Laman and Linzell, 2005)	PA	172	0	3 (47-88-37)	4 (PC)	10 x HP 12x74 (Weak Axis)
Porter Road Bridge	(Basu and Knickerbocker, 2005)	TN	318	27	2 (159-159)	4 (PC)	10 x HP 12x53 Piles

Frosch et al. (2005) monitored several jointless bridges to investigate their in-service behavior as well as the behavior of the piles supporting these structures. Based on the experimental study Chovichien (2004) made the following recommendations:

- Steel H-Piles are recommended because of their higher ductility and displacement capacity. Besides H-Piles result on lower moment at the interface with the abutment compared to CFT piles.

- Piles should be oriented for weak axis in order to maximize lateral displacement and minimize the moment at pile-abutment interface.
- Axial load should be limited to $9A_s$ (kips) for steel H-Piles and $0.25f_yA_s + 0.4f'_cA_c$ for CFT piles.
- Confinement reinforcement and/or deeper embedment length should be provided to improve pile-abutment connection.
- Local buckling in H-pile was observed for abutment movement above 1.0 in.

On the other hand the following conclusions were made based on the field studies by Frosch et al. (2005):

- End abutment movement because of thermal loads can be conservatively estimated by
$$\Delta L = \alpha.L.\Delta\theta$$
- Major movement of the abutment is longitudinal translation and abutment rotation can be ignored.
- Details utilized in pile-abutment connection (covering the embedded portion of the pile head with polystyrene) at SR-249 provided pinned connection and eliminated double curvature generally observed in integral connections.

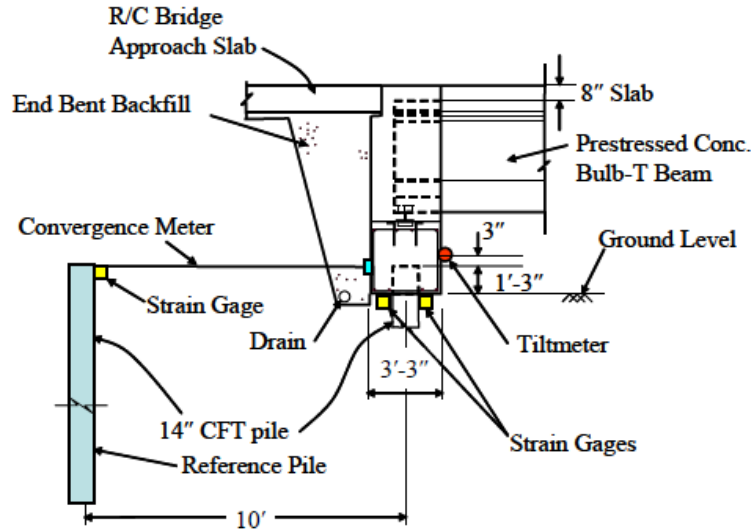


Figure 2-10- SR-18 End Bent Instrumentation (Frosch, Wenning and Chivivhien, 2005)

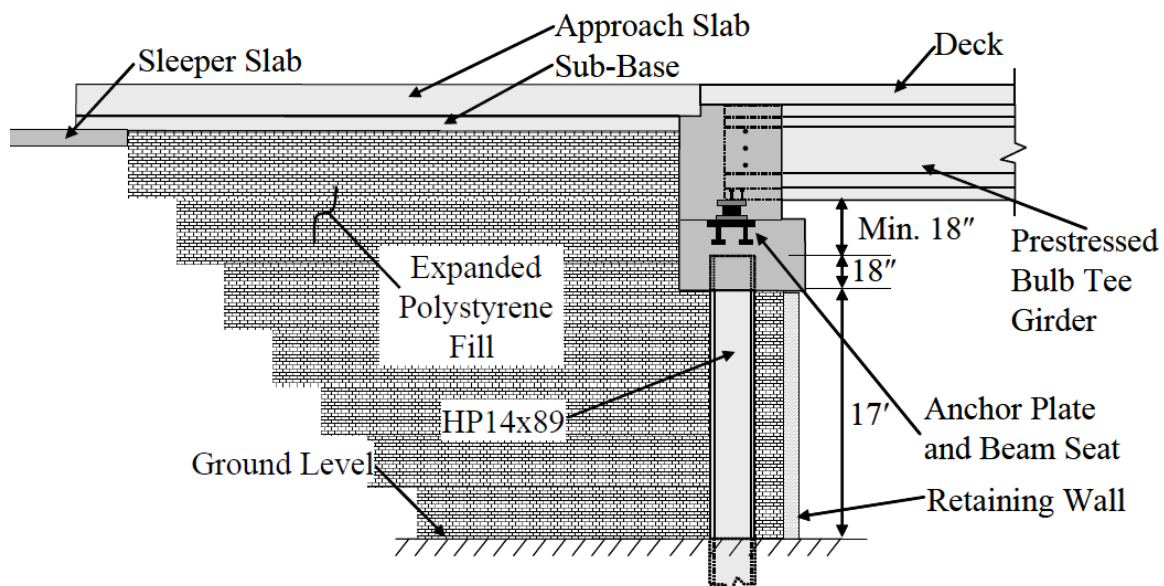


Figure 2-11- SR-249 End Bent Detail (Frosch, Wenning and Chivivhien, 2005)

Girton et al. (1991) monitored air and bridge temperature, bridge displacement and pile strains of two jointless bridges in Iowa. The following conclusions were made based on the results of the experimental and further analytical study:

- For design purposes, larger bridge temperature range should be selected compared to the recorded data.
- Steel and concrete bridges are not significantly different as related to bridge temperature range. A temperature range of 150° F for concrete and 140° F for steel bridges is recommended.
- Stresses due to bending of the bridge related to thermal movement can be modeled with two separate longitudinal and lateral frame models.
- Equivalent cantilever method is sufficiently accurate model for design purposes
- Stresses due to lateral movement of the skewed bridge should not be ignored.
- In order to increase the flexibility of the system, piles should be oriented for weak axis bending and also oversized pre-drilled holes should be used.
- In skewed bridges, to prevent lateral movement, battering the piles in the lateral direction should be used.

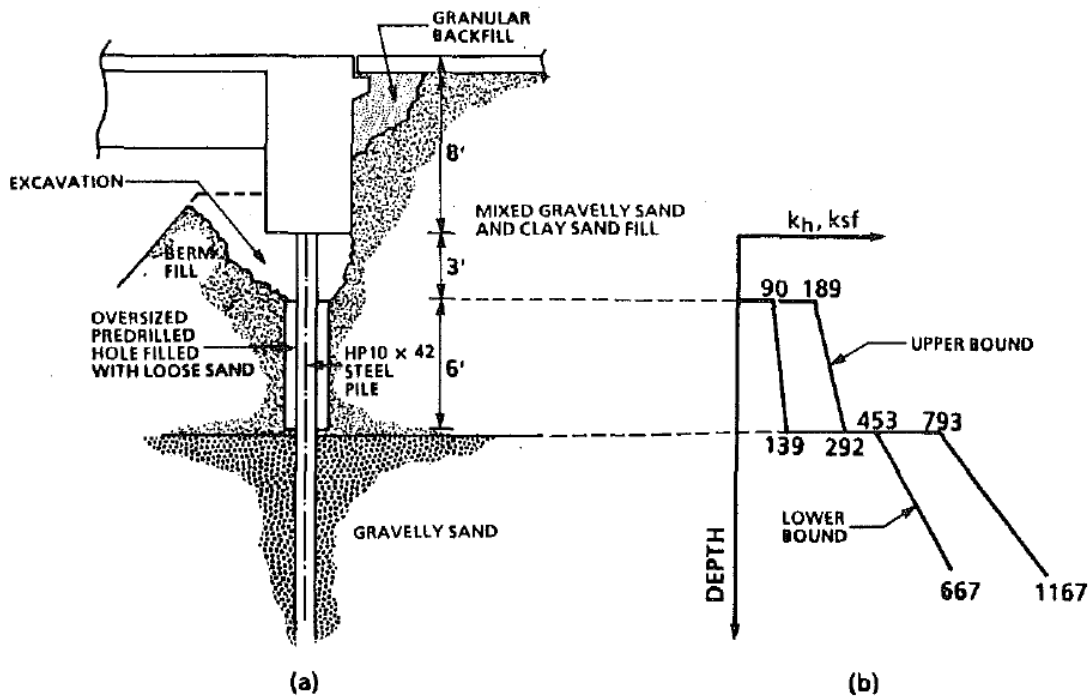


Figure 2-12- Boone River Bridge (a) Abutment Cross Section (b) Initial Stiffness vs. Depth (Girton, Hawkinson and Greimann, 1991)

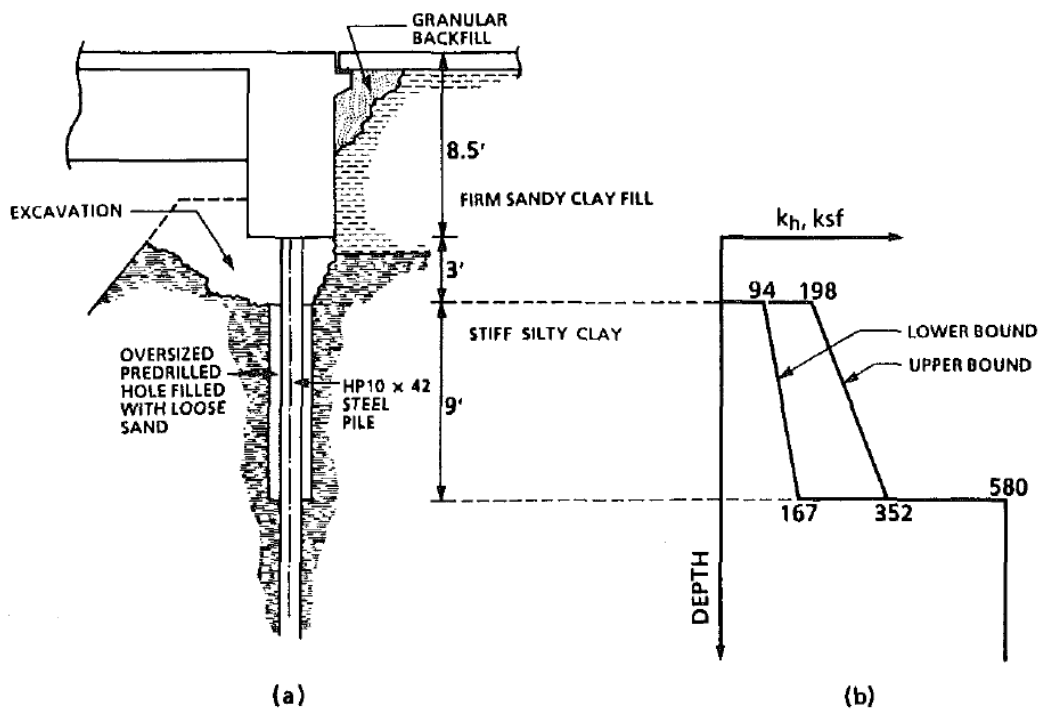


Figure 2-13- Maple River Bridge (a) Abutment Cross Section (b) Initial Stiffness vs. Depth (Girton, Hawkinson and Greimann, 1991)

Two prestressed concrete bridges in Iowa were monitored in a two year period by Abendroth and Greimann (2005). Instrumentation included displacement transducers, tilt-meter to measure bridge movement, strain gages, and thermometers to measure air and bridge temperatures. Pile strains exceeded the corresponding yield values in both bridges, while longitudinal strains in the girders were in the acceptable range. The inconsistency between the measured and calculated bridge movement due to thermal movement was not fully explained in this report. Based on the experimental study, design procedure is proposed for prestressed concrete bridges with steel piles to calculate design-temperature range, vertical-temperature gradients in the bridge superstructure, longitudinal displacements of the integral abutments, concrete creep and concrete-shrinkage effects, and coefficients of thermal expansion and contraction for the concrete.

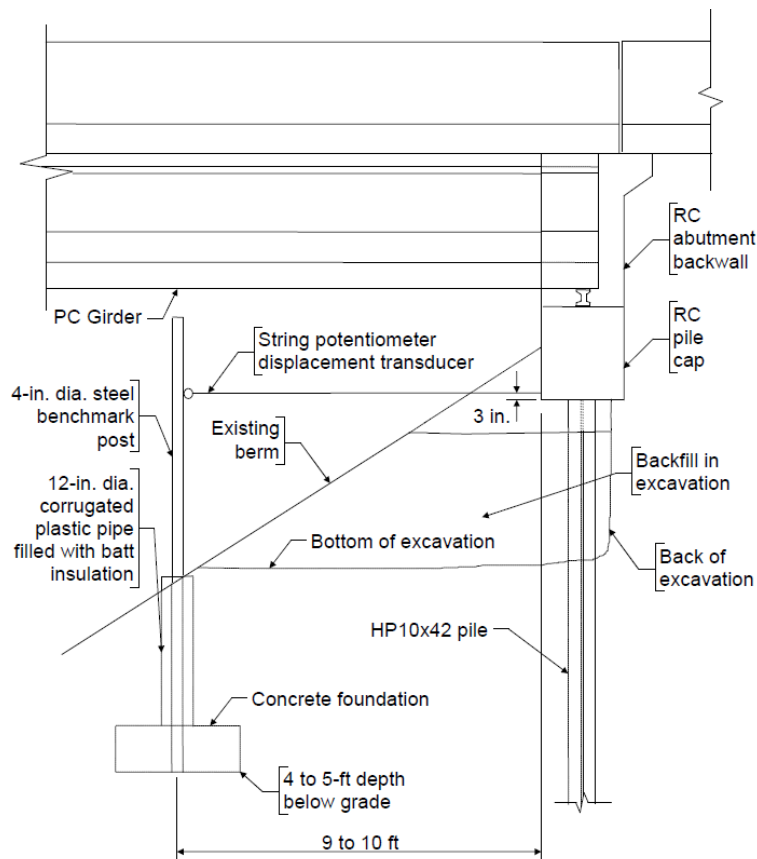


Figure 2-14- Typical longitudinal Cross Section near Abutment and Benchmark Post Installation for Story County Bridge and Guthrie County Bridge (Abendroth and Greimann, 2005)

In another research Abendroth et al. (2007) studied the behavior of the first jointless bridge in the state of Iowa with prestressed concrete piles. Several vibrating wire strain gages, displacement transducers and thermocouples were utilized to monitor the long term response of this bridge. The following is the result of instrumentation and monitoring of the bridge with prestressed concrete pile:

- Most of the longitudinal movement happened in the east abutment and the movement in the other abutment is negligible.
- The thermal gradient through the depth of the superstructures matches well with the AASHTO proposed values.

- Recorded data reveal that the carpet wrap provided to decrease the restraint at pile head is not effective and the pile head should be designed as fixed in this case.
- Cracking in the pile was observed.

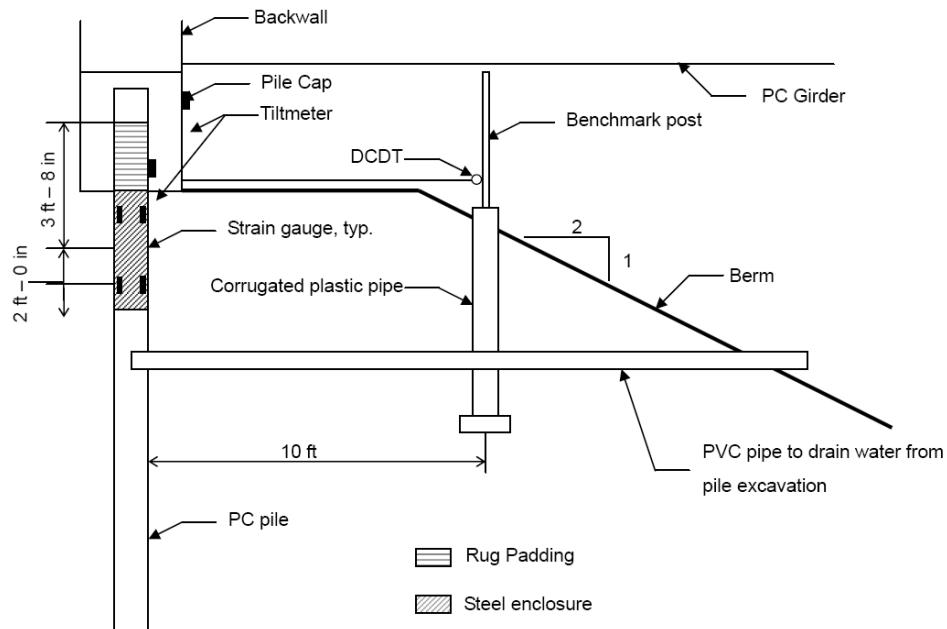


Figure 2-15- Instrumentation at Mid-Width of East Abutment for the Tama County Bridge (Abendroth, Greimann and LaViolette, 2007)

The behavior of a jointless bridge in the state of Massachusetts was studied by DeJong et al. (2004). The bridge was instrumented by Eighty five sensors as well as four inclinometer casings. Gages included earth pressure cells, joint meters, tilt meters, temperature gages, strain gages, and thermistors. The following conclusions were made from this study

- There is a correlation between the abutment displacement and rotation, and ambient temperature variation.
- Lateral earth pressure behind the abutment correlates with the temperature change and increases with depth.

- The measured backfill stiffness was less than the stiffness estimated using pressure meter tests by one order of magnitude.

No test data and conclusions from the instrumented bridge are reported in the corresponding paper. Some tests on single piles are reported which will be discussed in the next chapter.

Lawver et al. (2000) monitored the behavior of an integral abutment bridge near Rochester, Minnesota from the beginning of construction through several years of service using 180 instruments. Measured parameters included abutment horizontal movement, abutment rotation, abutment pile strains, backfill pressure, pier pile strains, prestressed girder strains, concrete deck strains, thermal gradients, steel reinforcement strains, girder displacements, approach slab settlement, frost depth, and weather. In this study, the main mode of abutment movement to accommodate expansion and contraction was found to be longitudinal movement rather than rotation. Static live load tests were also conducted on the bridge and the results revealed that the effect of environmental loading is as large as effect of live load. Although the performance of the bridge during the monitoring period was satisfactory but a loss of backfill material was observed within months after construction. Authors believe backfill plan need more attention including drainage detail and potential use of geo-textiles to stabilize the backfill and prevent its future settlement.

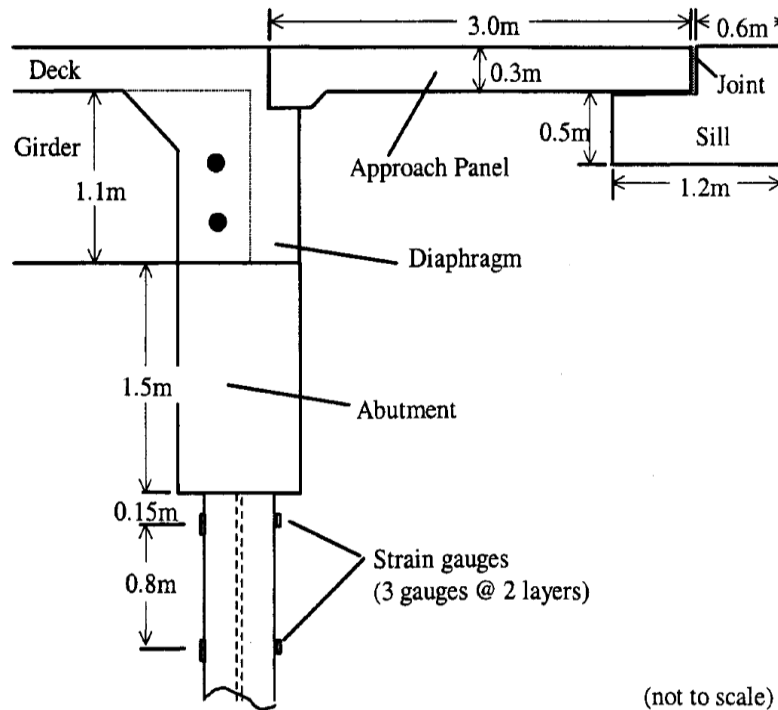


Figure 2-16- End Abutment Detail at Rochester Bridge (Lawver, French and Shield, 2000)

In a different study by Hassiotis et al.(2005) a jointless bridge on Scotch Road was monitored in a two year period. Strains gages were installed along the length of the pile. Soil pressure cells were also installed to measure the lateral pressure from the backfill. Inclinometers were used to monitor the rotations at the abutment-stringer interface. Besides, installed round displacement transducers measured the displacement at the relief slab while thermocouples monitored the temperature of the concrete slab as well as the steel stringers. Analysis of the experimental study revealed that bridge displacement is a linear function of temperature change and the stiffness of the integral abutment does not restraint temperature movement. Unfortunately this study does not offer useful information about the backfill pressure.

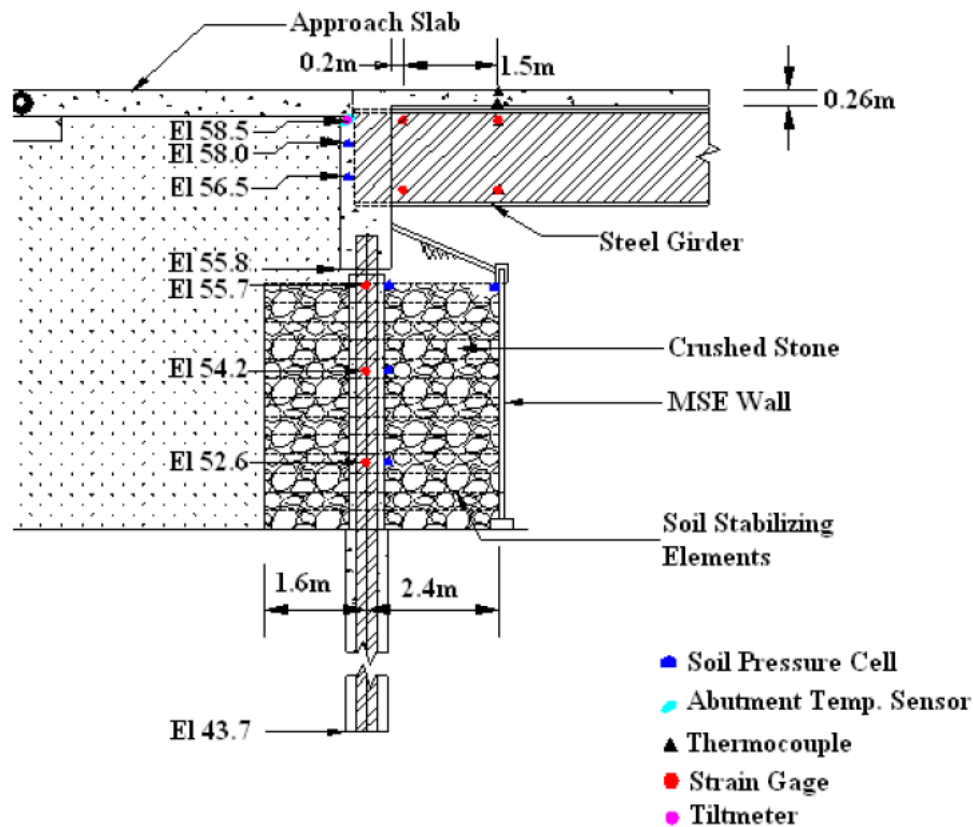


Figure 2-17- Instrumentation at Scotch Road Bridge (Hassiotis, Lopez and Bermudez, 2005)

In another study Fennema et al. (2005) used the field monitoring data from a bridge in Pennsylvania to refine the numerical models that were then used to predict the behavior of jointless bridges. 64 installed gages monitored pile strains, backfill pressure, abutment displacement and rotation, and girder rotations and strains during construction and thereafter. The following conclusions were made in this study:

- Pile responses in two and three dimensional models are the same. (Note that there is no skew in the bridge)
- The primary movement in jointless bridges is rotation about the base of the abutment not its longitudinal movement which is typically assumed in the design.

- Field data revealed that the girder-abutment connection is not rigid and it is better to assume hinge connection at girder ends although it is embedded in the abutment.
- Creep and Shrinkage may be important in axial behavior of the girders.
- Axial strains induced in the girders as a result of thermal changes are significant and should be considered in the design of the prestressed girders.

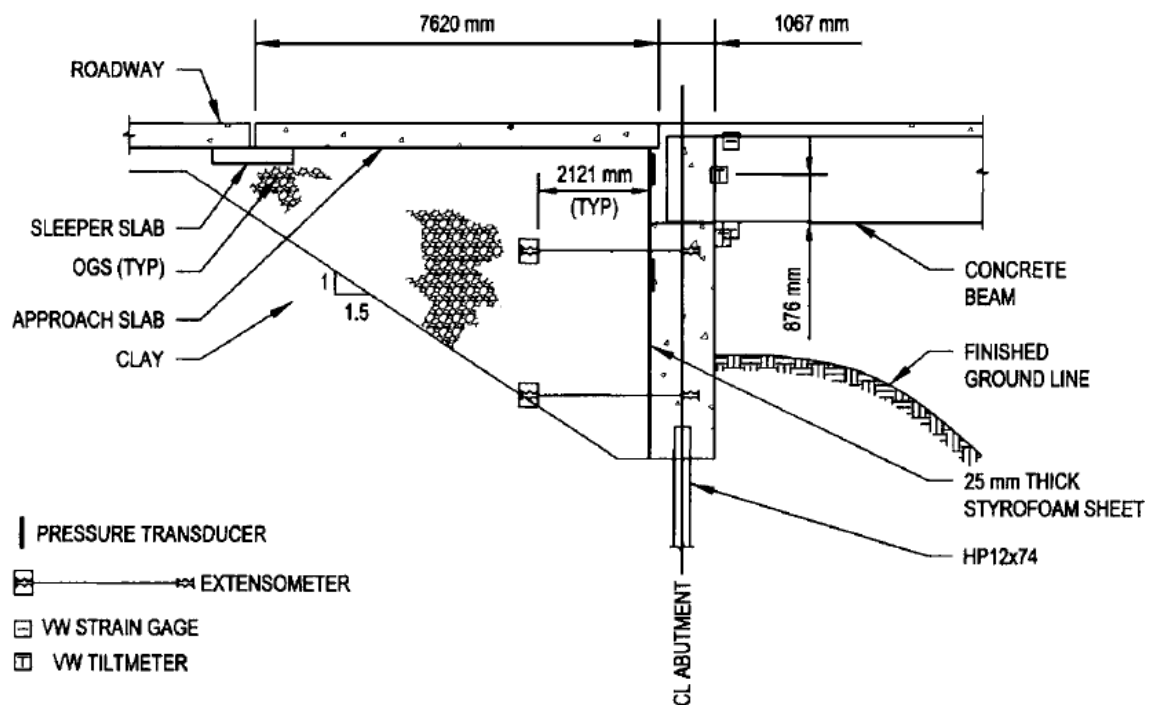


Figure 2-18- Port Matilda Bridge Abutment Section and Instrumentation Plan (Fennema, Laman and Linzell, 2005)

2.3.3. Field Tests on Single Piles

The following table summarizes all available literature on tests conducted on laterally loaded piles.

Table 2-8- List of all available literature on tests of laterally loaded single piles

Reference	State	Soil Type	Pile Type	Pile Width (in)	Embedded Length (ft)	Loading Type
(Burdette, Deathrage and Goodpasture, 2003)	Tennessee	Soft Clay	PC	14	36	Static-Cyclic
	Tennessee		H Piles	10	38	Static
(Cox, Reese and Grubbs, 1974)	Texas	Sand	Pipe	24 (3/8 thickness)	69	Static-Cyclic
(Reese, Cox and Koop, 1975)	Texas	Stiff Clay	Pipe	24 (3/8 thickness)	49	Static-Cyclic
(Matlock, 1970)	Texas	Soft Clay	Pipe	12.75 (0.5 thickness)	42	Static-Cyclic-Subsequent Reloading
(Bhushan, Haley and Fong, 1979)	California	Stiff Clay	RC	24 & 48	9-22	Static
(Reese and Welch, 1975)	Texas	Stiff Clay	RC	30	42	Static
(Cheang and Matlock, 1983)	Texas	Sand	Pipe	24 (0.5 thickness)	32	Static-Cyclic

University of Tennessee conducted several test experiments on prestressed concrete piles (Burdette, Deathrage and Goodpasture, 2003). In each four abutments tested, a 14 in square prestressed concrete pile was driven 36 ft through 7 in diameter pilot holes into undisturbed red clay soil. Piles were reinforced using six 0.5 in diameter low relaxation seven-wire grade 270 strands. Each pile was embedded 12 in. in the 36 in wide abutment. Cracks were observed on the piles just below the pile-abutment interface, when their head was displaced about an inch; however this cracking altered the load-displacement slightly and they were closed after the pulling load was removed. The main conclusion of this research was that prestressed concrete piles are appropriate for use in integral abutment bridges.

In another research study funded by Tennessee DOT conducted by University of Tennessee the behavior of pile-abutment systems supporting jointless bridges were investigated. During each test a single HP10x42 pile was loaded about its strong axis and

data were collected to estimate moment along the depth of the pile, and load versus displacement. Strain gages were installed along the top 18 ft of the embedded portion to determine the bending moment. Abutment rotation was restrained to simulate rotational restraint provided by the integral superstructure in a real bridge. More than fifty lateral displacement tests on five separate piles were carried out. In most of the tests the maximum lateral displacement was below 1 in. Local flange buckling was observed at the pile-abutment interface in a test which continued the loading up to 4.3 in. Authors believe that in most practical cases pile buckling is not a concern since the lateral support provided by the surrounding soil prevents any possibility of buckling. Unfortunately no information about the soil is provided.

A series of tests in sand were carried out on two 24 in piles instrumented to measure the bending moment along the pile length by Cox et al. (1974) in Mustang Island, Texas. The test piles were 24 in pipe piles with a wall thickness of 3/8 in embedded 69 ft into sand. Installed strain gages on piles were located along the top 32 ft embedded portion. Static and cyclic load tests were carried out on both piles to monitor the pile response in different loading conditions. Based on the tests conducted, Reese et al. (1974) proposed p-y curves for laterally loaded piles in sand.

Drilled pier laterally loaded in stiff clay was tested by Reese and Welch (1975). Tested foundation was a drilled pier constructed by drilling an open hole with a diameter of 30 in to a depth of 42 ft. The data taken during the test was used to develop p-y curves for different depths in stiff clay.

Lateral load tests were conducted on 12 drilled piers with diameters of 2 ft and 4 ft and lengths of 9 ft to 22 ft by Bhushan et al. (1979). Eight of these piers were constructed in level ground while the other four were tested on slopes ranging from 20° - 50° . Tests were carried out in four different sites with hard over-consolidated clays near Los Angeles, CA. Based on the load test data and some further analysis the following conclusions were made:

- Drilled piers in hard clays can carry high lateral loads (lateral loads in tests were up to 600 kips)
- The procedure proposed by Reese and Welch (1975) generally provides conservative predictions of the load-deflection relationship for rigid piers in hard clays.
- A limiting ground-line deflection can be used as a design criterion for short rigid piers.
- An approximate relationship is proposed for computing the ultimate lateral resistance on slopes.

Matlock (1970) conducted a series of experiments on laterally loaded pile for offshore structures with an instrumented pipe pile. Three loading conditions were applied including short term static, cyclic, and subsequent reloading with forces less than previous maximums. Based on the test results, a procedure was proposed for sub-merged clay soils which are naturally consolidated or slightly over-consolidated. It was assumed that the spacing between the piles is sufficient for independent action.

In another study, two 24 in diameter pipe piles driven into stiff clay were laterally loaded and the response was measured using installed strain gages on the top 32 ft embedded portion of the piles (Reese, Cox and Koop, 1975). The procedure of the testing and analysis was the same as their other experiment (Reese, Cox and Koop, 1974, Cox, Reese and Grubbs, 1974). Using the strain gage data the moment along the depth of the pile has been calculated and by twice differentiating the moment the soil response was evaluated and p-y curves were then developed. To validate the procedure, measured and computed values of moment along the depth were then compared for static and cyclic loadings, and a good agreement was observed.

Cheang and Matlock (1983) tested two driven piles which were previously used in another NSF funded project. The piles were instrumented to measure bending moment along the pile length. Applied loads and corresponding deflections at two different elevations above the ground surface were measured by strain-gaged load cells and LVDTs. Tests were conducted under three boundary conditions namely partially restrained head, free head, and fully restrained head. After the initial test loading permanent deflection of the pile near the ground surface was observed (about 0.3 inch). The SPASM program with nonlinear and inelastic soil model was used to model the system and satisfactory results were observed.

2.3.4. Creep and Shrinkage

The time-dependant response of concrete structures as a result of creep and shrinkage is a well-known phenomenon (Huang, French and Shield, 2004). In regular bridges, creep and shrinkage result in stress and deformations mainly in the

superstructure that is pre-stress loss, camber change, axial shortening, and secondary continuity forces. However, in jointless bridges, because of integrity of the system, effect of creep and shrinkage are more complicated.

In general, concrete creep and shrinkage are referred to as a result of water diffusion and redistribution, gel particle movement and micro-cracks in the concrete. Drying shrinkage is caused by withdrawal of free water in the concrete stored in unsaturated air as well as the volume change of particles due to removal of absorbed water.

Like shrinkage, Concrete creep is also related to moisture exchange between concrete and surrounding air (drying creep). This kind of creep may be caused by several mechanisms such as migration of solid particles during water diffusion out of the loaded gel, micro-pre-stress or micro-cracking due to concrete drying. Creep can also be caused by redistribution of capillary water within the structure of hardened cement paste and displacement of gel particles as a result of sustained stresses (basic creep).

Usually creep and shrinkage are disregarded in the analysis of jointless bridges (Haj-Najib, 2002, Chovichien, 2004, Fennema, Laman and Linzell, 2005, Bonczar, Brena, Civjan, Dejong, Crellin and Crovo, 2005, Thanasattayawibul, 2006); however they have great influence on the behavior of these bridges due to integrity of the system and should not be ignored (Oesterlie, Tabatabai, Lawson, Refai, Volz and Scanlon, 2002, Huang, French and Shield, 2004).

2.3.4.1. Creep

Concrete creep is affected by several factors such as sustained stress, concrete strength, aggregate size and type, water-cement ratio, slump, air content, loading age,

relative humidity, volume-surface ratio, and temperature. Concrete creep decreases with the increase of strength and aggregate content, and increases with the increase of slump and temperature. Relative humidity greatly affects drying creep. Smaller relative humidity and volume-surface ratio can greatly increase concrete creep. Furthermore, larger creep can be observed in concrete with lower loading age.

Extensive research related to concrete creep has been carried out by North Western University (Bazant, 1972, Bazant and Xi, 1995). Based on these studies, there are two ways to model the aging aspect of basic creep of concrete; (1) Age Adjusted Effective Modulus Method in which the material parameters involved in the creep model are quantified in empirical functions of age (2) Solidification Theory in which the material parameters for creep are considered to be age-independent but the volume fraction of the age-independent material increases with time.

Many researchers have modeled the creep of concrete using Age Adjusted Effective Modulus because of its simplicity and accuracy (Pugasap, Kim and Laman, 2009, Hedjazi, Rahai and Sennah, 2007). In this method, the modulus of elasticity of concrete is time dependant.

$$E(t, t_o) = \frac{E(t_o)}{1 + \chi(t, t_o)\phi(t, t_o)} \quad \text{Eq. 26}$$

Where, the creep coefficient $\phi(t, t_o)$, and aging coefficient $\chi(t, t_o)$, can be calculated either from ACI 209 or AASHTO LRFD Design Specification.

2.3.4.2. Shrinkage

The main factors affecting concrete shrinkage include water-cement ratio, water content, workability, aggregate content and type, and relative humidity. In a study by Brooks (1989) it was shown that with the increase of water-cement ratio between 0.2 and 0.6 shrinkage increases proportionally. The reason is that by increasing the water-cement ratio more evaporated water is stored in the concrete which result in larger shrinkage. On the other hand, increase of aggregate content and aggregate-cement ratio will decrease shrinkage. Besides, Concrete shrinkage increases with the increase of relative humidity.

Like creep, shrinkage is frequently ignored in the analysis of jointless bridges; however shrinkage has great influence especially in steel girder bridges, where creep is insignificant. Usually shrinkage is simulated by imposing a virtual temperature change on the concrete elements (Basu and Knickerbocker, 2005).

Pugasap et al. (2009) incorporated shrinkage in their model using the provisions of ACI 209.

2.3.5. Curved and Skewed Bridges

Haj-Najib (2002) studied the effect of skew on jointless steel bridges; however the secondary effects were ignored in this study. The following are the summary of the recommendations and conclusions provided:

- Piles should always be oriented to allow bending primarily about the weak axis. (Regardless of the skew angle, weak axis should be parallel to the abutment centerline)

- Place piles in pre-drilled holes in order to provide more flexibility and reduce the stresses in the piling system.
- Increasing the number of spans would reduce the stresses in the piles.
- Use granular backfill material behind the abutment with an acceptable drainage system. Backfill should be well-compacted to reduce settlement of the approach slab.

Although it is highly recommended to use the piles oriented so that they bend about their weak axis, it is recommended to further investigate the orientation along the strong axis.

In another research Thanasattayawibul (2006) investigated horizontally curved steel bridges with a degree of curvature ranging from 0 degree to 172 degrees based on a 1200 ft bridge length. Like the previous study, use of pre-drilled holes filled with loose granular soil, and orienting the piles along their weak axis is recommended.

Chapter 3

Soil-Structure Interaction

Soil-structure interaction is generally a complex problem. In jointless bridges, soil response affects the abutment and the piles. In soil-pile interaction problem, the response of deflected pile depends on the soil response and in return, the soil response is a function of pile deflection. Furthermore, the soil response is a nonlinear function of depth and pile's lateral movement. All these factors complicate the soil-pile problem.

In Section 3.1 first, the governing differential equation of embedded piles is discussed. Then the idea of p-y method is explained followed by some calibrated p-y curves for different soil types.

Soil-abutment interaction is briefly described in Section 3.2.

3.1. Soil-Pile Interaction

3.1.1. Governing Differential Equation of Pile

Hetenyi (1946) derived the differential equation for beam column. The behavior of the pile surrounded by soil is like a beam-column on elastic foundation. Figure 3-1 shows a segment of the pile bounded by two horizontal lines. As shown, the segment is displaced due to loading and it is assumed that the axial load is constant (Wang and Reese, 1993).

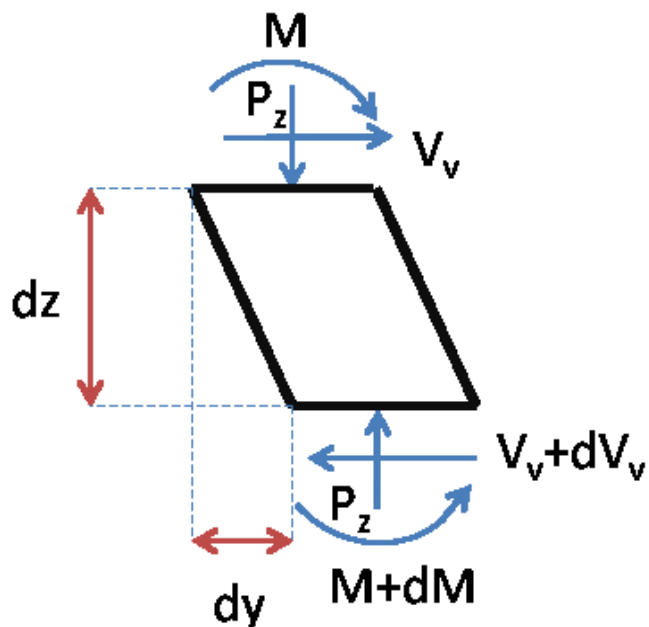


Figure 3-1- Beam-Column Segment Forces

Writing the equilibrium of moment, by ignoring second order terms, one will get:

$$(M + dM) - M + P_z dy - V_v dz = 0 \quad \text{Eq. 27}$$

$$\frac{dM}{dz} + P_z \frac{dy}{dz} - V_v = 0 \quad \text{Eq. 28}$$

Differentiating Eq. 28 with respect to z , the following equation is obtained:

$$\frac{d^2 M}{dz^2} + P_z \frac{d^2 y}{dz^2} - \frac{dV_v}{dz} = 0 \quad \text{Eq. 29}$$

Substituting M by $EI \frac{d^2 y}{dz^2}$, and $-\frac{dV_v}{dz}$ by p , Eq. 29 can be written as:

$$EI \frac{d^4 y}{dz^4} + P_z \frac{d^2 y}{dz^2} + p = 0 \quad \text{Eq. 30}$$

The term p represents the soil reaction per unit length. The response of the soil surrounding the pile is generally described in the form of p-y curves, which relate the soil

resistance to pile deflection at different depth below the ground level. These curves are generally nonlinear and depend on different parameters, including soil type, depth, and number of load cycles (Reese, 1977).

The differential equation for the pile embedded in soil can be written as follows:

$$EI \frac{d^4 y}{dz^4} + P(z) \frac{d^2 y}{dz^2} + p(z, y) = 0 \quad \text{Eq. 31}$$

In which z is the depth, y is the lateral displacement, $P(z)$ is the axial load in the pile and $p(z, y)$ is the soil reaction per unit length. Solution to abovementioned equation can either be obtained analytically or numerically. Analytical solutions are only available when the term $p(z, y)$ is constant. As mentioned before, the resistance of the soil to pile deflection is generally nonlinear which makes the analytical solution impossible in most of the cases. Besides, layered soils are very common in practice, which make the solution even more complicated. In these cases, the solution is obtained by a numerical finite-difference method. In this method, the pile is divided into n equal segments having length h (Figure 3-2). For a typical point i on the pile Eq. 31 is rewritten in the finite-difference format as follows: (Poulos and Davis, 1980)

$$EI \left[\frac{y_{i-2} - 4y_{i-1} + 6y_i - 4y_{i+1} + y_{i+2}}{h^4} \right] + P_i \left[\frac{y_{i-1} - 2y_i + y_{i+1}}{h^2} \right] + p_i = 0 \quad \text{Eq. 32}$$

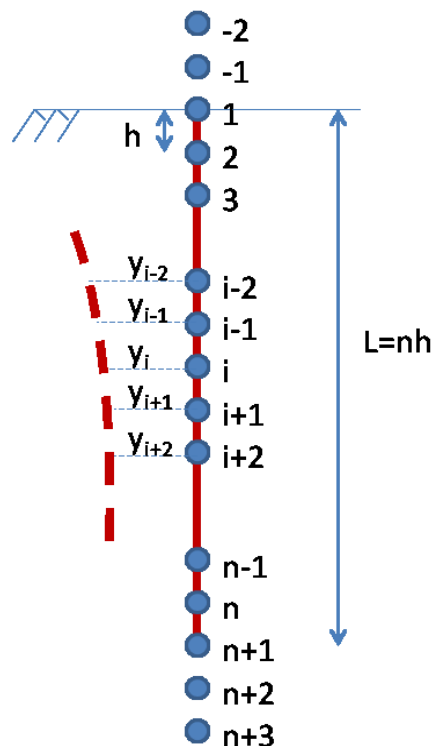


Figure 3-2- Finite Difference analysis of laterally loaded piles

Eq. 32 is then, applied to points 1 to $n+1$ which give $n+1$ equations. Four boundary conditions, two on the tip and two on the head, result in four further equations as follows

- Pile tip (Assuming a floating pile with a free tip):

- Zero Shear ($EI \frac{d^3 y}{dz^3} = 0$)

That is:

$$-y_{n-1} + 2y_n - 2y_{n+2} + y_{n+3} = 0 \quad \text{Eq. 33}$$

- Zero Moment ($EI \frac{d^2 y}{dz^2} = 0$)

That is:

$$y_n - 2y_{n+1} + y_{n+2} = 0 \quad \text{Eq. 34}$$

- Pile head:

- If fixed-head:

$$\text{Zero Rotation } \left(\frac{dy}{dz} = 0 \right)$$

That is:

$$y_2 - y_{-1} = 0 \quad \text{Eq. 35}$$

- If free-head:

$$\text{Zero Moment } \left(EI \frac{d^2y}{dz^2} = 0 \right)$$

That is:

$$y_2 - 2y_1 + y_{-1} = 0 \quad \text{Eq. 36}$$

$$\text{Shear} = H = EI \frac{d^3y}{dz^3}$$

That is:

$$-y_{-2} + 2y_{-1} - 2y_2 + y_3 = \frac{HL^3}{EI n^3} \quad \text{Eq. 37}$$

Using these four boundary conditions, four further equations will be identified and gives total of $n + 5$ equations which leads to the solution for $n + 5$ unknowns.

One of the main issues in solving the governing differential equation of the pile is the term related to the resistance of the soil against lateral movement.

3.1.2. Governing Differential Equation of Friction Piles

In friction piles the axial load along the pile would not be constant since a portion of the axial load is transmitted to the soil through skin friction. In this case, by differentiating the Eq. 28 with respect to z , the following equation is obtained:

$$EI \frac{d^4 y}{dz^4} + P(z) \frac{d^2 y}{dz^2} + \frac{dP(z)}{dz} \frac{dy}{dz} + p(z, y) = 0 \quad \text{Eq. 38}$$

In which, axial load at depth z can be calculated as

$$P(z) = P_o - \int_0^z f(z) dz \quad \text{Eq. 39}$$

Where, P_o is the axial load at the pile head, and $f(z)$ is the friction per unit length of the pile. Substituting Eq. 39 into Eq. 38 one can get:

$$EI \frac{d^4 y}{dz^4} + \left[P_o - \int_0^z f(z) dz \right] \frac{d^2 y}{dz^2} - f(z) \frac{dy}{dz} + p(z, y) = 0 \quad \text{Eq. 40}$$

Assuming linear variation of friction per unit length of the pile with depth (Heelis, Pavlovic and West, 2004) $f(z)$ can be written as follows

$$f(z) = \frac{2P_o(1-\mu)}{L} \left[f_1 + (f_2 - f_1) \frac{z}{L} \right] \quad \text{Eq. 41}$$

In this equation f_1 and f_2 are defined at the top and bottom of the pile respectively and should satisfy the following equation

$$f_1 + f_2 = 1 \quad \text{Eq. 42}$$

For example assuming $f_1 = f_2 = 0.5$ results in uniform friction along the pile. μ in Eq. 41 is the ratio of the tip axial load over applied head axial load (P_o).

$$\mu = \frac{P_o - P_{friction}}{P_o} \quad \text{Eq. 43}$$

Where, $P_{friction}$ is the total axial load transferred to the soil because of friction. A value of 1.0 for μ implies non-friction and a value of 0 implies pure friction pile.

3.1.3. p-y Method

The p-y method models the nonlinear behavior of the soil surrounding the pile and is an effective way for analysis and design of laterally loaded piles. Basically, the p-y curves are a set of curves corresponding to the soil response at certain depth. These curves are developed by calibrating test results of laterally loaded piles with analytical models. Using the p-y method, the deflections and forces in the pile can be calculated and used for design purposes.

3.1.3.1. Loading

One of the parameters affecting the response of the soil against lateral movement is the nature of loading. Generally, four types of loading can be considered (Reese, 1977)

- Static (short term)
- Cyclic (repeated)
- Sustained
- Seismic (dynamic)

3.1.3.2. Soft Clays below the Water Table

3.1.3.2.1. Static Loading

The following procedure is recommended to obtain appropriate curves for this case.

- Estimate variation of soil properties with depth such as undrained shear strength (c) and submerged unit weight (γ'). Also estimate ε_{50} which is one-half the maximum principal stress difference. If this value is not available, corresponding value from Table 3-1 can be used.

Table 3-1- Representative Values of ε_{50}

Consistency of Clay	ε_{50}
Soft	0.020
Medium	0.010
Stiff	0.005

- Calculate the ultimate resistance of the soil per unit length of the pile as the minimum of these values:

$$p_u = cD \left[3 + \frac{\gamma'}{c} + \frac{J}{D} z \right]$$

Eq. 44

$$p_u = 9cD$$

Where:

c = shear strength at depth z

D = pile width

γ' = average effective unit weight

z = depth below the ground

Based on experiments, Matlock (1970) suggested that the value of J for soft clay is about 0.5.

- Calculate the deflection at one-half the ultimate soil resistance as follows:

$$y_{50} = 2.5 \varepsilon_{50} D$$

Eq. 45

- Using the calculated values, the p-y curve is computed from the following equation:

$$\frac{p}{p_u} = 0.5 \left(\frac{y}{y_{50}} \right)^{1/3}$$

Eq. 46

The ratio of $\frac{p}{p_u}$ remains constant beyond $y = 8y_{50}$ (Figure 3-3(a))

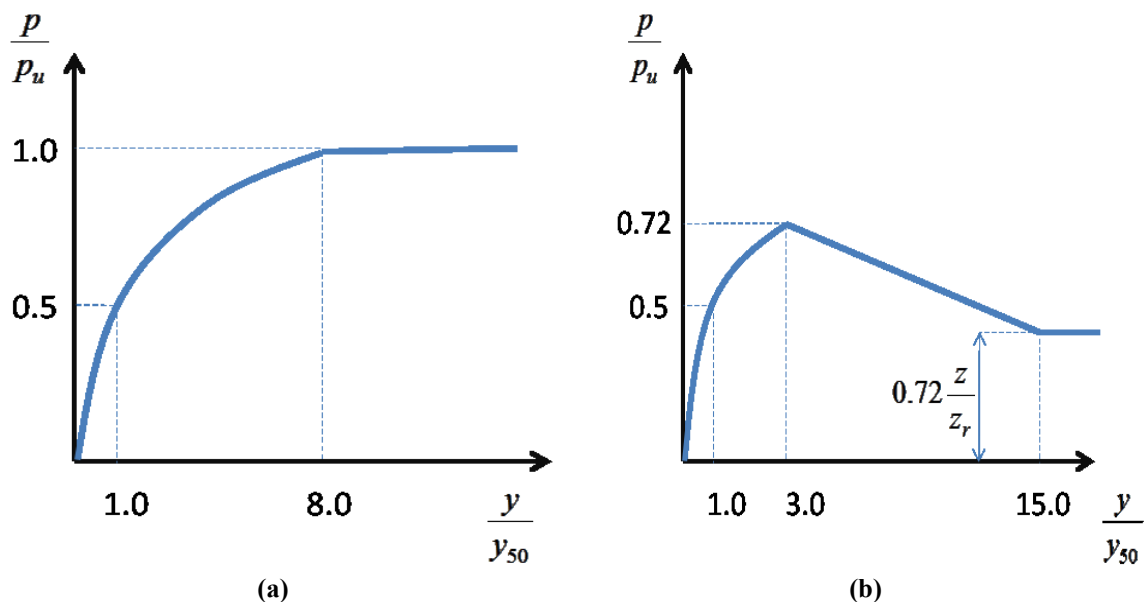


Figure 3-3- Characteristic shapes of p-y curves for soft clay below water table (a) static loading (b) cyclic loading (Matlock, 1970)

3.1.3.2.2. Cyclic Loading

The procedure for this case is the same as static loading up to $\frac{p}{p_u} = 0.72$.

Solving the two equations in Eq. 44 simultaneously, the value of z_r is obtained at each depth. If the unit weight and shear strength are constant z_r can be calculated as:

$$z_r = \frac{6cD}{\gamma' D + Jc}$$

Eq. 47

If $z \geq z_r$, then $\frac{p}{p_u} = 0.72$ for $y > y_{50}$

If $z < z_r$, then $\frac{p}{p_u}$ decreases linearly from 0.72 at $\frac{y}{y_{50}} = 3.0$, to $0.72 \frac{z}{z_r}$ at $\frac{y}{y_{50}} = 15.0$

and remains constant beyond this point.

3.1.3.3. Stiff Clay below the Water Table

A series of field tests on steel-pipe piles driven into stiff clay in Texas was performed (Reese, Cox and Koop, 1975). Based on this research, the following procedure is recommended for calculation of the p-y curves in stiff clays.

3.1.3.3.1. Static Loading

- Estimate soil properties such as undrained shear strength (c) and submerged unit weight (γ').
- Obtain the average undrained soil shear strength (c_a) at depth z .
- Calculate the ultimate soil resistance per unit length of the pile, using the smaller value from the following equations:

$$p_{ct} = c_a D \left[2 + \frac{\gamma' z}{c_a} + \frac{2.83}{D} z \right]$$

Eq. 48

$$p_u = 11cD$$

- Estimate the value of A_s from Figure 3-4.

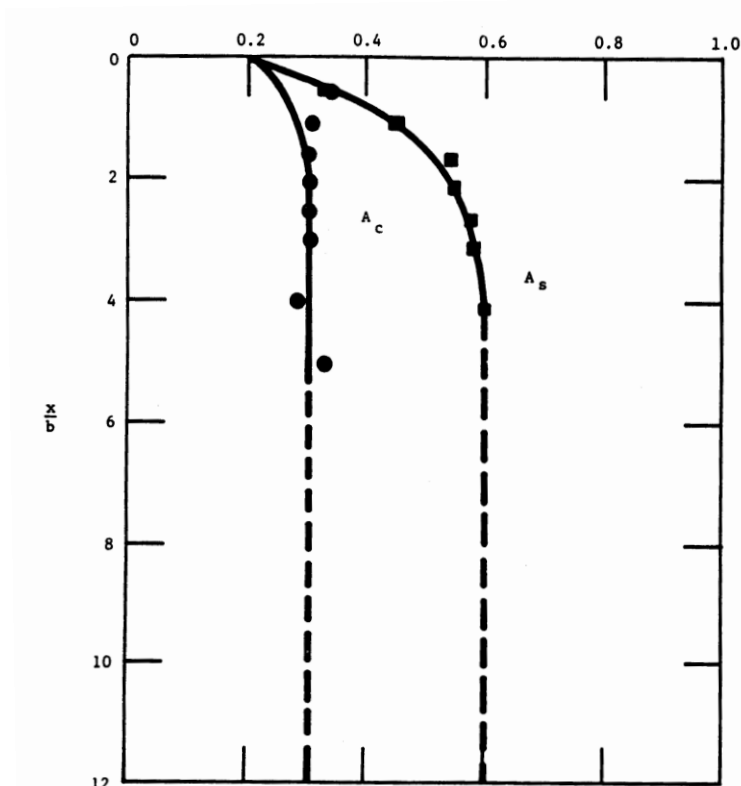


Figure 3-4- Values of A_s , and A_c (Reese, Cox and Koop, 1975)

- The first linear part of the graph is established by the following equation:

$$p = (kz)y \quad \text{Eq. 49}$$

Appropriate values for k_s (static) and k_c (cyclic) can be extracted from Table 3-2.

Table 3-2- Representative values of k and ε_{50} for stiff clay

	Average Undrained Shear Strength (ton/ft ²)		
	0.5-1.0	1.0-2.0	2.0-4.0
k_s (Static)	500	1000	2000
k_c (Cyclic)	200	400	800
ε_{50}	0.007	0.005	0.004

- The value of y_{50} is calculated as follows:

$$y_{50} = \varepsilon_{50}D \quad \text{Eq. 50}$$

- The first parabolic portion of the curve is then calculated as:

$$\left(\frac{p}{p_c}\right) = 0.5 \left(\frac{y}{y_{50}}\right)^{0.5} \quad \text{Eq. 51}$$

- The second parabolic portion of the curve from the point where y is equal to $A_s y_{50}$ to a point where y is equal to $6A_s y_{50}$ is defined as:

$$\left(\frac{p}{p_c}\right) = 0.5 \left(\frac{y}{y_{50}}\right)^{0.5} - 0.055 \left(\frac{y}{A_s y_{50}} - 1\right)^{1.25} \quad \text{Eq. 52}$$

- The next straight portion of the p-y curve from the point where y is equal to $6A_s y_{50}$ to a point where y is equal to $18A_s y_{50}$ is then calculated as:

$$\left(\frac{p}{p_c}\right) = 0.5(6A_s)^{0.5} - 0.411 - \frac{0.0625}{y_{50}}(y - 6A_s y_{50}) \quad \text{Eq. 53}$$

- Finally, the last straight portion of the curve for $y > 18A_s y_{50}$ is:

$$\left(\frac{p}{p_c}\right) = 0.5(6A_s)^{0.5} - 0.411 - 0.75A_s \quad \text{Eq. 54}$$

Or,

$$\left(\frac{p}{p_c}\right) = 1.225\sqrt{A_s} - 0.75A_s - 0.411 \quad \text{Eq. 55}$$

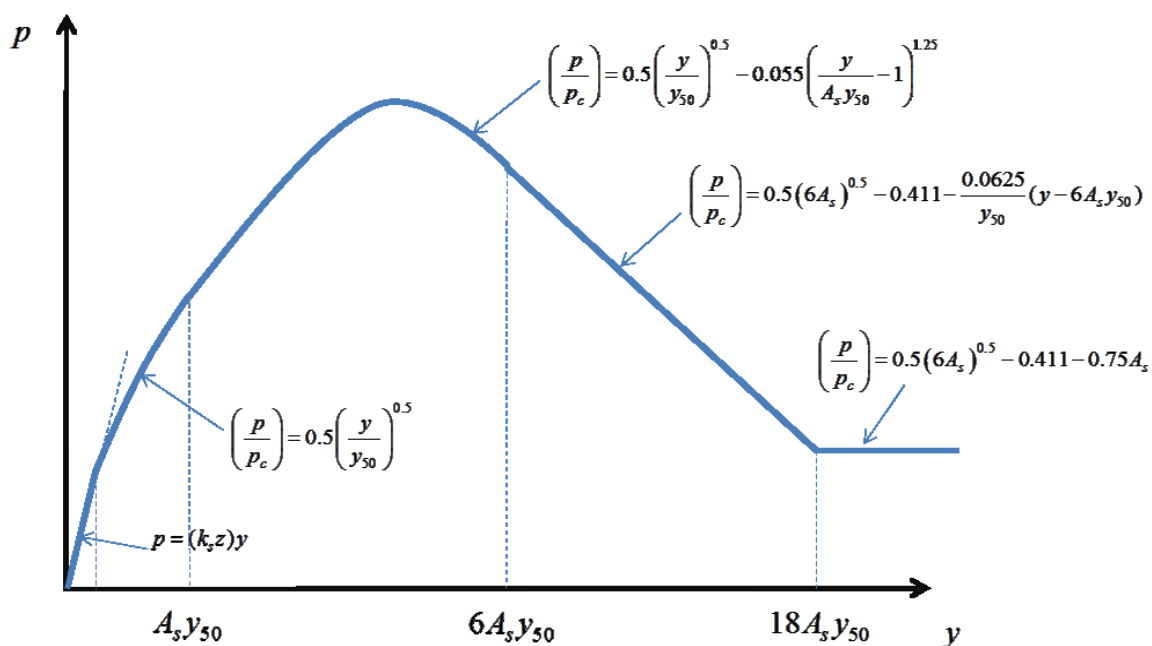


Figure 3-5- Characteristic shape of p-y curve for stiff clay (Reese, Cox and Koop, 1975)

3.2. Soil-Abutment Interaction

The magnitude of soil pressure behind the abutment wall and the nonlinear distribution of this pressure depend on wall displacement, soil type, depth, piles stiffness, and also direction of the displacement (Faraji, Ting, Crovo and Ernst, 2001). As a wall moves toward the backfill, passive pressure is engaged, and when it moves away from that, active pressure and surcharge pressure may be generated. Studies show that a minimum movement is required to reach the extremes for each of these types for pressure.

Full passive pressure builds up for relatively long bridge lengths. For shorter bridge lengths, only part of the passive pressure is developed for expansion as thermal expansion is limited. For all bridges, the maximum passive pressure force P_p is calculated as

$$P_p = \frac{1}{2} K_p \gamma H^2 \quad \text{Eq. 56}$$

Where,

K_p = the passive pressure coefficient

K_p is not necessarily the maximum K_p associated with full passive pressure. The value of K_p should be calculated using Figure 3-6 and Figure 3-7 (Clough and Duncan, 1991). The extreme values for expansion and contraction are proportional to the height of the wall. The movement required to reach the maximum passive pressure is on the order of ten times the movement required to reach the active soil pressure. The movement required to reach the extreme pressures are larger for loose soils than that for dense soils (Figure 3-6 and Figure 3-7). Table 3-3 highlights the required movements necessary to achieve maximum pressures.

The force-deflection design curves (Barker, Duncan, Rojiani, Ooi and Tan, 1991) shall be based on Figure 3-6 and Figure 3-7 (Clough and Duncan, 1991). The stiffness of the springs behind the abutment wall is nonlinear and depends on the type of the soil.

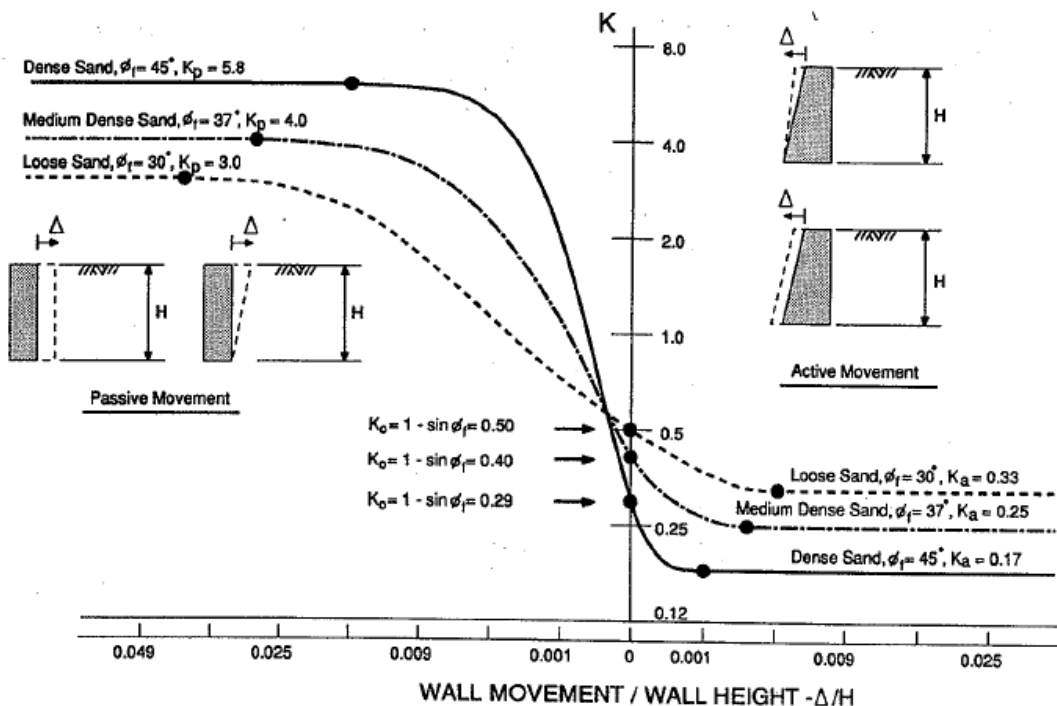


Figure 3-6- Relationship between wall movement and earth pressure (Clough and Duncan, 1991)

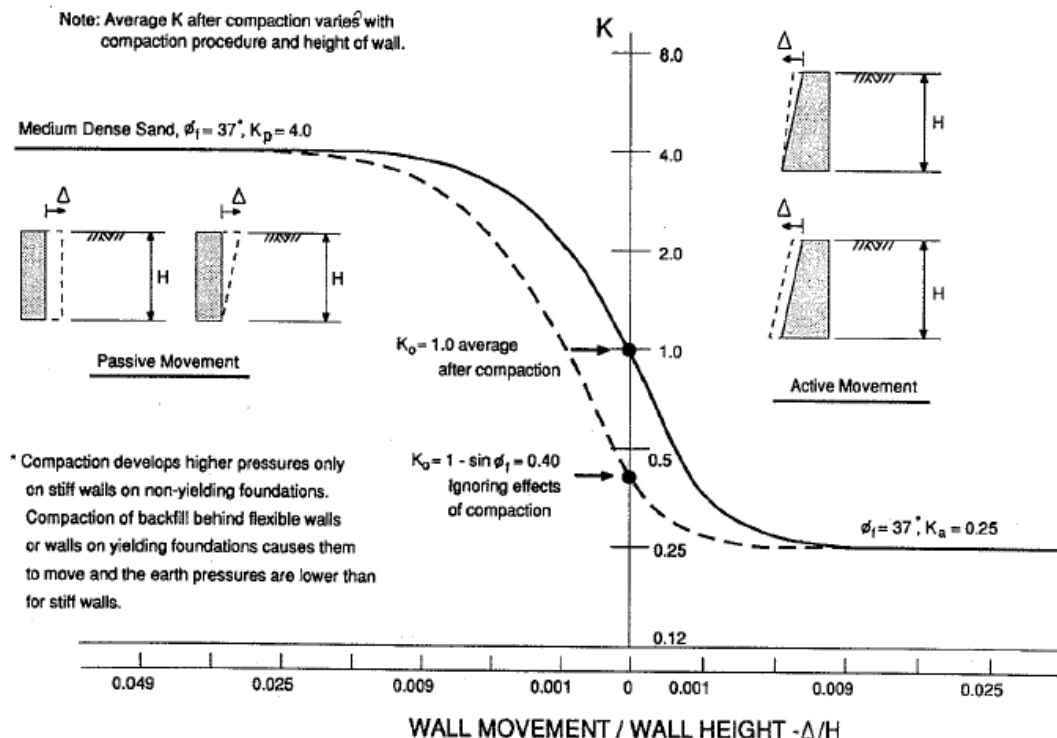


Figure 3-7- Relationship between wall movement and earth pressure for a wall with compacted backfill (Clough and Duncan, 1991)

Table 3-3- Approximate magnitudes of movements required to reach extreme soil pressure condition (Clough and Duncan, 1991)

Type of Backfill	Values of $\Delta/H^{(a)}$	
	Active	Passive
Dense Sand	0.001	0.01
Medium-Dense Sand	0.002	0.02
Loose Sand	0.004	0.04
Compacted Silt	0.002	0.02
Compacted lean clay	0.01 ^(b)	0.05 ^(b)
Compacted fat clay	0.01 ^(b)	0.05 ^(b)

(a) Δ = movement of top of the wall required to reach extreme soil pressure, by tilting or lateral translation, H = height of the wall

(b) Under stress conditions close to the minimum active or maximum passive pressures, cohesive soils creep continually. The movement shown would produce temporary passive pressures. If pressures remain constant with time, the movements shown will increase. If movement remains constant, active pressures will increase while passive pressures will decrease.

Chapter 4

Experimental program

4.1. Introduction

The experimental part of this study was conducted at UNL's structure's lab. The objective was to evaluate the behavior of the proposed detail as compared to the currently used detail. Two different connections were tested. The first specimen involved a relatively fixed pile/cap condition and represented current practice. The second specimen, however, consisted of the proposed connection detail and represented the relatively pinned connection. Axial load, modeling the gravity loads, was applied using the dywidag passed through the mid duct. The lateral load representing the thermal movements of the bridge was applied with two actuators. CFT piles were selected as they are axisymmetric.

4.2. Test Setup

Figure 4-1 shows the test setup for the experiments conducted in the structural lab. As shown, the pile was placed perpendicular to the loading frame. Two 3'x5'x4.7' concrete blocks were used to elevate the pile cap to reach the actuators level. The stack was finally post tensioned to the lab's floor using 4 dywidags.

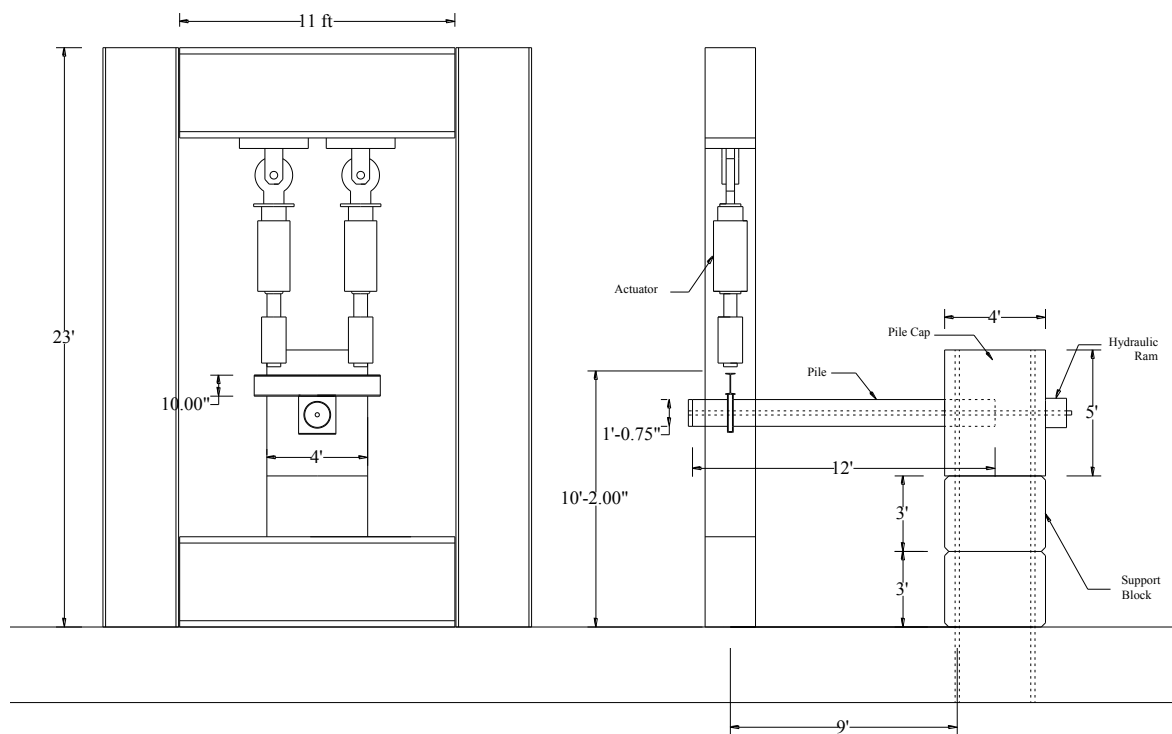


Figure 4-1- Test setup

Pile cap reinforcement is shown in Figure 4-2. The governing criteria in the design of these reinforcement was the minimum temperature and shrinkage reinforcement, since the stresses calculated from lateral load were below the allowable limits (see Appendix A)

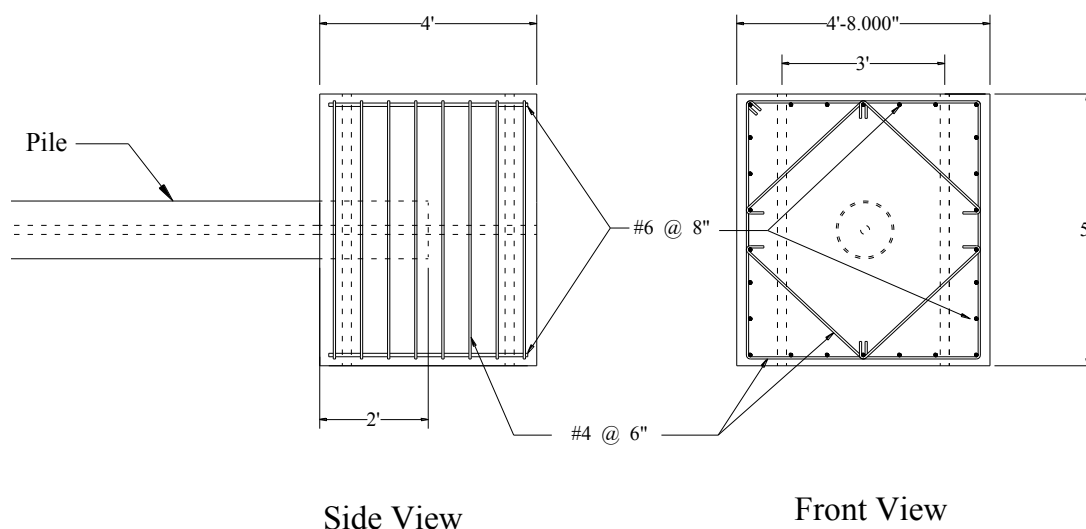


Figure 4-2- Pile cap reinforcement

4.2.1. Instrumentation

6 strain gages were used to measure the strains near the connection. The gages were located 2, 6, and 10'' away from the cap surface. 6 spring pots were also mounted on CFT close to the connection as shown in the following figure. For specimen #2, three threaded rods were tapped to the pile end and passed through $\frac{3}{4}$ '' copper ducts. These rods were attached to potentiometers to measure the deformation of the embedded portion of the CFT pile.

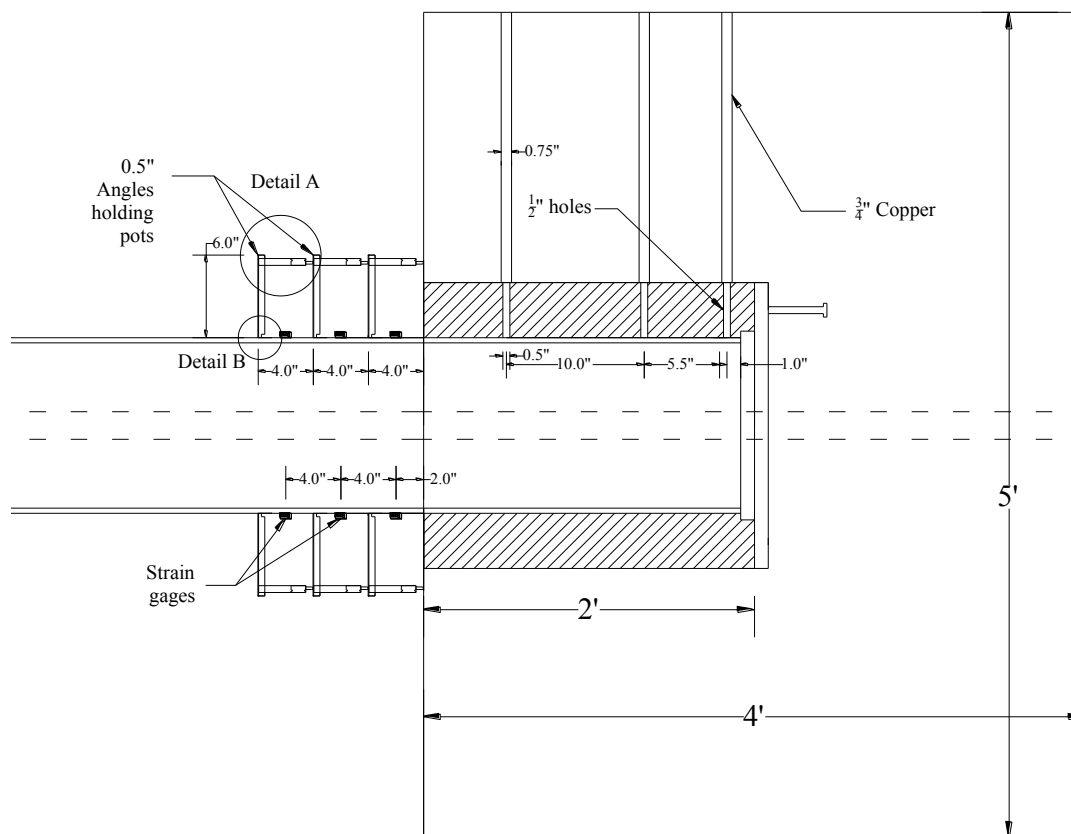
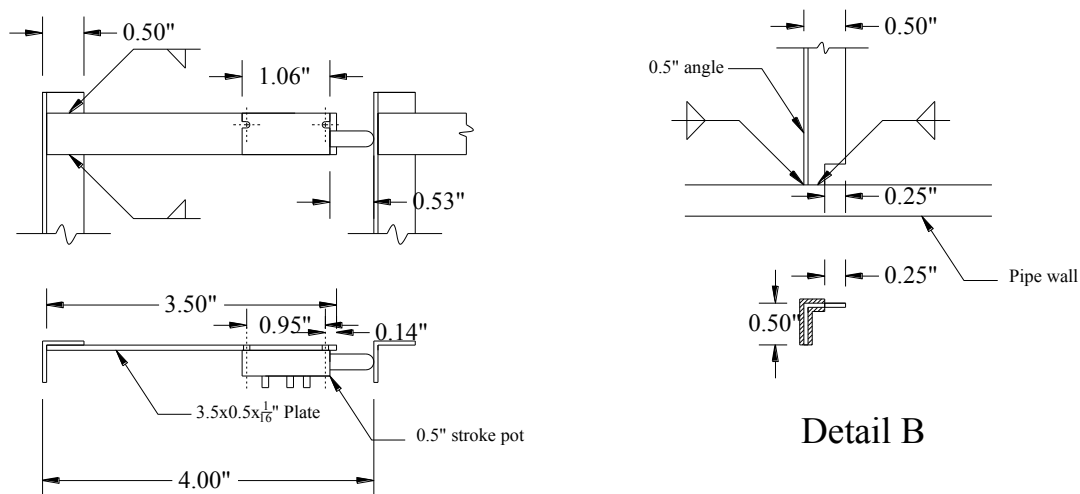


Figure 4-3- Instrumentation plan around the connection (specimen #2)

The following figure shows the details of attachment of the spring pots to the rod, and the rod to the CFT. Other than the three rods used for specimen #2, the other instrumentations were the same.



Detail A

Figure 4-4- details of mounting the spring pots

Two potentiometers (PNT and PNB) were mounted behind the cap to measure the possible rotation of the stack under the applied loads. The data extracted from the test show very small rotation which can be ignored. Although the deflection of the CFT under the load could be measured from the deflection of the actuators, another potentiometer (PB4) was mounted under the load.

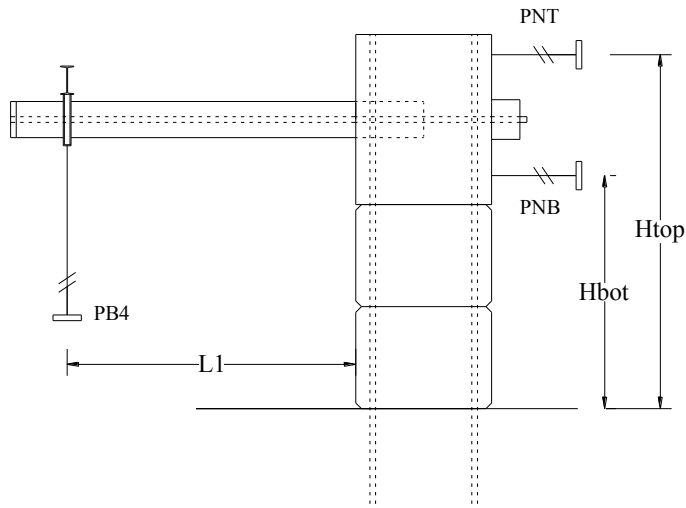


Figure 4-5- Instrumentation plan around the connection (specimen #2)

Table 4-1 lists the values of H_{top} , H_{bot} , and L_1 for two specimens.

Table 4-1- Location of pots (inch)

	Specimen #1	Specimen #2
H_{bot}	78.0	79.5
H_{top}	127.0	125.25
L_1	92	92

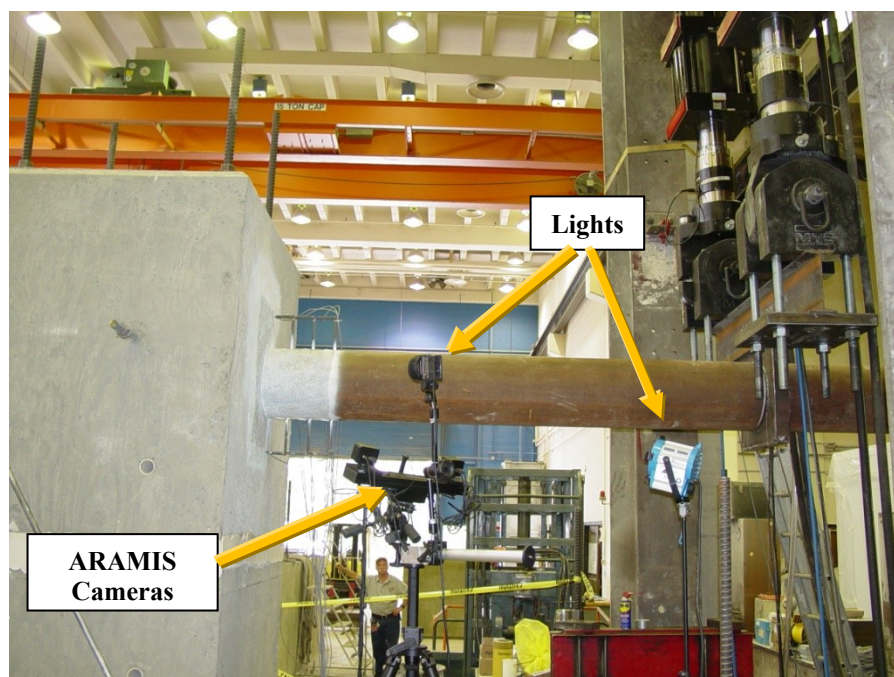
4.2.1.1. ARAMIS (Optical 3-D Deformation Analysis System)

ARAMIS is a non-contact and material independent measuring system providing, for static or dynamically loaded test objects, accurate 3D surface coordinates, 3D displacements and velocities, Surface strain values (major and minor strain, thickness reduction), and Strain rates. ARAMIS helps to better understand material and component behavior and is ideally suited to monitor experiments with high temporal and local resolution. ARAMIS is the unique solution delivering complete 3D surface, displacement and strain results where a large number of traditional measuring devices are required (strain gauges, LVDTs extensometers ...).

ARAMIS was used in parallel to regular measurement devices (strain gages, potentiometers ...) to assure the required precision and also measure the surface strain values at locations where no strain gage was available like concrete surface close to the connection, and elastomer surface. West half of the connection was painted with white spray, and then using markers 1/10" diameter dots were drawn on painted surfaces. The following table lists the load stages at which the data was recorded using ARAMIS system.

Table 4-2- Load stages at which ARAMIS system was used

	Load Stage	Used ARAMIS
Specimen #1	1	Yes
	2	No
	3	Yes
Specimen #2	1	Yes
	2	No
	3	No

**Figure 4-6- ARAMIS setup**

4.2.2. Building Specimens

Two pipes were fabricated by Midwest Steel as follows:

- 12” standard pipe x 12’-0”, prime painted (for specimen #1)
- 12” standard pipe x 12’-0” with a 13 ¾” diameter x 1” thick plate welded to one end, prime painted (for specimen #2)



Figure 4-7- Pipes before casting

The embedded plate was 1" thick, 20 3/4" diameter carbon steel plate with a 2" diameter hole in the center and sixteen 3/4 x 4" headed shear studs, which was fabricated and delivered to the structure's lab by Midwest Steel.



Figure 4-8- Embedded plate

The casts for the caps were made of plywood and were stiffened with 2x4" wood bars around the cast as shown in Figure 4-9.



Figure 4-9- Casts for the caps

Concrete with a maximum aggregate size of 3/4 in (47bd aggregate) was ordered from Concrete Industries. The specified 28-day strength of the concrete was 5.0 ksi. However, the compression tests on samples resulted in an average of 4.0 to 4.7 ksi in different pours. Based on the records from the vendor, the water-cement ratio was 0.434. After all pours, the surface of the wet concrete was covered with burlap after about 2 hours and the burlap was covered with plastic cover to keep moisture in. Burlaps were kept wet within 3 days after the pour to efficiently cure the fresh concrete. It was decided to pour the concrete in three stages, as the crane could hold one pipe at a time.

4.2.2.1. First Pour (March 7th 2011)

In the first stage on March 7th 2011 the bottom half of specimen #2's cap and the CFT's were cast. Using four 11" bars welded to one side of the embedded plate, it was held at the middle of the cap to be embedded in the concrete during the first pour.



Figure 4-10- Holding the embedded plate at the middle of the cap

Pipes were lifted with the crane and were held vertical by running the dywidags through the PVC pipes that were placed in the middle of the pipe section. PVC pipes were used as a duct for dywidag which applies the axial load during the tests. On the top end of each pipe, three tabs were welded to a 2.5" steel ring making a Mercedes shape, to hold the PVC at the top middle during the casting. On the bottom end of specimen #2 the PVC pipe was passed through the end plate, while a temporary plate with a 2.5" hole was tack welded to the bottom end of the specimen #1 pipe to keep the PVC pipe at the center. A lift truck was used to facilitate the casting procedure as shown in Figure 4-11.

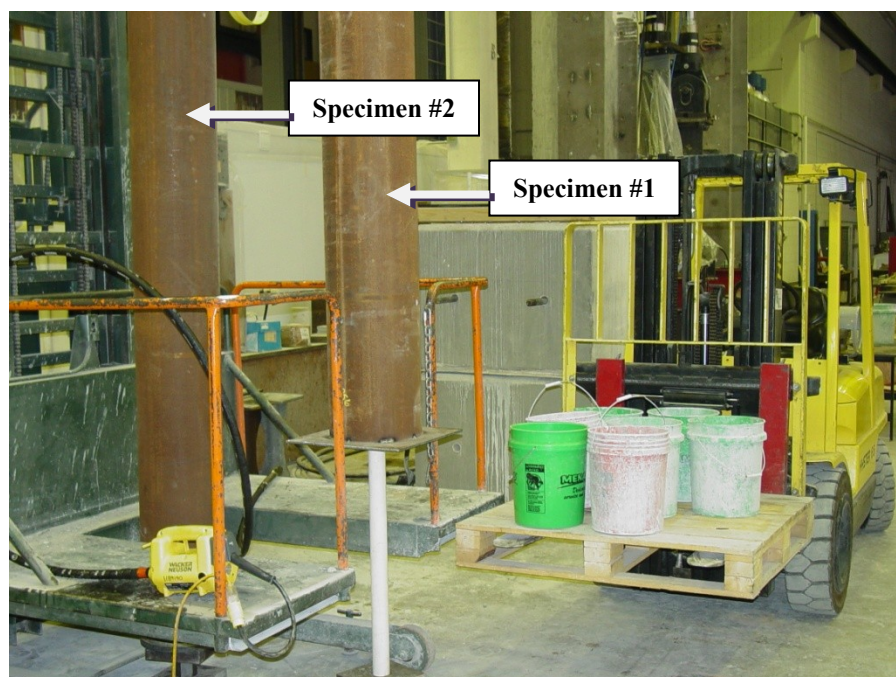


Figure 4-11- Preparing the pipes for the pour

The concrete was poured directly to the cap's cast, while buckets were filled with concrete and dumped into the pipes from the top. The buckets were lifted using the lift truck. A long concrete vibrator was used to minimize the air voids in the concrete.

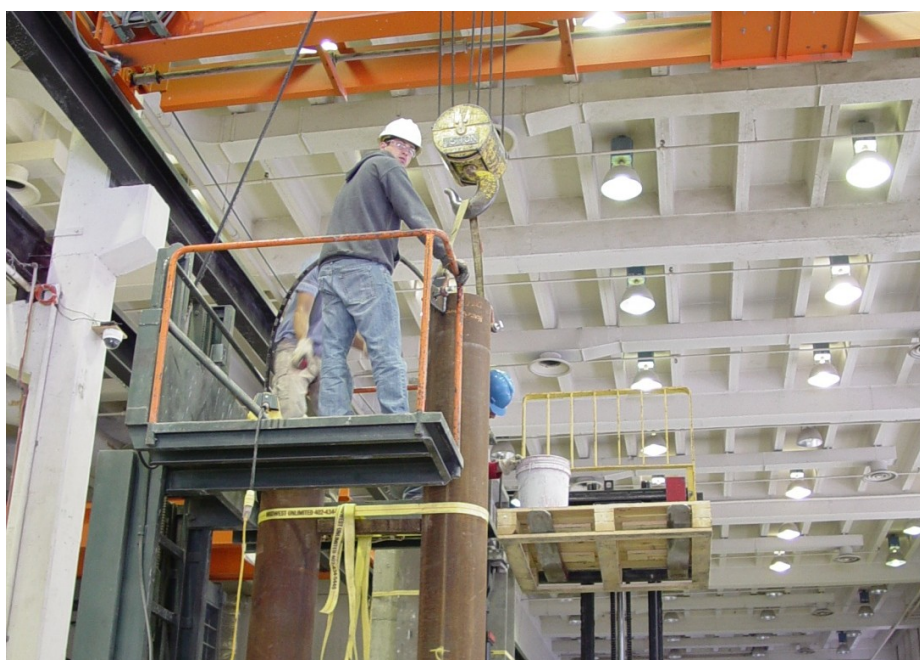


Figure 4-12- Pouring concrete into the pipe



Figure 4-13- First pour into Specimen #2

As mentioned the concrete was poured up to half of the cap to hold the embedded plate in place. The surface of the concrete was scratched to help the bond to the next pour.

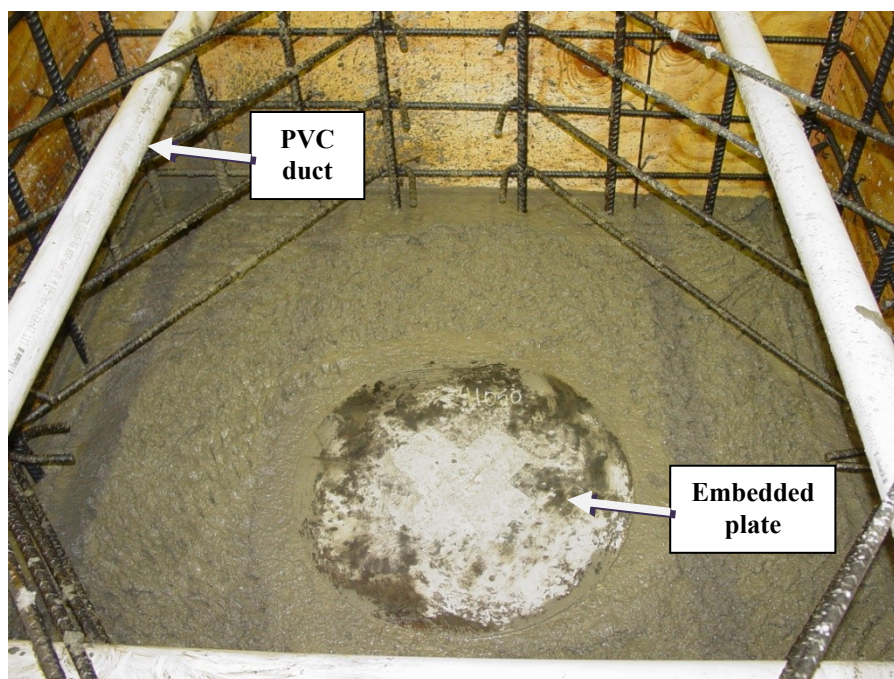


Figure 4-14- Specimen #2 after first pour (embedded plate at the middle)

A total of 12 samples (6x12” cylinders) were taken from the mix.

4.2.2.2. Second Pour (March 10th 2011)

In the second pour on March 10th the cap of specimen #1 was cast. In preparation for casting, the CFT was held vertical using the crane. Additional rebar were placed around the pipe and tied to the rebar cage to keep the CFT in place during the pour.

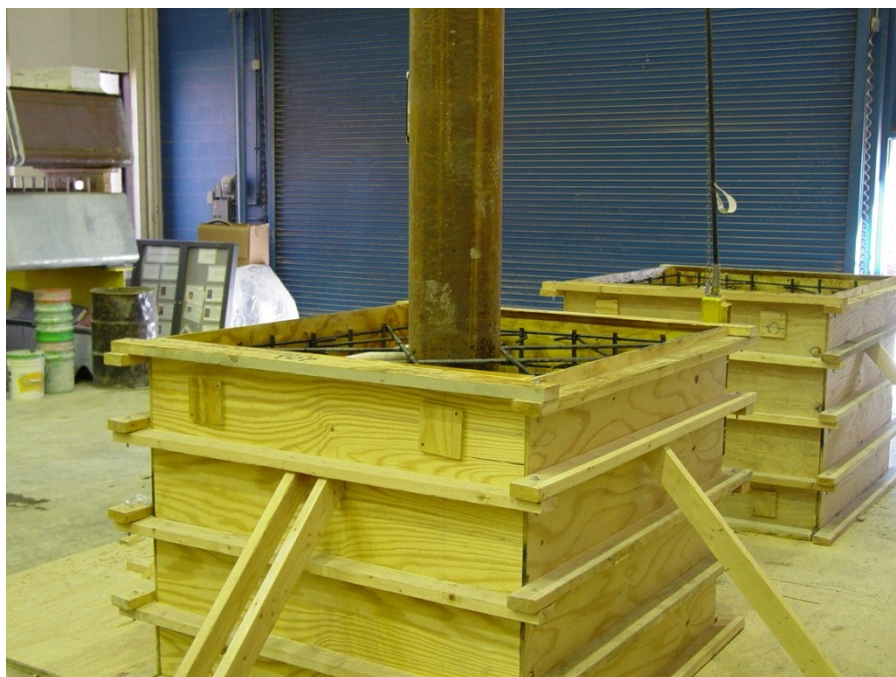


Figure 4-15- Specimen #1 before the pour

During the pour, the south side of the cast started to push out. Apparently, the lateral support from the 2x4” bars was not enough. Fortunately, by providing extra support and tying the dywidags passed through the PVC pipes the specimen was saved.



Figure 4-16- Specimen #1 after the pour

A total of 12 samples (6x12" cylinders) were taken from the mix.

4.2.2.3. Third Pour (March 15th 2011)

On March 15th, the top half of specimen #2's cap was cast.

The inner diameter elastomer fabricated for specimen #2 was less than the outer diameter of the CFT and did not fit around it. So, the elastomer was cut in half and using hose strap ties it was held around the CFT's head. Three threaded rods were tapped to the CFT and were passed through copper ducts. These rods were used to measure the deflection of the embedded portion of the pipe. The distance of the rods from the end face of the pipe was 2 ¼, 8 ¼, 18 ¼".



Figure 4-17- Preparing specimen #2

Silicone was used to seal the seam along the cut, and prevent the penetration of fresh concrete. Then the CFT was held against the embedded plate and a large dywidag was passed through the middle PVC to assure the correct alignment of the specimen.



Figure 4-18- Preparing specimen #2

The final set of concrete was cast on March 15th when the bottom half of the cap was 8 days old at the time (first pour).

4.2.3. Preparing the Test Setup

After the concrete pours, the load point that includes rectangular box around the pipe and the spreader beam was built. First, the rectangular box was assembled and then the

spreader beam was welded on top of that. Then, grout was injected to the box through holes made on the bottom flange of the spreader beam to ensure uniform distribution of the load throughout the test. The support blocks were then stacked and the specimen was lifted and placed on top of them.



Figure 4-19- Placing specimen #1 on top of support blocks

The gap between the blocks was filled with hydrostone in order to distribute the pressure evenly. Four wood panels were bolted on the two sides of the gaps and the openings were filled with silicone to seal the space between the blocks and facilitate the pumping of hydrostone. Two holes were driven in the wood panels on each side. A hand pump was then used to pump the fresh hydrostone into the gaps.



Figure 4-20- (a) preparing fresh hydrostone (b) pumping the hydrostone into the gaps

After placing the blocks, four vertical rods were post-tensioned to the lab floor using a hand pump and some washers. The target pressure in post-tensioning was 8.0 ksi.

Then the actuators were aligned completely vertical, followed by fastening eight bolts that tie the thick plates to the spreader were, with wrench.

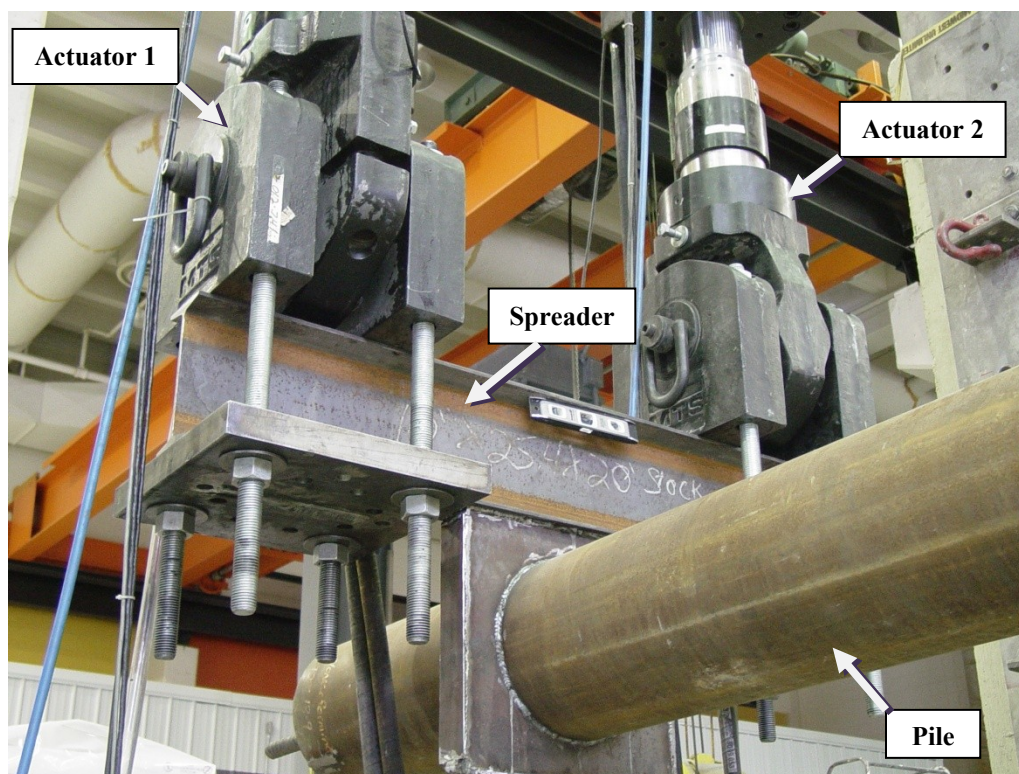


Figure 4-21- Load point configuration

4.2.4. Test Procedure on Specimen #1

4.2.4.1. Loading Schedule

Two regimens were considered for the experimental testing of specimen #1. In the first stage, increasing cyclic loads were applied in the form of tip displacement. In the second stage, constant cyclic load at two different axial load levels was applied, and finally increasing cyclic load until failure was conducted. Three load stages were considered.

- Increasing Cyclic Loading Up to ± 1 inch
- Constant Cyclic Loading (± 0.5 inch)
- Increasing Cyclic Loading up to Failure

4.2.4.1.1. Increasing Cyclic Loading Up to 1 inch

The following table shows the initial loading schedule. Note that two different axial load levels were applied.

Table 4-3- Load stage 1 (specimen #1)

Load stage	Disp. range (\pm in)	Cycles	Cumulative cycles	Axial load (kips)	Freq. (Hz)	Time (sec)
1-1-1	0.10	5	5	60	0.1	50
1-1-2	0.25	5	10	60	0.1	50
1-1-3	0.50	5	15	60	0.1	50
1-1-4	0.75	5	20	60	0.1	50
1-1-5	1.00	5	25	60	0.1	50
1-2-1	0.10	5	30	120	0.1	50
1-2-2	0.25	5	35	120	0.1	50
1-2-3	0.50	5	40	120	0.1	50
1-2-4	0.75	5	45	120	0.1	50
1-2-5	1.00	5	50	120	0.1	50

The following figure schematically show the displacement amplitude applied during load stage 1.

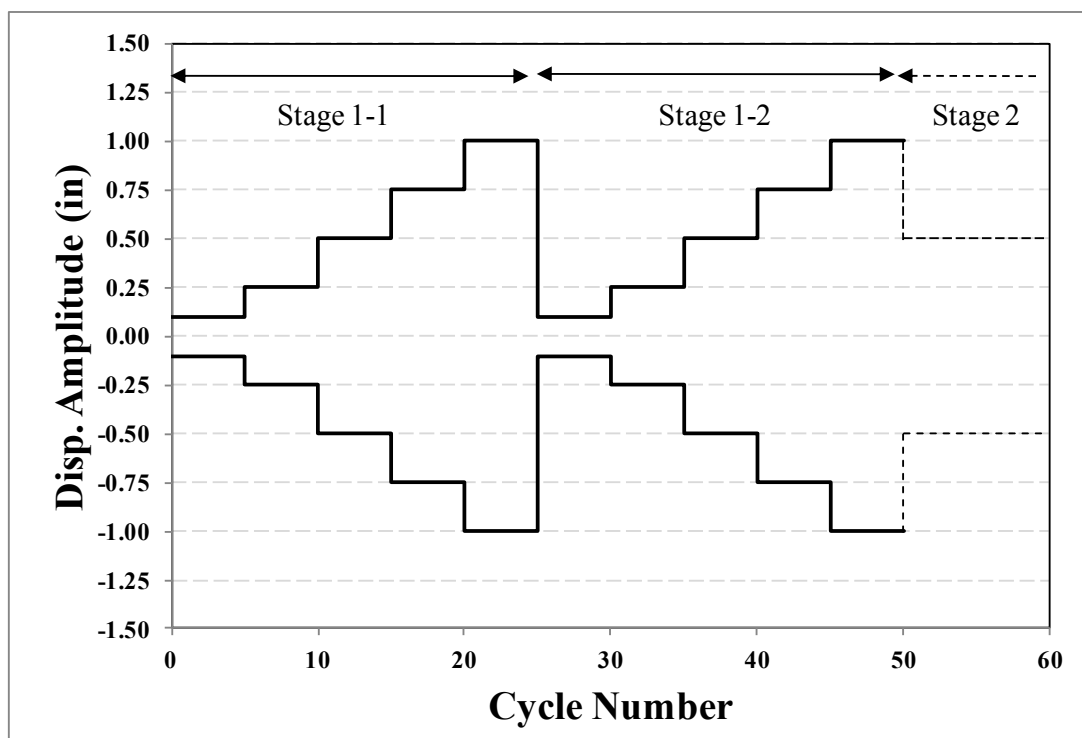


Figure 4-22- Typical pattern of lateral loading for stage 1 (specimen #1)

4.2.4.1.2. Constant Cyclic Loading (± 0.5 inch)

Constant cyclic loads were applied under two different axial load levels at ± 0.50 inch cycles. Although the initial plan was to conduct the constant cyclic loading at ± 1.00 , it was decided to reduce this range to ± 0.50 in since small residual strains were observed after load stage 1.

Table 4-4- Load stage 2 (specimen #1)

Load stage	Disp. range (\pm in)	Cycles	Cumulative cycles	Axial load (kips)	Freq. (Hz)	Time (hr)
2-1	0.50	36500	36550	60	0.2	20.2
2-2	0.50	36500	73050	120	0.2	20.2

4.2.4.1.3. Increasing Cyclic Loading up to Failure

The following table shows the loading schedule for stage 3. Target axial load was 120 kip in all stages. Note that the loading frequency was reduced for larger displacement levels.

Table 4-5- Load stage 3 (specimen #1)

Load stage	Disp. range (±in)	Cycles	Cumulative cycles	Axial load (kips)	Freq. (Hz)
3-1	0.25	5	73055	120	0.1
3-2	0.50	5	73060	120	0.1
3-3	0.75	5	73065	120	0.1
3-4	1.00	5	73070	120	0.1
3-5	1.25	5	73075	120	0.1
3-6	1.50	5	73080	120	0.1
3-7	1.75	5	73085	120	0.1
3-8	2.00	5	73090	120	0.06
3-9	2.25	5	73095	120	0.06
3-10	2.50	5	73100	120	0.06
3-11	2.75	5	73105	120	0.06
3-12	3.00	5	73110	120	0.04
3-13	3.25	5	73115	120	0.04
3-14	3.50	5	73120	120	0.04
3-15	3.75	5	73125	120	0.04
3-16	4.00	5	73130	120	0.04
3-17	4.25	5	73135	120	0.02
3-18	4.50	5	73140	120	0.02
3-19	4.75	5	73145	120	0.02

4.2.4.2. Conducting the Test

4.2.4.2.1. Load Stage 1

Increasing cyclic loads were applied to the specimen based on information provided in Table 4-3. Note that two axial load levels (60 kip and 120 kip) were applied. At first, one of the smaller rams (120 kip capacity) was used to exert the axial load. Since the effective area of these rams was smaller compared to the bigger rams (240 kip capacity) the pressure in the line was very high and resulted in leakage and pressure drop. To stop leakage, first the pressure cell was changed since it was leaking, but the load dropped again quickly. Then, the check valve was replaced, but the pressure dropped with almost the same rate. Subsequently, the small ram (120 kip) was replaced with another small ram with no success. Finally it was decided to change the ram to bigger ones (240 kip rams). As a result, the line pressure dropped and solved the leakage problem.

No visible distress was observed during or after the test. The cap remained intact and the pipe was almost the same as beginning. Small residual strains were tracked at load stage 1-1-5 (± 1.00 in). The axial load level was almost constant throughout the test.

4.2.4.2.2. Load Stage 2

Constant cyclic load was applied at two axial load levels as described in Table 4-4. The lateral displacement level was ± 0.50 in, at which the pile was cycling in the elastic range. No visual damage was observed during the test. The whole test took about 5 days.

4.2.4.2.3. Load Stage 3

Incremental cyclic loading was done as described in Table 4-5.

At load stage 3-8 (± 2.00 in) it was noticed that the west ram's swivel was not rotating smoothly. DS40 lubricant was used all around the swivel to facilitate its rotation with no success and noticeable kicks were observed throughout the rest of the test. However, this had negligible effect on the results.

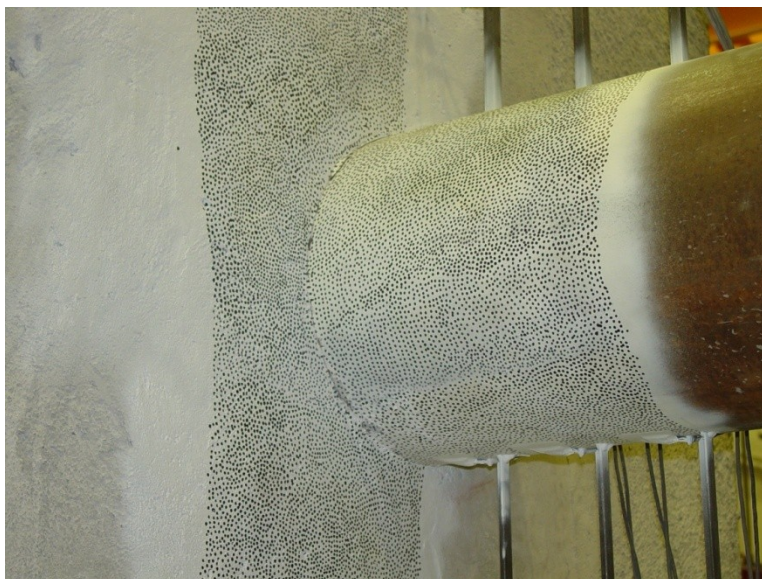


Figure 4-23- Condition of the connection at load stage 3-8 (± 2.00 in)

After load stage (± 2.00 in), the 2" plates were spot welded to the both sides of the I-shaped spreader beam to make sure that because of swivel rotation no slip will occur. Initially, the spreader was clamped between the swivels' foot and the thick plates.

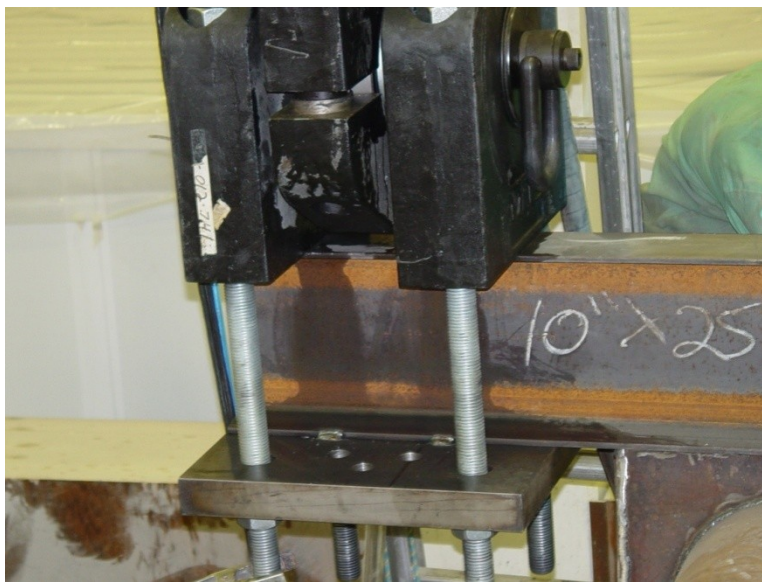


Figure 4-24- Welding the spreader beam's bottom flange to thick plate

Excessive deformation was observed close to the connection at stage 3-12 (± 3.00 in). Elephant foot failure mode was noticed at the top and the bottom of the specimen. At this time, the paint over the pipe started to peel off because of large strains. As a result of large deformation around the rod holding PT1, PT2 reached its stroke and needed reconfiguration.



Figure 4-25- (a) Excessive deformation near the first gages at load stage 3-16 (± 3.00 in) (b) large deformation around the rod holding PT1

The loading stages 3-1 to 3-16 was carried out on Friday May 13 2011. Since one of the pots reached its stroke and needed reconfiguration, the rest of the test was done on Tuesday May 17 2011.

Small crack at the bottom of the pipe around the strain gage GB1 was observed at stage 3-18 (± 4.50 in). At this load stage a little load drop was noticed in the last cycles. Strain gages GB1 and GT1 came off at stage 3-18 (± 4.50 in).



Figure 4-26- Condition of connection at load stage 3-18 (± 4.50 in) (a) huge crack at the bottom (b) large deformation at the top

At load stage 3-19 (± 4.75 in) the crack was fully opened and the crushed concrete came out of the cracked zone. The axial load dropped dramatically during this stage and the test was stopped.



Figure 4-27- Crack completely opened at load stage 3-19 (± 4.75 in)

4.2.5. Test Procedure on Specimen #2

4.2.5.1. Loading Schedule

Three regimens were considered for the experimental testing of specimen #2. In the first stage, increasing cyclic loads were applied in the form of tip displacement. In the second stage, constant cyclic load at 120 kip axial load level was applied, and finally ultimate loading up to failure.

Three load stages were considered in the loading schedule.

- Increasing Cyclic Loading Up to ± 4.5 inch
- Constant Cyclic Loading (± 4.25 inch)
- Ultimate loading up to Failure

4.2.5.1.1. Increasing Cyclic Loading Up to 4.5 inch

The following table shows the loading schedule for stage 1. Target axial load in all stages was 120 kip.

Table 4-6- Load stage 1

Load stage	Disp. range (±in)	Cycles	Cumulative cycles	Axial load (kips)	Freq. (Hz)
1-1	0.10	5	5	120	0.05
1-2	0.25	5	10	120	0.05
1-3	0.50	5	15	120	0.05
1-4	0.75	5	20	120	0.05
1-5	1.00	5	25	120	0.05
1-6	1.25	5	30	120	0.05
1-7	1.50	5	35	120	0.05
1-3a	0.50	5	40	120	0.05
1-5a	1.00	5	45	120	0.05
1-7a	1.50	5	50	120	0.05
1-3b	0.50	5	55	120	0.05
1-5b	1.00	5	60	120	0.05
1-7b	1.50	5	65	120	0.05
1-8	1.75	5	70	120	0.05
1-9	2.00	5	75	120	0.05
1-9a	2.00	5	80	120	0.05
1-10	2.25	5	85	120	0.05
1-11	2.50	5	90	120	0.05
1-3c	0.50	5	95	120	0.05
1-5c	1.00	5	100	120	0.05
1-7c	1.50	5	105	120	0.05
1-9c	2.00	5	110	120	0.05
1-11c	2.50	5	115	120	0.05
1-12	2.75	5	120	120	0.05
1-11d	2.50	25	145	120	0.05
1-13	3.00	5	150	120	0.05
1-14	3.25	5	155	120	0.025
1-15	3.50	5	160	120	0.025
1-16	3.75	5	165	120	0.025
1-17	4.00	5	170	120	0.025
1-7e	1.50	5	175	120	0.05
1-11e	2.50	5	180	120	0.05
1-15e	3.50	5	185	120	0.025
1-17e	4.00	5	190	120	0.025
1-18	4.25	5	195	120	0.025
1-19	4.50	5	200	120	0.025
1-18f	4.25	100	300	120	0.025
1-11g	2.50	5	305	120	0.05
1-15g	3.50	5	310	120	0.025
1-7g	1.50	5	315	120	0.05
1-3g	0.5	5	320	120	0.05
1-18h	4.25	100	420	120	0.04

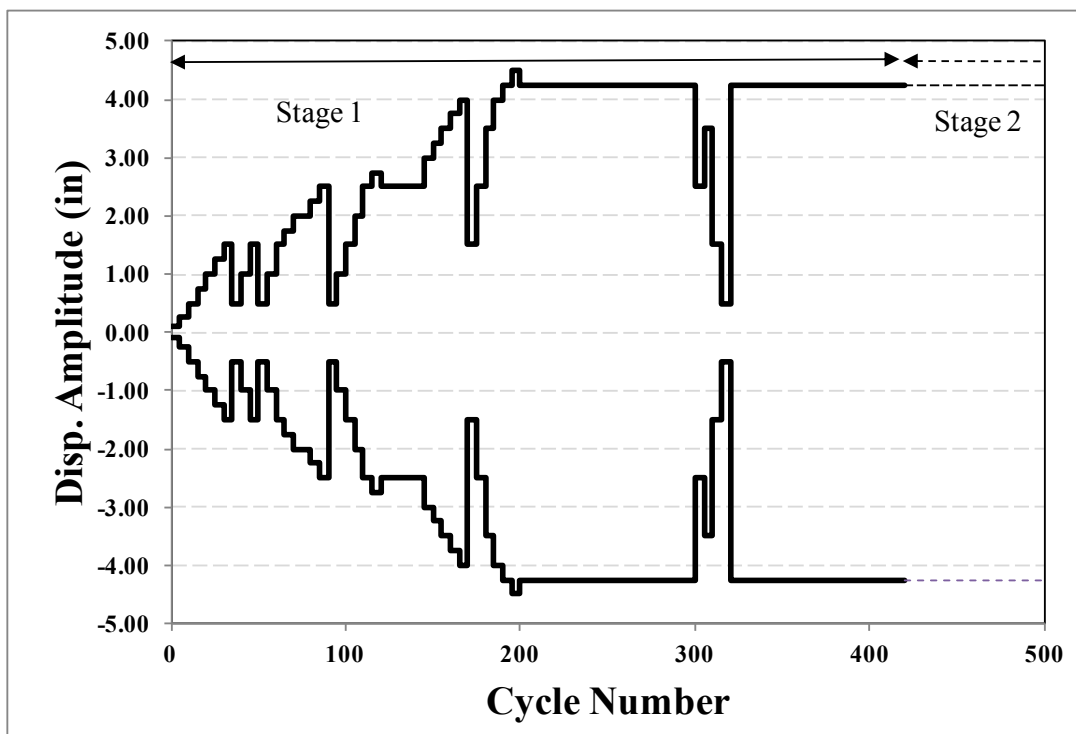


Figure 4-28- Typical pattern of lateral loading for stage 1 (specimen #2)

4.2.5.1.2. Constant Cyclic Loading (± 0.5 inch)

The following table shows the loading information for constant cyclic loading stage.

Table 4-7- Load stage 2 (specimen #2)

Load stage	Disp. range (\pm in)	Cycles	Cumulative cycles	Axial load (kips)	Freq. (Hz)
2-1	4.25	16000	73050	120	0.04

4.2.5.1.3. Ultimate Loading

At this load stage, the specimen was planned to be loaded until failure happens. It was not clear if the specimen will fail with available actuators stroke (10 in).

4.2.5.2. Conducting the Test

4.2.5.2.1. Load Stage 1

Increasing cyclic loading was applied on August 18th 2011 as described in Table 4-6. To investigate the behavior after unloading and check the damage to the specimen, the displacement range was reduced in several stages.

Loud noise was heard at the last cycle of load stage 1-9 (± 2.00 in). No visual damage was observed and the test was continued. At first, it was thought that the noise is because of sliding of steel against each other. However, later on the noise was referred to the slippage of the elastomer against the pipe's surface. At the beginning, this noise was noticed when the specimen traveled down from extreme top point.



Figure 4-29- Condition of the connection at stage 1-9 (± 2.00 in)

After a while during the test the noise was softened. Then, the noise was also noticed when the pile traveled on the bottom extreme at load stage 1-11d (± 2.50 in).



Figure 4-30- Condition of the connection around peak movement at stage 1-11d (± 2.50 in)

At load stage 1-15 (± 3.50 in) the seam in the elastomer started to open. The first row spring pots (PB1 and PT1) reached their stroke at load stage 1-16 (± 3.75 in).

Small spalling of concrete around the elastomer was observed after load stage 1-17 (± 4.00 in). This was because of large deformations and bulging of the elastomer.

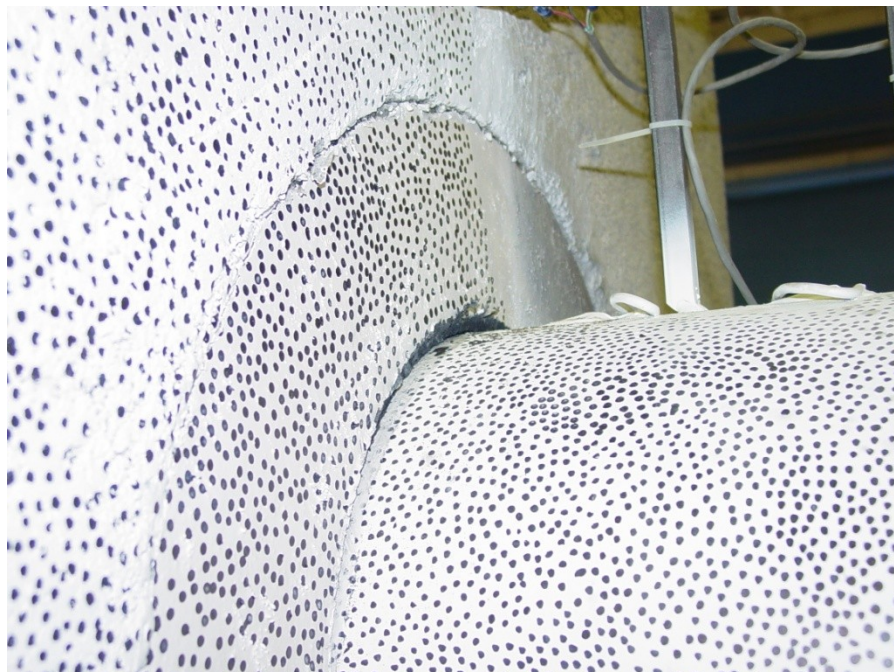


Figure 4-31- Condition of the top of the connection after stage 1-18h (± 4.25 in)

At load stage 1-19 (± 4.50 in) no visual damage was observed. Also, the noise was noticed only at the bottom extreme.

The string pots located on the top of the specimen were gone during the load stage 1-18f (± 4.25 in).

4.2.5.2.2. Load Stage 2

Constant cyclic loading (± 4.25 in) was applied on August 18 2011 after finishing the first load stage. During the initial cycles, it was decided to lubricate the surface between the elastomer and the steel pipe. WD40 was sprayed on the surfaces when the pipe was at the top and bottom extreme and the gap was wide open. Engine oil was also dispensed from the top three ducts placed for string pots PTBN, PTBM, PTBS. As a result, the noise was diminished after about 15 minutes.

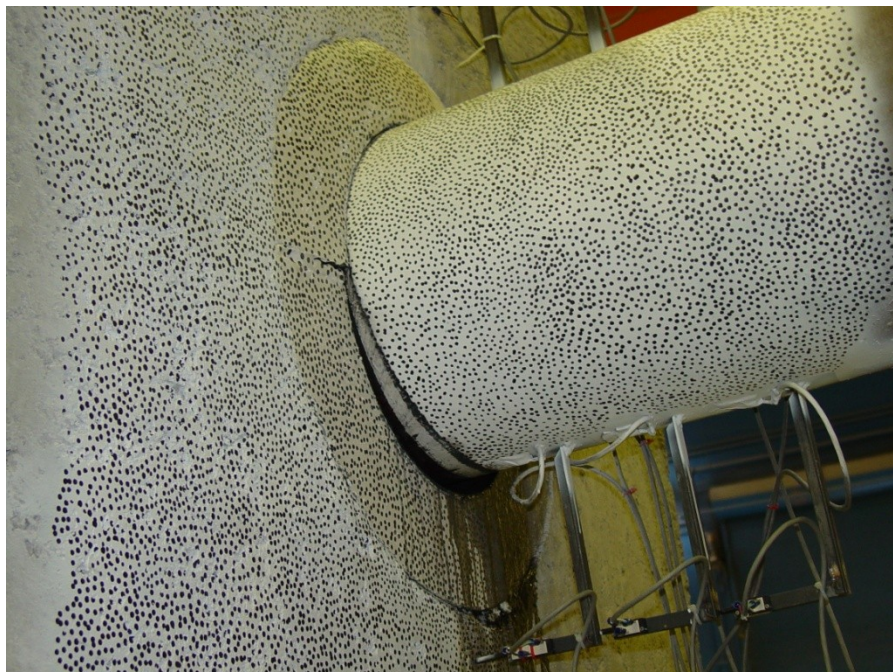


Figure 4-32- Specimen #2 after lubrication at peak displacement in load stage 2 (± 4.25 in)

On August 19th around 10:00 pm the test was stopped after around 600 cycles. The hydraulics was overheated. The test was restarted around midnight.

The noise was noticed again around noon on Aug. 20th. At this time, the top pots were switched to pile deflection outside the detail located at 2", 8", and 14" from the cap.

4.2.5.2.3. Load Stage 3

The ultimate test was carried out on Sep. 12th 2011. To provide more stroke during the ultimate test, four 11" cuts from a junk I section was cut and placed between the swivel's foot and the spreader beam. Calculations were made on capacity of the steel section for shear, and local buckling.

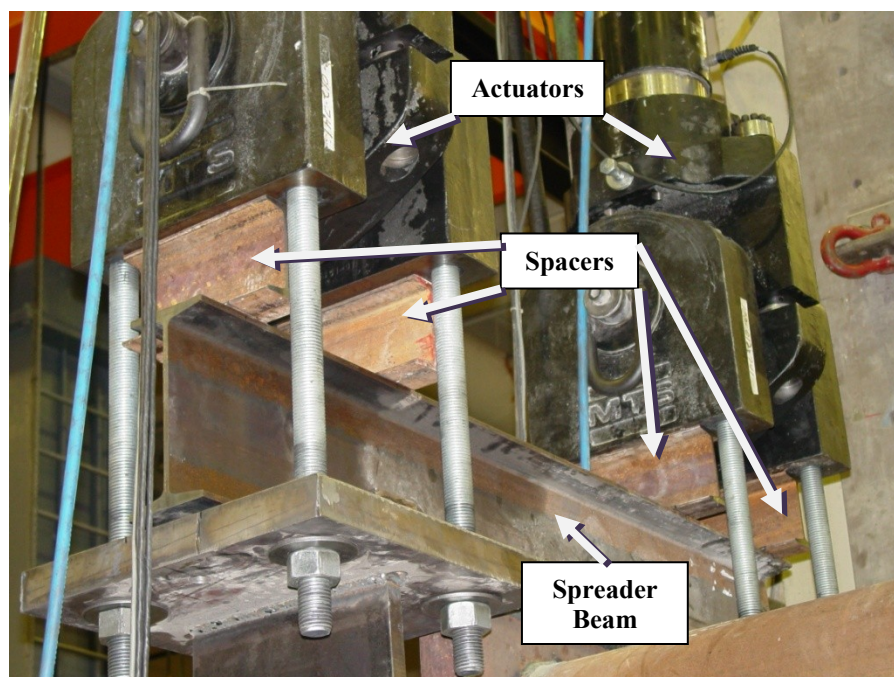


Figure 4-33- Spacers used for additional stroke

I-section was welded to the spreader to avoid possible slippage at large deformations.

The following figure depicts the setup at ultimate test.

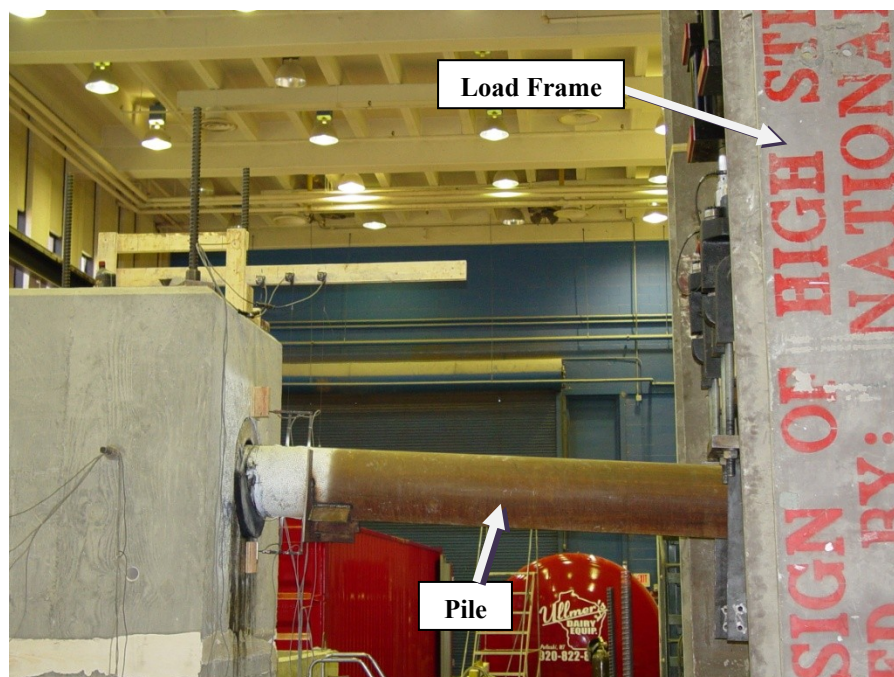


Figure 4-34- Ultimate test (specimen #2)

Unfortunately, at about 6 in deflection the dywidag, which applied the axial load throughout the test, failed and projected to the temporary storage room in front of the test setup. The front portion of the dywidag, which was almost 13ft, traveled through the back wall of the storage room and was stopped in the opposite wall. This accident happened when the axial load level (119 kip) was almost half the capacity of the rod. Fortunately, this accident did not cause any injuries or serious damage. The test was finished afterwards.



Figure 4-35- Failure of the dywidag

The following figure shows the failed section of the dywidag. Note that the failure happened right on the thicker section of the tread. After measurements it was found that the failure had happened next to the steel plates interface in the connection.



Figure 4-36- Failure of the dywidag

After finishing the test, the setup was disassembled and the CFT was extracted from the connection by welding two I sections to the sides of the pipe and using two hydraulic jacks as shown in Figure 4-37.

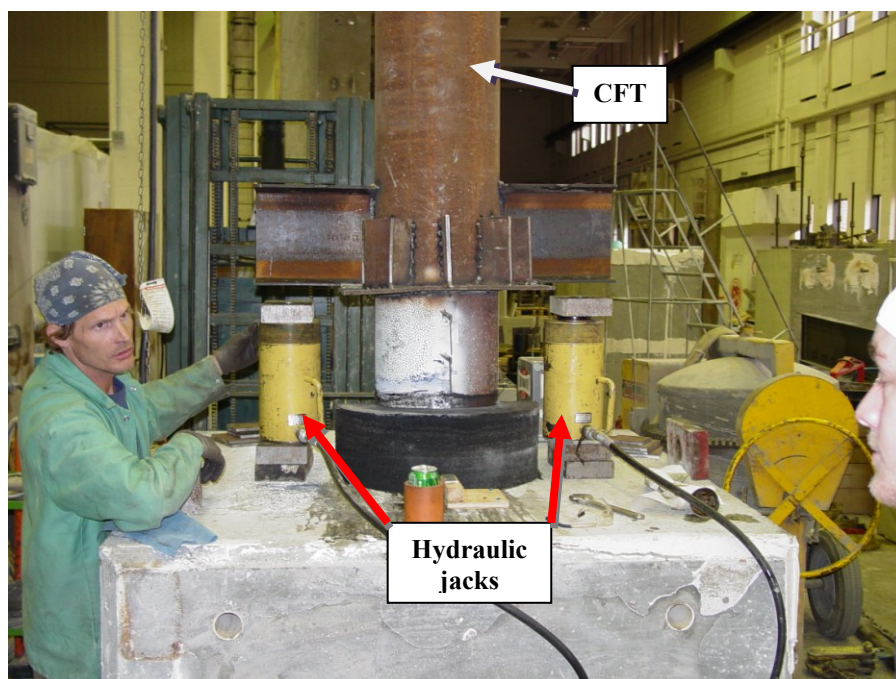


Figure 4-37- Setup used to Remove CFT

No serious damage was observed in the elastomer ring. However, the end of the CFT was damaged as the end plate was detached, and the pipe end was blossomed.



Figure 4-38- Pipe condition after the test

The embedded plate and the concrete behind it were intact and no damage was detected after removing the CFT. The analysis of results revealed that the damage has happened during the load stage 2 (constant cyclic loading). Apparently, weak weld and local crushing of the concrete had been the causes of this damage.

4.3. Analysis of Test Results

4.3.1. Specimen #1 (Fixed)

4.3.1.1. Load Stage 1

Figure 4-39 and Figure 4-40 show the load deflection of the specimen #1 at load stage 1-1 and 1-2 respectively. The lateral deflection of the pile is measured with a pot placed under the pipe at the load point (PB4). This value is slightly different from the target value (displacement of the rams) because of the deformation of the spreader beam. The load value is the sum of the applied loads by the two actuators.

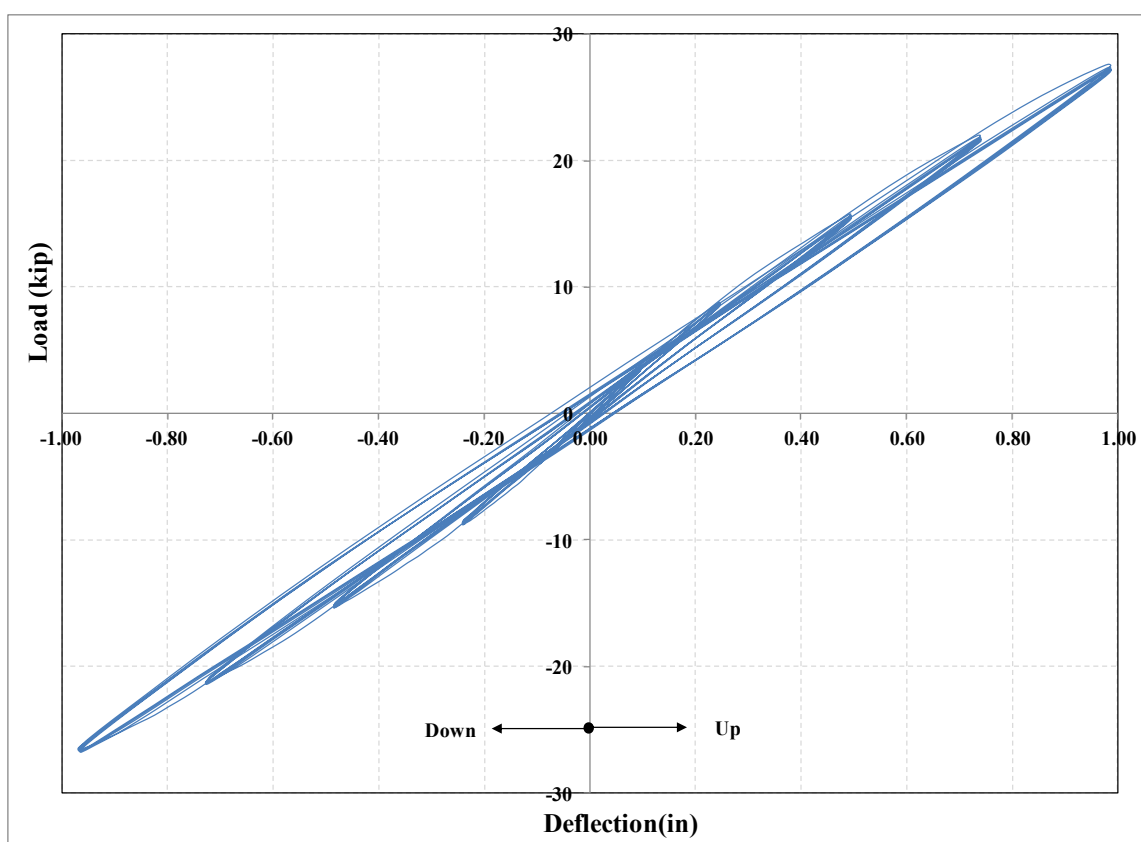


Figure 4-39- Load deflection curve for load stage 1-1

As shown, these curves are similar for the two different applied axial load levels.

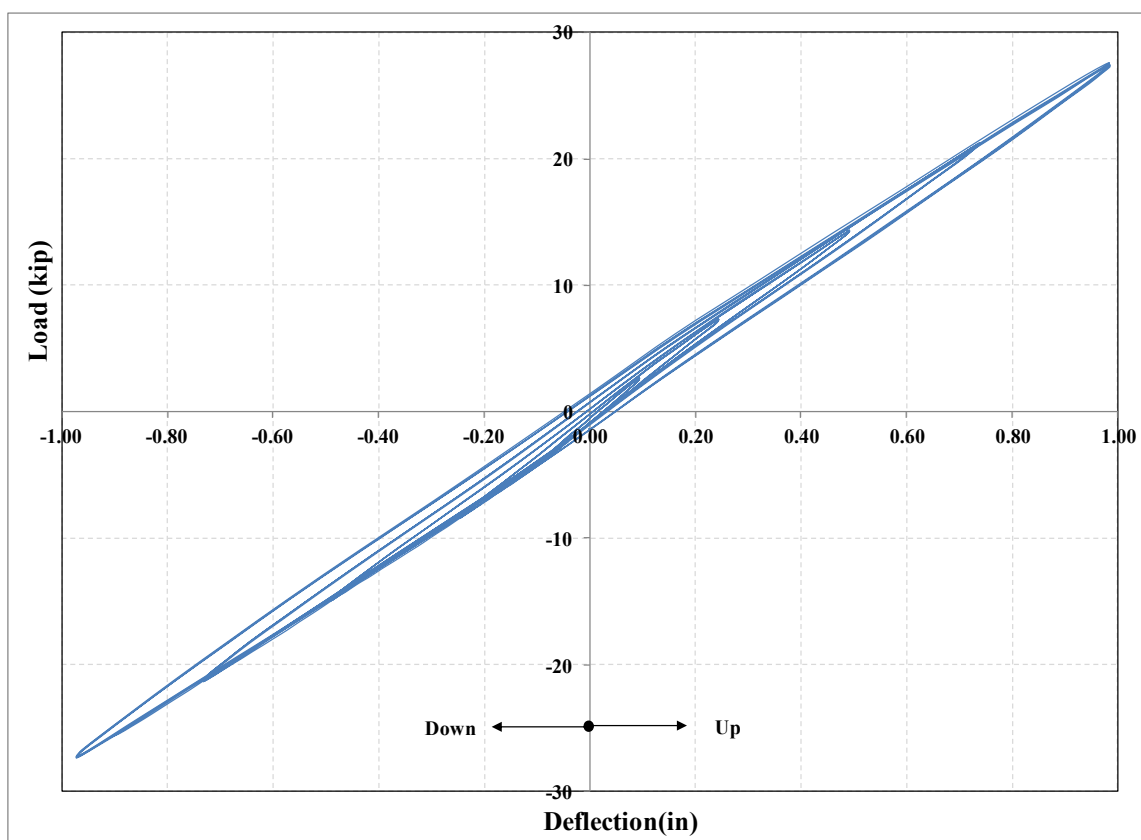


Figure 4-40- Load deflection curve for load stage 1-2

Figure 4-41 shows the envelope of load-deflection curve for load stages 1-1 and 1-2. The values in this chart represent the extreme values at the first cycle in each step. The stiffness at load stage 1-2 is smaller compared to load stage 1-1 to some extent, which can be referred to higher axial load level in the second stage. Also note that the initial slope of the load-deflection curve for stage 1-1 is larger. Although this type of connection is assumed as fixed, the results show minute rotation in specimen #1. At smaller movements of initial loadings, since there is cohesion between the pipe's surface and the surrounding concrete, rotation is not as easy. However, after some cycles, this bond fails and the stiffness drops. During the test a tiny gap was observed between at the connection which proves the rotation of the connection. The readings from the first row spring pots

also show some rotation which is further discussed in the moment-rotation calculations for load stage 1-3.

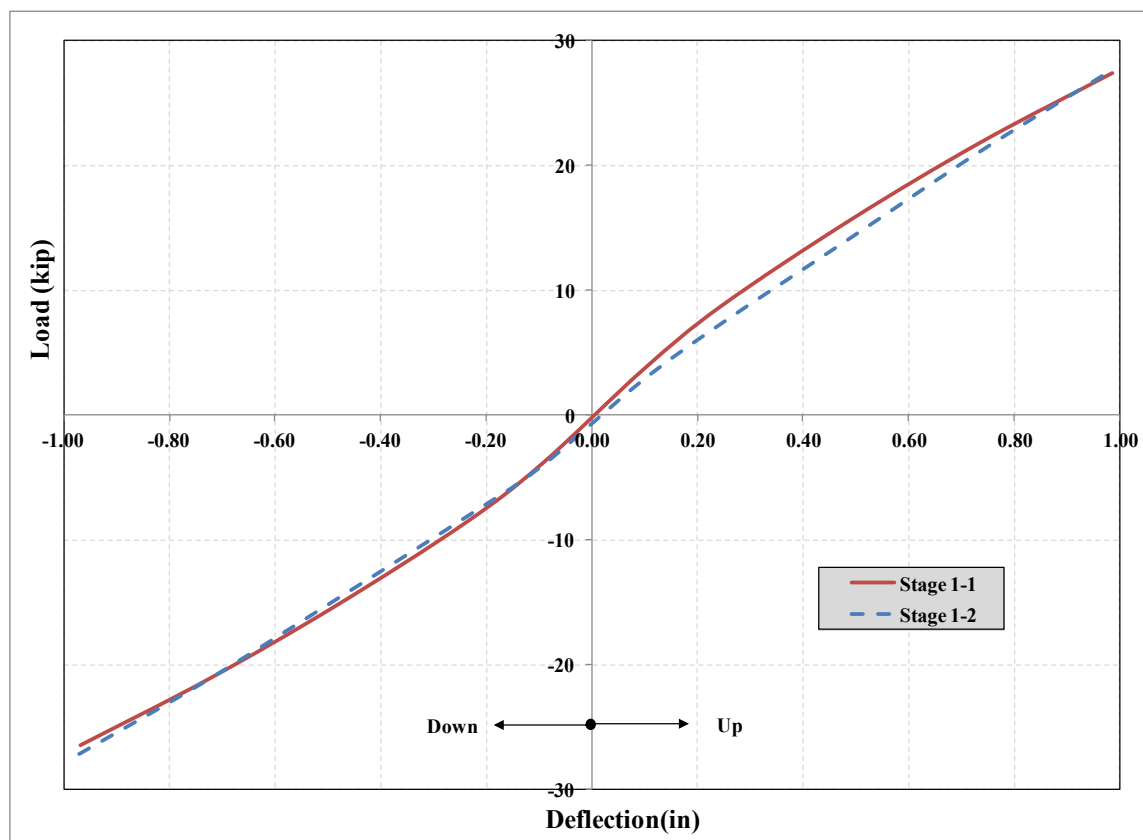


Figure 4-41- Envelope of load-deflection curve for stage 1

4.3.1.2. Load Stage 2

The maximum applied lateral load at load stage 2-1 is shown in Figure 4-42(a). As shown, this value remains relatively constant throughout the test. Also note that there is a small difference between the load applied by two actuators. Figure 4-42(b) shows the applied axial load during this load stage. The target axial load level for this load stage was 60 kips. Jumps in the curve are related to points when the axial load has been increased by the pump to cover gradual drops due to leakage of the hydraulic lining.

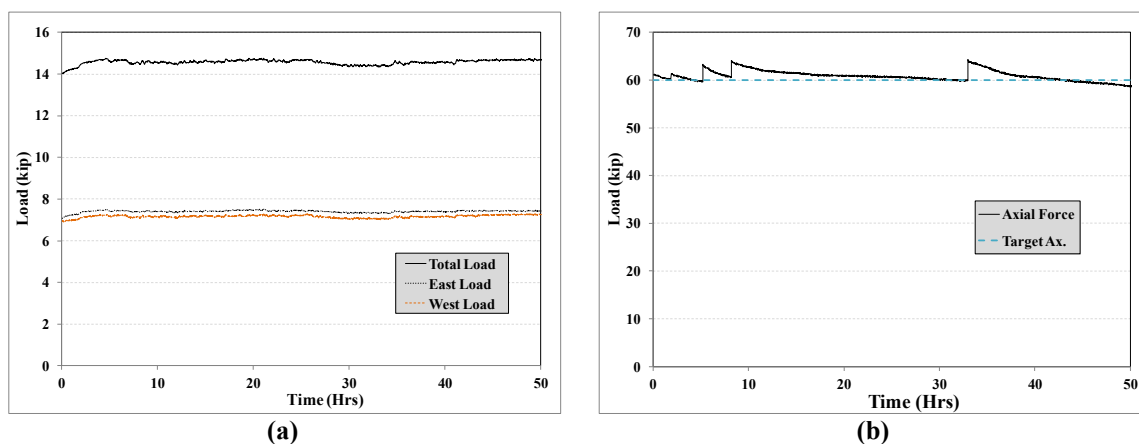


Figure 4-42- Applied forces in load stage 2-1 (a) maximum applied lateral load by actuators (b) applied axial load

The strains at peak displacements are shown in Figure 4-43. The strains in the top gages are close to each other, but the strain at the first strain gage in the bottom is almost twice as much as the other gages. As described earlier, some plasticity and residual strain was observed after load stage 1. This residual strain is propagated to load stage 2 and is apparent in data from strain gage GB1. It should be noted that the failure (at load stage 3) in the pipe happened on the bottom and close to this strain gage.

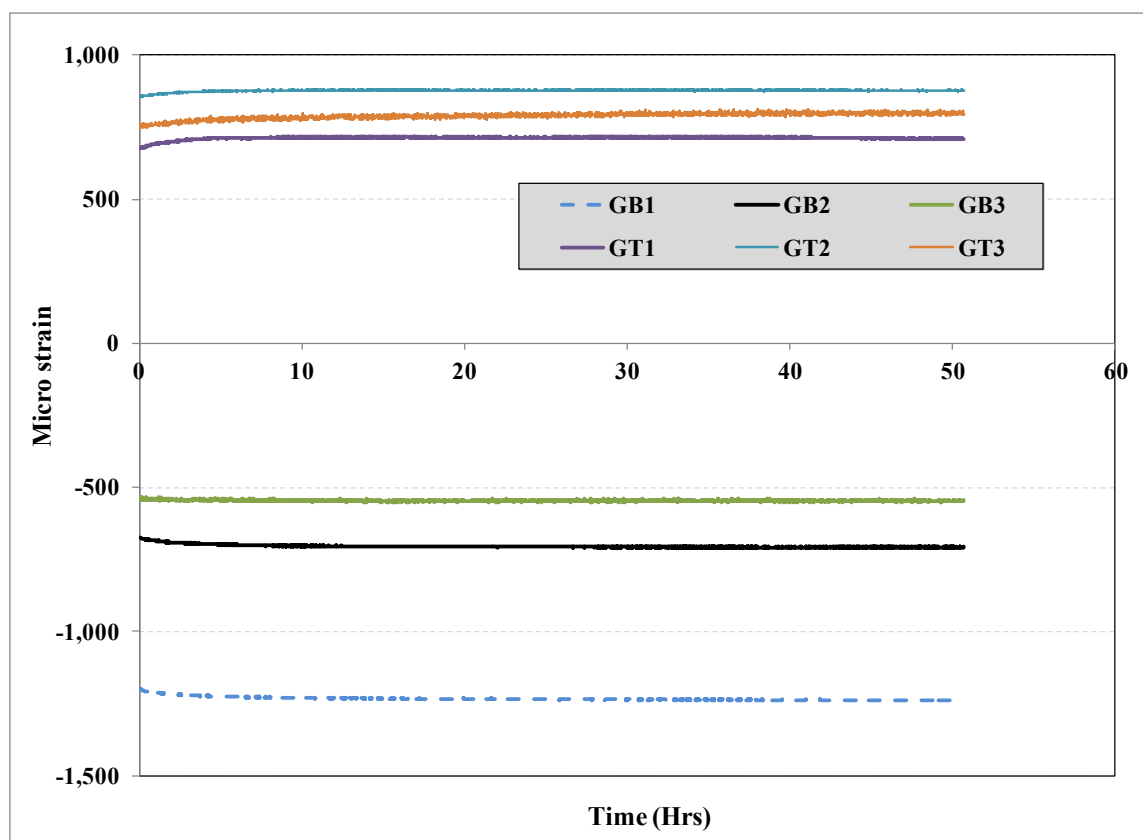


Figure 4-43- Maximum strains according to installed gages

4.3.1.3. Load Stage 3

Figure 4-44 shows the load deflection curves for this load stage. The load in this figure is the sum of the loads from two actuators. The deflection is based on the readings from the potentiometer placed under the load point (PB4). The drop in the last cycle at ± 4.50 in deflection is due to formation of the crack on the bottom of the pipe. As shown, the failure has happened at ± 4.75 in deflection where significant drop in the load is noticeable.

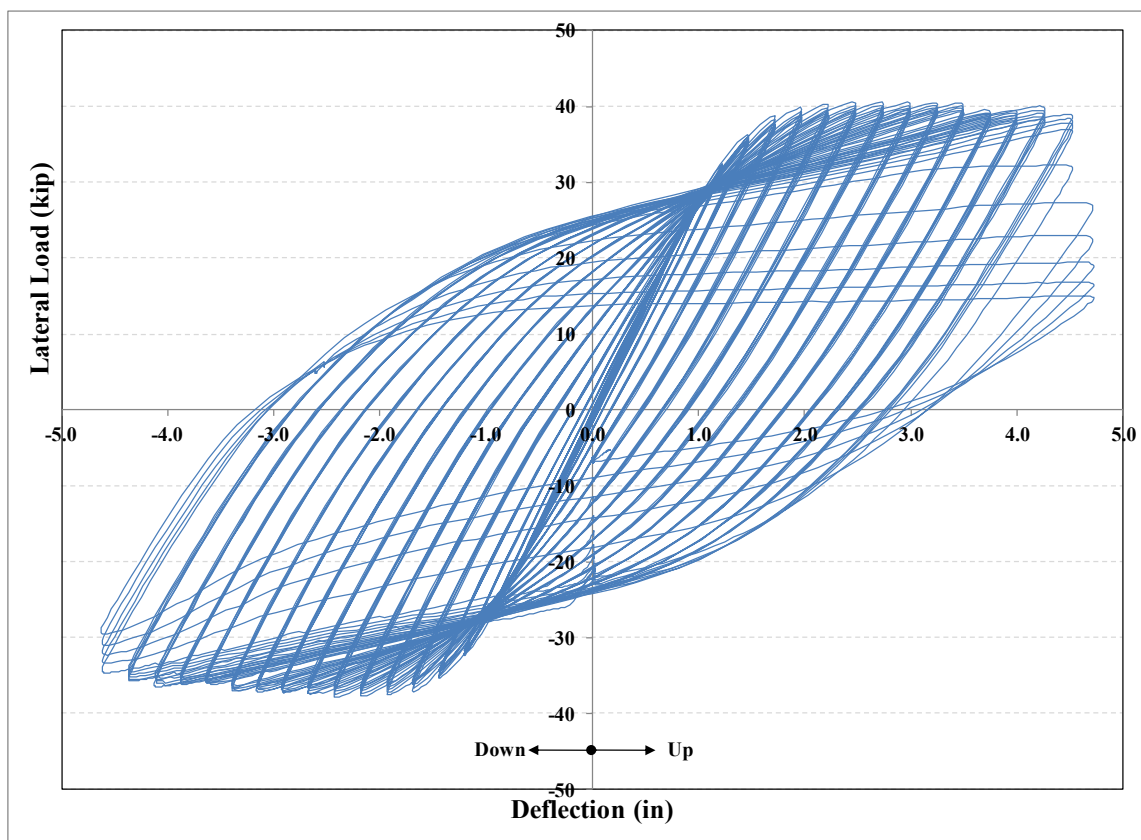


Figure 4-44- Load-deflection curve for specimen #1 at stage 3

The extreme load value in each step is depicted in Figure 4-45. These figures indicate that the specimen produce large hysteresis loops without significant drop in the level of the lateral load until ± 4.75 in. deflection where failure has happened.

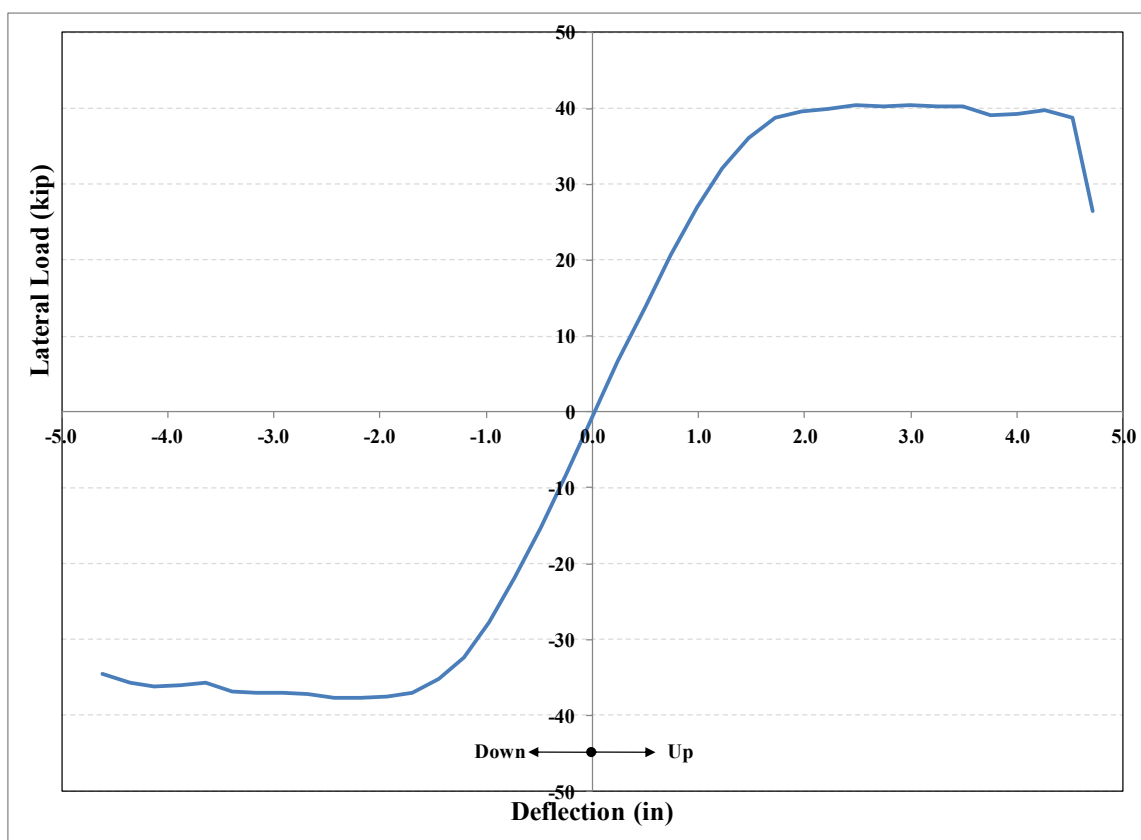


Figure 4-45- Envelope of load-deflection curve

The bending moment is calculated from the specimen geometry and loading and also taking into consideration the second order moments developed by the axial load due to the deflection of the CFT. The curvature is calculated using the strain data from the two strain gages located at the top and the bottom of the same cross section of the pipe. The average value of the curvature is calculated by dividing the difference between the two strains on the opposite sides of the cross section by the tube diameter. For convenience, positive curvature is considered to be in the direction of the initial loading.

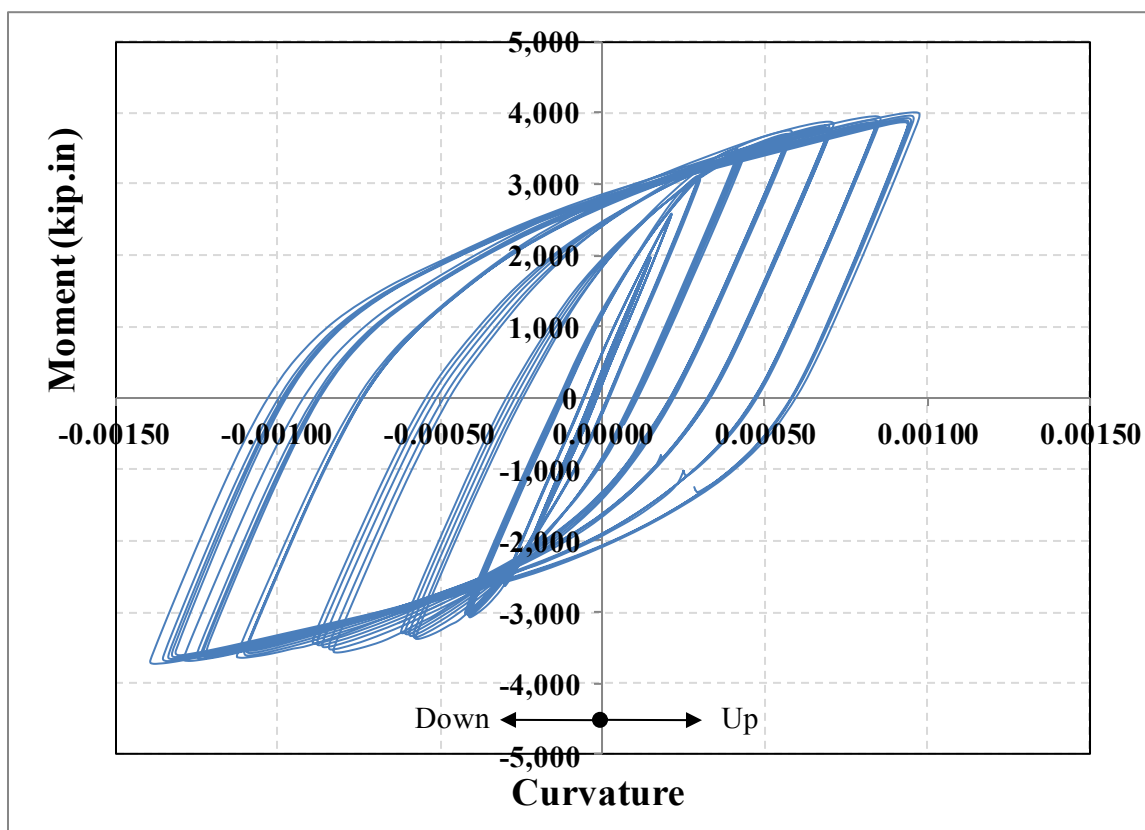


Figure 4-46- Moment-curvature curve for specimen #1 up to stage 3-10 (± 2.5 in)

The envelope of moment-curvature curve is shown in the following figure, compared to the estimated moment-curvature using the information provided in Appendix B.

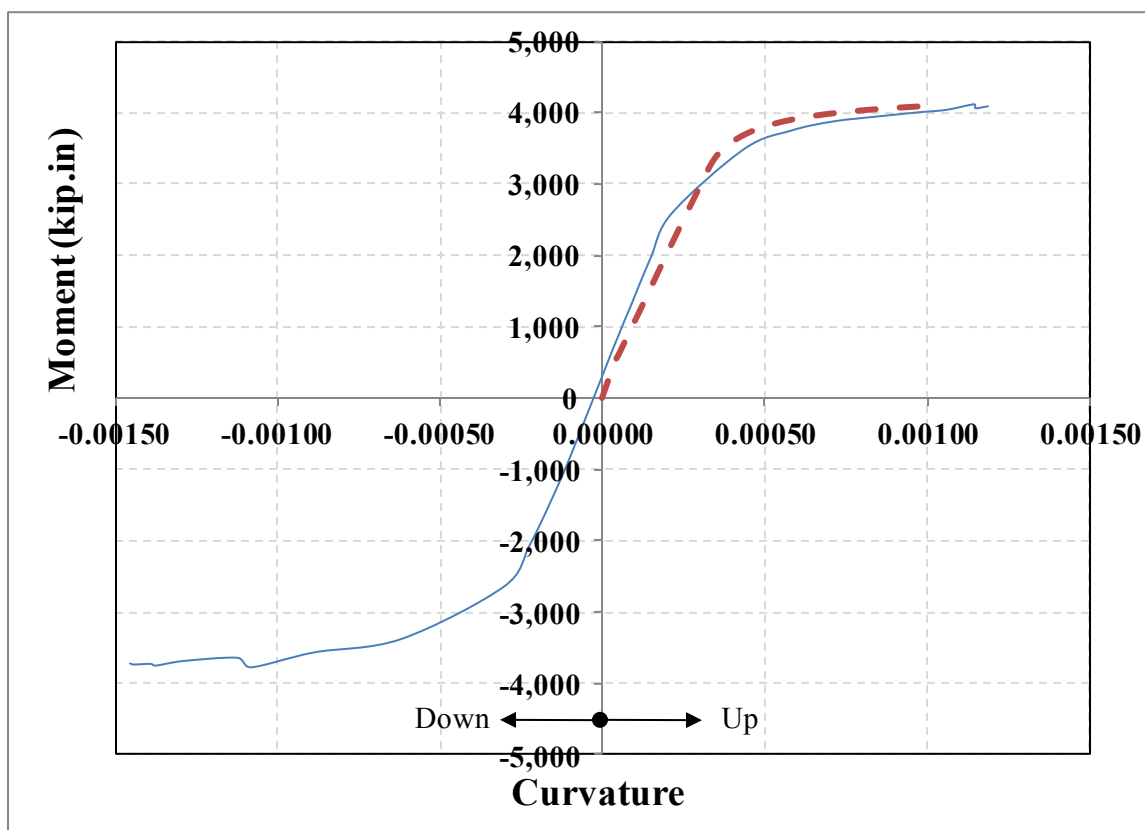


Figure 4-47- Moment-curvature curve for specimen #1 up to stage 3-10 (± 2.5 in)

Moment-rotation curve for this specimen is shown in Figure 4-48. The rotation is calculated based on the readings from the first row spring pots (PB1 and PT1). At larger deflections the because of local buckling of the pipe which happened at the vicinity of the rods holding the first row of spring pots (PB1 and PT1) the calculated values for rotation look strange and are not valid. The initial rotational stiffness of the connection is estimated about 694000 kip.in/rad.

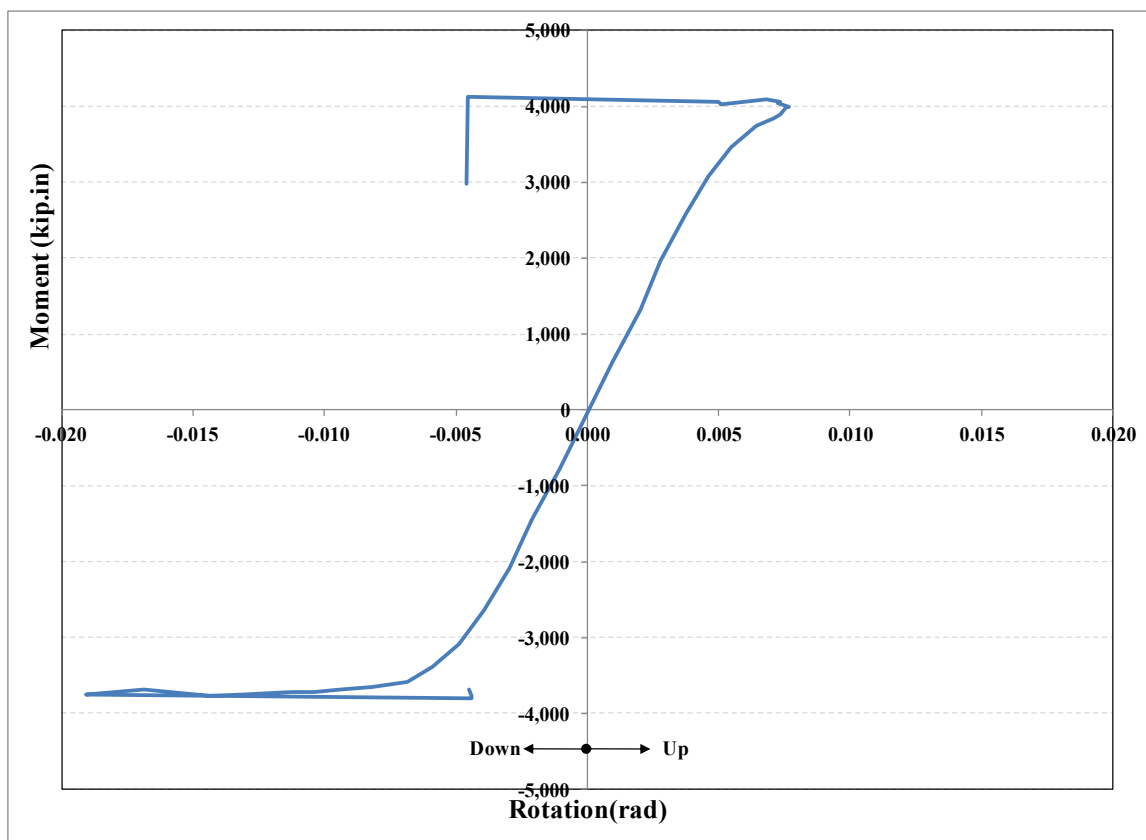


Figure 4-48- Moment-rotation curve for specimen #1

4.3.2. Specimen #2 (Pinned)

4.3.2.1. Load Stage 1

The following figure shows the load deflection points at extreme points for different load stages. Like specimen #1, the load in vertical axis is the sum of the loads from two actuators and the displacement is the reading from PB4.

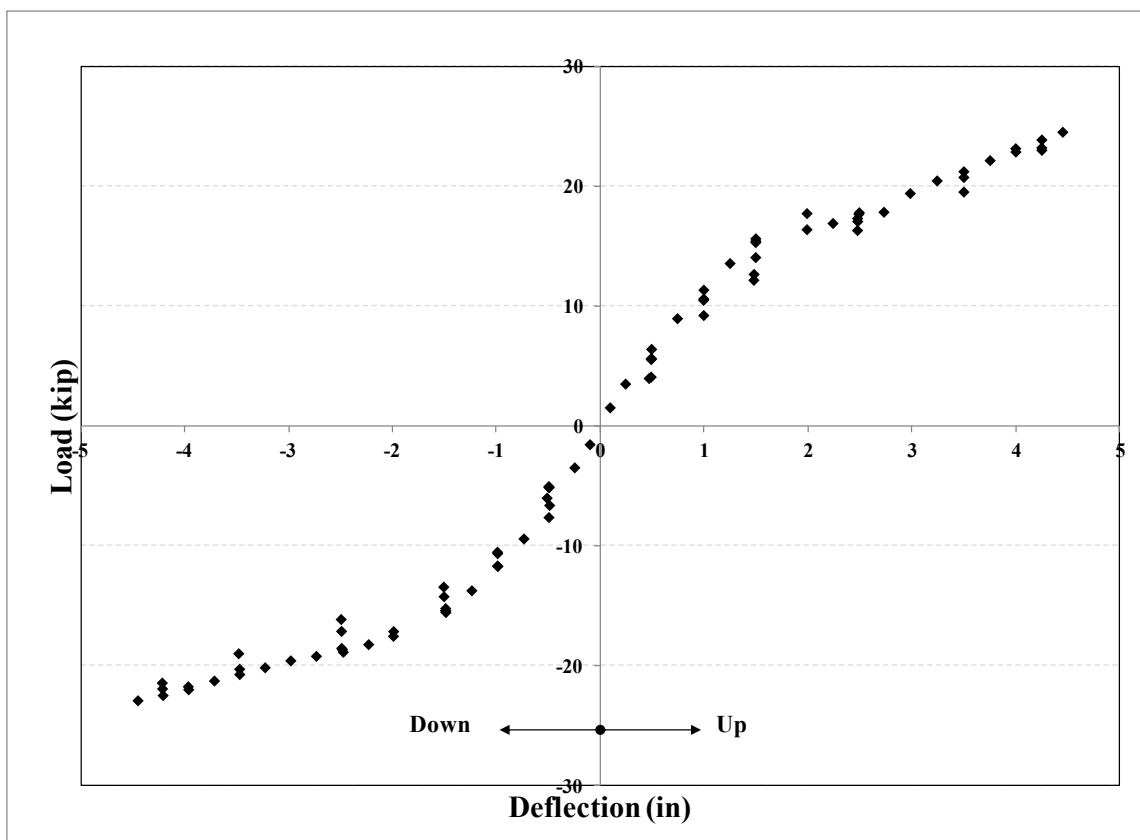


Figure 4-49- Load-deflection points for stage 1 (specimen #2)

As shown in this figure, the load dropped after 2 in displacement which can be addressed to the sliding of rubber against steel pipe. As mentioned before, the loud noise started at this point, and during the test the load drop was observed right when the noise was heard.

Figure 4-50 shows the load deflection curve for specimen #2. Note that these curves represent the first 5 cycles at each displacement level.

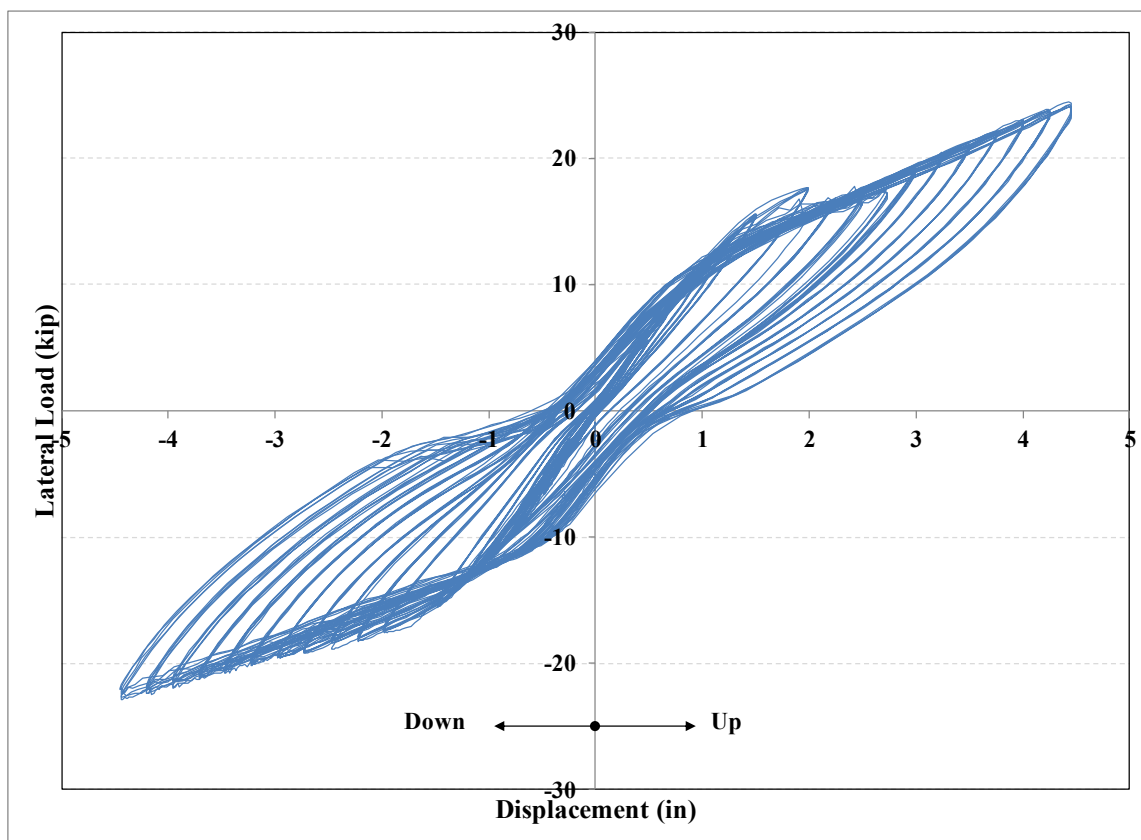


Figure 4-50- Load-deflection curve for stage 1 (specimen #2)

Moment-rotation curve for this specimen is shown in Figure 4-51. Like specimen #1, the bending moment is calculated from the specimen geometry and loading and also taking into consideration the second order moments developed by the axial load due to the deflection of the CFT. The rotation is calculated based on the readings from the first row spring pots (PB1 and PT1). At larger deflections the slope of the curve changes, which is related to separation of the spring pots (PB1 and PT1) from the concrete block on the tension side; thus, these values are not valid.

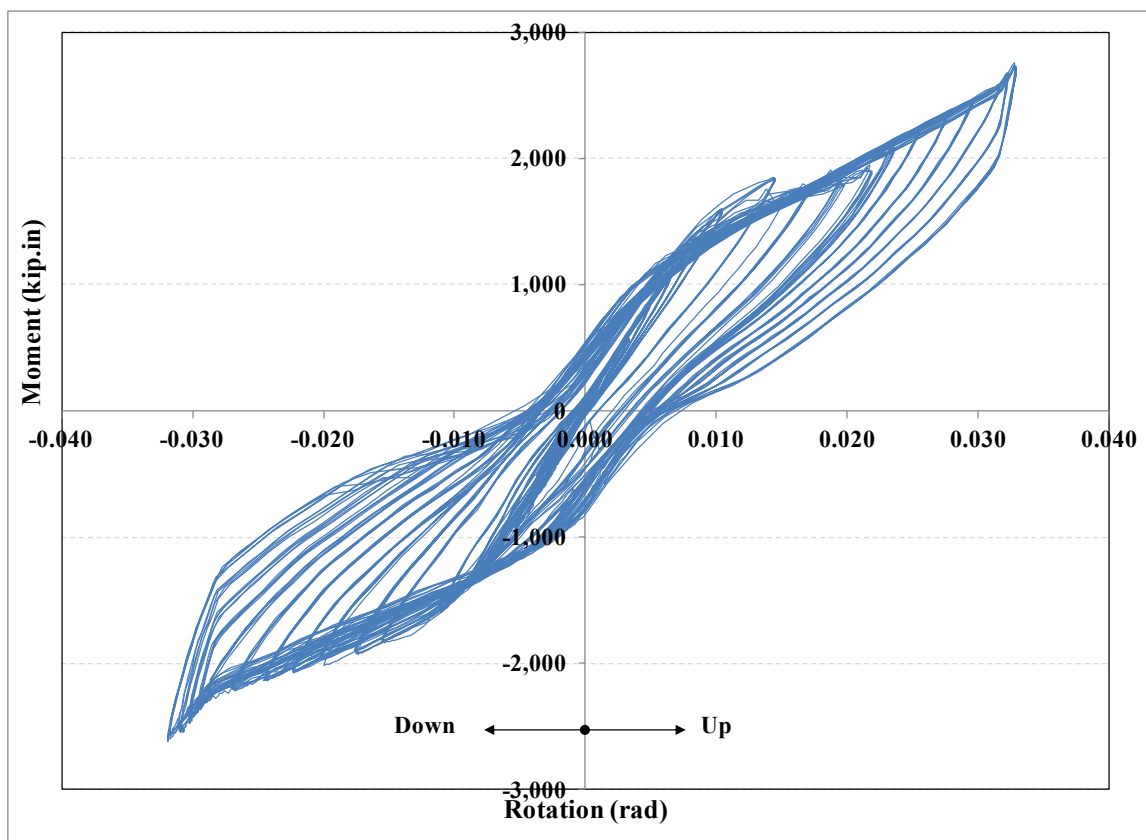


Figure 4-51- Moment-rotation curve for stage 1 (specimen #2)

Ignoring the data in large deformation and drawing the extreme values on the moment-rotation curve, the following figure is obtained, from which the initial and final rotational stiffness of the connection can be estimated about 167,000 and 27,000 kip.in/rad respectively.

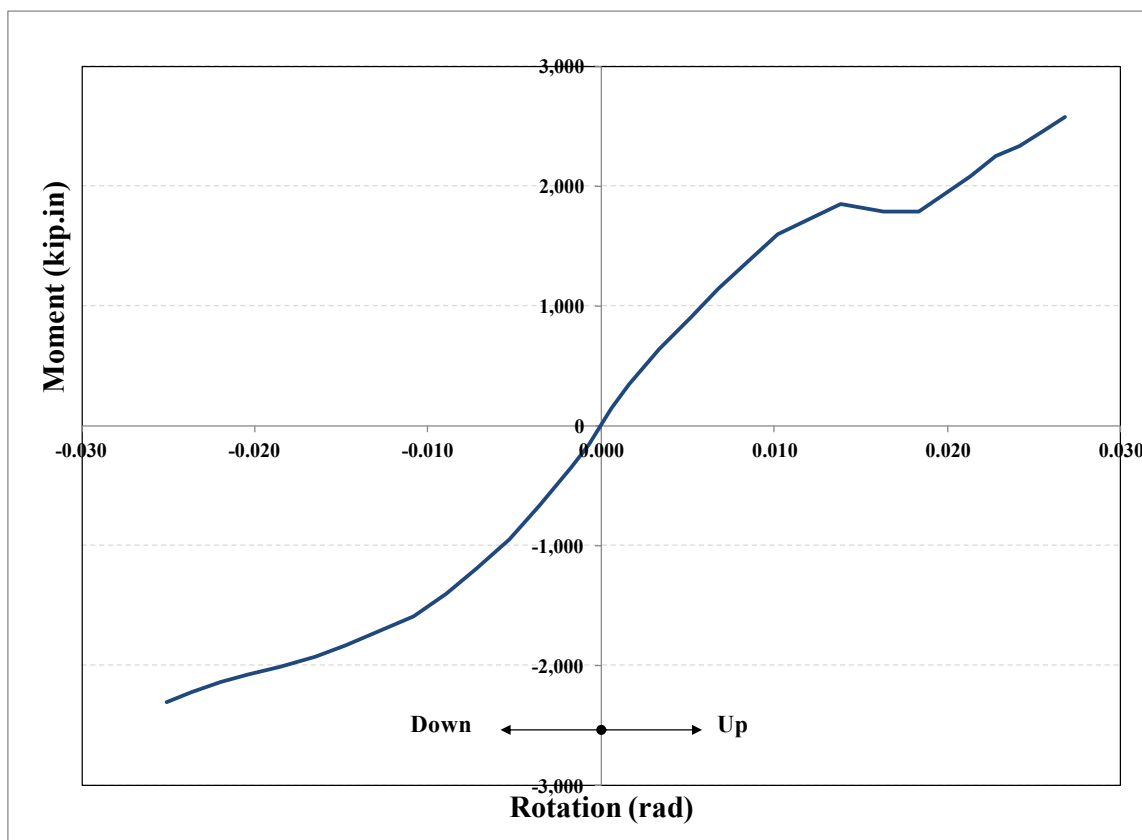


Figure 4-52- Envelope of moment-rotation curve for stage 1 (specimen #2)

The following figure shows the strains based on the first row strain gage readings (GB1 and GT1) during stage 1 for specimen #2.

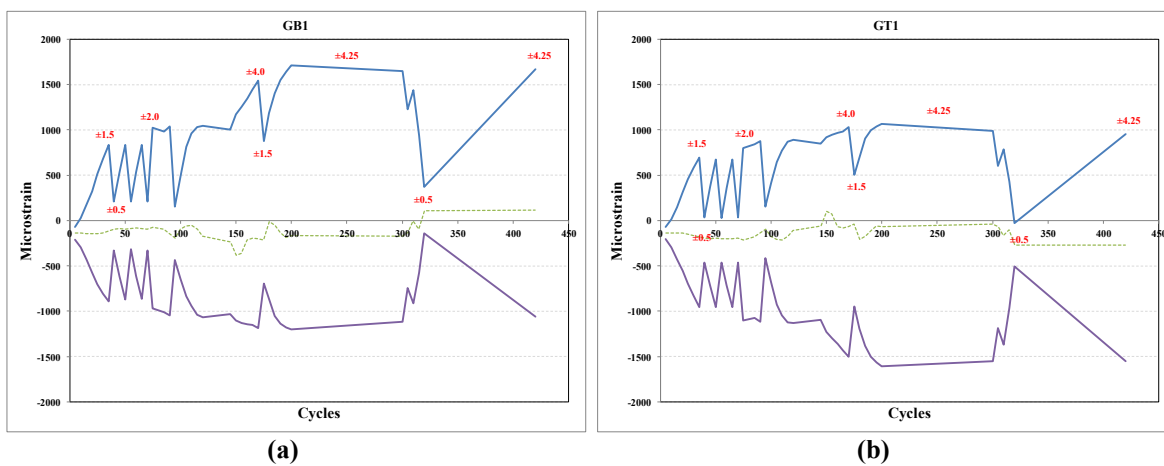


Figure 4-53- Maximum strains in stage 1 (specimen #2) (a) GB1 (b) GT1

4.3.2.2. Load Stage 2

Load-deflection curve for several cycles during this load stage is shown in Figure 4-54. Note that the specimen was not lubricated at the first cycle and as shown, the extreme loads are at its largest values. However after lubrication, the load has dropped to some extent. This is more evident when the direction of loading is downward, which can be due to the fact that more lubrication was deposited

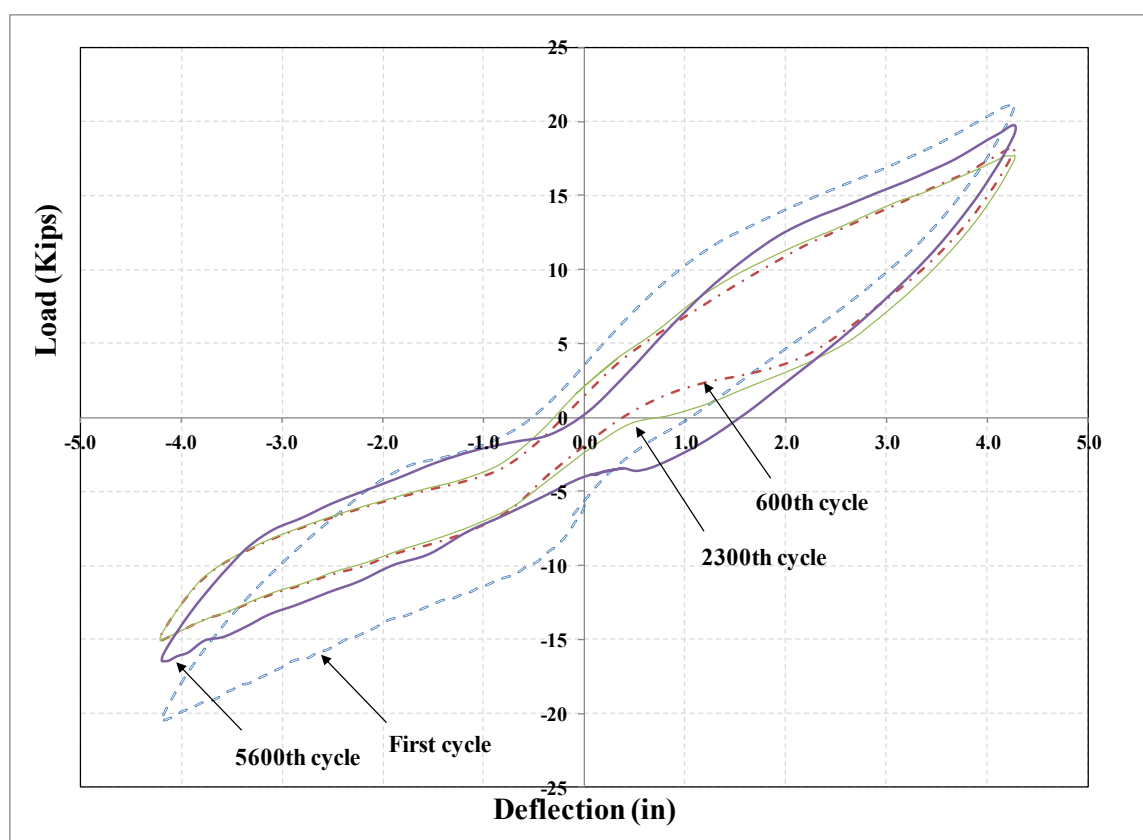


Figure 4-54- Calibrated moment-rotation curves

The following figure shows the values of the axial load and lateral load at maximum points of cycles. It is clear that after about 13000 cycles, the axial load level has decreased drastically. This is related to detachment of the end plate, blossom failure, and shortening of the pile. Since

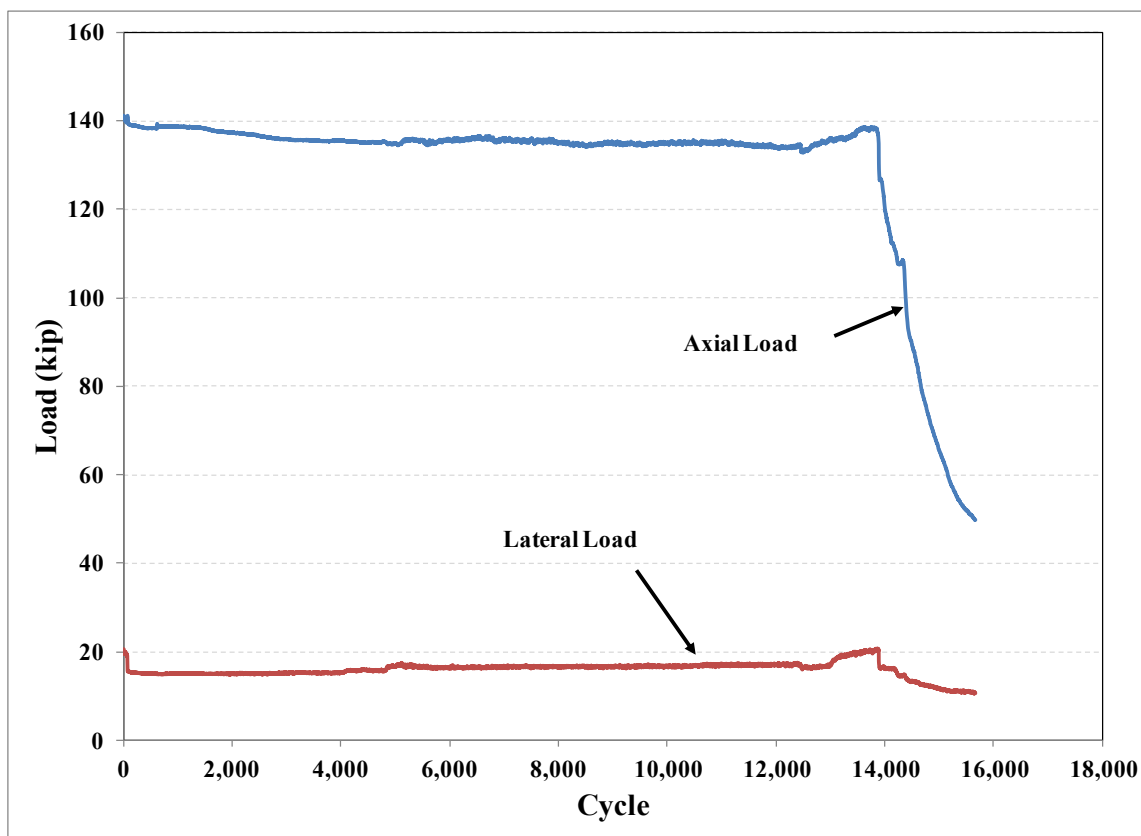


Figure 4-55- Axial and lateral load during load stage 2 (specimen #2)

The shortening of the specimen is further investigated through readings from the first row of spring potentiometers, PT1 and PB1 (top and bottom respectively), as shown in Figure 4-56. It is clear that after 13000 cycles, the top and bottom pots show some shortening. Note that the moving of the bottom half of the elastomer was noticed at about 16000 cycles and the test was stopped. After the detachment of the end plate and blossom failure, the blossomed portion of the pile had pushed the elastomer out, which has resulted in its moving.

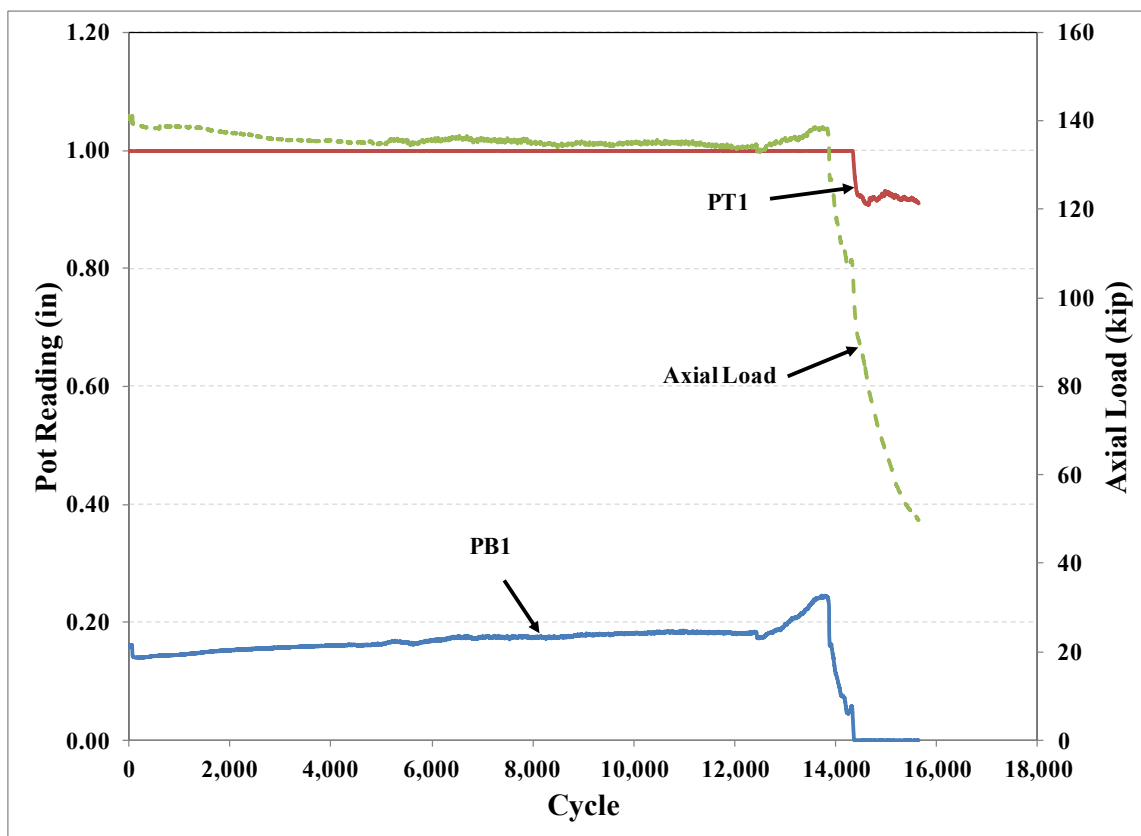


Figure 4-56- Readings from first row pots (specimen #2)

4.3.2.3. Load Stage 3

Load-deflection curve for load stage 3 is shown in Figure 4-57. At about 6 in deflection failure of the dywidag happened which concluded this test.

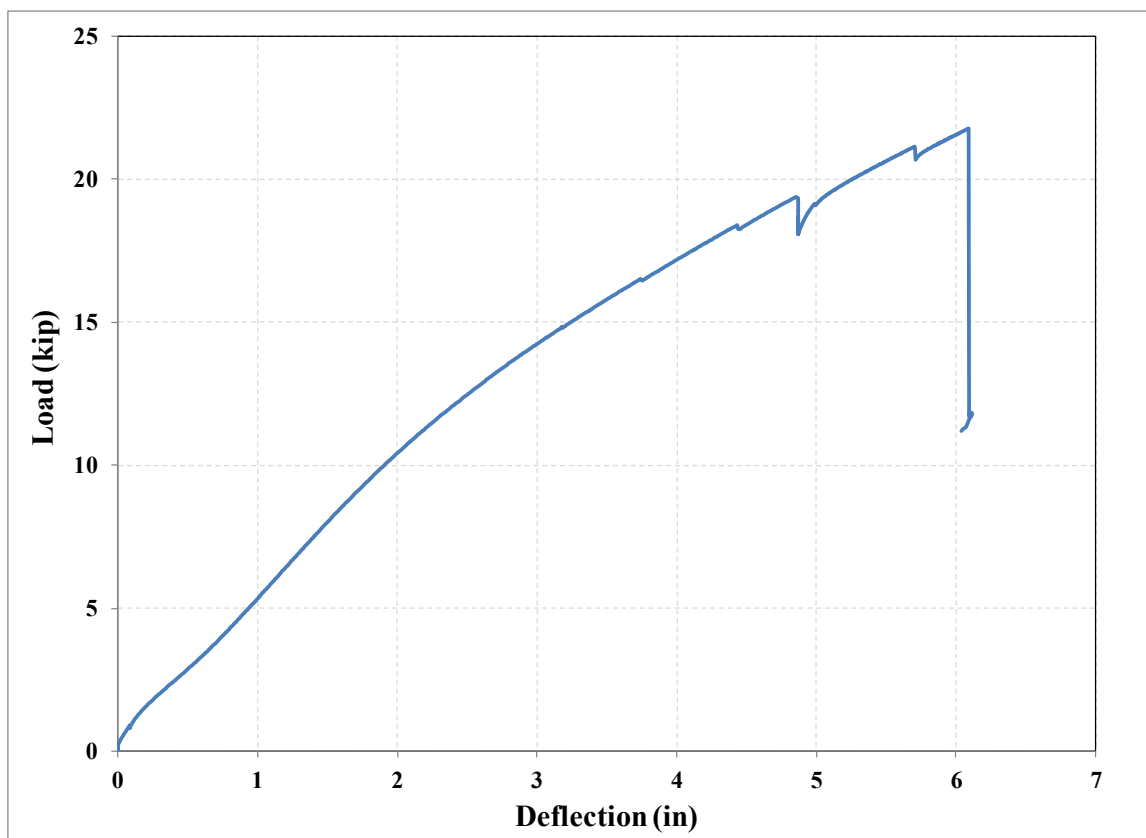


Figure 4-57- Load-deflection curve for load stage 3 (specimen #2)

Figure 4-58 shows the level of strains extracted directly from available strain gages.

Note that the rest of the gages were gone. The level of axial load is also shown in this figure. The axial load level at point of failure was about 119 kip.

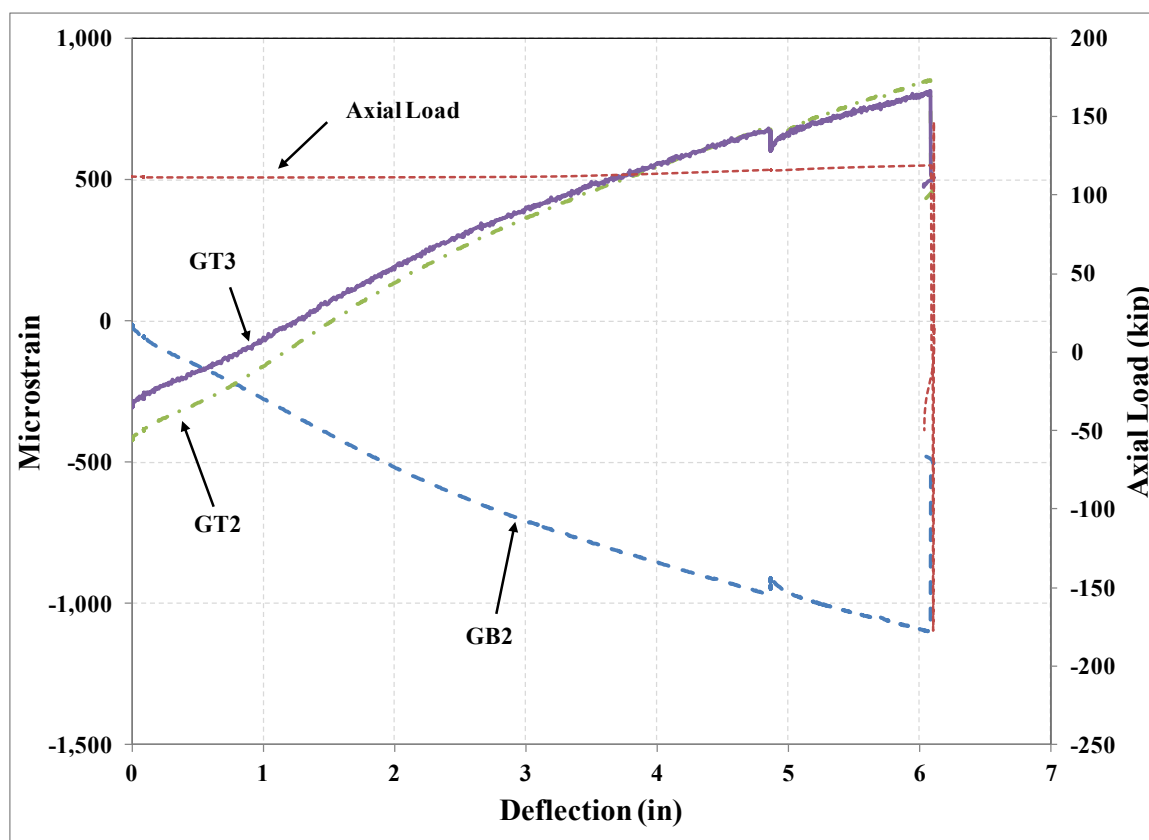


Figure 4-58- Load-deflection curve for load stage 3 (specimen #2)

4.3.3. Rotational Stiffness in SAP2000

In order to verify the estimated rotational stiffnesses, bilinear curve are fitted to the moment-rotation curves of the two specimens as shown in Figure 4-59.

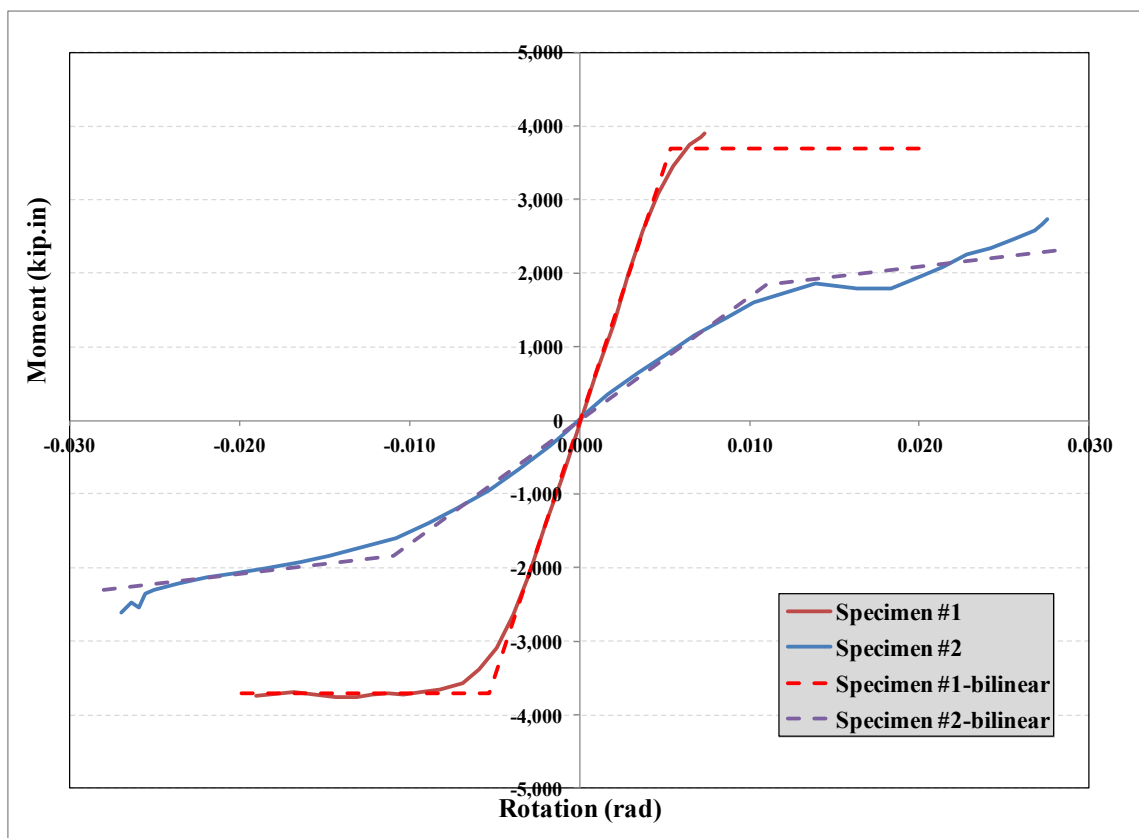


Figure 4-59- Calibrated moment-rotation curves

Then, the pile is modeled in SAP2000 using beam element and the nonlinear link element representing the connection's rotational stiffness is assigned to one end. The following table lists the nonlinear properties of the link elements used in SAP2000.

Table 4-8- Nonlinear properties of link element representing connection stiffness

	Initial Slope (kip.in/rad)	Final slope (kip.in/rad)	Rotation at slope change
Specimen #1	694000	0	±0.0053
Specimen #2	167000	27000	±0.011

120 kip axial load is applied to the free end of the beam. Then the lateral load is applied and the corresponding displacement is extracted from the analysis. Note that $P-\Delta$ effect is also considered in the analysis. Figure 4-60 shows the load deflection of the testes as compared to the analysis results from SAP2000. As expected, the curves match very nicely which proves the validity of moment-rotation stiffness calculations.

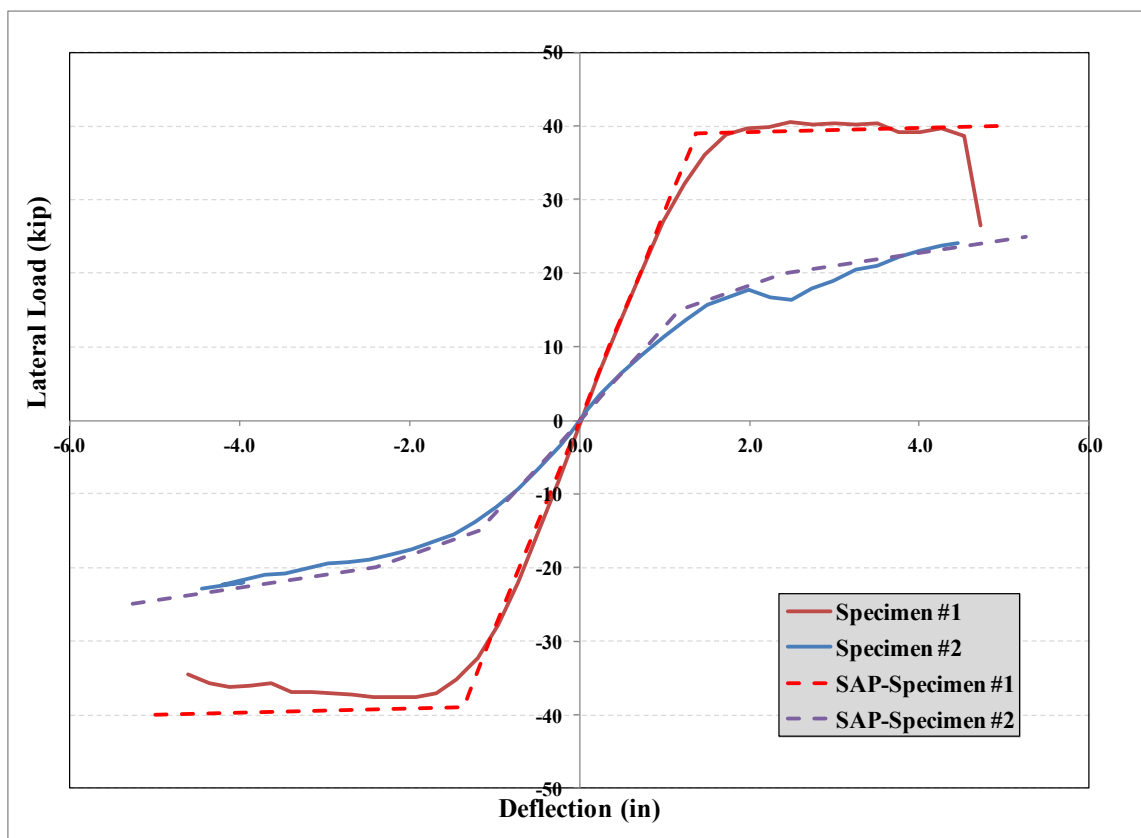


Figure 4-60- Load-deflection curves from tests and SAP2000

Using pushover analysis discussed in Chapter 5.3.2 the CFT pile is modeled in SAP2000. Four cases are studied to compare different boundary conditions as shown in Figure 4-61. In the first two models, the pile head connection is modeled using nonlinear link element based on values listed in Table 4-8. In the third and fourth model, however, completely fixed and pinned condition is modeled respectively.

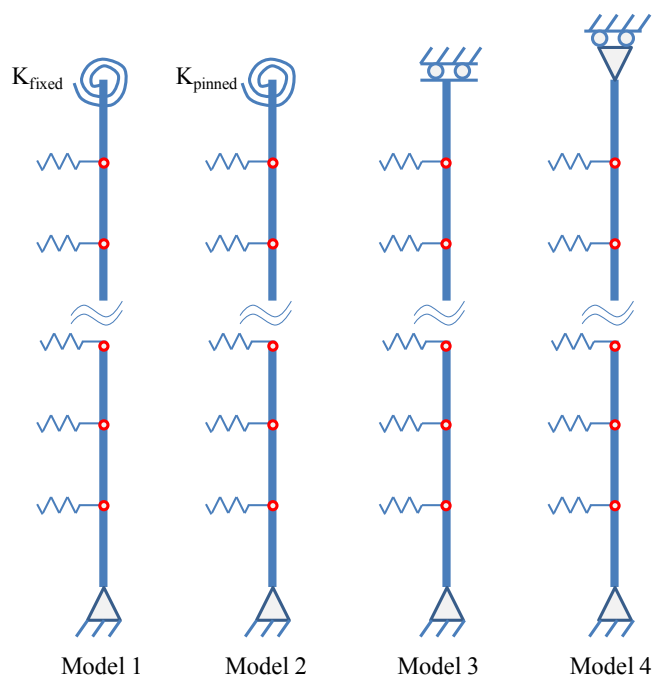


Figure 4-61- Schematic models used in SAP2000 analysis

As expected, the model with complete fixity (model 3) results in smaller maximum displacement compared to the fixed model with real rotational stiffnesses (model 1). On the other hand, in spite of increased stiffness, the pinned model with real rotational stiffnesses (model 2) gives more displacement capacity as compared to completely pinned model (model 4). This is due to the fact that the developed moment at the pile head in model 2, reduces the maximum opposite sign moment developed along the pile deep in the soil.

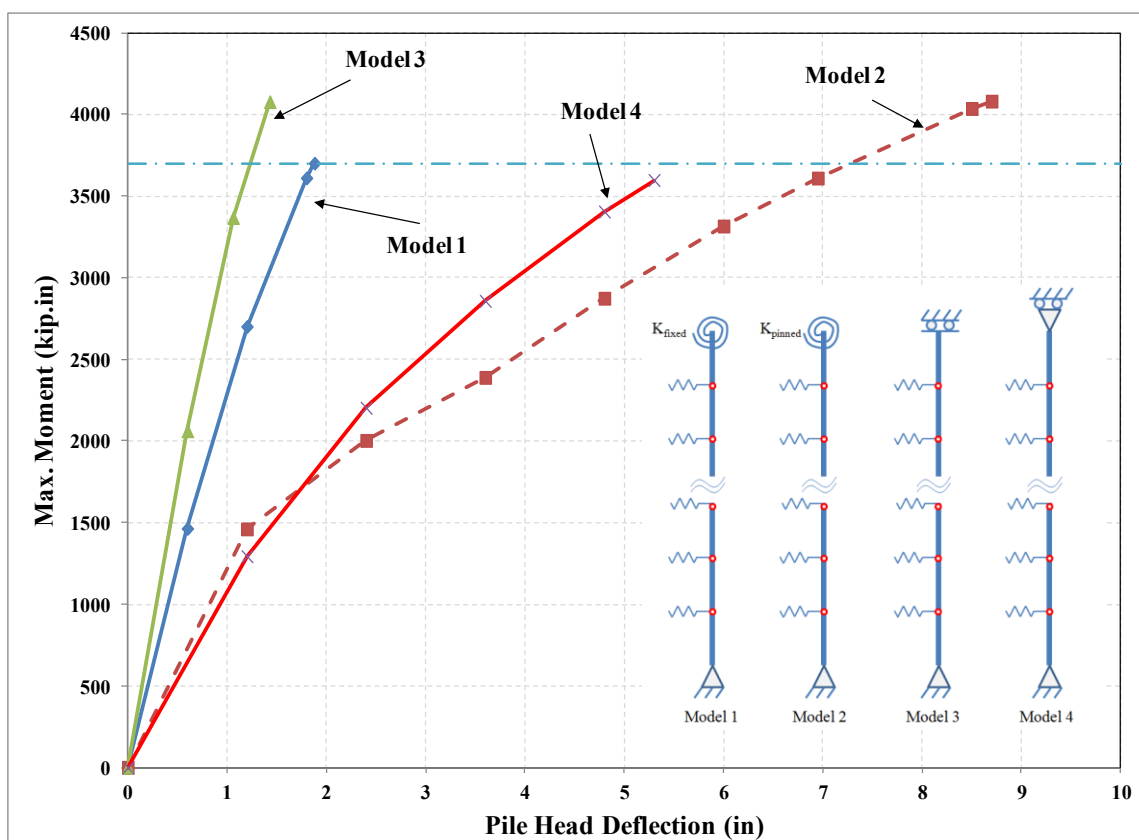


Figure 4-62- Pushover analysis results in medium clay for CFT piles tested

Assuming that the pile can reach the maximum moment of 3700 kip.in (the maximum moment observed in specimen #1), the following table summarizes the displacement capacities associated with different boundary conditions. It is observed that pinned connection can increase the lateral movement capacity up to 3.8 times (in medium clay).

Table 4-9- Comparison of different boundary conditions for CFT pile in Medium Clay

	Head condition	Displacement capacity (in)
Model 1	Nonlinear Link/Fixed	1.9
Model 2	Nonlinear Link/Pinned	7.3
Model 3	Fixed	1.3
Model 4	Pinned	5.7

4.4. Material Property Tests

4.4.1. Steel Tensions Tests

Samples were taken from the steel pipes after the tests were completed. Four samples were cut from the tip (free end) of the pile, and one sample next to them along the length. This region was selected since it did not undergo large deformations or major strains during the tests. Since the pipe was filled with concrete, grinder was used to cut the specimen instead of torch. Samples were machined in UNL machine shop based on the standard shape from ASTM A-370 as shown in the following figure.

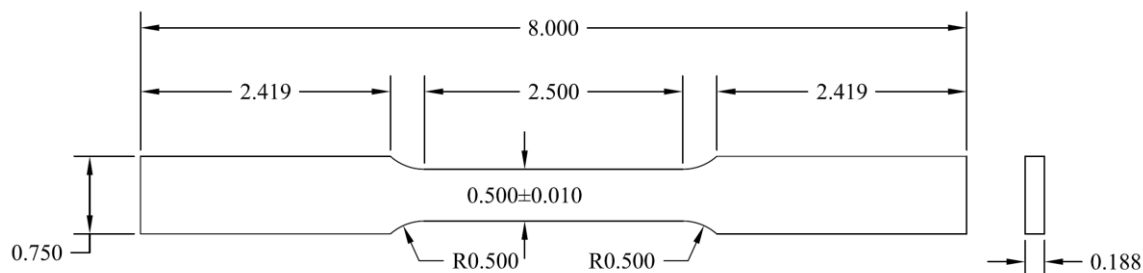


Figure 4-63- Tensile test dimensions

The following table lists the real dimensions of the specimen (measured with caliper) as well as the summary of the test results. Unfortunately, the data for sample 1-4 was lost because of the problem with extensometer and is not reported.

Table 4-10- Compression tests on first pour specimens (March 7th 2011)

	Sample	Thickness (in)	Width (in)	Yield stress (ksi)	Strain at failure	Comments
Specimen #1	1-1	0.189	0.500	54.8	0.381	tip
	1-2	0.189	0.500	53.1	0.366	tip
	1-3	0.188	0.499	58.9	0.351	tip
	1-4	0.189	0.500	--	--	tip
	1-5	0.183	0.500	55.2	0.350	next to tip
Specimen #2	2-1	0.187	0.497	61.90	0.365	tip
	2-2	0.187	0.497	62.40	0.334	tip
	2-3	0.187	0.498	59.40	0.414	tip
	2-4	0.188	0.499	56.30	0.393	tip
	2-5	0.188	0.495	56.80	0.4	next to tip

The following figures show the stress-strain curves for the testes samples. Since specific yielding plateau was not observed, 0.2% offset method was used to estimate the yield stress of the specimens.

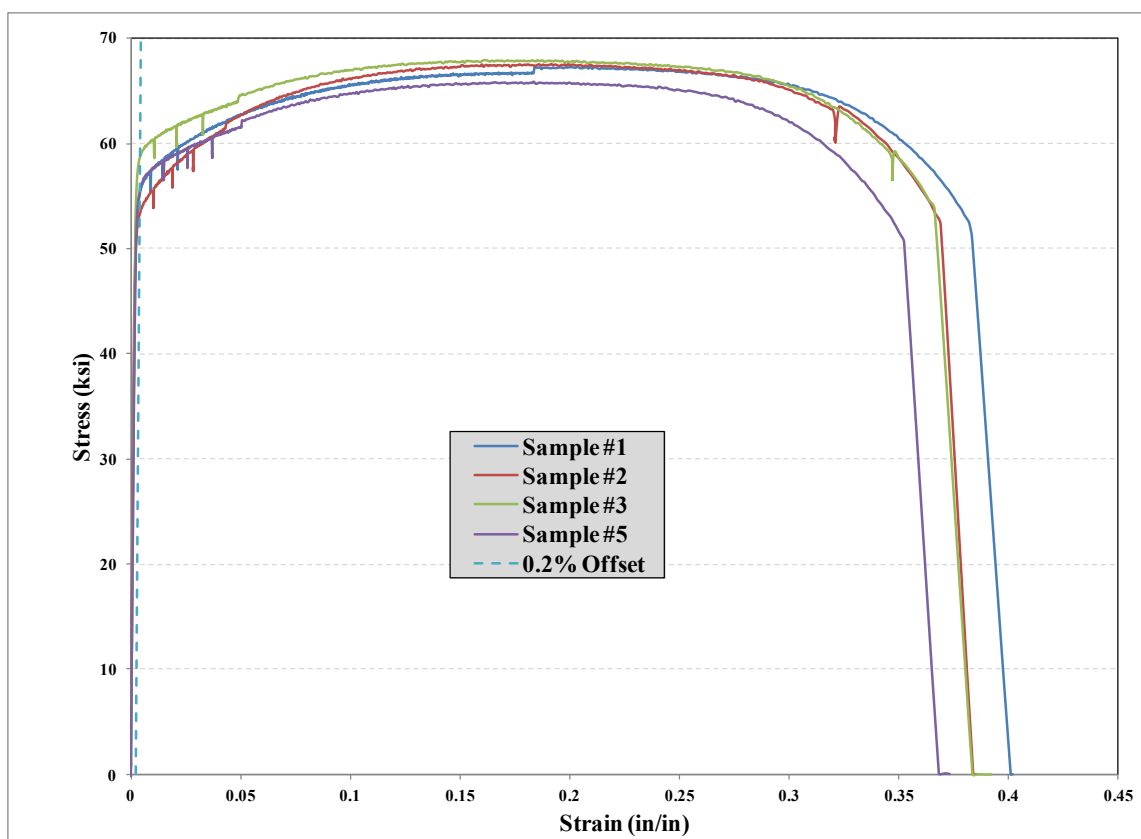


Figure 4-64- Stress-strain curves for samples from specimen #1

The average of yield stress was 55.4 ksi and 59.4 ksi for specimen #1 and specimen #2, respectively.

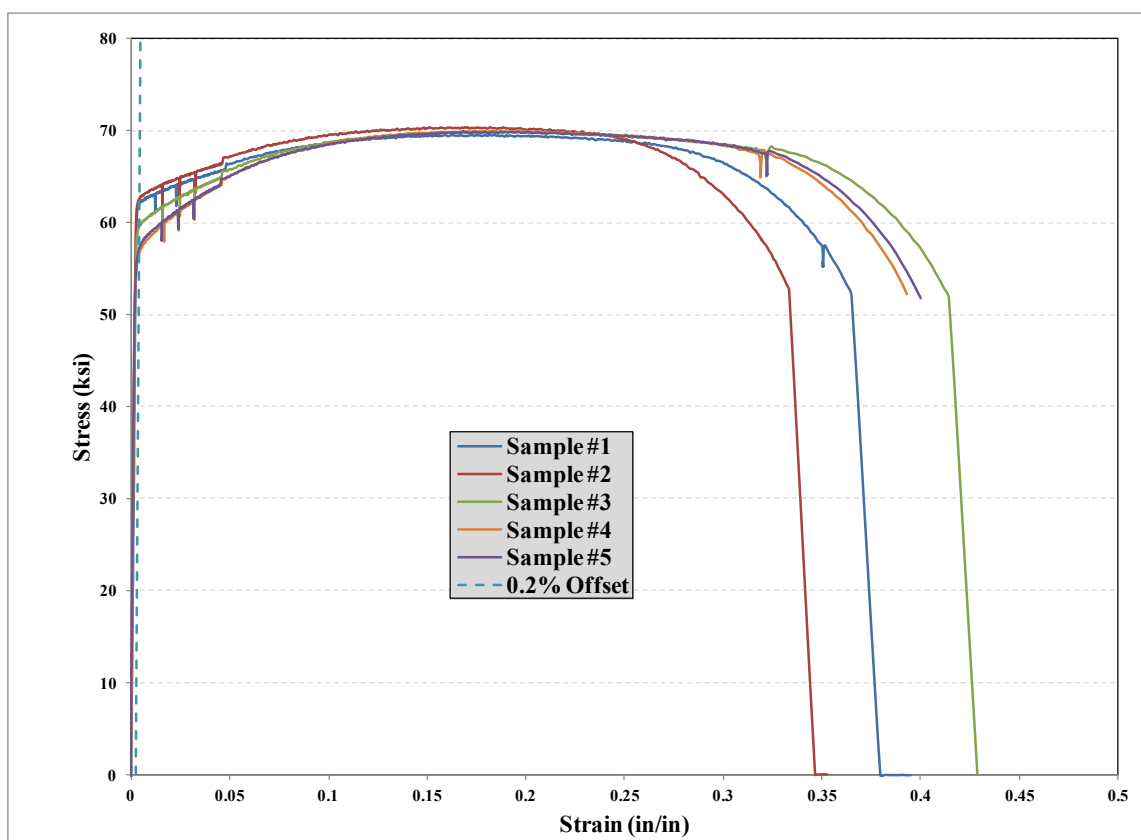


Figure 4-65- Stress-strain curves for samples from specimen #2

4.4.2. Concrete Compression Tests

4.4.2.1. Compression Test on First Pour Specimen

Compression tests were done on samples of the first pour.

Table 4-11- Compression tests on first pour specimens (March 7th 2011)

Date	Specimen	Age (days)	Compressive Strength (psi)	Comments
Apr. 5 th 2011	1-1	29	3462	28 day compressive strength
	1-2	29	4103	
	1-3	29	3870	
May 17 th 2011	1-4	71	4380	load stage 3 on specimen #1
	1-5	71	4632	
	1-6	71	4364	
Aug. 19 th 2011	1-7	165	4484	load stage 1 on specimen #2
	1-8	165	4670	
	1-9	165	4135	

The average of the compressive strength, f'_c , from the above table is 4.2 ksi.

4.4.2.2. Compression Test on Second Pour Specimen

Compression tests were done on samples of the second pour.

Table 4-12- Compression tests on second pour specimens (March 10th 2011)

Date	Specimen	Age (days)	Compressive Strength (psi)	Comments
Apr. 7 th 2011	2-1	28	4496	28 day
	2-2	28	4527	compressive
	2-3	28	4409	strength
May 17 th 2011	2-4	68	4881	load stage 3 on
	2-5	68	4917	specimen #1
	2-6	68	4864	

The average of the compressive strength, f'_c , from the above table is 4.7 ksi.

4.4.2.3. Compression Test on Third Pour Specimen

Compression tests were done on samples of the third pour.

Table 4-13- Compression tests on third pour specimens (March 15th 2011)

Date	Specimen	Age (days)	Compressive Strength (psi)	Comments
Apr. 12 th 2011	3-1	28	4602	28 day
	3-2	28	4649	compressive
	3-3	28	4368	strength
Aug. 19 th 2011	3-4	157	4003	load stage 1 on
	3-5	157	2523	specimen #2
	3-6	157	3654	

The average of the compressive strength, f'_c , from the above table is 4.0 ksi.

4.4.3. Soft Material Compression Tests

4.4.3.1. Delpatch Elastomeric Concrete

The package for Delpatch consists of three components, two of which are resin elements. The big portion is, however, the mixture of fine sand and fiberglass. Table 4-14 lists the weight of different components that were used in the mix to make four 2" cubic samples.

Table 4-14- Mix ratios for 2” cube specimens

Component	Amount (lb)
Resin A	0.72
Resin B	0.36
Aggregate	2.38

First, the two resin components were mixed and stirred with hand drill for about 1 minute then the aggregate was added and mixed for another 90 seconds.

**Figure 4-66- Delpatch mixing procedure**

In the first attempt, the samples were made in wooden molds, but the mix adhered to the molds and the samples were not useful (Figure 4-67). The same mix was then poured in plexiglass molds which resulted in better samples, although tiny defects were developed on the surface.

4.4.3.1.1. Wooden Mold

Wooden molds were built for four 2” cubic samples. Interior surfaces of the molds were oiled to facilitate the de-bonding after the mix was cured, but unfortunately it adhered to the mold as shown in Figure 4-67. The mix was made on Nov. 1st 2010 at 11:50 am.



Figure 4-67- Samples made in wooden molds

4.4.3.1.2. Plexiglass Mold

New molds were then made from plexiglass and were lubricated using WD40. New concrete mix was also prepared based on the ratios listed in Table 4-14 and poured at 1:30 pm on Nov. 2nd.

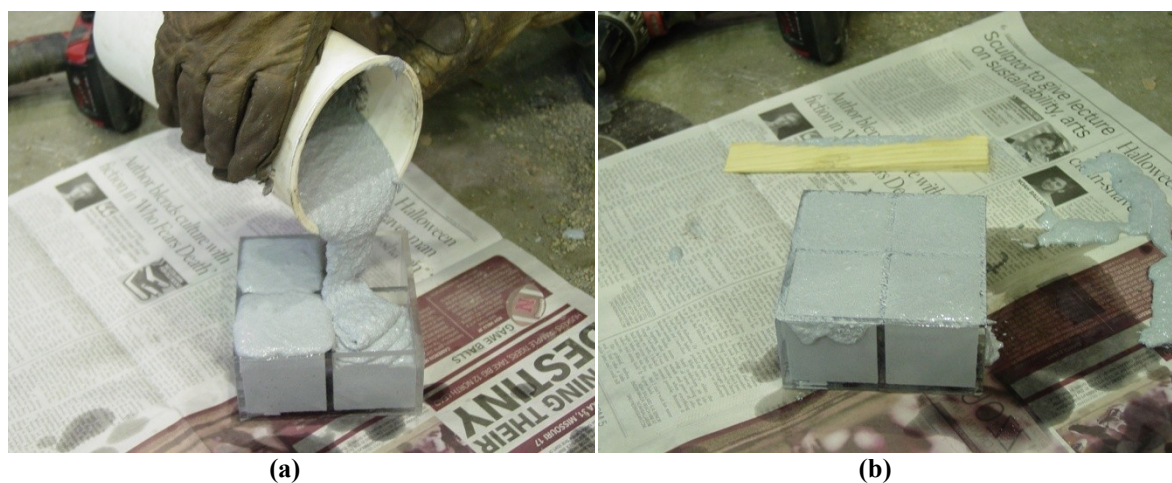


Figure 4-68- (a) Pouring the mix (b) leveled top surface

4.4.3.1.3. Cyclic Test

In order to investigate the behavior of the elastomeric concrete after several loadings, cyclic load was applied to the 2” cube samples. The MTS frame with load capacity of 22 kips is used for loading the specimen. Since the platforms were not found for the compression setup, two square plates were made, and bolted to the grips. The setup was completed on November 23rd 2010, and the machine was programmed to load the samples. The specimen was 21 days old when tested for cyclic loading.

Table 4-15- Compression tests on elastomeric concrete specimens

Test #	Specimen	Direction	Strain	Cycles	Freq (Hz)
EC-C-1	1	Upright	5%	36500	2
EC-C-2	1	Upright	10%	8000	2



Figure 4-69- MTS Load frame for cyclic load test

4.4.3.1.3.1. 5% Strain Cyclic Test

First the sample was statically loaded up to 0.1 in deflection (5% strain) to obtain the stress-strain curve for compression of the specimen. At this stage the material had not experienced any loading.

After the first step, 36500 cycles of 0.1 in deflection (5% strain) was applied with the frequency of 2 Hz. As expected, the specimen heated up during the cyclic step. It was observed that the required load for the abovementioned displacement was about 4.0 kips at the initial cycles, but it dropped to around 2.5 kips at the final cycles.

After the cyclic step was completed, another static compression test (0.1 in deflection) was conducted to obtain the stress-strain curve for the specimen, which by then, had some loading history (Figure 4-70 (a)).

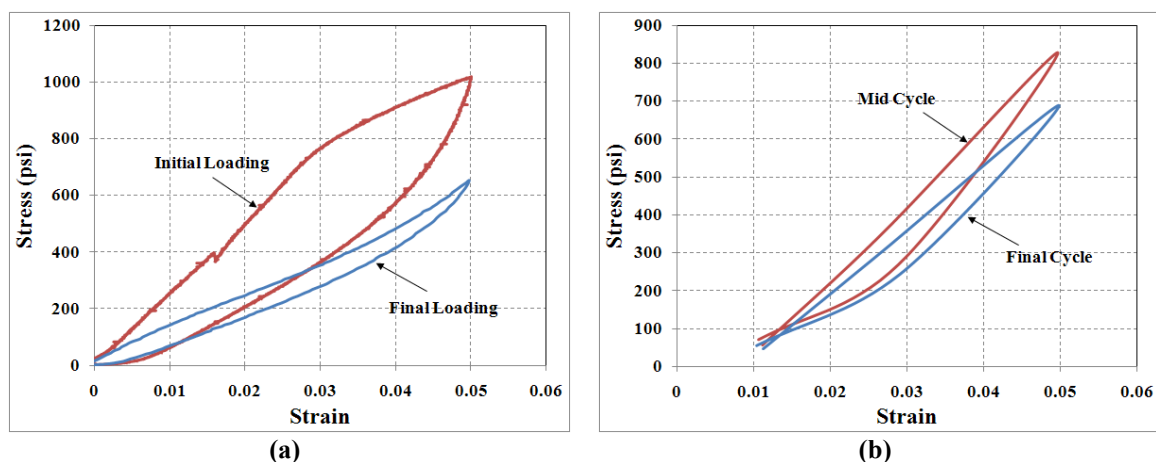


Figure 4-70- Stress-strain curves for (a) static loading up to 5% strain (b) cyclic loading

4.4.3.1.3.2. 10% Strain Cyclic Test

On the next day, the specimen was loaded up to 0.2 in deflection (10% strain). Note that the specimen was previously tested for 5% cyclic loading. First the stress-strain data was collected for the static compression test up to 10%. Then the specimen was subjected to cyclic loading of 10% deflection (36500 cycles as target).



Figure 4-71- (a) Cracks forming on the opposite side of the specimen (b) dislocation of the specimen and cracks after about 8000 cycles

After about 1000 cycles some cracks were observed in the specimen. These cracks were mainly on the imperfect side of the specimen. Because of cyclic deflections, some aggregate spalled from the cracked zone. The surface of the specimen was warmer than

the 5% test. The test was stopped after about 8000 cycles, because the specimen was dislocating on the platform and the cracks were developed on all sides of the specimen.

During the test, the load dropped from about 5.5 kips to 1.5 kips.

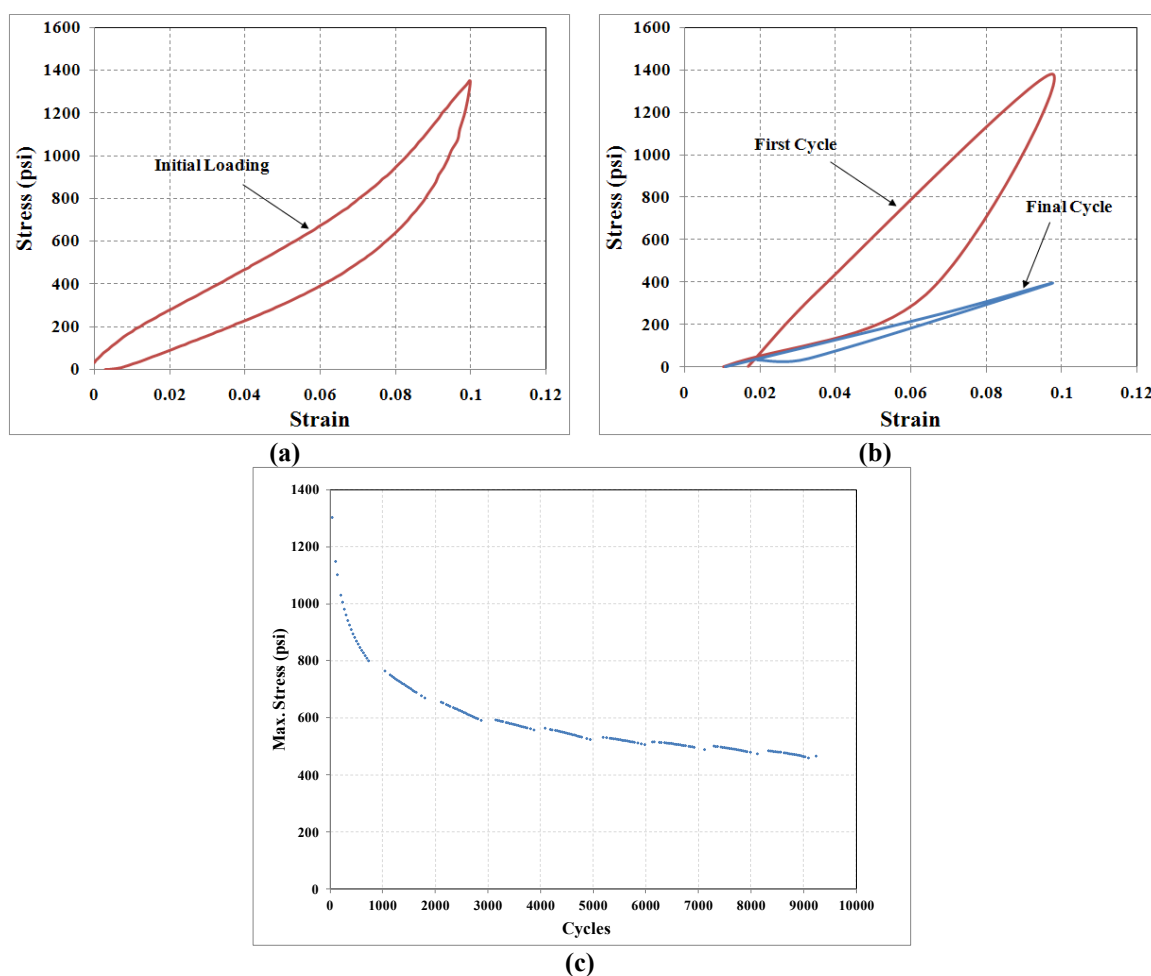


Figure 4-72- Stress-strain curves for (a) initial static loading up to 10% strain (b) cyclic loading (c) max load change during the cyclic loading

4.4.3.2. Fiberlast (Elastomeric Material)

Compression tests were also conducted on 2” cube samples of Fiberlast material. Samples were provided by Voss Company, which is the vendor of the elastomer ring used in the experimental study. Table 4-16 shows the list of compression tests conducted on different specimens.

Table 4-16- Compression tests conducted on Fiberlast specimen

Test #	Specimen	Direction	Strain	Cycles	Freq (Hz)
F-C-1	1	Upright	10%	36500	2
F-C-2	2	Upright	10%	36500	2
F-C-3	2	Side	10%	36500	2
F-C-4	2	Upright	30%	100	1
F-C-5	3	Upright	5%	36500	2
F-C-6	3	Upright	15%	36500	2

Figure 4-73 through Figure 4-78 show stress-strain curves for different tests conducted.

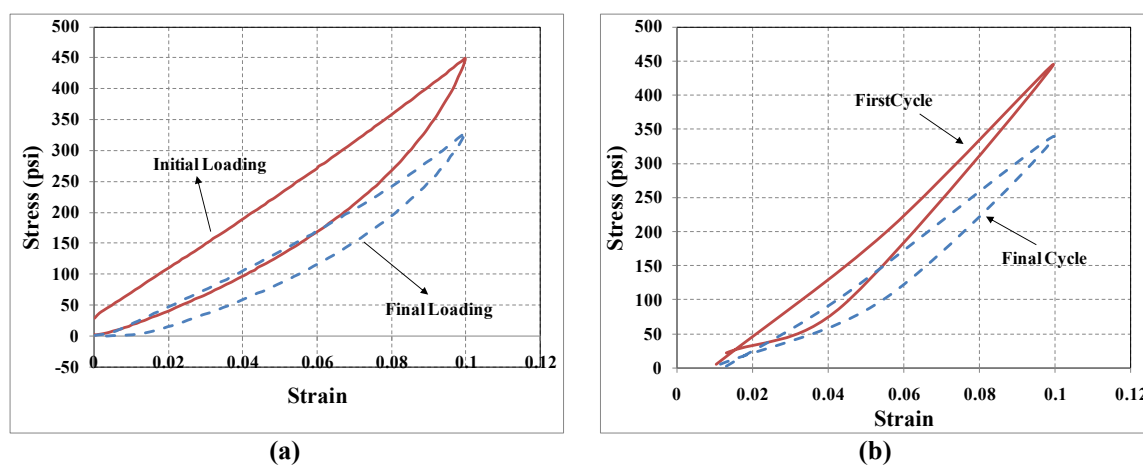


Figure 4-73- Stress-strain curves for test F-C-1 (a) static loading up to 10% strain (b) cyclic loading

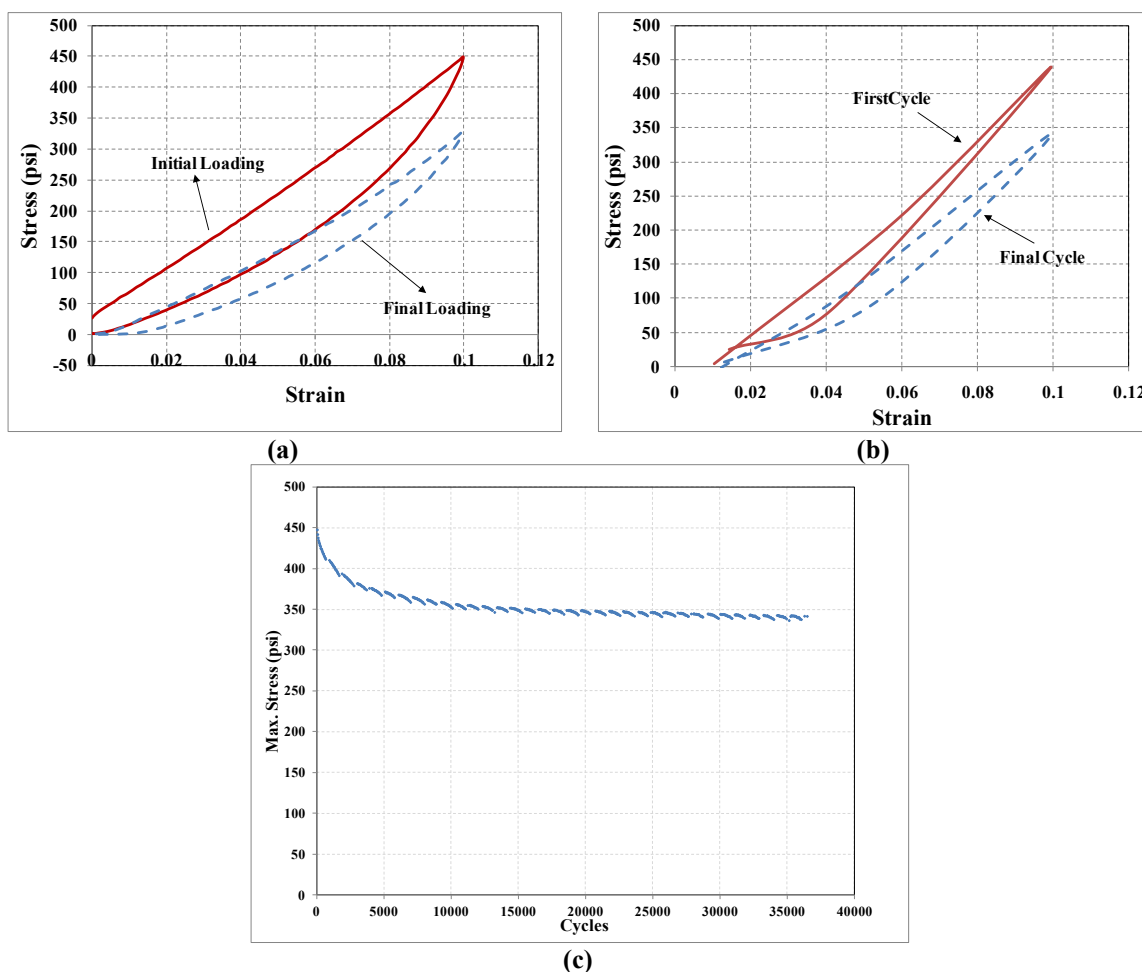


Figure 4-74- Stress-strain curves for test F-C-2 (a) static loading up to 10% strain (b) cyclic loading (c) max load change during the cyclic loading

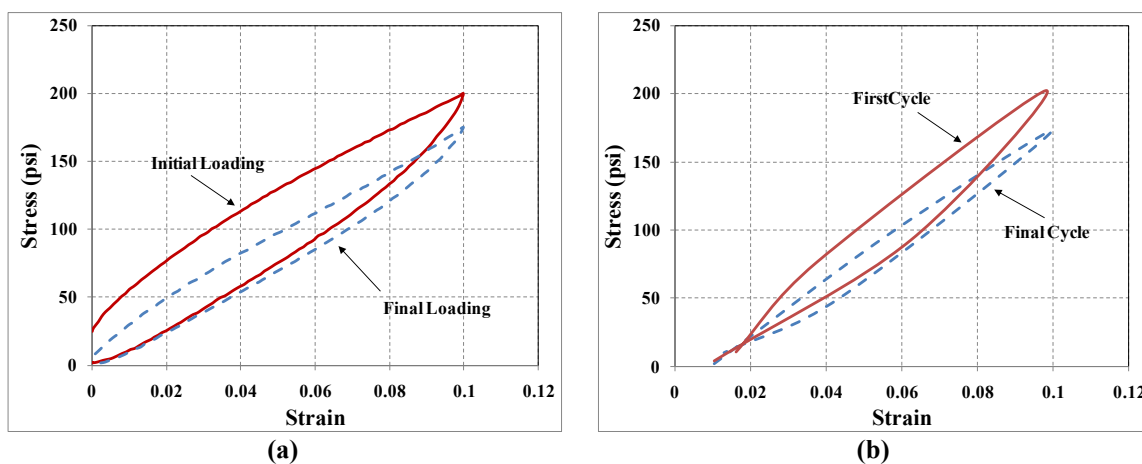


Figure 4-75- Stress-strain curves for test F-C-3 (a) static loading up to 10% strain (b) cyclic loading

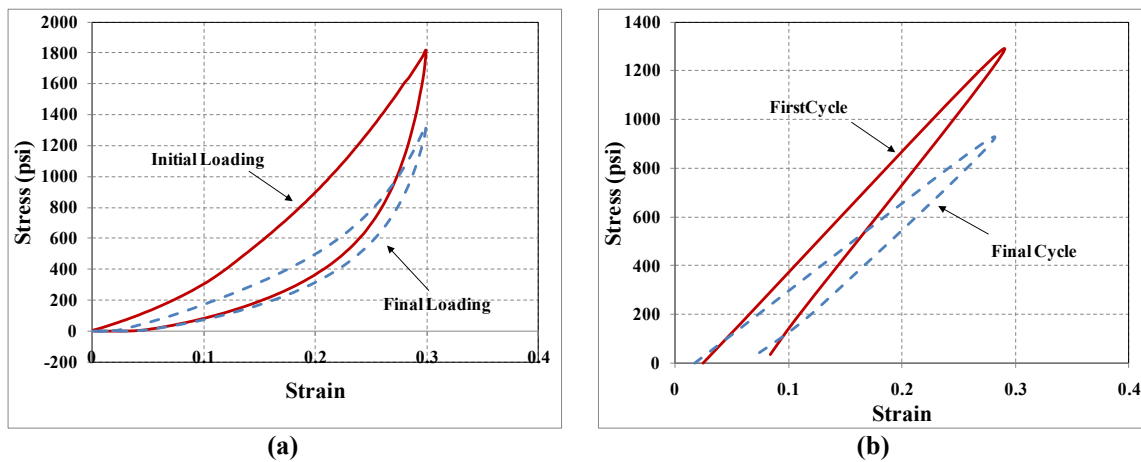


Figure 4-76- Stress-strain curves for test F-C-4 (a) static loading up to 30% strain (b) cyclic loading

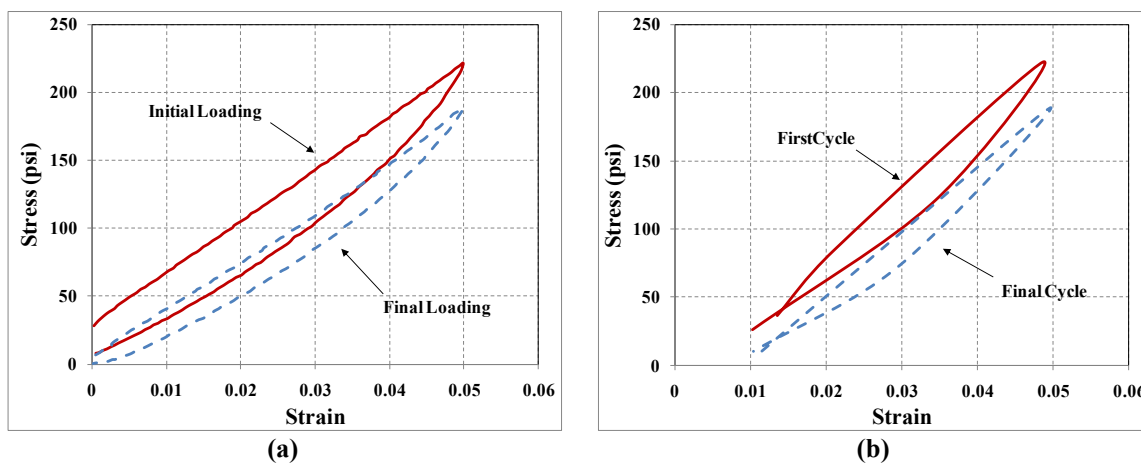


Figure 4-77- Stress-strain curves for test F-C-5 (a) static loading up to 5% strain (b) cyclic loading

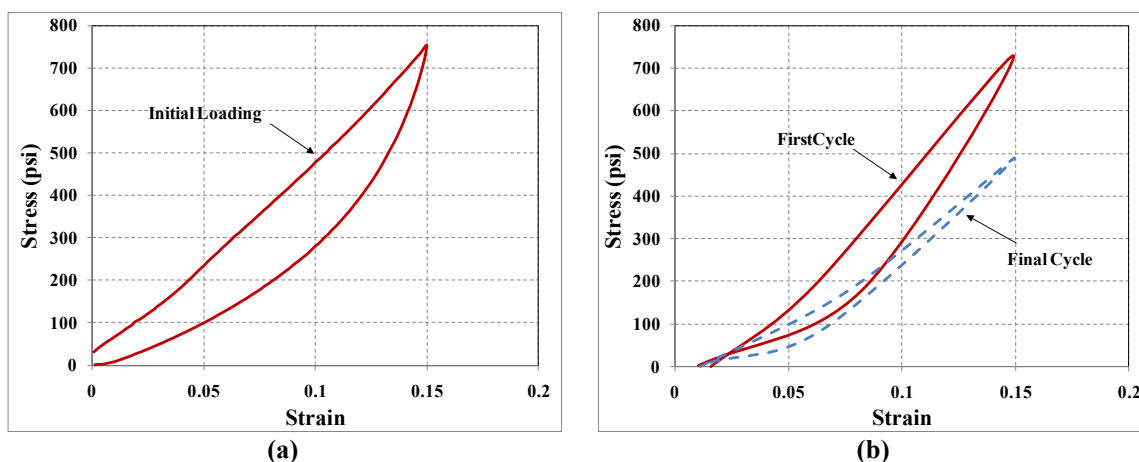


Figure 4-78- Stress-strain curves for test F-C-6 (a) initial static loading up to 15% strain (b) cyclic loading

4.5. Conclusions of Experimental Study

The following conclusions can be made from the experimental study conducted:

- Pinned pile/cap connection can effectively reduce the stiffness of the piling system and also increase the lateral displacement capacity of the piles. Two different boundary conditions were studied. In the first specimen, relatively fixed connection was investigated where the pile head is embedded in the concrete. Yielding, elephant foot buckling, and failure was observed at about 0.75 in, 3.00 in, and 4.50 in deflection respectively. In the second specimen the pile head was encased in the elastomer material (Fiberlast) which was embedded in the concrete cap. Small residual strains were observed at final stages of loading; however the condition of the pipe at the interface was intact. Blossom failure at the end of the pile happened in the cyclic testing stage after about 13000 cycles. The end plate was detached because of weld failure, followed by blossom failure, shortening of the specimen, and moving of

the bottom half of elastomer. Nevertheless, the embedded plate, concrete cap, and end plate were intact.

- Cyclic compression tests were conducted on 2” samples of elastomeric concrete (Delpatch) and elastomeric material (Fiberlast). Noticeable damage was observed in elastomeric concrete sample at 10% strain, whereas elastomeric material performed much better and the damage level was very small. Based on these tests, elastomeric material was chosen as the casing for the detail.

Chapter 5

Analytical Study

In this chapter the analytical studies conducted on different aspects of jointless bridges are summarized.

Unlike regular column elements, the calculation of elastic buckling load in embedded piles is not straight forward, because of the lateral support provided by the surrounding soil. A new approach is proposed Section 5.1 which combines the energy method with nonlinear p-y curves to estimate the critical axial load for the piles supporting jointless bridges.

The idea of a pinned pile/cap connection is further discussed and analytical investigations are presented in Section 5.2. First finite element model of a prestressed pile embedded in clay is calibrated and then the new connection concept is applied to the model. Finally, the finite element model of the tested specimens are generated and compared to the test results.

The design approach based on fatigue and strength criteria is presented in Section 5.3. In this approach, the maximum allowable strain is determined based on Miner's rule. Then, the maximum allowable curvature is calculated based on the maximum allowable strain. The maximum allowable moment is then extracted from the moment-curvature curve for the specific axial load level. Finally, using nonlinear pushover analysis the maximum allowable head displacement is estimated.

Using the design approach in Section 5.3, and adding the local and global stability criterion, a complete design approach is proposed in Section 5.4.

5.1. *Elastic Buckling of Embedded Steel Piles*

Since piles are relatively slender elements, their buckling is always a concern to designers. However, their critical load cannot be evaluated easily because of their interaction with the surrounding soil. Several studies have focused on the buckling analysis of piles. Davisson (1963) presented the solution for the buckling of fully embedded end-bearing pile problem using non-dimensionalized parameters. Davisson and Robinson (1965) estimated the critical buckling load of piles assuming constant and linearly increasing modulus of subgrade reaction. Reddy and Valsangkar (1970) obtained pile's critical load using the energy method for fully and partially embedded piles. They considered different boundary conditions assuming constant and linear soil modulus variation with depth for clays and sands, respectively. Prakash (1987) used the energy method to estimate the critical buckling load of fully embedded piles but the soil reaction was assumed linear in his calculations. Results were comparable to the solutions from Davisson (1963) and it was concluded that the energy method is a valid approach for this purpose. Gabr and Wang (1994) developed a model for calculation of piles' buckling load assuming uniform variation of skin friction as a function of depth. Gabr et al. (1997) assumed linear behavior for the soil-pile interaction in the lateral direction and developed a model for evaluating the critical buckling load of slender friction piles. In their study, several boundary conditions and different subgrade reaction distributions were investigated. Heelis et al. (2004) presented a non-dimensional solution for fully or

partially embedded general piles using Winkler springs. In these studies, because of numerous parameters involved, non-dimensional parameters were defined to make the problem simpler. The major issue with all previous studies is that for simplification, they assumed that the soil reaction is a linear function of the lateral displacement while nonlinear behavior is studied herein.

Based on AASHTO LRFD (2010), pile design should address nominal axial resistance, pile group interaction, and minimum penetration length. Axial resistance of the piles is generally evaluated by calculation of buckling load as well as axial strength of the cross section of the pile. Current design practice for buckling includes determination of equivalent cantilever length of the embedded portion of the pile while ignoring the surrounding soil.

There are, however, issues regarding the abovementioned design method. The theory behind the modulus of subgrade reaction is basically a linear assumption and technically represents the reaction of the surrounding soil as a linear function of the lateral displacement. Besides, in this method the effect of the soil on the equivalent cantilever length, which is defined as the depth below which the displacements and moments are very small, is completely ignored for analysis simplification.

Herein, the buckling capacity of piles is estimated by combining the energy method and p-y curves. Pile head displacement is also incorporated into capacity calculation. In this method, the soil reaction is a nonlinear function of lateral displacement and can efficiently model the soil-structure interaction.

5.1.1. Pile Design for Jointless Bridges

Several methods are available for the design of piles. In one approach, the pile, as a structure member, is designed only based on axial loads it is likely to experience during its lifetime (Kunin and Alampalli, 1999). This method is valid for the cases in which the pile does not undergo lateral movements, or these movements are negligible as in semi-integral bridges.

In jointless bridges with integral abutments, deformations induced by temperature changes, creep, and shrinkage from the superstructure are transferred to the substructure and consequently, the piles will experience fairly large movements depending on the length of the structure. Therefore, piles in jointless bridges with integral abutments shall be designed to withhold axial loads as well as the moments and loads introduced by lateral movement (Oesterlie, Tabatabai, Lawson, Refai, Volz and Scanlon, 2002, Wasserman and Walker, 1996, Burke Jr, 2009).

Abendroth et al. (1989) proposed the equivalent cantilever method for design of laterally loaded piles based on the study by Davisson and Robinson (1965). In this method, piles are represented as idealized cantilever columns having a fixed base at some depth below ground surface. Three equivalencies are recommended in this approach including horizontal stiffness of the soil and pile system, maximum moment in the pile, and elastic buckling of the pile. Equivalent cantilever lengths are presented in a non-dimensionalized format as shown in Figure 5-1. In a relatively long pile, l_c is the length below which the lateral displacements are a small percentage of the pile head displacement and is calculated as:

$$l_c = 4\sqrt[4]{\frac{EI}{k_h}} \quad \text{Eq. 57}$$

Where, EI is the pile's flexural stiffness and k_h represents the initial horizontal stiffness of the soil. In Figure 5-1 l_u is the un-embedded length of the pile, and l_e is the equivalent cantilever length.

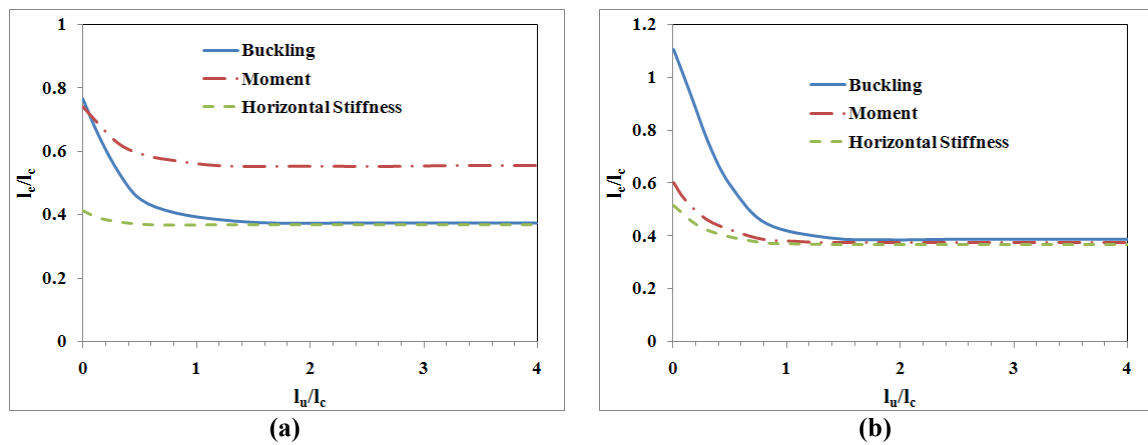


Figure 5-1- Equivalent cantilevers in uniform soils for (a) pinned head piles (b) fixed head piles (Abendroth, Greimann and Ebner, 1989)

5.1.2. Numerical Study

Because of the term related to soil contribution in the governing differential equation of the pile, this equation can't be solved conveniently. Some researchers have assumed simplified forms for the soil response to facilitate the solution (Davisson, 1963, Davisson and Robinson, 1965, Prakash, 1987, Gabr, Wang and Zhao, 1997, Heelis, Pavlovic and West, 2004), but finding a closed form solution is impossible because of the complexity of the problem.

To solve the governing differential equation of the pile, a MATLAB code is developed. General information of the problem such as pile and soil information are defined in the main code. Since the governing differential equation is an ODE problem

with boundary values, the `bvp4c` function is utilized which solves boundary value problems for ordinary differential equations. This function requires the differential equation defined as a function as well as the boundary conditions inputted as a separate residual function, and an initial guess.

5.1.2.1. *p-y Curves for Soft Clay*

Matlock (1970) tested instrumented pipe piles and developed *p-y* curves for soft clay based on the results of that experimental study. The tested pile was 324x12.7 mm (12.75x0.5 in) steel pipe embedded 12.8 m (42 ft) into the ground. 35 pairs of strain gages were installed on the pile to determine the bending moment along the pile length.

During the experimental study, static loadings at four levels were applied to the pile while providing free rotation at the head.

Based on the results of the experiment, *p-y* curves were proposed for design of laterally loaded piles in soft clay for static loading as follows:

$$\begin{aligned}
 p(z, y) &= 0.5 p_u \left(\frac{y}{y_c} \right)^{1/3} && \text{if } y < 8y_c \\
 p(z, y) &= p_u && \text{if } y > 8y_c
 \end{aligned}
 \tag{Eq. 58}$$

Where, $p(z, y)$ is the soil response to lateral displacement, p_u is the ultimate soil resistance per unit length of the pile and is a function of the soil properties and the depth, y is the lateral displacement, and y_c is a function of soil properties.

The proposed *p-y* equation is defined as a function in the MATLAB (2007) code and is used in solving the governing differential equation of the laterally and axially loaded pile.

5.1.2.2. Energy Method

Energy is stored in different forms. The strain energy of the bending pile is:

$$V_{bending} = \frac{1}{2} \int_0^H E_p I_p \left(\frac{d^2 y}{dz^2} \right)^2 dz \quad \text{Eq. 59}$$

Where, E_p is modulus of elasticity of the pile, I_p is moment of inertia of the pile's cross section, and H is length of the pile. The potential energy of the axial load is:

$$V_{axial} = -\frac{1}{2} \int_0^H P \left(\frac{dy}{dz} \right)^2 dz \quad \text{Eq. 60}$$

Where, P is axial load in the segment. The potential energy stored in the soil medium is:

$$V_{soil} = \int_0^H \int_0^y p(z, y) dy dz \quad \text{Eq. 61}$$

Where, $p(z, y)$ is the response of the soil to lateral deformation, and can be estimated by p-y curves.

The current method is a step by step incremental approach. In each step, the governing differential equation of the pile is solved for a specific axial load and the energy values are evaluated based on the solution using Eq. 59 and Eq. 60. Then for the next step, the axial load is increased by a specific increment and the energy values are calculated once again. This sequence is continued until singularity is observed in the calculated energy values (see Figure 5-2). The corresponding axial load is identified as the critical bucking load of the pile.

5.1.2.3. Verification of Buckling Calculations

5.1.2.3.1. Simple Unsupported Column

In order to verify the validity of buckling calculations the differential equation of a simple beam-column is considered which is written as follows:

$$EI \frac{d^4 y}{dz^4} + P(z) \frac{d^2 y}{dz^2} + \frac{dP(z)}{dz} \frac{dy}{dz} + q(z) = 0 \quad \text{Eq. 62}$$

Where, EI is the flexural stiffness, $P(z)$ is the axial load, and $q(z)$ is the lateral load on the beam-column. Assuming that the axial load is constant and the lateral load is zero, Eq. 62 can be summarized to:

$$EI \frac{d^4 y}{dz^4} + P \frac{d^2 y}{dz^2} = 0 \quad \text{Eq. 63}$$

The eigenvalue solution for Eq. 63 results in the calculation of the elastic buckling load which is equal to:

$$P_e = \frac{\pi^2 EI}{(kl)^2} \quad \text{Eq. 64}$$

The pile used in the test by Matlock (1970) is considered (12.8 m long 324x12.7 mm pipe). Two different end conditions are investigated. First, pinned condition is assigned to both ends of the column. Effective length factor for this condition would be equal to 1.0 which leads to a buckling load of 1726.6 KN (388.0 kips) as shown in Figure 5-2(a). In the second condition, both ends of the column are fixed. Effective length factor for fix-fix condition is 0.5 which gives a buckling load of 6906.4 KN (1552.0 kips) (Figure 5-2(b)).

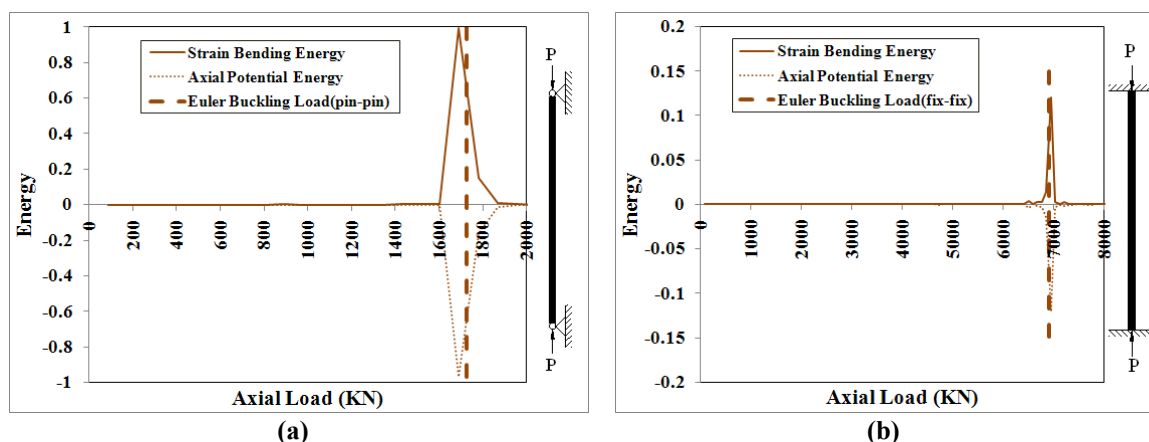


Figure 5-2- Buckling load estimation for a pipe column using energy method (a) pin-pin (b) fix-fix.

To check the validity of the code, axial load of the column is increased in 89 KN (20 kips) steps. Energies in the form of bending and axial are integrated in MATLAB (2007) for each step. Singularities are observed in the vicinity of the theoretical buckling load which verifies that numerical singularity has occurred in the solution of the differential equation and the corresponding axial load is the buckling load of the column (Figure 5-2). Same approach is used to estimate the critical load of the piles embedded in soil medium. In this approach, the axial load of the pile is increased up to the point where singularity is observed in the energies. MATLAB (2007) code can track these jumps and reports the corresponding axial load as the critical buckling load.

5.1.2.3.2. Pile Buckling Test

It should be noted that because of the nature of the problem limited test information is available in the literature. Here, the test by Vogt et al. (2009) on scaled piles is considered (Figure 5-3-a). In this test the pile's flexural stiffness was 37.3 KN.m² (12988 kip.in²) and its length was 4 m (157.5 in). In one test the soil's shear resistance was 12.4 kPa (1.80 psi) and the corresponding buckling load was about 220 KN (49.4 kips). It is

reported that the unsupported buckling capacity of the pile was about 23.0 kN (5.2 kips). It is clear that the soil has provided some lateral support and has increased the critical buckling load to some extent.

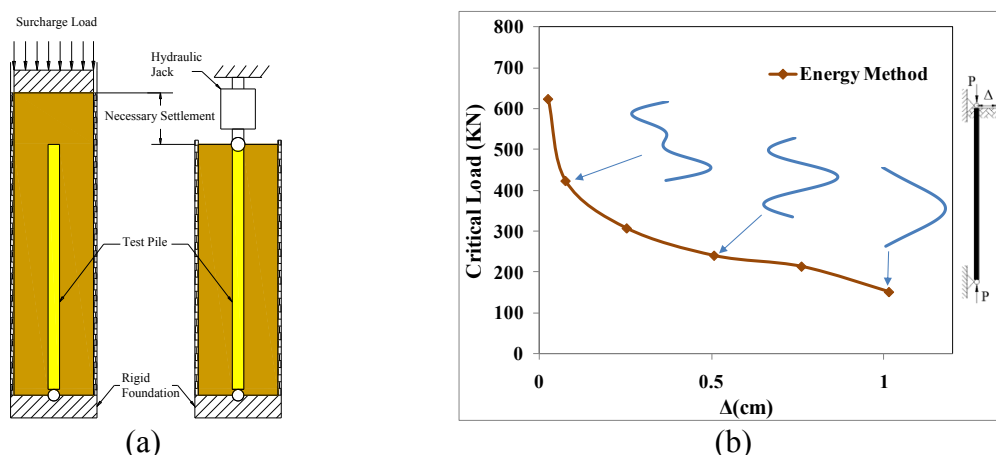


Figure 5-3- (a) Test setup (b) buckling load estimation for the pile tested by Vogt et al. (2009).

Figure 5-3-b shows the results of buckling analyses using the energy method. Theoretical buckling shapes obtained from MATLAB (2007) are also presented in this figure. As shown, for relatively small head movements, higher modes of buckling occur and consequently larger critical loads are estimated. However, due to imperfection lower modes of buckling are possible and are closer to the test result. It should be noted that the reported mode of buckling for this pile matches with the buckling shape corresponding to 0.5 cm (0.2 in) head movement from the energy method at which the critical load is very close to the test result.

On the other hand, using the same information in the equivalent cantilever length, and assuming 3445.0 kPa (72 kips / ft²) for the modulus of subgrade reaction based on Oesterle et al. (2005), l_c is estimated as:

$$l_c = 4\sqrt[4]{\frac{EI}{k_h}} = 4\sqrt[4]{\frac{37.3 \times 10^3}{3445 \times 10^3}} = 1.29 \text{ m}$$

Since the pile is fully embedded in this case, the ratio of un-embedded length over fixity length is zero and using Figure 5-1-a, which is for pinned head pile, the ratio of $\frac{l_e}{l_c}$ for buckling is about 0.8. So the effective length would be

$$l_e = (0.8)l_c = (0.8)(1.29) = 1.03 \text{ m}$$

Since the pile head is pinned the length factor would be equal to 0.7 and the critical load is estimated as:

$$P_{cr} = \frac{\pi^2 EI}{(kl)^2} = \frac{\pi^2 (37.3 \times 10^3)}{(0.7 \times 1.03)^2} = 708.2 \text{ KN}$$

It is clear that the critical load estimated by equivalent cantilever method is much larger than the measured load.

5.1.2.4. Another Comparison with Current Method

To compare the result of this analysis with equivalent cantilever method, the pile from the test by Matlock (1970) is considered. Based on Oesterle et al. (2002) Modulus of subgrade reaction for soft clay can be assumed constant and equal to 3445.0 kPa (72 kips / ft²). Using the equivalent cantilever method one can write:

$$l_c = 4\sqrt[4]{\frac{EI}{k_h}} = 4\sqrt[4]{\frac{(3.01 \times 10^7)}{(3.445 \times 10^6)}} = 6.88 \text{ m}$$

$$\frac{l_u}{l_c} = \frac{0.30}{6.88} = 0.04$$

Using Figure 5-1-a (pinned head pile in uniform soil), the ratio of $\frac{l_e}{l_c}$ for buckling is

about 0.8. So the effective length would be:

$$l_e = (0.8)l_c = (0.8)(6.88) = 5.5 \text{ m}$$

Total equivalent length of the pile can then be calculated as the sum of the un-embedded length and the equivalent cantilever length:

$$l = l_u + l_e = (0.3) + (5.5) = 5.8 \text{ m}$$

Since the pile head is assumed to be pinned, the effective length factor is 0.7. Critical buckling load is estimated as:

$$P_{cr} = \frac{\pi^2 EI}{(kl)^2} = \frac{\pi^2 (3.01 \times 10^7)}{(0.7 \times 5.8)^2} = 18022 \text{ KN}$$

The energy method is used to compare the buckling load estimated from two methods. It is assumed that the pile head movement before applying the axial load is 2 cm. As shown in Figure 5-4 the buckling load from the energy method can be estimated about 5607 KN (1260 kips) which is much lower than the value calculated from equivalent cantilever method. This shows that the equivalent cantilever method is very un-conservative and the pile may buckle under loads much lower than that estimated by this method.

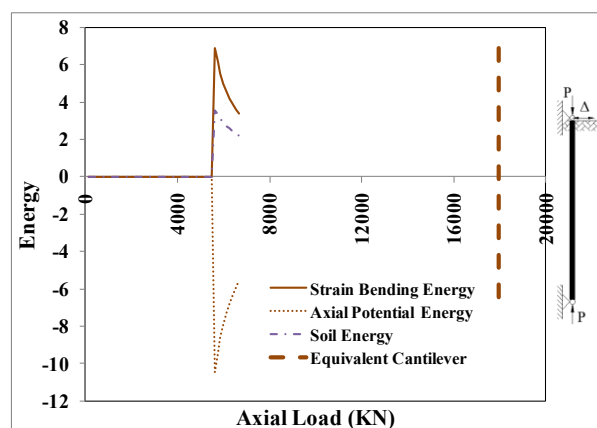


Figure 5-4- Buckling load estimation for a pile using energy method ($\Delta=2.0$ cm)

In the problem solved, Eq. 31 is used to estimate the buckling load since it is assumed that the axial load along the length of the pile is constant. It is clear that this is a simplifying assumption, and in reality, piles transfer some of the axial load to the soil in the form of friction along their length and axial load is no longer constant. To account for the effect of friction along the pile length, Eq. 38 should be used in the analysis instead of Eq. 31. Since the axial load in the pile decreases along the pile, it is clear that in friction piles, the axial critical load would be larger than the case with constant axial load. For this reason, the constant axial load assumption is a conservative assumption which can reduce analysis time. In order to compare the difference between the two cases, linear axial load is assumed with tip load equal to half of the applied load on the top. In this case the critical axial load is estimated about 5940 KN (1335 kips) which is slightly larger than the case with constant axial load. Because of this small difference, it is preferred to do the rest of the study based on the constant axial load assumption.

5.1.3. Results and Discussion

A parametric study has been conducted to determine the effects of various parameters involved in soil-pile interaction problem on the buckling load. The parameters

are pile head deflection (Δ), flexural stiffness of the pile (EI), pile length (L), and soil shear strength (c). For this purpose the values involved in the test by Matlock (1970) have been set as baseline. When a parameter varies, the other parameters are set to be the reported values from the experiment. Table 5-1 lists the range of parameters used in the parametric study. In each case, four different boundary conditions are applied including pinned and fixed at both ends of the pile.

Table 5-1- Range of parameters in the parametric study

Parameter	Unit	Baseline Value	Min. Value	Max. Value
Pile Head Movement (Δ)	mm	0	50.8	0
Moment of Inertia (I)	mm ⁴	1.50x10 ⁸	3.01 x10 ⁷	3.01x10 ⁸
Embedded Length (L)	m	12.8	4.27	42.72
Soil Shear Resistance (c)	kPa	13.02	9.65	15.85

5.1.3.1. Effect of Pile Head Deflection

At first, pile head movement does not seem to be a big factor, but results show that larger pile head movement reduces the buckling capacity drastically. This fact can be related to the lateral support provided by the soil. At very small head movements most of the surrounding soil is in the elastic range and has not reached its ultimate capacity. In this case, the lateral support is so high that the buckling happens in the second mode as shown in Figure 5-5. In larger movements (>0.75 cm) though, parts of the soil reach their ultimate load resistance and cannot provide further stiffness to the system, and as a result the buckling in the first mode becomes possible and consequently buckling load drops severely.

On the other hand, the buckling analysis is carried out in MATLAB (2007) using linear soil response as in the theory of modulus of subgrade reaction, assuming $k_h = 3445.0$ kPa (72 kips / ft²). In this case because of the linearity of the system,

buckling load remains constant as the pile head movement increases. Furthermore, the buckling happens in the second mode and is comparable to the results of the analysis by p-y method at low head movements.

Buckling mode shapes in the following figure are derived from the analysis of the pile under the corresponding axial load with certain head lateral movement.

Since piles in integral jointless bridges will undergo lateral movement, pile buckling calculation shall be done at some level of lateral movement. Results show that for movements above 0.75 cm (0.3 in) first mode of buckling occur (Figure 5-5). Usually in jointless bridges because of thermal induced deflections, piles will undergo larger movements at their head. In the rest of analyses, 2 cm pile head movement is assumed.

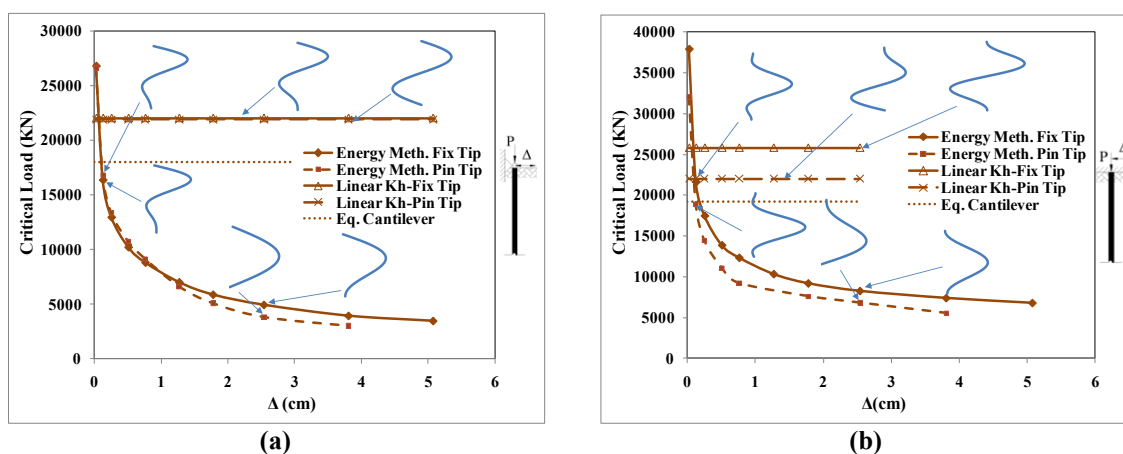


Figure 5-5- Effect of pile head movement on critical buckling load (a) pinned head (b) fixed head.

5.1.3.2. Effect of Pile's Flexural Stiffness

To study the effect of flexural stiffness, the modulus of elasticity is assumed to be fixed, while changing the cross section's moment of inertia. Result of buckling analysis for different moment of inertia is presented in Figure 5-6. This figure also shows the axial load that causes yielding of the cross section. In the calculation of the yield load, P_y , it is

assumed that the cross section is pipe with 12.7 mm (0.5 in) thickness. Further, the yield stress of the cross section is assumed 292.8 MPa (42.5 ksi). As shown in the figure, equivalent cantilever method overestimates the buckling load. Furthermore, one can conclude that the section yields before it reaches the buckling load.

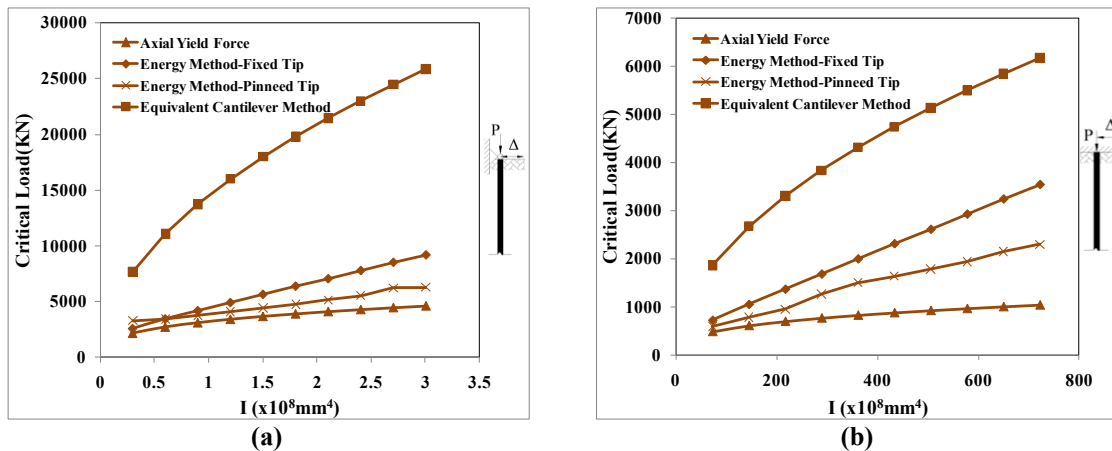


Figure 5-6- Effect of pile flexural stiffness on critical buckling load (a) pinned head (b) fixed head ($\Delta=2.0$ cm)

5.1.3.3. Effect of Embedded Length

Figure 5-7 illustrates the effect of pile length on the buckling load. As expected, it is observed that the buckling load decreases as the length increases and almost remains constant after a certain length. This fact is due to the lateral support provided by the surrounding soil.

In design, generally, the point of fixity is defined as the point after which displacements and moments are fairly small. However it cannot be a practical definition since in larger head deformations this point goes deeper in the soil (Chovichien, 2004).

Instead of the current definition of fixity point, it can be referred to as a point after which the buckling load remains constant. So to obtain the fixity point, a buckling analysis is recommended using available information of the soil and the pile. For the

problem solved, the fixity length can be estimated around 12.7 m (500 in) for pinned head which is close to the pile length used in the test, and 17.8 m (700 in) for fixed head.

Figure 5-7 also shows that after a certain length, the tip condition of the pile does not affect the critical load and the two curves corresponding to the fixed and pinned tip condition merge together. This length is about the same as the length after which the buckling load remains constant.

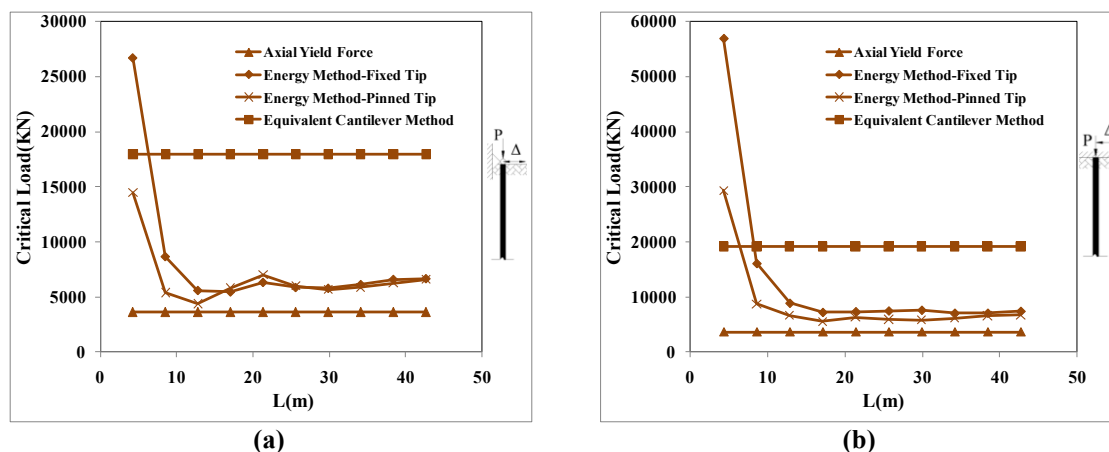


Figure 5-7- Effect of pile length on critical buckling load (a) pinned head (b) fixed head ($\Delta=2.0$ cm)

5.1.3.4. Effect of Soil Shear Resistance

To investigate the effect of the soil around the pile, the main parameter of the cohesive soil, which is its shear resistance, is varied. In order to have a comparison between the two methods, it is assumed that the relationship between shear resistance and modulus of subgrade reaction is linear. It is observed that the buckling load is not very sensitive to the soil's shear resistance and it remains fairly constant as the soil resistance increases (Figure 5-8). Furthermore, like other cases, critical load estimated by equivalent cantilever method is much larger than the one calculated using the energy method.

Besides, except for very small shear resistances, the critical load is above the yield limit, which means that the buckling does not govern the design.

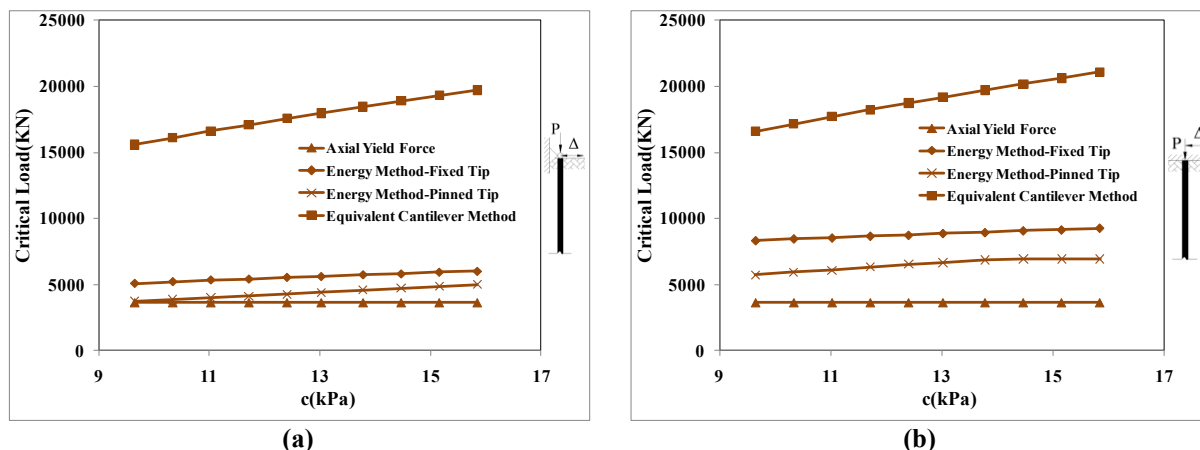


Figure 5-8- Effect of soil shear resistance on critical buckling load (a) pinned head (b) fixed head ($\Delta=2.0$ cm)

5.1.4. Conclusions

In this study the governing differential equation of a pile is used to estimate the behavior of laterally loaded piles under axial loading. The energy method is employed to estimate the buckling load of piles. Based on the analyses and the parametric study, the following conclusions are made:

- Verification examples provided for simple beam prove that the energy method is a valid approach to estimate the critical load of piles. In the method presented, nonlinear soil behavior is considered while in previous methods the soil reaction is a linear function of the lateral displacement.
- Pile head movement has a great effect on the level of buckling load. For small head movements the energy method and equivalent cantilever method are comparable.

However, for larger head movements buckling loads estimated by the energy method drop severely.

- It is shown that for soft clay the buckling load corresponding to 2 cm pile head movement does not govern the design as the pile will fail before reaching the critical axial load because of yielding. This conclusion can be expanded for medium and stiff clay since the lateral support provided by these types of soils is larger which increases the critical load in this case.
- The equivalent cantilever method is not a valid design method for buckling of piles in integral jointless bridges since the estimated loads by this method are highly above the values estimated by the energy method at larger pile head movement.

5.2. Pile Head Detail

In order to reduce the induced loads from the substructure to the superstructure, typically flexible foundations are recommended which consist of one row of piles to accommodate longitudinal movements and provide maximum flexibility (Burke Jr, 2009). Furthermore, to increase the flexibility of the piling against longitudinal thermal movements several methods are utilized.

Weak axis bending: The easiest way to reduce the stiffness of the piling system is to align the piles such that they bend along their weak axis when the bridge moves longitudinally (Haj-Najib, 2002, Chovichien, 2004, Girton, Hawkinson and Greimann, 1991, Thanasattayawibul, 2006). Most of the states use this method (Kunin and Alampalli, 1999, Haj-Najib, 2002); however, the study by Oesterlie et al. (2002) revealed

that local buckling and yielding of the pile is possible at the critical section which is the interface between the pile and the cap.

Pre-drilled holes: This method is also popular among different agencies. Since the top portion of the pile plays the most important role in its response to the lateral movement, by replacing the top portion of the surrounding soil with non-compacted granular soil, more flexibility is achieved (Haj-Najib, 2002, Girton, Hawkinson and Greimann, 1991). After the embankment is placed and compacted, holes are drilled and in some cases plastic sleeves are placed in the hole. Then the pile is driven and finally the hole is filled with granular soil. Although this seems to be an efficient method, but some studies have revealed that the granular soil becomes compacted after a while and larger response is observed from the soil.

Rotation over the pile head: A simple study revealed that providing pin connection at the pile head can effectively reduce the stiffness, and also lower the moments developed in the pile as a result of lateral movement, since the pile will deform in a single curvature shape rather than double. Some researchers have studied different details to provide rotational capacity over the pile head. However, all of these details can handle relatively small movements and in some cases their real behavior is unknown.

Kamel et al. (1996) proposed a connection which allows the abutment to slide and rotate over the pile head. In this detail, the pile head is encased in 2 in expanded polystyrene, while a bearing pad is located between the top of the pile and the abutment. Further information about this detail is not available. However, as mentioned by authors,

this detail can handle relatively small movements (below 1 in). Besides, the performance of the bearing pad located above the pile head is questionable.

Another detail that was believed will reduce stiffness of jointless bridge piling was tested by Arsoy et al. (2002). In this detail, the pile cap and abutment backwall are constructed separately, and the shear between these two elements is transferred by dowels. No signs of distress were observed in the test conducted, however, the performance of this detail under larger deformation and also its behavior in skewed bridges is debatable.

Abendroth et al. (2007) studied the behavior of a jointless bridge in which the tops of the abutment piles be wrapped with a double thickness of rug padding to permit rotation to occur between the top of the abutment piles and the abutment pile cap. However, based on monitoring results it was observed that the connection does not provide enough of rotational capacity to be assumes as pinned.

Frosch et al. (2009) tested a pile head connection that consisted of 1in polystyrene pads wrapped around the H-Pile head. Apparently Indiana DOT has used this detail to provide rotational capacity over the pile head. However, there are concerns regarding walking and unintentional lateral movement of the pile head under cyclic loading. Although no sign of distress was observed in the tests, but Frosch et al. (2009) believe that the lateral load resisting of this detail is substantially less than regular connection.

5.2.1. FEM Modeling of an Embedded Pile

As a basic investigation, the field test by Burdette et al. (2003) is considered. In this test the behavior of prestressed concrete piles in cohesive soil was studied.

The pile used in the test was 14”x14” prestressed concrete reinforced with six 0.5 in diameter 270 k, low relaxation seven wire strands. The pile was embedded 12 inch in an abutment and was driven 36 ft into the ground. The soil in which the pile was driven was residual red clay. The test setup was designed to simulate a real integral abutment supported by prestressed concrete piles (Figure 5-9)

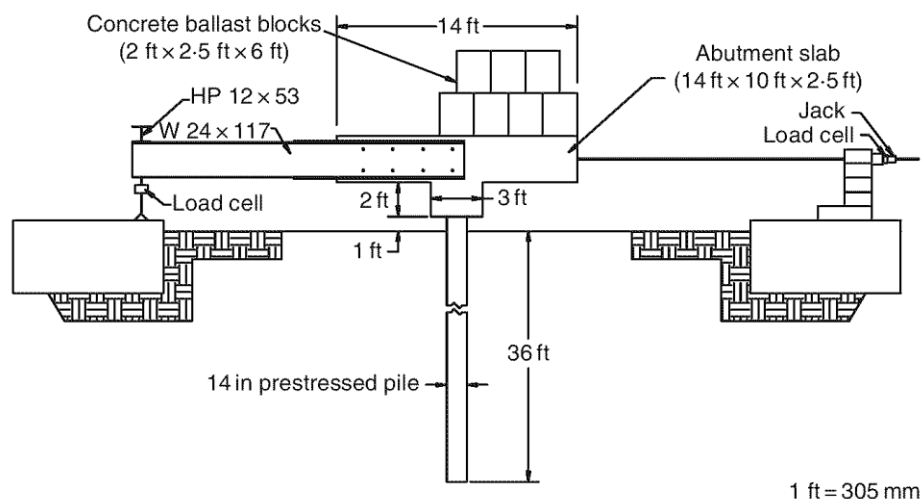


Figure 5-9- Test setup by Burdette et al.

The abovementioned test is modeled in ABAQUS to investigate the piling system behavior and study the new concept. All the elements used in the test are precisely modeled to simulate the real test conditions. Concrete material is simulated using concrete damaged plasticity model. Pre-stressing of the strands is modeled with *INITIAL CONDITIONS in ABAQUS, and then the lateral load is applied to the abutment.

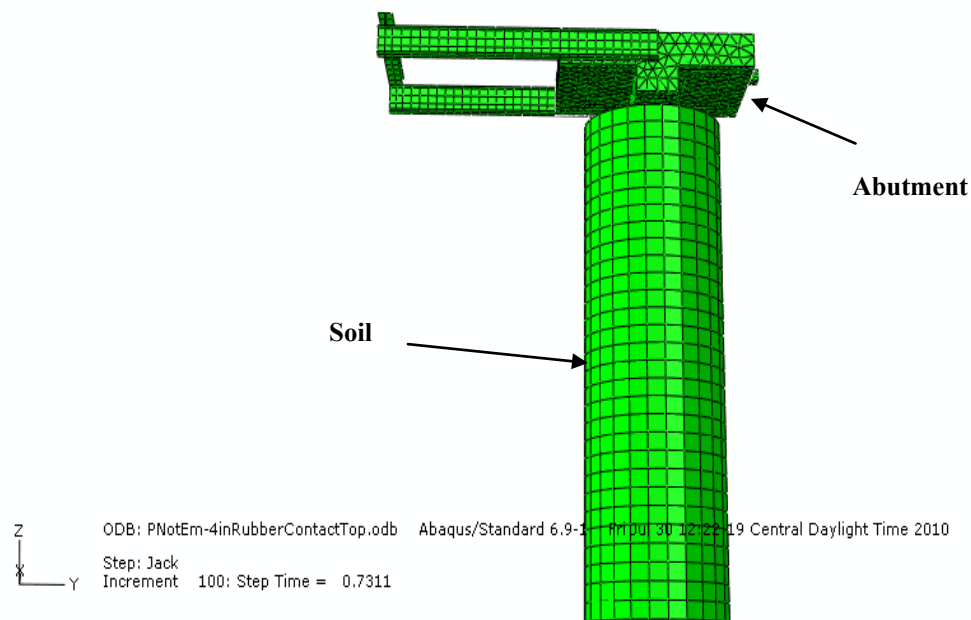


Figure 5-10- FEM model of the test by Burdette et al.

In the field test because of full fixity at the pile-abutment connection, the maximum moment happened at the interface and cracks were observed at this location after 1 in movement.

In order to investigate the pin connection, 4 in rubber with modulus of elasticity of 10,000 psi is placed around the pile head.

Drucker-Prager model is used to model the soil nonlinear behavior in ABAQUS. Laboratory unconfined compression test data are used in the modeling. Elastic-perfectly plastic model is utilized and it is assumed that the soil yield stress is 20 psi.

Contrary to steel, modeling the concrete behavior is a very difficult task. Generally ABAQUS contains two specific models for concrete, the smeared cracking model and the damaged plasticity model. The first model can be unstable in post buckling analysis, and often stops due to numerical difficulties prior to experimental ultimate load. Concrete

damage plasticity model is utilized to model nonlinear behavior of the concrete due to its satisfactory accuracy in representing reinforced concrete. This model assumes two major failure mechanisms for concrete; cracking under tensile and crushing under compressive stresses.

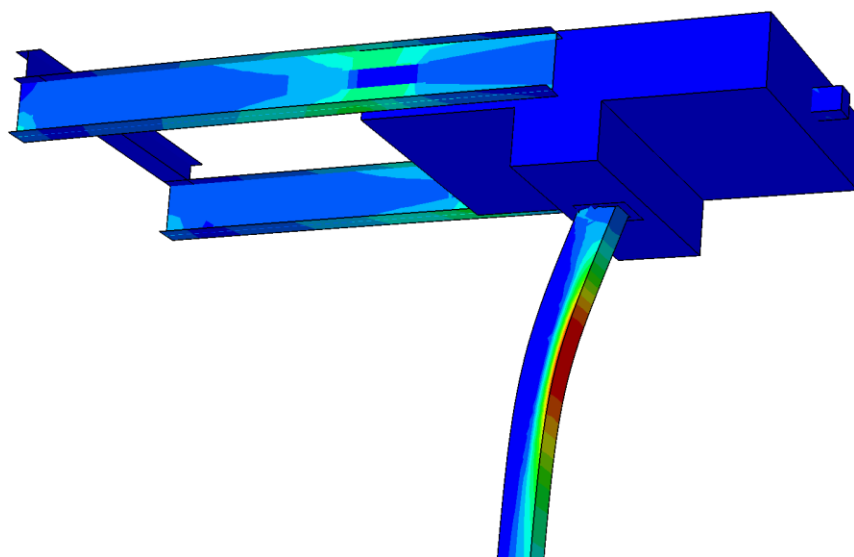


Figure 5-11- Stresses in pinned system at 1.84 in ground deflection.

Figure 5-12 depicts the maximum principal plastic strain in prestressed pile. This parameter is a criterion in determination of crack patterns in concrete elements using concrete damaged plasticity model. As shown in this figure, the value of maximum principal plastic strain at 1 in ground level deflection for the test model (fixed head condition) is almost twice as much as the corresponding value at 1.84 in ground level deflection for the model with 4" rubber casing. Note that at these deflections for both models, the maximum stress in prestressing strands was 288 ksi. Burdette et al. (2003) reported visible cracks after 1 in ground level deflection right at the pile-cap interface. Based on their observations, they recommended 1.5" maximum lateral deflection for prestressed piles.

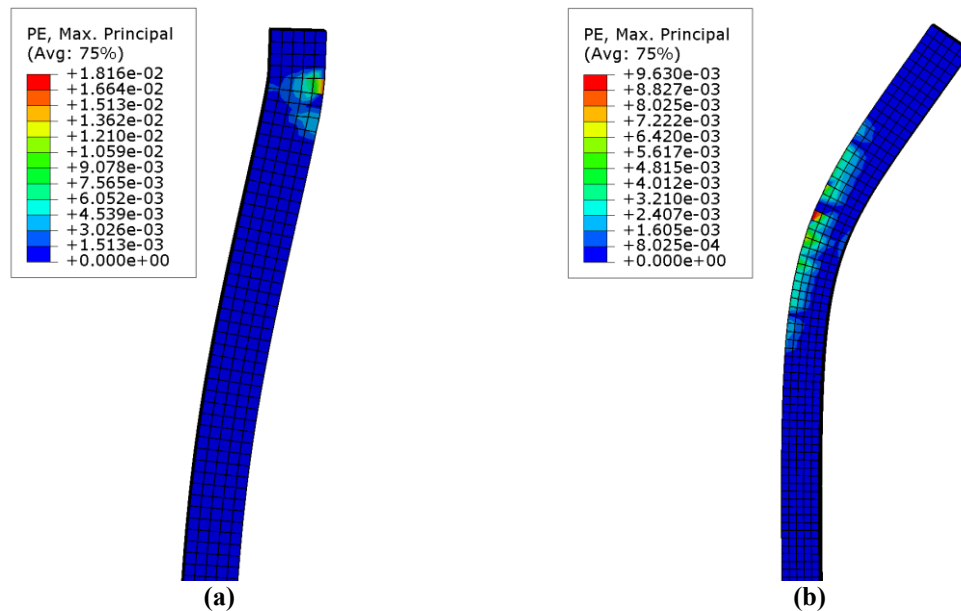


Figure 5-12- Principal maximum plastic strain (a) fixed head at 1.0 in ground level deflection (b) pinned head at 1.84 in ground level deflection.

Load-deflection curves are illustrated in Figure 5-13. First the finite element model for real experiment is calibrated, and then the pinned model is built based on the first model. It can be concluded that encasing the pile head in soft material can efficiently reduce the piling stiffness.

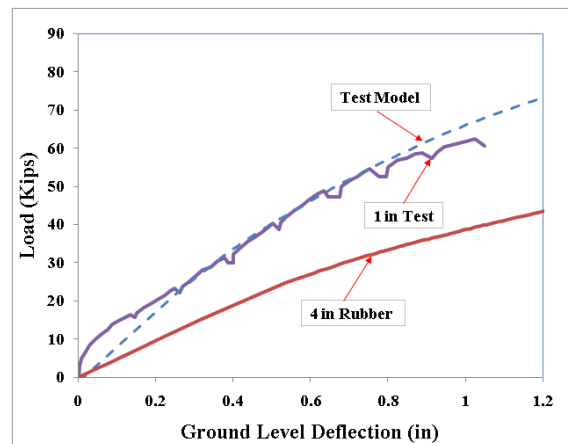


Figure 5-13- Load deflection curve (a) comparison of test result with FEM model (b) comparison of FEM results for full fixity, 1 in rubber, and 4 in rubber

5.2.2. FEM Modeling of the Specimens

ABAQUS has been used to model the specimens described in Chapter 4.

5.2.2.1. Description of the Model

Concrete damage plasticity model has been employed for concrete in of the cap and CFT. It is assumed that the concrete's compression strength, f'_c , is 4.0 ksi. Bilinear model with $F_y = 57.4 \text{ ksi}$, $F_{ult} = 65.0 \text{ ksi}$ and $\epsilon_{ult} = 0.35$ is utilized for steel plasticity. It is assumed there would be no slippage between the pipe's inner surface and the filled concrete. Therefore, the related interface is attached using tie option. Pipe, filled concrete, elastomer, plates, and the cap are modeled using 8-noded solid elements (C3D8R).

The axial load is applied by applying uniform pressure on the end surface of the CFT. Then, the lateral displacement is applied on the load points.

5.2.2.1.1. Specimen #1

CFT in this specimen is embedded in the concrete cap. The cap is modeled as a rectangular cube with 12.75 in diameter hole extended 24 in representing the connection of the pipe to the cap. Surface/surface contact with hard normal behavior is assigned to pipe/cap interface.

5.2.2.1.2. Specimen #2

In this specimen the pile head is encased in the elastomer ring which is then embedded in the concrete cap. Elastomer/cap interface is bound with tie option, whereas pipe/elastomer interface is modeled with contact, as the corresponding surfaces may separate during loading. Hard normal behavior with relatively rough tangential behavior is assigned to this interaction. The embedded plate is tied to the end of the hole in the cap,

while the endplate/embedded plate interface is modeled with contact option as they can slide against each other and separate.

5.2.2.2. Results of Analysis

The results of FEM analyses are compared to the load-deflection envelope of the tests specimens in Figure 5-14.

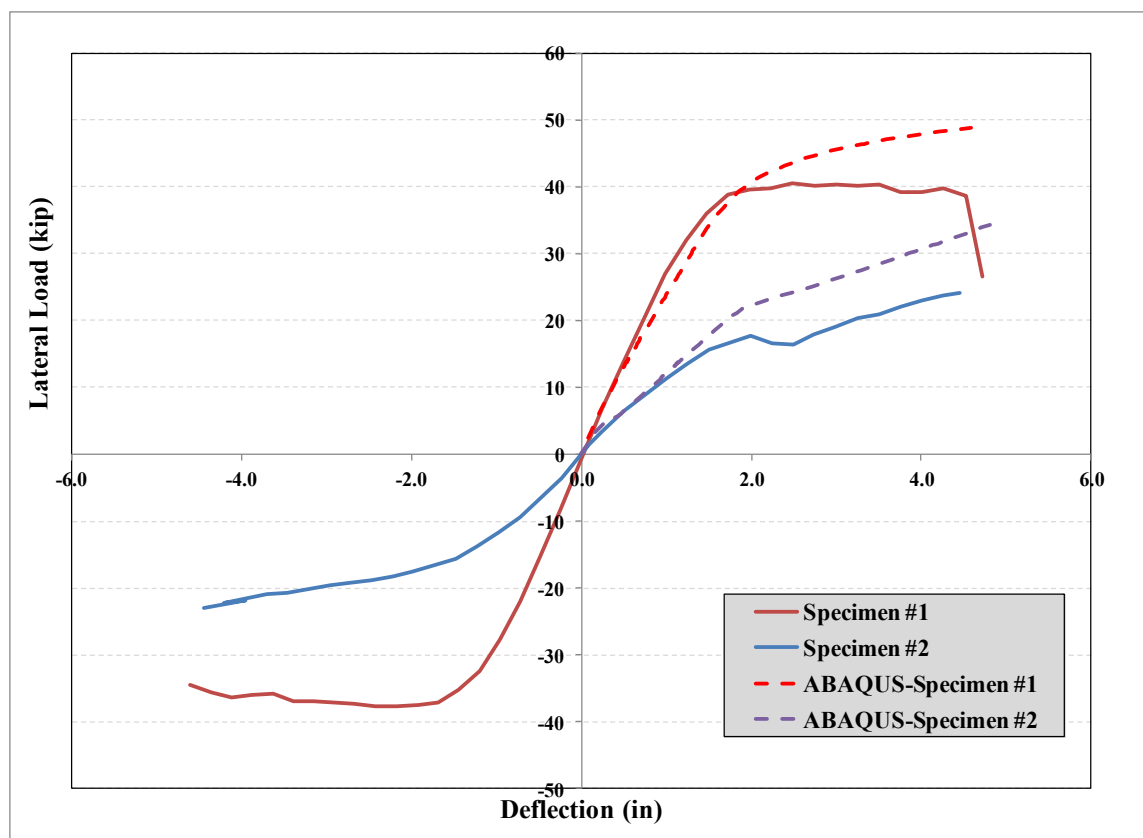


Figure 5-14- Load deflection curves comparing the test results with FEM models

Maximum principal plastic strains at 4.0 in deflection are compared in the following figure for the two models at mid cross section cut.

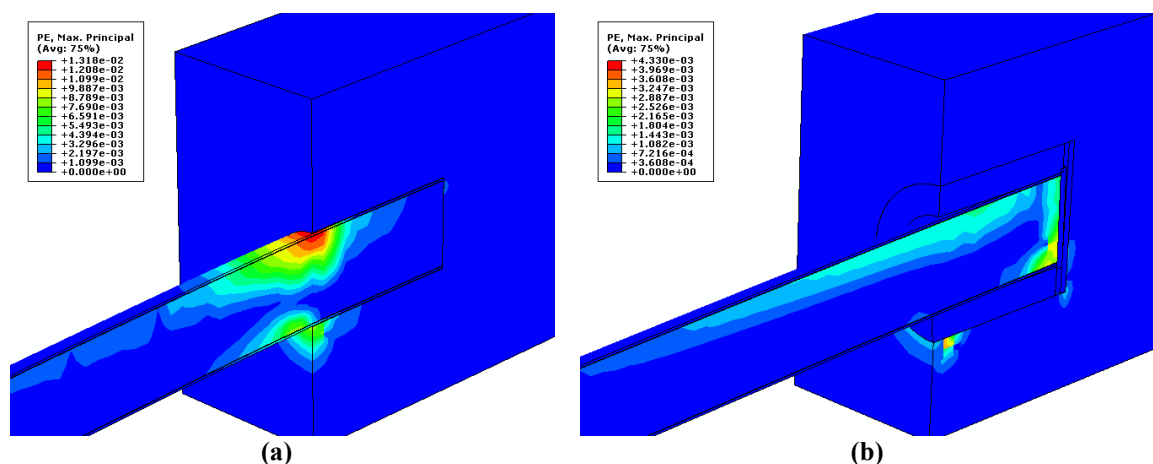


Figure 5-15- Maximum principal plastic strains at 4.0 in deflection (a) specimen #1 (b) specimen #2

The following table compares the maximum principal plastic strains in different elements at 4.0 in deflection.

Table 5-2- Maximum principal plastic strain in different elements

	Specimen #1		Specimen #2	
	Maximum	Location	Maximum	Location
Pipe	1.32e-2	interface	1.96e-4	Pile tip
Filled Concrete	1.30e-2	interface	4.33e-3	Pile tip
Cap	9.48e-3	interface	3.60e-3	interface
Elastomer	NA	NA	0	NA

The maximum Von-Mises stress at 4.0 in deflection, in the filled concrete was about 11.6 ksi and 4.7 ksi for specimen #1 and specimen #2 respectively. Clearly, the filled concrete had crushed in specimen #1.

Calibrated finite element models prove the validity of the concept and show that by providing rotational capacity in the pile/cap interface larger displacement capacity can be obtained.

5.3. Design of Piles for Fatigue

5.3.1. Estimation of Maximum Allowable Strain

Thermal induced longitudinal movement of the jointless bridges result in one dominant cycle through a year because of seasonal temperature change and numerous small cycles due to daily temperature changes (Dicleli and Albhaisi, 2004). Based on several field test data on jointless bridges Karalar and Dicleli (2010) concluded that the bridge undergoes an average of 148 small but effective cycles. Besides, the amplitude of the small strain cycles was 0.25times the amplitude of the large strain cycles on average. It should be noted however, that the difference between the setting point (construction temperature) and the extreme seasonal temperature may not be different for summer and winter times. Therefore, the amplitudes of strain cycles in positive (ϵ_{ap}) and negative (ϵ_{an}) corresponding to summer and winter times may not be equivalent. As range of strain amplitude is important in the fatigue design, Dicleli and Albhaisi (2004) assumed that the positive and negative strain amplitudes are equal.

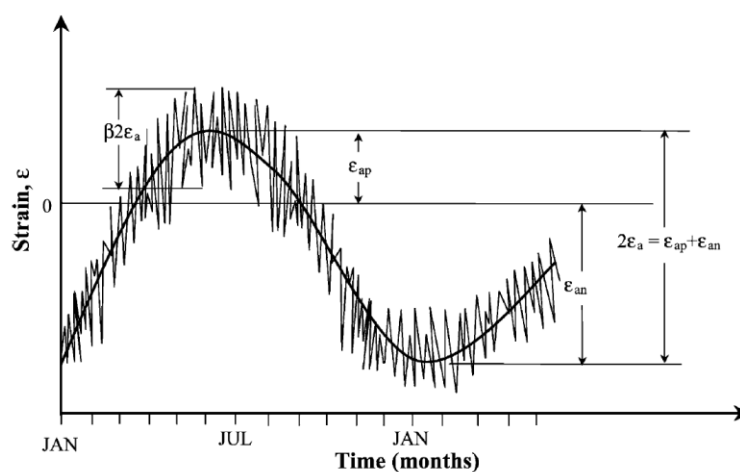


Figure 5-16- Pile strain as a function of time (Dicleli and Albhaisi, 2004)

Piles in jointless bridges undergo lateral movement that may develop significant amount of plastic strains. In strain-based fatigue life estimation of a structure, the number of displacement cycles that lead to failure of a component is determined as a function of

the localized plastic strain. This approach is used here in determining the fatigue life of steel H piles supporting jointless bridge abutments.

Based on several fatigue experiments, Koh and Stephens (1991) proposed an equation based on the total strain amplitude, ε_a to calculate the number of constant amplitude cycles to failure of steel sections under low cycle fatigue.

$$\varepsilon_a = M(2N_f)^m \quad \text{Eq. 65}$$

Where, $M = 0.0795$, $m = -0.448$, and N_f is the number of cycles to failure. As the temperature induced strains in steel H piles have variable amplitudes consisting of large and small cycles, therefore Eq. 65 can't be used directly. Dicleli and Albhaisi (2004) used Miner's rule, in which the cumulative fatigue damage in a structural member undergoing different strain amplitude is defined as follows:

$$\sum_{i=1}^n \frac{n_i}{N_i} \leq 1 \quad \text{Eq. 66}$$

Where, n_i is the cycle associated with the loading number i , and N_i is the number of cycles to failure for the same case. Applying the above equation to the large and small amplitude strains in the piles, the following expression is obtained (Dicleli and Albhaisi, 2004):

$$\frac{n_s}{N_{fs}} + \frac{n_l}{N_{fl}} = 1 \quad \text{Eq. 67}$$

Where, n_s and n_l are respectively, the number of small and large amplitude strain cycles due to temperature changes during the service life of the bridge, and N_{fs} and N_{fl}

are the total number of cycles to failure for the corresponding small and large amplitude strain cycles, respectively. For a bridge with 100 years of service life, the number of small amplitude cycles is $n_s = 14800$, and the number of large amplitude cycles are $n_l = 100$. Using Eq. 65 the small and large amplitude strains are then expressed as (Dicleli and Albhaisi, 2004):

$$\varepsilon_{as} = M \left(2N_{fs} \right)^m \quad \text{Eq. 68}$$

$$\varepsilon_{al} = M \left(2N_{fl} \right)^m \quad \text{Eq. 69}$$

The small strain amplitude, ε_{as} , may be expressed as a fraction of the large strain amplitude, ε_{al} , as follows:

$$\varepsilon_{as} = \beta \varepsilon_{al} \quad \text{Eq. 70}$$

Where β is estimated to have an average of 0.25 (Karalar and Dicleli, 2010). By substituting Eq. 70 into Eq. 68 and solving the numbers of small and large amplitude cycles to failure are obtained as follows (Dicleli and Albhaisi, 2004):

$$N_{fs} = \frac{1}{2} \left(\frac{\beta \varepsilon_{al}}{M} \right)^{\frac{1}{m}} \quad \text{Eq. 71}$$

$$N_{fl} = \frac{1}{2} \left(\frac{\varepsilon_{al}}{M} \right)^{\frac{1}{m}} \quad \text{Eq. 72}$$

By substituting Eq. 71 and Eq. 72 into Eq. 67 and solving for ε_{al} , the maximum large amplitude strains a pile may sustain is then obtained as (Dicleli and Albhaisi, 2004):

$$\varepsilon_{al} = \left(\frac{2n_s}{\left(\frac{\beta}{M}\right)^{\frac{1}{m}}} + \frac{2n_t}{\left(\frac{1}{M}\right)^{\frac{1}{m}}} \right) \quad \text{Eq. 73}$$

Applying $n_s = 14800$, $n_t = 100$, $\beta = 0.25$, $M = 0.0795$, and $m = -0.448$, ε_{al} is estimated to be 0.00297.

Based on the calculated maximum large strain amplitude, $\varepsilon_{al} = 0.002967$, the maximum cyclic curvature amplitude at fatigue failure of the pile is expressed as :

$$\psi_f = \frac{2\varepsilon_{al}}{d_p} \quad \text{Eq. 74}$$

Where, d_p is the width of the pile in the direction of the cyclic displacement. The cyclic moment amplitude corresponding to the calculated curvature amplitude is then obtained from the piles moment-curvature diagram. This moment is used in pushover analysis as control flag to determine the displacement capacity of the steel H piles.

5.3.2. Pushover Analyses

Static nonlinear pushover analysis in SAP2000 is used here to estimate the cyclic displacement capacity of H piles based on fatigue limit. Based on ductility requirement mentioned in Section 6.2.5.2.1, only the two compact sections (HP10x57 and HP12x84) are considered in the analyses.

5.3.3. Soil-Pile Interaction Model

5.3.3.1. Pile driven in Clay

p-y curve can be simplified to bilinear response for piles driven in clay as shown in the following figure.

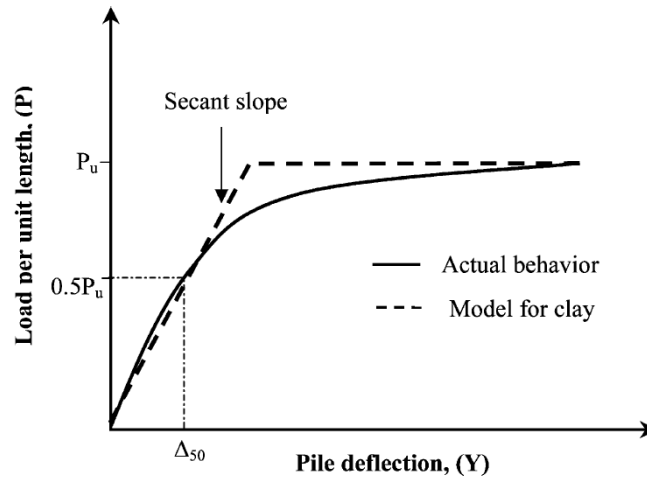


Figure 5-17- Actual and modeled p-y curves for clay (Diciceli and Albhaisi, 2004)

The ultimate response, P_u , is estimated as:

$$P_u = 9C_u d_p \quad \text{Eq. 75}$$

Where, C_u is the undrained shear strength of the clay, and d_p is the pile width. The elastic modulus of the clay soil can be estimated as:

$$E_s = \frac{9C_u}{5\varepsilon_{50}} \quad \text{Eq. 76}$$

Where, ε_{50} is the soil strain at 50% of ultimate soil resistance. The following table lists the corresponding values of C_u and ε_{50} for different clay soils:

Table 5-3- Representative Values of C_u and ε_{50}

Consistency of Clay	C_u (psi)	ε_{50}
Soft	2.9	0.020
Medium	5.8	0.010
Stiff	17.4	0.005

5.3.4. Description of the Model

The pile is modeled using SAP2000 beam elements and divided into 1 ft elements. 40 ft length of the pile is modeled. The models show that this length is enough to provide relative fixed condition in the lower parts of the pile. The pile tip is restrained from movements in all the direction, which is a valid assumption based on the modeled length of the pile.

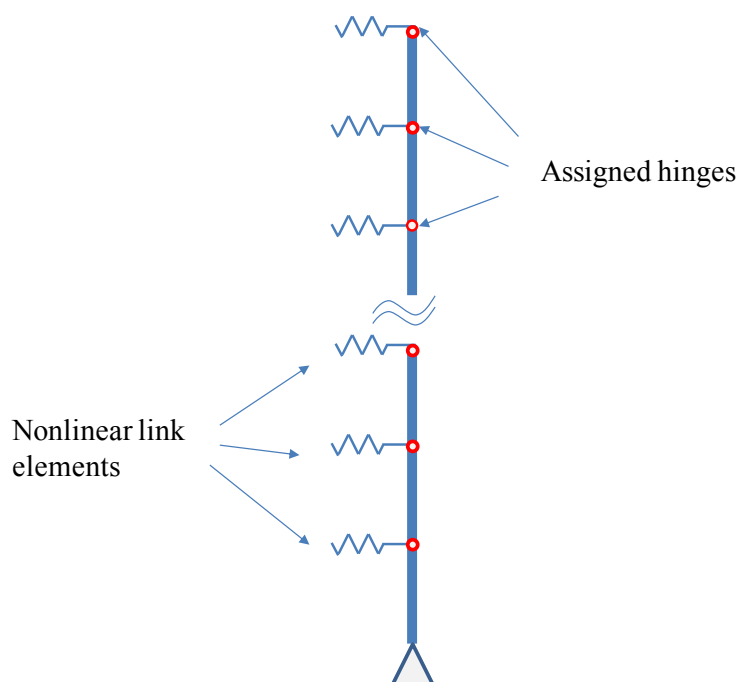


Figure 5-18- Schematic model used in SAP2000

Desired boundary conditions are applied to the pile head based on pinned or fixed condition. The soil response to lateral deflection is modeled using nonlinear link elements placed at every 12". The load deflection properties of the link elements are defined based on the model discussed in the previous section. 36 ksi steel is assigned to the pile sections in all the models. Hinges are assigned to all the beam elements start and end locations. The properties of these hinges are defined based on the orientation and the level of axial load on the pile. Nonlinear pushover load case is defined and a target

displacement is assigned to the top node of the pile. Then the pushover load case is run and based on the target moment, the corresponding lateral displacement is extracted.

5.3.5. Results of the Analyses

Using the described method, and by running pushover analyses the maximum displacement capacity of 36ksi steel piles are estimated and shown in the following figures.

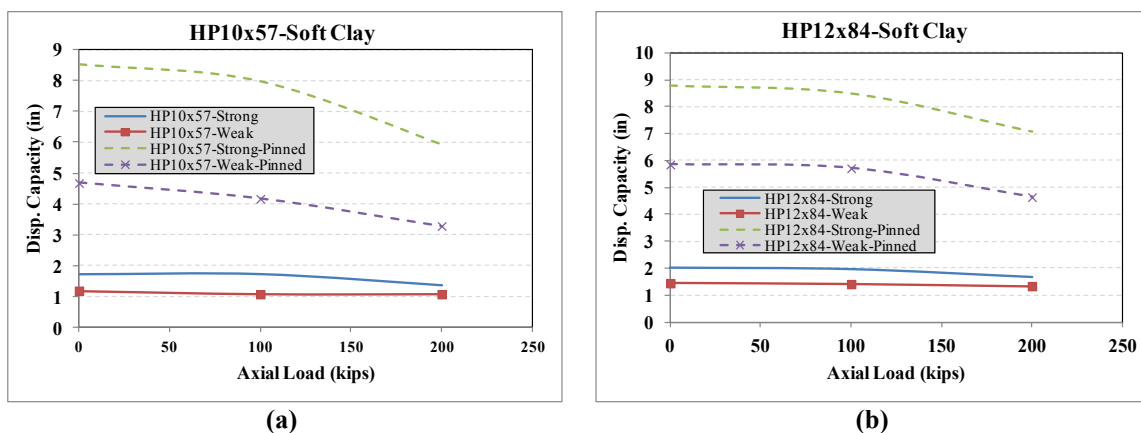


Figure 5-19- Displacement capacity of compact HP sections in soft clay ($c_u = 2.9$ psi) (a) HP10x57 (b) HP12x84

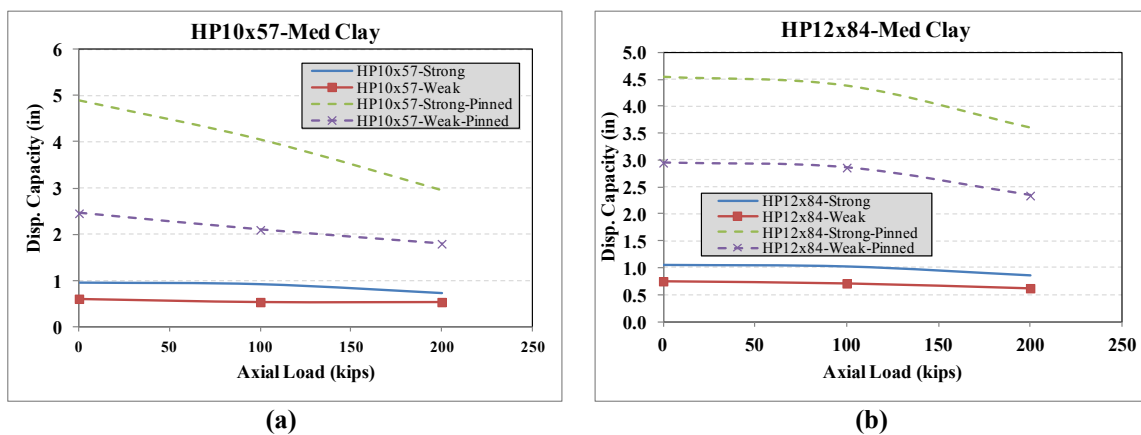


Figure 5-20- Displacement capacity of compact HP sections in medium clay ($c_u = 5.8$ psi) (a) HP10x57 (b) HP12x84

Based on these figures, it can be concluded that the strong axis bending provides more capacity. Besides, by providing rotational capacity over the pile head the lateral displacement capacity can be increased up to 4 times.

5.3.5.1. Example Problem

Consider an HP12x84 pile embedded in medium clay ($c_u = 5.8 \text{ psi}$). Assume this pile is not carrying any axial load. The lateral displacement capacity of this pile for different conditions is estimated as follows.

5.3.5.1.1. Strong Axis Bending

For strong axis bending, the moment-curvature diagram of the cross section of the pile is shown in the following figure.

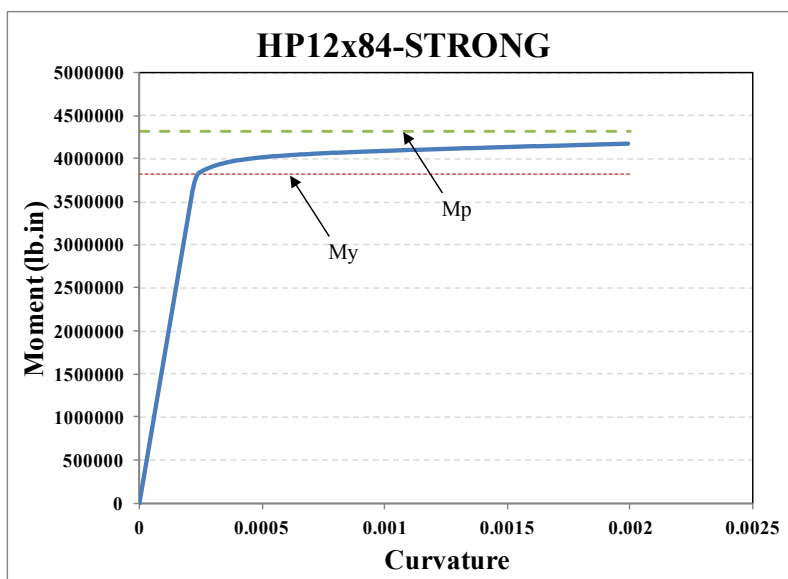


Figure 5-21- Moment-curvature for HP12x84 bending along strong axis with no axial load

As mentioned in section 5.3.1 the maximum allowable strain for 100 years of service life based on Eq. 73 is 0.00297. The maximum curvature corresponding to this strain can be estimated by using Eq. 74 as follows

$$\psi_f = \frac{2\varepsilon_{al}}{d_p} = \frac{(2)(0.00297)}{(12.3)} = 0.00048$$

The moment corresponding to this curvature using the moment-curvature curve shown in Figure 5-21 is about 4016 kip.in. In pushover analysis the displacement corresponding to this maximum moment along the pile represents the lateral displacement capacity of the pile. The following figure depicts the maximum moment along the length of the pile for two the different boundary conditions at pile head location. As shown the lateral displacement capacity for fixed and pinned head condition are 1.04 and 4.55 in respectively.

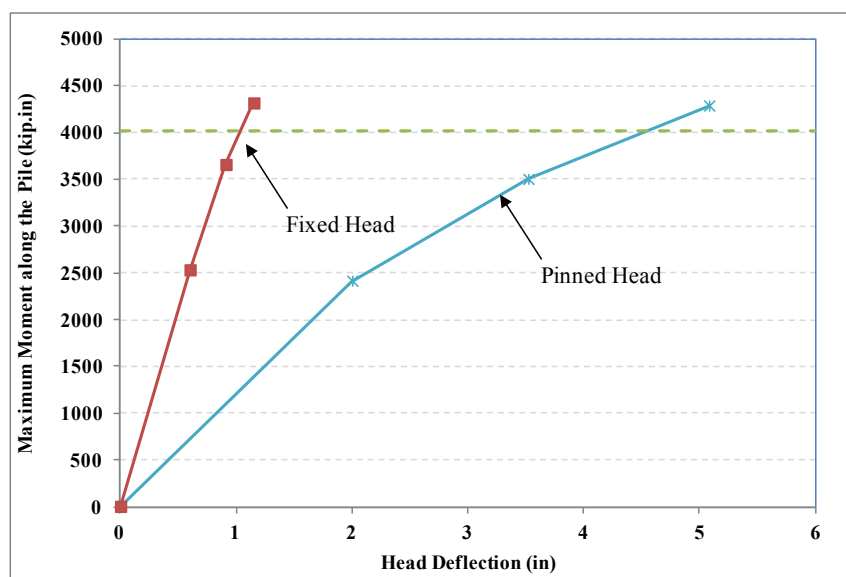


Figure 5-22- Moment-curvature for HP12x84 bending along strong axis with no axial load

5.3.5.1.2. Weak Axis Bending

For weak axis bending, the moment-curvature diagram of the cross section of the pile is shown in the following figure.

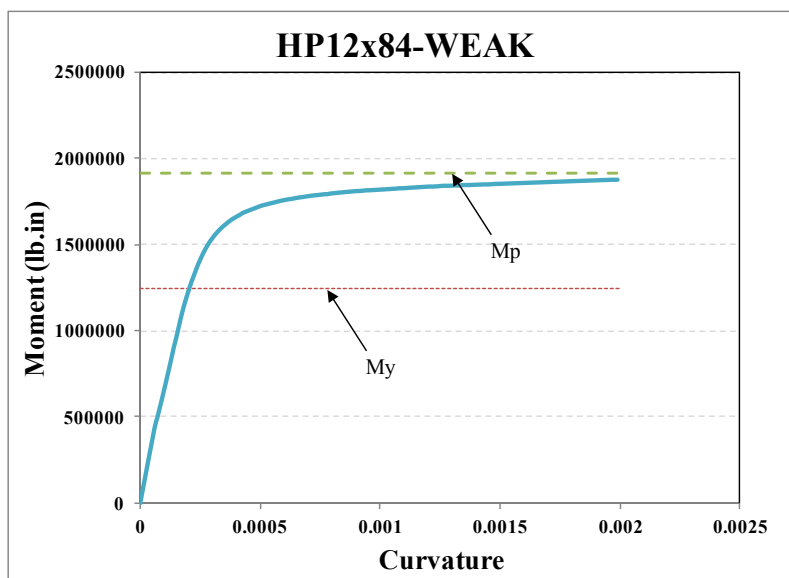


Figure 5-23- Moment-curvature for HP12x84 bending along strong axis with no axial load

Like before, the maximum allowable strain based on fatigue requirement is 0.00297.

The maximum curvature corresponding to this strain can be estimated by using Eq. 74 as follows

$$\psi_f = \frac{2\varepsilon_{al}}{d_p} = \frac{(2)(0.00297)}{(12.3)} = 0.00048$$

The moment corresponding to this curvature using the moment-curvature curve shown in Figure 5-23 is about 1776 kip.in. In pushover analysis the displacement corresponding to this maximum moment along the pile represents the lateral displacement capacity of the pile. The following figure depicts the maximum moment along the length of the pile for two different boundary conditions at pile head location. As shown the lateral displacement capacity for fixed and pinned head conditions are 0.75 and 2.95 in respectively.

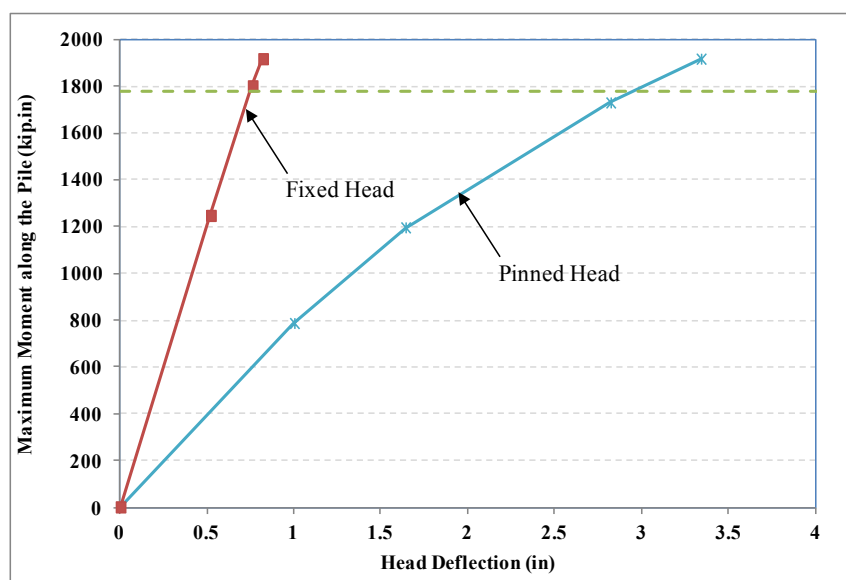


Figure 5-24- Moment-curvature for HP12x84 bending along strong axis with no axial load

5.4. Development of the Design Provisions for Piles

Although jointless bridges have been used for more than 50 years, their implementation has been a matter of intuition, experiment and observation rather than exact science; the main reason being the complexity of soil-structure, and specifically soil-pile interaction problem (Wasserman and Walker, 1996). Despite the lack of analytical tools, bridge engineers have pushed the limits by building longer bridges. In soil-pile interaction problem, the response of deflected pile depends on the soil response and in return, the soil response is a function of pile deflection. Furthermore, the soil response is a nonlinear function of depth and pile's lateral movement. Using the governing differential equation of the pile the soil-pile interaction problem can be solved by using finite difference (Poulos and Davis, 1980) or numerical methods (as described in Chapter 5.1.2). The most popular technique in estimation of the soil response to pile lateral movement is the p-y method.

Based on AASHTO (2010) four criteria should be checked in the pile design process:

- Global stability (buckling)
- Ductility (local buckling)
- Fatigue
- Strength

5.4.1. Global Stability

Equivalent cantilever method has been used for a long time (Abendroth, Greimann and Ebner, 1989, Davisson, 1963, Davisson and Robinson, 1965). In this method the length after which the deflections and the moments are negligible is calculated based on the flexural stiffness of the pile as well the soils' modulus of subgrade reaction. Then using some factors, effective length for calculation of maximum moment, buckling capacity, and ductility is estimated. Then the soil is completely ignored and the pile is analyzed as a cantilever. Since this method models the soil as a linear medium, estimated values of critical loads are larger than real values and result in an un-conservative design.

Elastic buckling of steel piles embedded in cohesive soil using energy method and p-y curves is studied in Section 5.1. In this study, it is shown that the critical axial load is a function of head displacement. By increasing the head displacement, the critical axial load decreases as the lateral support from the soil is reduced because of its nonlinear response. It is also observed that the estimated values are beyond the axial compressive strength of the section and will not govern the design.

5.4.2. Ductility

Compactness of steel sections is important factor in their ability to accommodate large plastic deformations without local buckling (Dicleli and Albhaisi, 2004). Based on article 6.10.8.2.2 from AASHTO LRFD (2010) the limiting slenderness ratio for a compact flange is:

$$\lambda_{pf} = 0.38 \sqrt{\frac{E}{F_{yc}}} \quad \text{Eq. 77}$$

Since large inelastic deformations are required in piles undergoing lateral deformations, piles should satisfy the compactness requirement. The following table lists compactness of HP cross sections:

Table 5-4- Compactness of HP sections

Cross Section	b_f (in)	t_f (in)	$b_f / 2t_f$	$F_y = 36 \text{ ksi}$ $\lambda_{pf} = 10.8$	$F_y = 50 \text{ ksi}$ $\lambda_{pf} = 9.2$
HP 8x36	8.16	0.445	9.17	Compact	
HP 10x42	10.1	0.42	12.02		
HP 10x57	10.2	0.565	9.03	Compact	Compact
HP 12x53	12	0.435	13.79		
HP 12x63	12.1	0.515	11.75		
HP 12x74	12.2	0.61	10.00	Compact	
HP 12x84	12.3	0.685	8.98	Compact	Compact
HP 14x73	14.6	0.505	14.46		
HP 14x89	14.7	0.615	11.95		
HP 14x102	14.8	0.705	10.50	Compact	
HP 14x117	14.9	0.805	9.25	Compact	

As shown in this table, only 6 and 2 HP sections meet the compactness requirement for $F_y = 36 \text{ ksi}$ and $F_y = 50 \text{ ksi}$ respectively. The designer should select the pile cross section among the compact ones; otherwise local buckling of the flanges may happen.

5.4.3. Fatigue

Based on the method described in Section 5.3 the following figures summarize the maximum allowable pile head displacement in soft and medium clay for 36 ksi steel pipes.

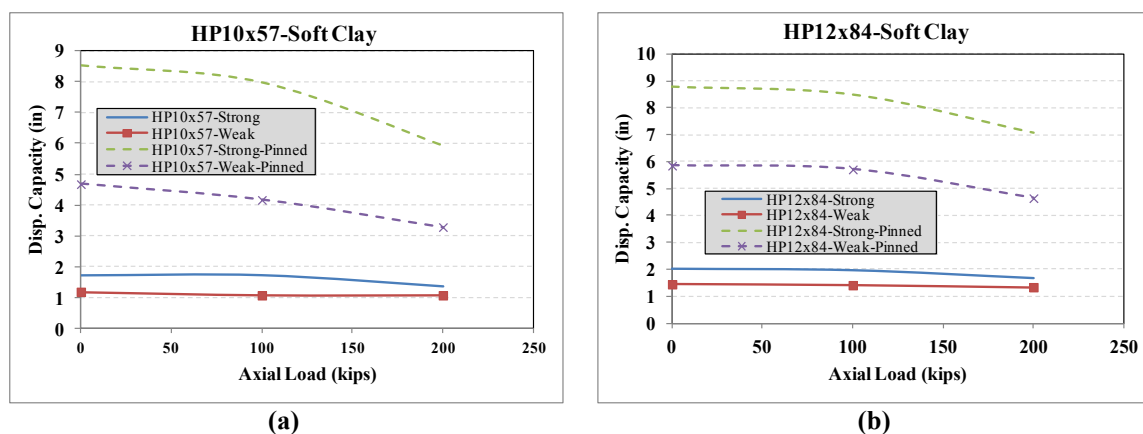


Figure 5-25- Displacement capacity of compact HP sections in soft clay ($c_u = 2.9$ psi) (a) HP10x57 (b) HP12x84

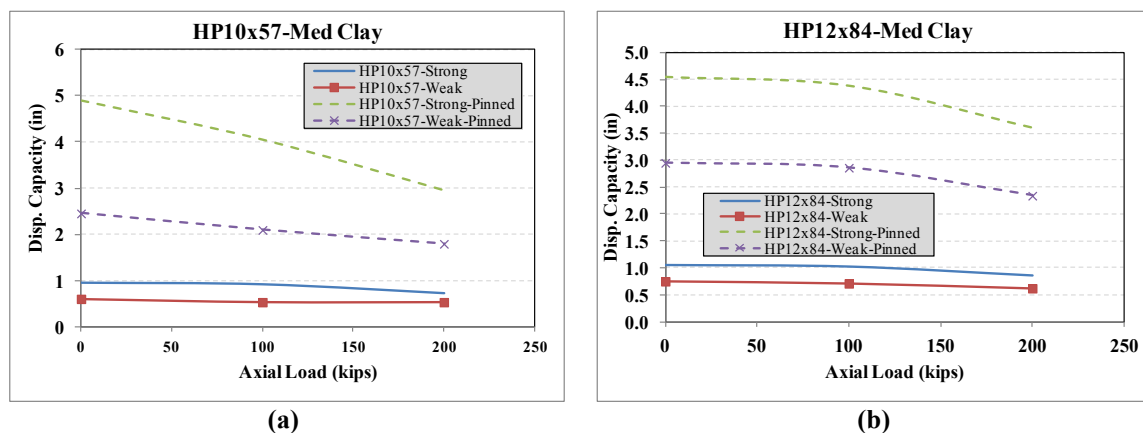


Figure 5-26- Displacement capacity of compact HP sections in medium clay ($c_u = 5.8$ psi) (a) HP10x57 (b) HP12x84

The maximum displacement of the pile head should not exceed the values obtained from this figure.

5.5. Findings

Buckling analyses using energy method show that the old method in calculation of critical buckling capacity of embedded piles is un-conservative. Nevertheless, estimated values were beyond the compressive strength of the investigated sections, and as a result buckling calculations will not govern the design.

Using calibrated FEM models, the idea of pinned pile/cap connection is further investigated for a prestressed pile and the specimens tested in the lab. Results of these analyses clearly verify the validity of the concept, and show that larger displacement capacity can be obtained.

Nonlinear pushover analyses in SAP2000 show that strong axis bending provides more displacement capacity in the pile, although stiffness to lateral displacement would be larger compared to weak axis bending. Moreover, pinned condition at pile head can increase the pile's displacement capacity up to 4 times.

Chapter 6

Conclusions and Recommendations

6.1. Conclusions

The following conclusions were made based on conducted research:

- The main objective in this study was to expand the length of jointless bridges. In these bridges thermal movements are accommodated in their substructure as the whole structure is integral. To reduce the induced forces due to soil-structure interaction, flexible foundations, which include single row of piles, are utilized. Technically, the length of these bridges is limited based on their supporting piles' lateral capacity. In this study it has been shown that the lateral displacement capacity of embedded piles supporting jointless bridges can be increased up to four times by providing rotational capacity at pile head level. Since thermal movement at ends of the bridge is linearly dependant on the length of the bridge, the length of jointless bridges can be expanded four times.
- Results of different surveys have shown that different agencies have different strategies for aligning the piles. Most states recommend weak axis bending. Further studies revealed that this detailing is an engineering judgment rather than a scientific approach. The only reason for weak axis bending is its lower lateral stiffness, but the more important factor which is lateral displacement capacity is always ignored. Nonlinear pushover analyses revealed that the pile's displacement capacity can be increased 1.5 to 2 times if the piles are oriented to bend along the strong axis. Based

on these results it is highly recommended to allow for strong axis bending. Even in skewed or curved bridges, it is recommended to determine the principal direction of movement at pile locations and orient the piles for strong axis bending.

- Experimental studies were carried out in the structure's lab on two specimens. The first specimen involved a relatively fixed pile/cap condition and represented current practice. The second specimen, however, consisted of the proposed connection detail and represented the relatively pinned connection. Axial load, modeling the gravity loads, was applied using the dywidag passed through the mid duct. The lateral load representing the thermal movements of the bridge was applied with two actuators. As expected, test results show that the stiffness of the second specimen is smaller. Besides, lateral displacement capacity was much larger and could not be reached with available setup. Note that in the first specimen yielding, local buckling, and failure happened at about 0.75 in, 3.0 in, and 4.75 in respectively, whereas no yielding or visual buckling was observed in the second specimen throughout the test.
- A new design approach is proposed for steel H-piles supporting jointless bridges. In this method, only compact sections are accepted as the piles will undergo relatively large strains and local instability is not desired. Based on AASHTO limitation for slenderness ratio of compact flange, only two HP sections (HP10x57 and HP12x84) are recommended (for $F_y = 50 \text{ ksi}$). After applying the ductility requirements, the fatigue and strength criteria are considered. First, the maximum allowable strain is estimated using Miner's rule. Then, using this strain and the section depth, the maximum allowable curvature is calculated. Using the moment-curvature relationship

for the specific axial load level, the maximum allowable moment is estimated. Finally, using nonlinear pushover analysis, the corresponding head displacement, which results in a maximum moment along the pile equal to the estimated moment, is evaluated. These steps are summarized into design charts where designer can estimate the lateral displacement capacity based on the pile, the surrounding soil, and the axial load level.

- The energy method was used in parallel to nonlinear p-y curves to estimate the buckling capacity of the embedded pile supporting jointless bridges. In this study, the governing differential equation of the pile was solved and then the energies stored in different forms were estimated. By increasing the axial load and tracking singularity in the energy level, the critical axial load level was estimated. Parametric study was then conducted on different important parameters. It was shown that the critical load is highly dependent on the pile's top lateral displacement level. Besides, the current approach, which is based on linear soil response, was compared to the new approach and it was proven that the current approach is very un-conservative in the sense that it gives much larger critical loads. In any case, the level of critical loads was beyond the compressive resistance of the considered piles.

6.2. Future Research

- Conducted experimental study involved CFT piles, which despite all its great advantages, is not employed by all agencies. Analysis of survey responses as well as DOT's design guides for jointless bridges revealed that all the agencies recommend

HP sections for piles, while some of them allow for CFT piles. Further experimental study on pinned connection for HP sections is recommended.

- As shown in Chapter 4.2.5.2.3 after extracting the CFT pile from the connection it was observed that the end plate had been detached from the end of the pile and because of stress concentration the end of the pile had blossomed. This had happened during the load stage 2 (constant cyclic at ± 4.25 in) as the behavior of the connection was the same after several unloading during load stage 1. Future research is needed to optimize the end plate connection detailing.

References

- [1] Abendroth, R. E., Greimann, L. F., and Ebner, P. E. (1989). "Abutment Pile Design for Jointless Bridges." *Journal of Structural Engineering, ASCE*, 115(11), 2914-2929.
- [2] AASHTO (2010). *AASHTO LRFD Bridge Design Specifications*, Washington D.C.
- [3] Kunin, J., and Alampalli, S. (1999). "Integral Abutment Bridges: Current Practice in the United States and Canada." New York State Department of Transportation, Albany, New York.
- [4] Haj-Najib, R. (2002). "Integral Abutment Bridges with Skew Angles." *PhD Dissertation*, University of Maryland, College Park, Maryland.
- [5] Maruri, R. F., and Petro, S. H. (2005). "Integral Abutments and Jointless Bridges 2004 Survey Summary." *Proc., Integral Abutment and Jointless Bridges (IAJB 2005)*, Federal Highway Administration – USDOT, 12-29.
- [6] Oesterlie, R. G., Tabatabai, H., Lawson, T. J., Refai, T. M., Volz, J. S., and Scanlon, A. (2002). "Jointless and Integral Abutment Bridges." *Final Report to FHWA*.
- [7] Clough, G. W., and Duncan, J. M. (1991). "Earth Pressures." *Foundation Engineering Handbook*, Van Nostrand Reinhold, New York, NY, 223-235.
- [8] Faraji, S., Ting, J. M., Crovo, D. S., and Ernst, H. (2001). "Nonlinear Analysis of Integral Bridges: Finite Element Model." *Journal of Geotechnical and Geoenvironmental Engineering*, 454-461.
- [9] Barker, R. M., Duncan, J. M., Rojiani, K. B., Ooi, P. S. K., and Tan, C. K. (1991). "Manuals for the Design of Bridge Foundations." National Cooperative Highway Research Program (NCHRP), Washington, D.C.
- [10] Pugasap, K., Kim, W., and Laman, J. A. (2009). "Long-Term Response Prediction of Integral." *ASCE Journal of Bridge Engineering*, 14(2), 129-139.
- [11] Basu, P. K., and Knickerbocker, D. J. (2005). "Behavior of Jointless High Performance Concrete Bridges." Tennessee Department of Transportation, Nashville, TN.
- [12] Broms, B. B. (1956). "Design of Laterally Loaded Piles." *Proc., American Society of Civil Engineers*, 77-99.
- [13] Poulos, H. G., and Davis, E. H. (1980). *Pile Foundation Analysis and Design*, John Wiley & Sons, Inc., United States of America.
- [14] Matlock, H., and Ripperger, E. A. (1958). "Measurement of Soil Pressure on a Laterally Loaded Pile." *Proc., American Society for Testing Materials*, 1245-1259.
- [15] Matlock, H. (1970). "Correlation for Design of Laterally Loaded Piles in Soft Clay." *Proc., Second Annual Offshore Technology Conference*, 577-594.

- [16] Reese, L. C. (1971). "The Analysis of Piles under Lateral Loading." *Proc., Symposium on the Interaction of Structure and Foundation*, University of Birmingham, 206-218.
- [17] Reese, L. C., Cox, W. R., and Koop, F. D. (1974). "Analysis of Laterally Loaded Piles in Sand." *Proc., Fifth Annual Offshore Technology Conference*.
- [18] Reese, L. C., Cox, W. R., and Koop, F. D. (1975). "Field Testing and Analysis of Laterally loaded Piles in Stiff Clay." *Proc., Seventh Offshore Technology Conference*.
- [19] API (1993). *Recommended Practice for Planning, Designing and Constructing Fixed Offshore Platforms*, American Petroleum Institute.
- [20] Trochanis, A., Bielak, J., and Christiano, P. (1991). "Three-Dimensional Nonlinear Study of Piles." *ASCE Journal of Geotechnical Engineering*, 117(3), 429-447.
- [21] Khodair, Y. A., and Hassiotis, S. (2005). "Analysis of Soil-Pile Interaction in Integral Abutment." *Journal of Computers and Geotechnics*, 32, 201-209.
- [22] Miao, L. F., Goh, A. T. C., Wong, K. S., and Teh, C. I. (2006). "Three-Dimensional Finite Element Analyses of Passive Pile Behaviour." *International Journal for Numerical and Analytical Methods in Geotechnics*, 30, 599-613.
- [23] Frosch, R. J., Wenning, M., and Chivivhien, V. (2005). "The In-Service Behavior of Integral Abutment Bridges: Abutment Pile Response." *Proc., 2005 FHWA Conference on Integral Abutment and Jointless Bridges (IAJB 2005)*, 30-40.
- [24] Chovichien, V. (2004). *The Behavior and Design of Piles for Integral Abutment Bridges*, Purdue University.
- [25] Girton, D. D., Hawkinson, T. R., and Greimann, L. F. (1991). "Validation of Design Recommendation for Integral Abutment Piles." *Journal of Structural Engineering*, 117(7), 2117-2135.
- [26] Abendroth, R. E., and Greimann, L. F. (2005). "Field Testing of Integral Abutments." Iowa State University, Ames, Iowa.
- [27] Abendroth, R. E., Greimann, L. F., and LaViolette, M. D. (2007). "An Integral Abutment Bridge with Precast Concrete Piles." Center of Transportation Research and Education, Ames, Iowa.
- [28] Hartt, S. L., Sanford, T. C., and Davis, W. G. (2006). "Monitoring a Pile-Supported Integral Abutment Bridge at a Site with Shallow Bed Rock." University of Maine, Orono, Maine.
- [29] Sanford, T. C., and Elgaaly, M. (1993). "Skew Effects on Backfill Pressures at Frame Bridge Abutments." *Transportation Research Record*, 1415, 1-11.
- [30] DeJong, J. T., Howey, D. S., Civjan, S. A., Brena, S. F., Butler, D. S., Crovo, D. S., Hourani, N., and Connors, P. (2004). "Influence of Daily and Annual Thermal Variations on Integral Abutment Bridge Performance." *Proc., Proceeding of Geotrans 2004*, ASCE, 496-505.

- [31] Lawver, A., French, C., and Shield, C. K. (2000). "Field Performance of Integral Abutment Bridge." *Transportation Research Record*, 1740, 108-117.
- [32] Kamel, M. R., Benak, J. V., Tadros, M. K., and Jamshidi, M. (1996). "Prestressed Concrete Piles in Jointless Bridges." *PCI Journal*, 41(2), 56-67.
- [33] Hassiotis, S., Lopez, J., and Bermudez, R. (2005). "Full-Scale Testing of an Integral Abutment Bridge." *Proc., 2005- FHWA Conference on Integral Abutment and Jointless Bridges (IAJB 2005)*, FHWA, 199-210.
- [34] Jorgenson, J. L. (1983). "Behavior of Abutment Piles in an Integral Abutment in Response to Bridge Movement." *Transportation Research Record*, 903, 72-79.
- [35] Fennema, J. L., Laman, J. A., and Linzell, D. G. (2005). "Predicted and Measured Response of an Integral Abutment Bridges." *Journal of Bridge Engineering*, 10(6), 666-677.
- [36] Burdette, E. G., Deathrage, J. H., and Goodpasture, D. W. (2003). "Behavior of Laterally Loaded Piles Supporting Bridge Abutments Phase II Prestressed Concrete Piles." University of Tennessee, Knoxville, TN.
- [37] Cox, W. R., Reese, L. C., and Grubbs, B. R. (1974). "Field testing of Laterally Loaded Piles in Sand." *Proc., Proceedings of Sixth Offshore Technology Conference*, Offshore Technology Conference, 459-472.
- [38] Bhushan, K., Haley, S. C., and Fong, P. T. (1979). "Lateral Load Tests on Drilled Piers in Stiff Clays." *American Society of Civil Engineers, Journal of the Geotechnical Engineering Division*, 105, 969-985.
- [39] Reese, L. C., and Welch, R. C. (1975). "Lateral Loading of Deep Foundations in Stiff Clay." *Journal of the Geotechnical Engineering Division*, 101(7), 633-649.
- [40] Cheang, L., and Matlock, H. (1983). "Static and Cyclic Lateral Load Tests on Instrumented Piles in Sand." The Earth Technology Corporation, Long Beach, California.
- [41] Huang, J., French, C. E., and Shield, C. K. (2004). "Behavior of Concrete Integral Abutment Bridges." Minnesota Department of Transportation, St. Paul, MN.
- [42] Bonczar, C., Brena, S., Civjan, S., Dejong, J., Crellin, B., and Crovo, D. (2005). "Field Data and FEM Modeling of the Orange-Wendell Bridge." *Proc., 2005-FHWA Conference on Integral Abutment and Jointless Bridges (IAJB 2005)*, FHWA, 163-173.
- [43] Thanasattayawibul, N. (2006). *Curved Integral Abutment Bridges*, University of Maryland, College Park, MD.
- [44] Bazant, Z. P. (1972). "Prediction of Concrete Creep Effects Using Age Adjusted Effective Modulus Method." *ACI Journal*, 69, 212-217.
- [45] Bazant, Z. P., and Xi, Y. (1995). "Continuous Retardation Spectrum for Solidification Theory of Concrete Creep." *Journal of Engineering Mechanics*, 121(2), 281-288.

- [46] Hedjazi, S., Rahai, A., and Sennah, K. (2007). "Evaluation of Creep Effects on the Time-Dependent Deflections and Stresses in Prestressed Concrete Bridges." *Journal of Bridge Structures*, 3(2), 119-132.
- [47] Brooks, J. J. (1989). "Influence of Mix Proportions, Plasticizers and Superplasticizers on Creep and Drying Shrinkage of Concrete." *Magazine of Concrete Research*, 41(148), 145-153.
- [48] Hetenyi, M. (1946). *Beams on Elastic Foundation*, University of Michigan Press, Ann Arbor, Michigan.
- [49] Wang, S.-T., and Reese, L. C. (1993). "COM624P- Laterally Loaded Pile Analysis Program for the Microcomputer Version 2.0." U.S. DOT, Federal Highway Administration, Washington D.C.
- [50] Reese, L. C. (1977). "Laterally Loaded Piles: Program Documentation." *Journal of the Geotechnical Engineering Division*, 287-305.
- [51] Heelis, M. E., Pavlovic, M. N., and West, R. P. (2004). "The Analytical Prediction of the Buckling Loads of Fully and Partially Embedded Piles." *Geotechnique*, 54(6), 363-373.
- [52] Davisson, M. T. (1963) "Estimating Buckling Loads for Piles." *2nd Pan American Conference on Soil Mechanics and Foundation Engineering*, 351-369.
- [53] Davisson, M. T., and Robinson, K. E. (1965) "Bending and Buckling of Partially Embedded Piles." *Sixth International Conference on Soil Mechanics and Foundation Engineering*, 243-246.
- [54] Reddy, A. S., and Valsangkar, A. J. (1970). "Buckling of Fully and Partially Embedded Piles." *ASCE Journal of Soil Mechanics and Foundation Division*, 96(6), 1951-1965.
- [55] Prakash, S. (1987). "Buckling Loads of Fully Embedded Vertical Piles." *Computers and Geotechnics*, 4, 61-83.
- [56] Gabr, M. A., and Wang, J. (1994). "Buckling of friction piles supporting bridge foundations." *Transportation Research Record*, 93-101.
- [57] Gabr, M. A., Wang, J. J., and Zhao, M. (1997). "Buckling of piles with general power distribution of lateral subgrade reaction." *Journal of Geotechnical and Geoenvironmental Engineering*, 123, 123-130.
- [58] Heelis, M. E., Pavlovic, M. N., and West, R. P. (2004). "The analytical prediction of the buckling loads of fully and partially embedded piles." *Geotechnique*, 54, 363-373.
- [59] Wasserman, E. P., and Walker, J. H. (1996). *Integral Abutments for Steel Bridges*, American Iron and Steel Institute.
- [60] Burke Jr, M. P. (2009). *Integral and Semi-Integral Bridges*, Wiley-Blackwell.
- [61] Vogt, N., Vogt, S., and Kellner, C. (2009). "Buckling of Slender Piles in Soft Soils." *Bautechnik*, 86(S1), 98-112.

- [62] Oesterlie, R. G., Tabatabai, H., Lawson, T. J., Refai, T. M., Volz, J. S., and Scanlon, A. (2002). "Jointless and Integral Abutment Bridges." FHWA.
- [63] Kamel, M. R., Benak, J. V., Tadros, M. K., and Jamshidi, M. (1996). "Prestressed concrete piles in jointless bridges." *PCI Journal*, 41(Compendex), 56-67.
- [64] Arsoy, S., Barker, R. M., and Duncan, J. M. (2002). "Experimental and Analytical Investigations of Piles and Abutments of Integral Bridges." Virginia Polytechnic Institute and State University, Charlottesville,.
- [65] Frosch, R. J., Kreger, M. E., and Talbott, A. M. (2009). "Earthquake Resistance of Integral Abutment Bridges." Purdue University, West Lafayette, IN.
- [66] Dicleli, M., and Albhaisi, S. M. (2004). "Effect of cyclic thermal loading on the performance of steel H-piles in integral bridges with stub-abutments." *Journal of Constructional Steel Research*, 60, 161-182.
- [67] Karalar, M., and Dicleli, M. (2010). "Development of a new cycle counting method for cyclic thermal strains in integral bridge piles." *Bridge Maintenance, Safety, Management and Life-Cycle Optimization*, 3296-3301.
- [68] Koh, S. K., and Stephens, R. I. (1991). "Mean stress effects on low cycle fatigue for a high strength steel." *Fatigue and Fracture of Engineering Materials and Structures*, 14, 413-428.
- [69] Neogi, P. K., Sen, K. H., and Chapman, J. C. (1969). "Concrete-filled tubular steel columns under eccentric loading." *Structural Engineer*, 47(5), 187-195.
- [70] Gourly, B. C., and Hajjar, J. F. (1994). "Cyclic Nonlinear Analysis of Three-Dimensional Concrete Filled Steel Tube Beam-Column and Composite Frames." University of Minnesota.
- [71] Salmon, C. G., and Johnson, J. E. (1996). *Steel Structures Design and Behavior*, HarperCollins Publisher Inc.
- [72] Hognestad, E. (1951). "Study of combined bending and axial load in reinforced concrete members." University of Illinois, Urbana, IL, United States, 128.
- [73] Kent, D. C., and Park, R. (1971). "Flexural Members with Confined Concrete." *Journal of the Structural Division*, 97(7), 1969-1990.
- [74] Oesterle, R. G., Tabatabai, H., Lawson, T. J., Refai, T. M., Volz, J. S., and Scanlon, A. (2005). "Jointless Bridges, Volume III, Summary Report." *Final Report to FHWA*.
- [75] Moulton, L. K., Gangarao, H. V. S., and Halvorsen, G. T. (1985). "Tolerable Movement Criteria for Highway Bridges." *Report No. FHWA/RD-85/107* Washington, DC, 109.
- [76] Hearn, G. (1995). "Faulted Pavements at Bridge Abutments." *Colorado Transportation Institute Synthesis*, University of Colorado at Boulder, 181.

- [77] Beavers, J. A., and Durr, C. L. (1998). "Corrosion of Steel Piling in Nonmarine Applications." *NCHRP Report No. 408*, Transportation Research Board, Washington D.C.
- [78] Decker, J. B., Rollins, K. M., and Ellsworth, J. C. (2008). "Corrosion rate evaluation and prediction for piles based on long-term field performance." *Journal of Geotechnical and Geoenvironmental Engineering*, 134, 341-351.
- [79] Elias, V., Barry, P. E., and Christopher, R. (1997). "Mechanically stabilized earth walls and reinforced soil slopes design and construction guidelines : FHWA demonstration project 82, Reinforced soil structures WSEW and RSS.", US Dept. of Transportation, Federal Highway Administration, Washington, D.C.
- [80] Nicholson, B. A., Barr, J. M., Cooke, R. S., Hickman, R. P., Jones, C. J. F. P., and Taylor, H. P. J. (1997). "Integral Bridges: Report of a Study Tour to North America." Concrete Bridge Development Group, U.K., 93.
- [81] Hassiotis, A. (2007) "Data Gathering and Design Details of an Integral Abutment Bridge." *18th ASCE Engineering Mechanics Division Conference (EMD)*.
- [82] Lui, D., Magliola, R. A., and Dunker, K. F. (2005). "Integral Abutment Bridges – Iowa and Colorado Experience." *Proc., FHWA Conference on Integral Abutment and Jointless Bridges, (IAJB2005)*.
- [83] Doust, S. E., and Azizinamini, A. (2011). "End Displacement and Pile Orientation in Straight and Curved Integral Abutment Bridges." *Submitted to ASCE Journal of Bridge Engineering*.
- [84] Kosmatka, S. H., and Panarese, W. C. (1988). "Design and Control of Concrete Mixtures." *Portland Cement Association (PCA)* Skokie, IL, 151-162.
- [85] Bazant, Z. P., and Panula, L. (1980). "Creep and Shrinkage Characterization for Analyzing Prestressed Concrete Structures." *Journal - Prestressed Concrete Institute*, 25, 86-122.
- [86] Oesterle, R. G. (2005). "Jointless Bridges, Volume II, Analytical Research and Proposed Design Procedures." *Final Report*, FHWA.
- [87] Oesterle, R. G., and Volz, J. S. (2005). "Effective Temperature and Longitudinal Movement in Integral Abutment Bridges." *Proc., FHWA Conference on Integral Abutment and Jointless Bridges (IAJB2005)*.
- [88] Science, N. A. o. (1979). "Expansion Joints in Buildings." *Technical Report No. 65*, Federal Construction Council.
- [89] Emanuel, J. H., and Hulsey, J. L. (1977). "Prediction of the Thermal Coefficient of Expansion of Concrete." *Journal of The American Concrete Institute*, 74, 149-155.
- [90] Tabatabai, H., Oesterle, R. G., and Lawson, T. J. (2005). "Jointless Bridges, Volume I, Part 3, Experimental Research and Field Studies." *Final Report*, FHWA.

- [91] Chandra, V. (1995). "Draft Report on Precast Prestressed Concrete Integral Bridges, State-of-the-Art." Precast/Prestressed Concrete Institute, 113.
- [92] Oesterle, R. G., and Lotfi, H. R. (2005). "Transverse Movement in Skewed Integral Abutment Bridges." *Proc., FHWA Conference on Integral Abutment and Jointless Bridges (IAJB2005)*, 16-18.
- [93] Freyermuth, C. L. (1969). "Design of continuous highway bridges with precast, prestressed concrete girders." *Journal of the Prestressed Concrete Institute*, 14(2), 14-39.
- [94] Oesterle, R. G., Glikin, J. D., and Larson, S. C. (1989). "Design of Precast Prestressed Bridge Girders Made Continuous." *NCHRP Report 322*, Transportation Research Board, 97.
- [95] Oesterle, R. G., Mehrabi, A. B., Tabatabai, H., Scanlon, A., and Ligozio, C. A. (2004). "Continuity considerations in prestressed concrete jointless bridges." *Proc., Proceedings of the 2004 Structures Congress - Building on the Past: Securing the Future, May 22, 2004 - May 26, 2004*, American Society of Civil Engineers, 227-234.
- [96] Oesterle, R. G., Mehrabi, A. B., Tabatabai, H., Scanlon, A., and Ligozio, C. A. (2004). "Evaluation of Continuity in Prestressed Concrete Jointless Bridges." *Proc., 2004 Concrete Bridge Conference*.
- [97] Mirmiran, A., Kulkarni, S., Castrodale, R., Miller, R., and Hastak, M. (2001). "Nonlinear continuity analysis of precast, prestressed concrete girders with cast-in-place decks and diaphragms." *PCI Journal*, 46, 60-80.
- [98] Miller, R. A., R., C., Mirmiran, A., and Hastak, M. (2004). "Connection of Simple-Span Precast Concrete Girders for Continuity." *NCHRP Report 519*, Transportation Research Board, 55.
- [99] AASHTO (2007). *AASHTO LRFD Bridge Design Specifications*, Washington, D.C.
- [100] ENR (1994). "Temperature gradient cracks viaduct girders." *Engineering News-Record*, 232, 14-14.
- [101] AL-DOT (1994). "Cracks in Precast Prestressed Bulb Tee on Structure Nos. I-565-45-11.5 A& B on I-565 in Huntsville, Alabama." Alabama DOT.
- [102] Telang, N. M., and Mehrabi, A. M. (2003). "Cracked Girders." *Public Roads (FHWA)*, 67(3).
- [103] Sherafati, A., and Azizinamini, A. (2011a). "Expanding Jointless Bridge Lengths by Providing Rotational Capacity over the Pile Head-Part I: Theory." *Submitted to Journal of Bridge Engineering*.
- [104] Sherafati, A., and Azizinamini, A. (2011b). "Expanding Jointless Bridge Lengths by Providing Rotational Capacity over the Pile Head-Part II: Experimental Study." *Submitted to ASCE Journal of Bridge Engineering*.
- [105] Schaefer, V. R., and Koch, J. C. (1992). "Void Development Under Bridge Approaches." *Report No. SD90-03*, South Dakota State University, Brookings, SD, 147.

- [106] Gangarao, H. V. S., and Thippeswamy, H. K. (1996). "Study of Jointless Bridge Behavior and Development of Design Procedures." *Report No. FHWA-WV89*, West Virginia DOT, Charleston, WV.
- [107] Jung, Y. S., Zollinger, D. G., and Tayabji, S. D. (2007). "Best Practices of Concrete Pavement Transition Design and Construction." *Report No. FHWA/TX-07/0-5320-1*, Texas Department of Transportation, 92.
- [108] Caner, A., and Zia, P. (1998). "Behavior and design of link slabs for jointless bridge decks." *PCI Journal*, 43, 68-80.
- [109] Gastal, F., and Zia, P. (1989). "Analysis of Bridge Beams With Jointless Decks." *Proc., IASBE Symposium*, 555-560.
- [110] Zederbaum, J. (1969). "Factors Influencing the Longitudinal Movement of Concrete Bridge Systems With Special Reference to Deck Contraction." *Concrete Bridge Design, ACI Publication SP 23*, American Concrete Institute, Detroit, MI, 75-95.
- [111] Krauss, P. D. (1996). "Transverse cracking in newly constructed bridge decks." *NCHRP Report 380*, Transportation Research Board, National Research Council.
- [112] Briaud, J. L., James, R. W., and Hoffman, S. B. (1997). "Settlement of bridge approaches (the bump at the end of the bridge)." *NCHRP Synthesis 234*, Transportation Research Board, National Research Council, Washington, D.C.
- [113] Leathers, R. C. (1990). "Bridge Deck Joint Rehabilitation." *FHWA Technical Advisory T5140.16*, U.S. Department of Transportation, Federal Highway Administration.
- [114] Connor, R. J., Dexter, R., and Mahmoud, H. (2005). "Inspection and Management of Bridges with Fracture-Critical Details." *NCHRP Synthesis 354*, Transportation Research Board, Washington D.C.
- [115] Maberry, S., Camp, J. D., and Bowser, J. (2005). "New Mexico's Practice and Experience in Using Continuous Spans for Jointless Bridges." *Proc., FHWA Conference, Integral Abutment and Jointless Bridges*.

Appendix A.

Design of Specimens

A1. Design of Pile Cap

Figure A1 shows the moments and shears developed in the pile cap, assuming that the pile reaches its full moment capacity, M_p (Wasserman and Walker, 1996).

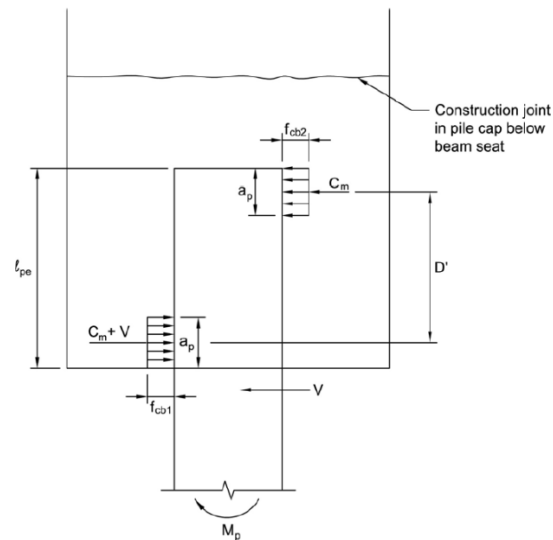


Figure A1- Transfer of pile moments to pile cap (Wasserman and Walker, 1996)

As illustrated above, this moment can be developed by bearing stress of f_{cb} between the pile and the concrete. The depth of stress block can be estimated as:

$$a_p = 0.85 \left(\frac{l_{pe}}{2} \right) \quad \text{Eq. A1}$$

Where,

l_{pe} = the embedment length of the pile.

Setting the resisting couple equal to the moment capacity of the pile gives:

$$M_p = C_m D' = a_p b f_{cb2} (l_{pe} - a_p) \quad \text{Eq. A2}$$

$$f_{cb2} = \frac{M_p}{a_p b (l_{pe} - a_p)} \quad \text{Eq. A3}$$

$$f_{cb1} = f_{cb2} + \frac{V}{a_p b} = \frac{M_p}{a_p b (l_{pe} - a_p)} + \frac{V}{a_p b} \quad \text{Eq. A4}$$

Where,

C_m = bearing force developed between the face of the pile and the concrete over the length a_p

D' = distance between the center of the compressive stress zones on the top and bottom

b = Width of the pile.

The suggested limit for f_{cb1} is about $1.9f'_c$.

Two moment curvature analysis on the cross section of the pile is shown in Figure A2.

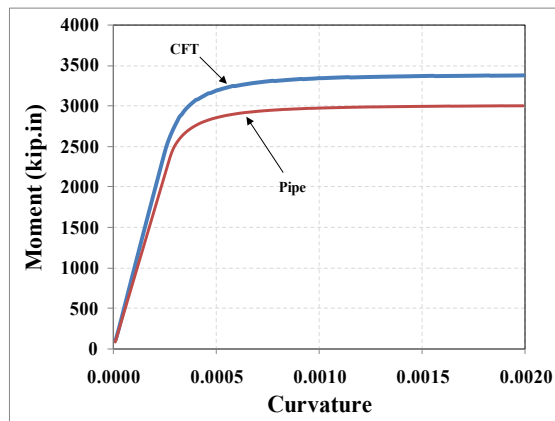


Figure A2- Moment-curvature analysis of the cross section of the pile

Table A1 lists assumed information for the moment curvature analyses.

Table A1- Assumed information in the moment-curvature analysis

	Outside diameter (in)	Tube thickness (in)	Tube yield stress (ksi)	Ultimate stress (ksi)	Concrete compressive stress (ksi)
EPP Steel Model	12.75	0.375	50.0	NA	4.0
Bilinear Steel Model	12.75	0.375	50.0	80.0	4.0

As shown in Figure A2, the ultimate moment capacity of the 12” standard pipe filled with concrete can be estimated about 3373 kip.in. Note that in moment-curvature analysis, it is assumed that no slip will occur between the tube and the concrete. Also, in the analysis, the axial load is ignored. Using Eq. A1 the depth of stress block can be estimated as:

$$a_p = 0.85 \left(\frac{l_{pe}}{2} \right) = 0.85 \left(\frac{24}{2} \right) = 10.2 \text{ in}$$

Using Eq. A3 the bearing stress at the top region can be estimated as:

$$f_{cb2} = \frac{M_p}{a_p b (l_{pe} - a_p)} = \frac{3373 \times 10^3}{(10.2)(12.75)(24 - 10.2)} = 1879 \text{ psi}$$

Since the test is done on a cantilevered pile, the ultimate moment is developed by the lateral load, V , equal to:

$$V = \frac{M_p}{l} = \frac{3373 \times 10^3}{(8.5)(12)} = 33.1 \text{ kips}$$

So, the bearing stress over the bottom region can be calculated using Eq. A4 as follows:

$$f_{cb1} = f_{cb2} + \frac{V}{a_p b} = (1879) + \frac{(33100)}{(10.2)(12.75)} = 2134 \text{ psi}$$

As shown, both of the bearing stresses are below the compressive strength of the concrete (f'_c).

If bilinear steel is assumed in moment curvature analysis, then the ultimate moment capacity of the 12" standard pipe filled with concrete can be estimated about 5600 kip. in. Note that in moment-curvature analysis, it is assumed that no slip will occur between the tube and the concrete. Also, in the analysis, the axial load is ignored.

Using Eq. A3 the bearing stress at the top region can be estimated as:

$$f_{cb2} = \frac{M_p}{a_p b (l_{pe} - a_p)} = \frac{5600 \times 10^3}{(10.2)(12.75)(24 - 10.2)} = 3120 \text{ psi}$$

Since the test is done on a cantilevered pile, the ultimate moment is developed by the lateral load, V , equal to:

$$V = \frac{M_p}{l} = \frac{5600 \times 10^3}{(8.5)(12)} = 54.9 \text{ kips}$$

So, the bearing stress over the bottom region can be calculated using Eq. A4 as follows:

$$f_{cb1} = f_{cb2} + \frac{V}{a_p b} = (3120) + \frac{(54900)}{(10.2)(12.75)} = 3542 \text{ psi}$$

As shown, both of the bearing stresses are below the compressive strength of the concrete (f'_c). The suggested limit for f_{cb1} is about $1.9f'_c$.

A2. Cap Reinforcement Design

Since the stresses corresponding to the applied loads is minor, shrinkage and temperature reinforcement would be sufficient.

Based on Article 5.10.8 of AASHTO LRFD, the area of reinforcement per foot, on each face and in each direction, shall satisfy:

$$A_s \geq \frac{1.30bh}{2(b+h)f_y}$$

So the required reinforcement to satisfy the above criterion will be equal to:

$$A_s \geq \frac{1.30bh}{2(b+h)f_y} = \frac{(1.3)(48)(56)}{(2)(48+56)(60)} = 0.28$$

Use #6 @ 8" on vertical sides and #6@ 8" on horizontal sides.

A3. Design of Spreader Beam

The maximum load that the CFT pile will experience would be about 54.9 kips. Since this load is applied using two rams located about 3 ft apart, the maximum moment developed in the spreader beam would be equal to:

$$M_{spreader,max} = \frac{Vl_{spreader}}{4} = \frac{(54.9)(3)}{4} = 41.2 \text{ kip.ft}$$

The spreader beam in the lab is S10x25.4 with section modulus (S) of 24.6 in³. The nominal elastic capacity of this section is calculated as:

$$M_{y,nominal} = S_{10x25.4} F_y = (24.6)(50) = 102.5 \text{ kip.ft}$$

Shear resistance of this section can be estimated as:

$$V_{nominal} = 0.58F_y A_w = (0.58)(50)(0.311)(9.02) = 81.35 \text{ kip}$$

This is much larger than the maximum shear in the spreader beam.

$$V_{\text{spreader,max}} = V/2 = 28.3 \text{ kip}$$

So the S10x25.4 is good to be used as the spreader.

The maximum deflection associated with the above load (maximum load) would be:

$$\delta_{\text{max}} = \frac{Vl^3}{48EI} = \frac{(56 \times 10^3)(36)^3}{(48)(2.9 \times 10^7)(123)} = 0.015 \text{ in}$$

Appendix B. Moment-Curvature Analysis

Since the CFT piles are used in this analysis, flexural failure will take place before any instability. Moment-curvature analysis was selected to evaluate the capacity of the specimens.

Since the moment-curvature relationship depends on the level of the applied axial load, for a given axial load, the moment-curvature is obtained for the specimen, by computing the moment on its cross section for various values of curvature. The moment is calculated by summation of the moments of small subsections. For this purpose, the cross section is divided into number of horizontal strips. Figure B1 shows a schematic of the discretization of the cross section. The density of the mesh shown in this figure is significantly reduced for illustration purposes. In this study the section is divided into 100 subsections (strips). Such a fine mesh minimizes the error of calculations due to approximations made.

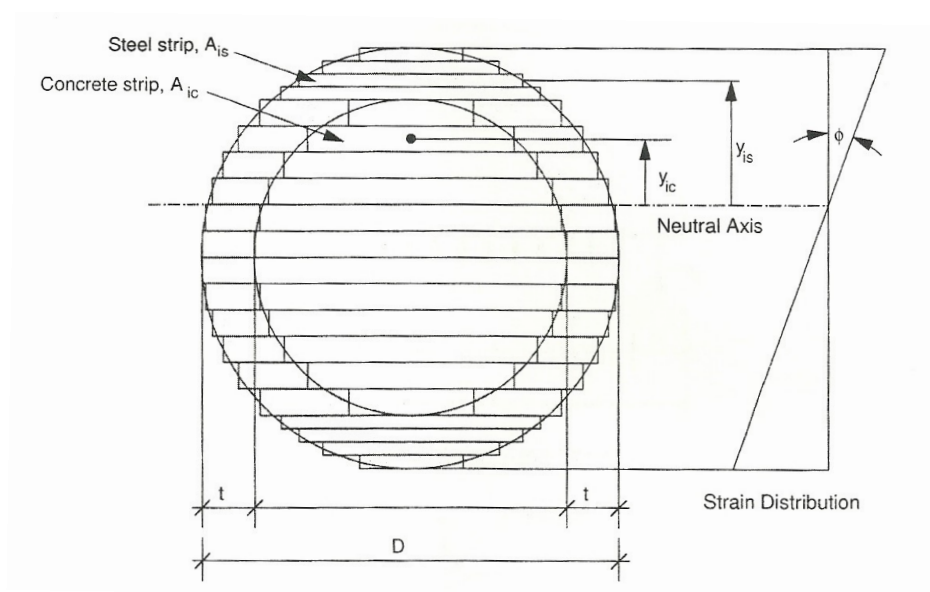


Figure B1- Discretization of the cross section for moment-curvature analysis

For the given value of the axial load and curvature the corresponding moment is calculated through an iterative process. At the beginning, the initial value of compressive strain is assumed. Given the curvature and the compressive strain at the top fiber, and assuming linear strain distribution over the cross section, the location of the neutral axis and the strain at the middle of each strip is calculated. The linear strain distribution implies perfect bond exists between the concrete and the steel. Most of the previous researches conducted on CFT columns have incorporated the same assumption (Neogi, Sen and Chapman, 1969, Gourly and Hajjar, 1994)

Knowing the strain in each strip, stresses for steel and concrete elements are computed by using the corresponding constitutive model described in page 209. The force in each strip is then calculated by multiplying the area of the strip times its stress. The resultant axial force in the cross section is computed by summation of the forces in the strips as follows:

$$F = \sum_{ic=1}^j \sigma_{ic} A_{ic} + \sum_{is=1}^k \sigma_{is} A_{is} \quad \text{Eq. B1}$$

Where j and k are the number of concrete and steel strips, respectively, A_i is the area of each strip, and σ_i is the stress at the centroid of the strip. Calculated internal axial force, F , is then compared to the applied axial load, P . If the difference between the two values is not within the prescribed tolerance, the top compressive strain is adjusted and the process is repeated until convergence is achieved. The moment is then calculated by summing the moment produced by each strip as follows:

$$M = \sum_{ic=1}^j \sigma_{ic} A_{ic} y_{ic} + \sum_{is=1}^k \sigma_{is} A_{is} y_{is} \quad \text{Eq. B2}$$

Where, y_i is the distance from the neutral axis of the cross section to the centroid of the strip. The given curvature and calculated moment obtained from Eq. B2 correspond to one point on the moment-curvature diagram. The complete moment-curvature diagram for a given level of axial load is obtained by increasing the curvature incrementally and repeating the process for each curvature value.

B1. Constitutive Models

B1.1. Steel Model

Bilinear model is utilized for steel shell of the CFT. This model takes into account strain hardening of steel. Steel behaves linear-elastically below the yield strain (ϵ_y). The modulus of elasticity is taken as 29000 ksi. After the steel yields, the stress stays constant up to a certain stress, denoted as the onset of strain hardening (ϵ_{st}) which is about 15 to 20 times the yield strain (Salmon and Johnson, 1996). For strains greater than ϵ_{st} , the stress increases, but with a much flatter slope than the elastic slope, E . The slope of the stress-strain curve beyond ϵ_{st} is known as the strain hardening modulus, E_{st} .

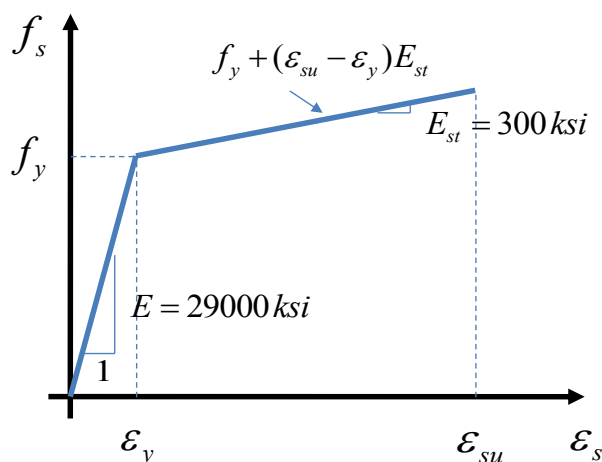


Figure B2- Bilinear stress-strain curve for steel

B1.2. Concrete Model

Since the concrete core is confined by the steel tube, a confined concrete stress-strain model should be considered. Different models used in other studies are discussed herein. All of these models include a curve up to maximum stress followed by a line to failure.

B1.2.1. Modified Hognestad Model (Hognestad, 1951)

The modified Hognestad stress-strain curve consists of a second-degree parabola followed by a line up to failure (Figure B3). The stress corresponding to given strain in the parabola portion is given by

$$f_c = f_c'' \left[\frac{2\varepsilon_c}{\varepsilon_0} - \left(\frac{\varepsilon_c}{\varepsilon_0} \right)^2 \right] \quad \text{Eq. B3}$$

The maximum stress is assumed to be equal to $f_c'' = 0.85f_c'$ corresponding to the strain of $\varepsilon_0 = 2 \frac{f_c'}{E_c}$, where E_c is the concrete's modulus of elasticity taken as $57000\sqrt{f_c'}$.

The ultimate strain for un-confined concrete is limited to 0.003, however, for confined concrete a value of 0.050 can be assumed. The stress corresponding to the ultimate strain is equal to $0.85f_c'' = 0.72f_c'$. The equation of the linear portion is given as

$$f_c = f_c'' \left[1 - 0.15 \left(\frac{\varepsilon_c - \varepsilon_0}{\varepsilon_{cu} - \varepsilon_0} \right) \right] \quad \text{Eq. B4}$$

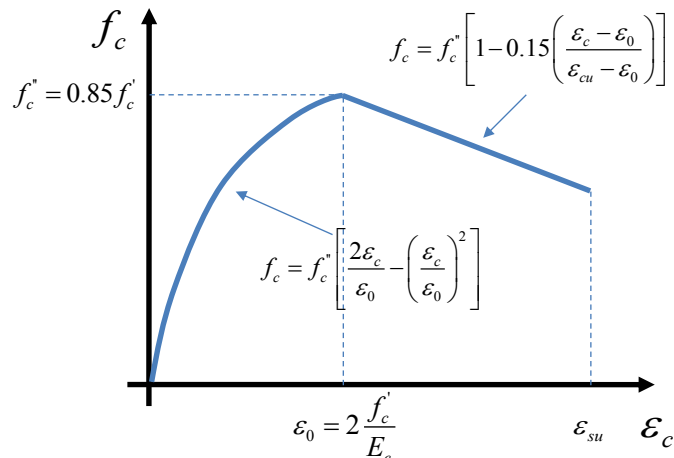


Figure B3- Modified Hognestad Model (Hognestad, 1951)

B1.2.2. Kent and Park Model (Kent and Park, 1971)

This model is generally developed for concrete confined with spirals. It is assumed that the confining steel has no effect on the second order parabola curve until a concrete strain of 0.002. Following this strain, the stress decreases linearly to $0.2f'_c$ at a strain of ε_{20c} upon which, it becomes constant. This model is presented in Figure B4. Z_c in the descending line is a function of the spacing of spirals.

Since this model is mainly used for concrete confined with spirals, it is not applicable to CFT piles and is not used in this work.

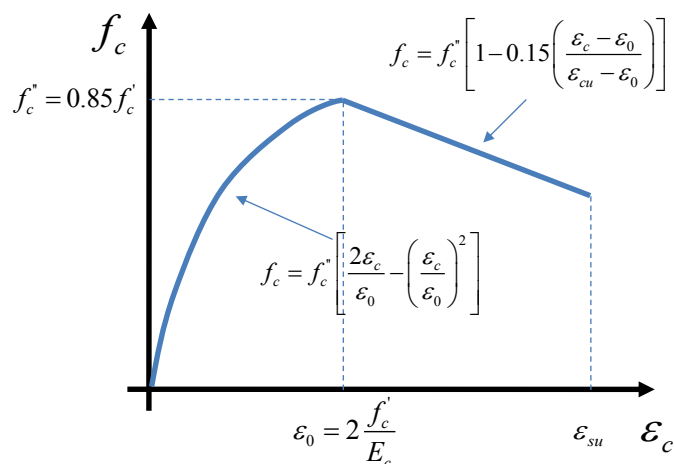


Figure B4- Kent and Park Model (Kent and Park, 1971)

Appendix C.

Design Guide for Jointless Bridges

C1. Introduction

A jointless bridge, by definition, has a continuous deck with no expansion joints over the superstructure, abutments, and approaches. In this type of bridge structure, all movement due to thermal, creep, and shrinkage strain is accommodated either within the system itself or at the ends of the approach slabs where the slabs abut the pavement. Because they are jointless, ride quality is improved and maintenance can be greatly reduced.

This chapter of the guide provides the summary of design, construction and maintenance provisions related to use of jointless bridges.

C2. History of Jointless Bridges

A detailed history of jointless bridges is provided by Burke Jr. (2009). The first integral bridge in the United States was the Teens Run Bridge. It was built in 1938 near Eureka in Gallia County, Ohio. It consists of five continuous reinforced concrete slab spans supported by capped pile piers and abutments. Since that time construction of integral bridges has spread throughout the United States and abroad. The United Kingdom recently adopted them for routine applications. Japan completed its first two in 1996. South Korea completed its first such bridge in 2002.

On the basis of a nationwide mail survey of state and province transportation departments, it appears that the Ohio highway department was one of the first agencies to

initiate the routine use of continuous construction for the design and construction of multi-span bridges (Burke Jr, 2009).

In conjunction with the development and adoption of continuous construction for all moderate length highway bridges, Ohio DOT was also the first to routinely eliminate deck joints at abutments. This was accomplished for continuous reinforced concrete slab bridges by providing embankments and stub-type integral abutments supported by flexible piles in lieu of movable deck joints and wall type abutments. A version of this integral abutment design has been used in Ohio on hundreds of bridges ever since. However it was not until early 1960s that the integral concept was first used by Ohio DOT for a steel beam bridge. Since that time most of steel bridges with skews 30 degree or less and lengths not longer than 300 ft were of integral construction.

The Tennessee Department of Transportation now is leading the way in construction of continuous bridges. For example the Long Island bridge of Kingsport was constructed in 1980 using 29 continuous spans without a single intermediate movable deck joint.

Continuous integral bridges with steel main members have performed successfully for years in the 300 ft range in such states as North Dakota, South Dakota and Tennessee. Continuous integral bridges with concrete main members 500 to 800 ft long have been constructed in Kansas, California, Colorado and Tennessee.

As of 1987, eleven states reported building continuous integral bridges in the 300 ft range. Missouri and Tennessee reported even longer lengths. Missouri reported steel and concrete bridges in length of 500 and 600 ft respectively. Tennessee reported length of

400 and 800 ft for similar bridges. Sixty percent of those departments responding to the 1987 survey were using integral construction for continuous bridges.

More recently, Tennessee DOT completed the Happy Hollow Creek Bridge, a seven-span prestressed concrete curved integral bridge with a total length of over 1175 ft. In that bridge, tall flexible twin circular column piers support the superstructure. A single row of steel H-piles is used to support each abutment. Although to some engineers, the length of this structure may seem extreme, it is well within Tennessee DOT's bridge design policy statement regarding the length of integral bridges.

Seamless bridges are another type of jointless decks introduced by SHRP R19A for U.S. practice. The seamless bridge system was first introduced by Russell Bridge in Australia for continuously reinforced concrete pavement. Most commonly used pavements in the U.S. are either jointed plain concrete (JPCP) or flexible pavement. Seamless bridges do not have any joints, even at the ends of a transition slab (hence seamless). Instead, a pavement transition zone is used to dissipate the thermal displacements of the bridge. Although seamless, the transition zones can be rather lengthy, relative to the bridge. The benefit is that movements at the end of the transition zone are very small.

C3. Types of Jointless bridges

Three main types of jointless bridges are described in this chapter. The integral and semi-integral jointless bridges are commonly used in practice. A new class of jointless bridges, referred to as seamless jointless bridges is also introduced in this chapter. The

main characteristic of this system is that expansion joints are eliminated altogether and the bridge deck is connected to the road pavement with no joint.

Figure C1 shows a rendering of a typical layout of a jointless bridge, shown with the superstructure cast in an integral abutment.

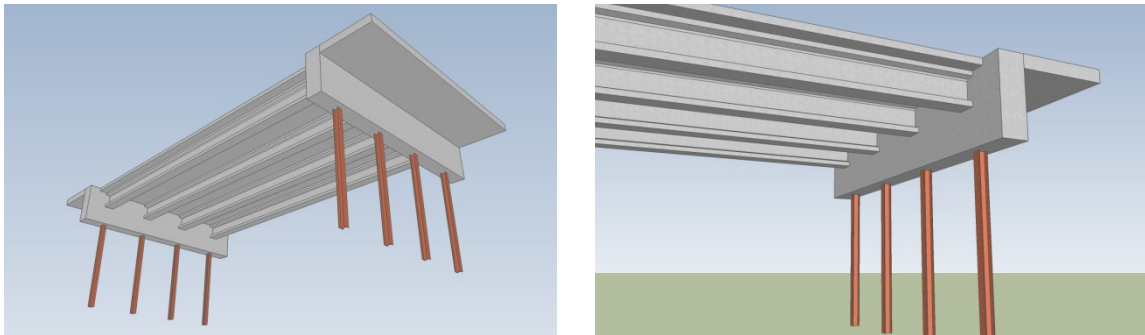


Figure C1- Elements of jointless integral bridges

C3.1. Integral Bridges

Integral bridges are defined as a superstructure constructed monolithically with the abutments, encasing the ends of the superstructure within the backwall. The system is structurally continuous and the abutment foundation is flexible longitudinally. The movement of the superstructure is accommodated by the foundation.

Figure C1 shows, schematically, the main elements of an integral bridge system. The main elements of the system consist of bridge deck, integral cast abutments, and approach slabs. The bridge movement is accommodated at the ends of the approach slabs. Also, sleeper slabs are commonly used to provide vertical support for the ends of the approach slab where the slabs abut the pavement (not shown in Figure C1). In addition, jointless integral bridges can be continuous multi-span structures with intermediate piers (also not shown in Figure C1). Various details are described in greater detail in Section C7.

C3.2. Semi-Integral Bridges

Semi-Integral bridges are defined as having an end diaphragm serving as the backwall stem and it is cast encasing the superstructure ends. In this system, the superstructure rests on bearings and the end diaphragm is not restrained longitudinally with respect to the pile cap. The deck may be sliding, or cast monolithically with the backwall stem, but does not have a joint above the abutment. The foundation is rigid longitudinally, where superstructure movement is accommodated through providing bearings.

Figure (XX) shows, schematically, the main elements of a semi-integral bridge system. The main elements of the system consist of bridge deck, pier cap and bearing seat, integral cast diaphragm backwall, approach slab, and sleeper slab. The bridge movement is accommodated at the ends of the approach slabs. The various details are described in greater detail in Section C7.

C3.3. Seamless bridges

The seamless bridge system is characterized by eliminating the need for expansion joints, even at the ends of the approach slabs, while allowing the longitudinal expansion and contraction of the bridge superstructure. The foundation requirements are very similar to those of Integral abutments. A seamless bridge system, for the types of pavements used in the U.S., is developed by SHRP2 R19A project.

Figure C2 shows, schematically, the main elements of seamless bridge system. The main elements of the system consist of bridge deck, transition zone and pavement. The bridge movement is accommodated within the transition zone and the movement at the

end of transition zone is very small (less than 0.1 inches). The thickness of the transition zone near the abutment is increased to account for lack of support from soil below (approach slab). The details of the transition zone and design provisions for the seamless bridge system are provided in Section C7.

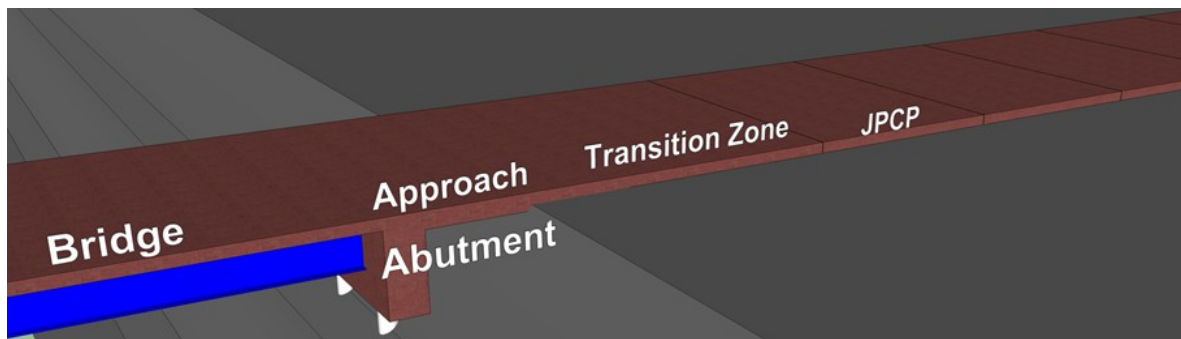


Figure C2- Seamless bridge system

C3.4. Advantages of Jointless Bridges

Henry Derthick, former engineer of structures at the Tennessee Department of Transportation, once stated, “The only good joint is no joint.” In keeping with this statement, known advantages of the jointless bridge systems include:

- Lower initial cost
- Lower maintenance cost
- Longer service life
- Preventing leakage of moisture to bridge elements below deck
- Improved ride quality
- Easier and faster construction
- Easier inspection

- Simplifying bridge details
- Elimination of bearings (except for Semi-integral)
- Ideal for bridges with skew and curvature or located in high seismic areas
- Enhancing the buoyancy characteristics of the bridge.

Because of these advantages, many DOT's have started using jointless bridges. However, the design provisions vary significantly from one State to another.

C3.5. Cost effectiveness of Jointless Bridges

Jointless bridges have a significant cost savings advantage as compared to traditional bridges with expansion joints. As mentioned above, cost savings are realized both during initial construction and throughout the life of the bridge with reduced maintenance. This is particularly true for bridges with integral abutments.

Most components of typical bridges with joints and jointless bridges are similar in construction and cost (deck, beams, cross frames, etc.). Thus, a comparison is made relative to the different components that distinguish each type of construction, e.g. the costs of the abutments and expansion joints. Additionally, since per unit pricing of each item is not consistent from region to region nor over time, a qualitative comparison is made using relative costs.

It is recognized that different states and municipalities have different specifications and construction techniques; however, initial construction of a typical abutment with an expansion joint will most often include the following:

- Excavation

- 2 rows of Piling
- Concrete cap, stem, diaphragms and backwall with reinforcing (3 pours)
- Elastomeric bearings, per beam
- Expansion joint
- Porous Backfill

Similarly, with an integral bridge the typical construction includes:

- Excavation
- 1 row of Piling
- Concrete cap, integral backwall and diaphragm (2 pours)
- Integral abutment joint seal
- Sleeper slab with reinforcement
- Porous Backfill

The important differences between an integral abutment and a standard jointed deck include a lack of expansion joint, no bearings, reducing the number of required piles, reducing the number of concrete pours, and inclusion of a sleeper slab. Taking these into consideration, the cost savings are readily apparent. The sleeper slab will add a few cubic yards of concrete and an extra detail to the cost, but removal of the expansion joint, removal of the second row of piling (overall reduced number of piles), reducing the required concrete and reinforcing in the stem/backwall unit, and elimination of beam bearings at the abutment greatly reduce the cost relative to adding the sleeper slab. The

overall reduction in initial construction cost can be over 40% for each abutment (% difference was estimated using Ohio 2010 bid planning costs for a typical 32' wide bridge).

The life cycle cost of the two types of abutments differs as well. A design life of 100 years is used for the comparison, although it is acknowledged that differences in estimated design life can affect the parameters. For standard jointed bridges, common armored expansion joints typically require gland replacement on the order of 8-12 years depending on condition severity. Additionally, the entire joint including armor will need to be replaced along with the deck at least once (based on an estimated life of a deck between 30-50 years). Again, this depends on the severity of the conditions. It is also expected that the bearings will need replacing at least once over the life of the bridge, the cost of which includes jacking of the bridge.

Similar to expansion joints, the integral abutment joint seal will require replacement on the same (or at least similar) schedule. Likewise, the deck will need replacing on a similar schedule. Deck replacement of an integral bridge does require additional consideration of certain construction items, but does not require a significant increase in construction cost as compared to traditional deck replacement.

So, for comparative purposes, consider that a typical bridge abutment with expansion joints will require:

- Expansion gland replacement every ~10 years
- Deck replacement every ~50 years
- Expansion joint replacement every ~50 years

- Bearing replacement every ~50 years

A typical Jointless bridge abutment will require:

- Joint seal replacement every ~10years
- Deck replacement every~50 years

Cost is similar for deck replacement, and gland and seal replacement. There is a significant increase in cost when replacing the expansion joint, however.

A qualitative cost comparison is presented in Figure C3 and Figure C4. Both Figures consider the difference in the initial cost at year 0, and the accumulated cost difference over the life of the bridge. The figures show the difference in costs, that is, similar costs have been removed from the equation (i.e. the cost of replacing the deck itself is removed from the equation since it is similar). Figure C3 shows the estimated cost comparison through the 100 year life of the structure overtime. Figure C4 shows the cost comparison differentiating the initial difference in the construction costs, the lifetime maintenance costs, and the overall total difference over the life of the bridge.

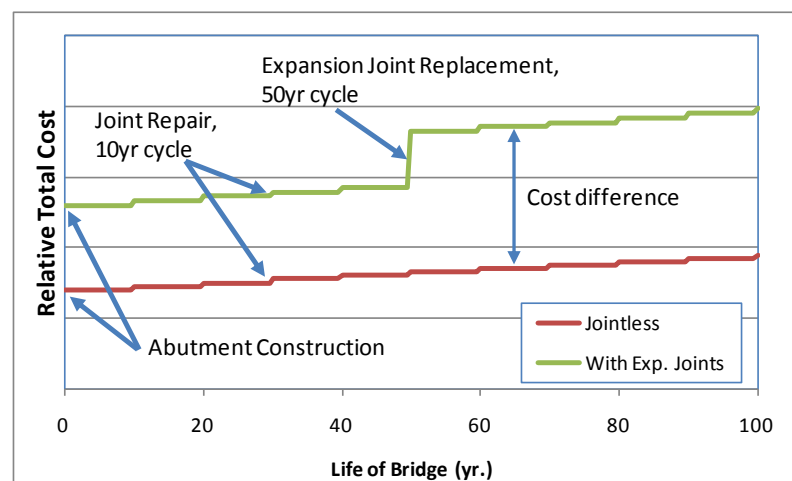


Figure C3- Life-time cost analysis of jointed vs. jointless bridge over time

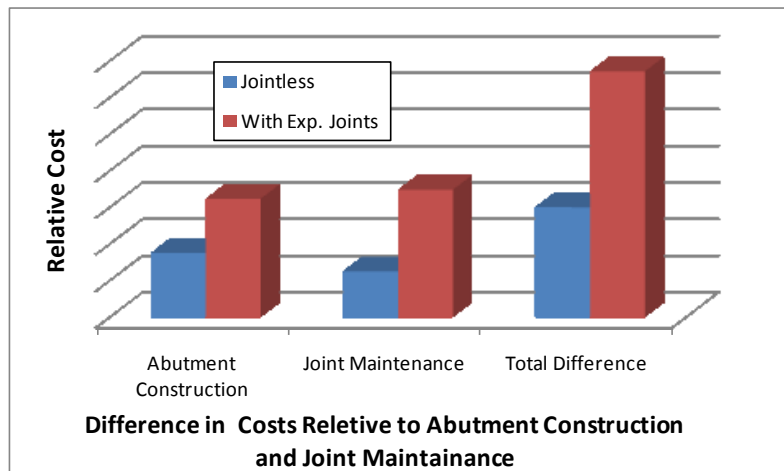


Figure C4- Life-Time cost differential analysis of jointed vs. jointless bridge

C4. Factors Affecting Performance of Jointless Bridges

C4.1. Curvature

Horizontal curvature changes the internal forces of the integral abutment bridges. These changes are more profound when the length over radius ratio of the bridge exceeds 0.5 or the radius of curvature the bridge is less than 1000 feet. For bridges which the length over radius ratio is less than or equal to 0.5 and the radius of curvature is larger than 1000 feet, the response of the curved bridge can be estimated by the response of a straight bridge of the same length. This estimation is not valid for the internal forces during construction.

C4.2. Skew

Theoretically, a bridge with a skew angle of $\theta > 20^\circ$ may rotate in the plane of the superstructure because of the transverse component of the passive soil pressure resisting thermal expansion. Therefore, in heavily skewed bridges, abutment will move in the transverse direction because of longitudinal expansion, unless this movement is restrained (Oesterle, Tabatabai, Lawson, Refai, Volz and Scanlon, 2005).

C4.3. Bearing

In the case of integral bridges with rigid piers, superstructure seats on piers by means of bearing devices. In curved bridges or wide straight bridges, fixed disc or pot bearings are not recommended except at the points of zero movement. In curved bridges, there may be no point of zero movement throughout the bridge. Also, guided disc or pot bearings are not recommended for curved and wide straight bridges because the displacements do not happen just in a particular direction. In such cases, guided bearing behave like a fixed bearing, creating large internal forces in the piers.

Elastomeric and sliding bearings are the proper types of bearings for integral bridges. If such bearings are used, the superstructure movement is mainly controlled by the integral abutments. Stop blocks may also be employed to limit the movements in extreme event limit states.

C4.4. Connection between Superstructure and Substructure

The choice of how the superstructure is connected to the substructure has a significant impact on how the bridge will behave. The types of jointless bridges were presented in Section C3 noting the associated abutments, and the methodology for designing the abutments is presented in Section C6. Choosing the abutment type sets the major design considerations for the bridge with respect to jointless behavior.

Equally important, however, is the consideration for the connection to the piers. The superstructure can be made integral with a pier or designed to transfer loads to the pier with more traditional assumptions. What is important to note in the planning stages is how the pier will react as the bridge expands and contracts. Piers must be sufficiently designed, whether it is intended to flex with the structure (slender piers), or if it is design to resist the movement (stout piers). The latter case is generally not preferable as it often

leads to oversized substructures since the movement from the continuous deck superstructure can generally be accommodated by simply using an expansion bearing to accommodate the movement. Overall, design using an integral pier has advantages and disadvantages that are discussed in more detail in Section C6.2.10.

C4.5. Other Considerations

There are other factors that can affect the performance of jointless bridges, primarily associated with the conditions of the foundation.

C4.5.1. Site Condition

Integral abutments for jointless bridges are usually supported on a single row of piles to provide flexibility. Also, piles are typically used to minimize settlement of the abutment and differential settlement within the superstructure. However, when rock is close to surface, a different type of foundation may be required. One solution is to use semi-integral abutments as described in Section C3.2. The abutment foundations are keyed into the rock. The end diaphragm serving as the backwall stem and encasing the superstructure ends rest on bearings supported by the abutment foundations. The deck and approach slabs are cast monolithically with the backwall stem. The abutment foundations are rigid and the longitudinal movement of the superstructure is accommodated through the bearings.

As an alternate to the semi-integral abutments, spread footings may potentially be appropriate for integral abutments when rock is close to the surface, or even when competent soil is near the surface, particularly for single-span bridges. Differential settlement would be a concern for use of spread footings on soils to support abutments for multi-span continuous bridges. There is however, some evidence that differential

settlement may not be significantly increased by using spread footings. With respect to differential settlement within the superstructure, Moulton et al. (1985), and Hearn(1995) indicate that there is essentially no difference in the settlement magnitude between the abutments on piles and the abutments on spread footings. Therefore, it should be possible to use spread footings under integral abutments for multi-span bridges. However, there is very little experience with the actual use of spread footings for integral abutments either on rock or on competent soil near the surface. Hence, it is recommended that experience be gained by starting with relatively short simple-span bridges. Use can then progress to longer structures and multispan structures as successful experience is gained.

The following recommendations pertain to the abutments supported by relatively shallow spread footings, where end movement may be accommodated by sliding:

1. For footings founded on rock, a layer of granular fill should be used (on top of a leveling layer of fill concrete, as needed) between the footing and rock to facilitate sliding. Do not key the footing into rock.
2. For footings founded on soil embankments, steps should be taken to minimize abutment settlement, such as allowing the maximum time feasible for embankment settlement before completing construction and establishing superstructure continuity or preloading the embankment to accelerate settlement. Also, with conditions susceptible to scour, footing should not be founded on soil above the scour line.

3. Design forces for the spread footing abutment should consider passive pressure similar to an abutment on piles. However, design forces should also include sliding friction on the bottom of the footing. For multispan continuous superstructures, friction should be calculated using a normal force that includes additional vertical load resulting from the negative moment on the girder related to these soil forces.
4. The abutment wall should be designed for shear and moments resulting from both expansion and contraction movements. The resistance to contraction should include friction on the bottom of the footing and soil pressure from the berm soil on the front face of the abutment.
5. Sufficient drainage, distance from the face of the slope, and slope protection are essential to keep soil from washing out below the footing. For footings supported on a layer of granular soil for sliding on rock, use of geotextile material may be considered to contain the granular soil. For footings supported on soil, mechanical stabilization of the soil below the footing may be appropriate.

Another possible solution for conditions when rock is close to surface is to drill large diameter holes in the rock and use piles, which would consequently allow use of typical integral abutment construction.

It must be noted that the concepts of integral abutments supported on spread footings or supported of piles placed in holes drilled into rock are not common practice. These two concepts are suggested for consideration when site conditions that may otherwise inhibit use of typical jointless construction.

C4.5.2. Deterioration of Piling

Accelerated pile deterioration is generally not considered except in specialized corrosive locations. Designers should consult with either a geotechnical engineer or geologist to mitigate possible impacts for this condition. More commonly, corrosion is generally thought of as a minimal concern for piles but it has been recorded (Beavers and Durr, 1998) and more recently evaluated (Decker, Rollins and Ellsworth, 2008). Additionally, the State of Iowa has been investigating deterioration of piles just below the pile cap of integral abutments (reference: Wade, C., 2011). Initial results note that the State has discovered corrosion immediately below abutment footings of what would be considered normal conditions.

Piling deterioration is of increased importance for integral abutments due to the additional strains placed on the substructure from the longitudinal expansion of the superstructure. The potential for section loss based on soil conditions should be accounted for as presented by AASHTO 10.7.5 which states minimum considerations for the effects of corrosion and deterioration of piling. Adhering to these guidelines should provide sufficient protection against advanced corrosion and thus failure of the integral abutment system.

C4.5.3. Jointless Bridge Abutments with MSE Walls

For locations where it is impractical to set the abutment on top of an embankment slope or to reduce the total bridge length, full height abutments with mechanically stabilized earth (MSE) retaining wall may be considered in the design of jointless bridges. When MSE walls are used, steps must be taken to prevent excess pressure on the retaining wall introduced by the movement of the backwall and pile.

For integral abutments, per FHWA Demonstration Project 82 (Elias, Barry and Christopher, 1997) the horizontal force and its distribution with depth may be developed using pile load/deflection methods (p-y curves) and added as a supplementary horizontal force to be resisted by the MSE wall reinforcements. This force will vary depending on the level of horizontal load, pile diameter, pile spacing, and distance from the pile to the back of the panels.

Per the FHWA Demonstration Project, the following additional design details have successfully been used:

- Provide a clear horizontal distance of 0.5m between the back of the panels and the front edge of the pile
- Provide a casing around piles, thru the reinforced fill, where significant negative skin friction is anticipated

Where pile locations interfere with the reinforcement, specific methods for field installation must be developed. Simple cutting of the reinforcement is not permissible.

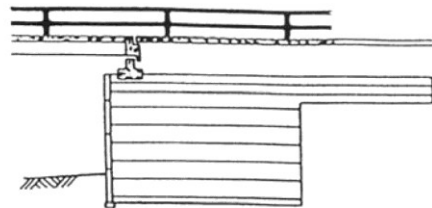
Alternatives for use of MSE walls with jointless bridge abutments suggested by Nicholson (1997) are shown in Figure C5. Figure C5a illustrates use of a semi-integral abutment or stub integral abutment on spread footings. In this approach, the MSE reinforcement should be designed for the sliding forces in the bearings of the semi-integral abutment or the frictional sliding forces of the spread footings.

Figure C5b illustrates use of pile encased in a pressure relieving sleeve that isolates the pile movements from the surrounding soil. Hassiotis (2007) has reported tests with an integral abutment supported on pile encased in corrugated steel sleeves backfilled with

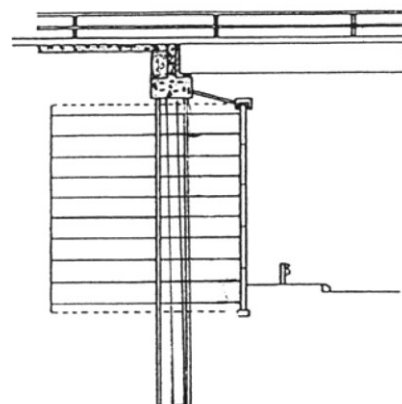
sand. Lui et al. (2005) indicate Iowa DOT criteria for use of MSE walls with integral abutments requires each pile to be encased in a corrugated metal sleeve. The reinforced earth should include sand up to the bottom of the sleeve and the remainder is to be filled with bentonite to the top of the sleeve.

Figure C5c illustrates use of a semi-integral abutment supported on a pier in front of the MSE wall. No additional considerations are necessary for semi-integral abutments since the lateral movement is dissipated through the bearings. For integral abutments and for seamless bridges, MSE walls can still be used, but they must be sufficiently isolated from the soil movement caused by the movement of the piles. One strategy that has been suggested by Nicholson (1997) is shown in Figure C5. The piles are encased in a pressure relieving sleeve that isolates the pile movements from the surrounding soil. This procedure can be used where full height abutments are necessary.

- (a) Semi-integral or stub integral abutment on spread footing. The reinforced soil must be allowed to settle before constructing the bridge and approach pavement.



- (b) Piled integral abutment. The piles are surrounded by an earth-pressure relieving sleeve.



- (c) Semi-integral abutment in front of reinforced soil.

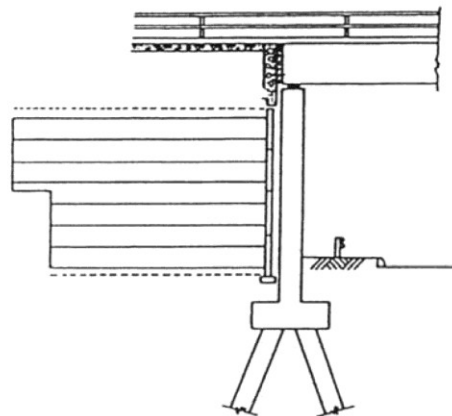


Figure C5- Alternatives to integral full-height wall abutments using reinforced soil retaining structure (Nicholson, Barr, Cooke, Hickman, Jones and Taylor, 1997)

C5. Strategy Selection Process

Each type of jointless construction has a range of parameters that suits particular bridges or provides various advantages over another type of system. The following Tables help to guide the proper selection of bridge type based on limiting parameters

Table C1 assists in the selection of the primary system.

Table C1- Strategy table for abutment in jointless bridges- straight bridges

Strategy	Maximum Bridge Length Used	Typical Details	Advantages	Disadvantages	Qualitative longitudinal movement demand	Qualitative maintenance ranking	Applicability to Existing Bridges
Integral	800'	Section C7 Figure C53, Figure C54, Figure C55	Eliminates need for bearings	Difficult to inspect damage to piles due to pile movement	Low	Low	Yes
Semi-Integral	1500'	Section C7 Figure C56, Figure C57	No longitudinal force transfer to piles	Needs bearings	Medium	Medium	Yes
Seamless	infinite	Section C7 Figure C45, Figure C46	Eliminates need for any expansion joints anywhere. Eliminates concerns when there is skew or curvature. Eliminates need for bearings; no need for sleeper slab	Possible, initial higher cost. Difficult to inspect damage to piles due to pile movement; long transition zone off bridge	Low	Low	Yes

Table C2 provides further guidance on the substructure type that is appropriate for use with each type of jointless bridge.

Table C2- Strategy table for foundation at abutment in jointless bridges-straight bridges

Strategy		Typical Details	Advantage	Disadvantage	Qualitative longitudinal movement demand	Potential for achieving 100 plus years of service life
Integral Abutment	Strategy 1- H-pile	Section C7 Figure C53	Economical for small movements. Easy to construct	Relatively Low strength, ductility and buckling capacity	Low	Medium
	Strategy 2- Pre-stressed Pile	Section C7 Figures X, Y, Z	Very stiff and high axial load capacity	Prone to concrete deterioration and corrosion of strands	Medium	Medium
	Strategy 3- Concrete Filled Tube (CFT) Pile	Section C7 Figures X, Y, Z	CFT has high strength and ductility and higher buckling capacity, which will use much larger bridge length	Higher initial cost	High	High
Semi-Integral Abutment	Any foundation type could be used with the semi-integral abutment.					
Seamless	Strategy for selection of seamless foundations is the same as those for integral abutments. The detailing for seamless bridges is primarily in the transition zones at the ends of the bridge as detailed in page 312.					

Table C3 provides guidance on the types of connections and bearings used at the piers when used in a jointless bridge.

Table C3- Strategy Table for Connection Between Piers and Superstructure in Jointless Bridges-Straight Bridges

Strategy		Detail Figure	Advantage	Disadvantage	Qualitative longitudinal movement demand	Qualitative maintenance ranking	Degree of difficulty to apply to existing bridges	Potential for achieving 100 plus years of service life
Girders continuous over pier	Strategy 1- Integral-Frame Action	Section C7 Figure C47a, Figure C49	Eliminates need for bearings over pier	May cause transverse cracking in the pier	Low	Low	Medium	High
	Strategy 2- Fixed Bearing(Rotational Movement Allowed)	Section C7 Figure C47b	No longitudinal movement requirement for bearing over pier	May cause transverse cracking in the pier	Low	Medium	Medium	Medium
	Strategy 3- Expansion Bearing	Section C7 Figure C47c	No bending of pier column	Bearing designed for both rotation and longitudinal movement	High	Medium	Low	Low
Girders not continuous over pier	Strategy 4- Simple for Dead and Continuous for Live Load	Section C7 Figure C47b, Figure C47c, Figure C50	Eliminates joints and protects girder ends; viable option for seismic retrofit	Restraint moments and cracking in diaphragms.	Varies with bearing type	Low	Low	High
	Strategy 5- Link Slab	Chapter 7 Figure C47d, Figure C51	Low cost	May crack and cause leakage over joint	Varies with bearing type	High	Low	Medium

C6. Design Provisions for Jointless Bridges

Two design approaches are presented in this section. Method A is a simple approach and is applicable to bridges meeting the limitations stated in Table C4. Method B is a detailed design approach and is applicable to all bridges. Many of the design provisions

stated in Method B is automatically satisfied, when limitations of Table C4 are met and it is sufficient to use Method A design approach (Doust and Azizinamini, 2011).

Table C4- Requirements for Using Method A

Requirement	Limitations	
	Method A	Method B
Skew	<20 deg.	>=20 deg.
Total Bridge Length and Curvature	L/R<1/2 and L<400'	L/R>=1/2 or L>=400'

C6.1. Method A

When Method A is selected to design a bridge, the designer can ignore the secondary load effects and use a conventional two dimensional analysis method which can be either hand calculations or finite element modeling. When Method B is chosen, all loads and load effects including secondary effects should be considered. In the latter case, a three dimensional finite element analysis is preferred.

C6.2. Method B

Method B is a general approach to design jointless bridges. There are no limitations on total bridge length, skew, or curvature, for using Method B. Method B uses more detailed design process, accounting for the effects of exceeding the limits of Table C4. Many of the Method B design provisions are met, when Table C4 limitations for Method A are satisfied. Method A design provisions are small subset of Method B design provisions.

C6.2.1. Loads

C6.2.1.1. Dead Loads

Dead loads include the weight of all components including superstructure and substructure elements and need to include all permanent loads according to AASHTO

LRFD Article 3.5. The dead loads are distributed to the foundation through traditional assumptions or in accordance with the owner's bridge design provisions.

C6.2.1.2. Live Loads

Live Loads and the associated impact are applied in accordance with AASHTO LRFD (2010) Article 3.6, or in accordance with the owner's bridge design provisions. Note that for integral abutments and piers, application of live loads will cause rotation and induce moments that will need to be considered in the design.

Horizontal live load (braking force and centrifugal force) are subject to distribution with respect to the stiffness of the integral and semi-integral abutments. In traditional design, longitudinal forces are distributed to the substructure based on bearing fixity (expansion vs. fixed against horizontal movement) and relative substructure flexibility. For jointless bridges, the backfill is in full contact with the end diaphragm (backwall) and provides a great amount of stiffness relative to the other substructure components. In particular for integral abutments, where the bearing condition is fixed, it is acceptable to assume for bridges with one to three spans that the longitudinal forces are absorbed by the passive pressure and stiffness provided by the backfill soil. This should be verified by a geotechnical engineer. As bridges get longer and more substructure units are introduced, a relative stiffness analysis should be performed. However, even with multiple piers with some having fixed-expansion bearings, integral abutments can still be expected to absorb as much as 80% of the longitudinal force.

C6.2.1.3. Soil Loads

C6.2.1.3.1. Soil Load on Abutment

The magnitude of soil pressure behind the abutment wall and the nonlinear distribution of this pressure depend on wall displacement, soil type, depth, piles stiffness, and also direction of the displacement (Faraji, Ting, Crovo and Ernst, 2001). As a wall moves toward the backfill, passive pressure is engaged, and when it moves away from that, active pressure and surcharge pressure may be generated. Studies show that a minimum movement is required to reach the extremes for each of these types for pressure.

Full passive pressure builds up for relatively long bridge lengths. For shorter bridge lengths, only part of the passive pressure is developed for expansion as thermal expansion is limited. For all bridges, the maximum passive pressure force, P_p is calculated as

$$P_p = \frac{1}{2} K_p \gamma H^2 \quad \text{Eq. C1}$$

Where,

K_p = the passive pressure coefficient

K_p is not necessarily the maximum K_p associated with full passive pressure. The value of K_p should be calculated using Figure C6 and Figure C7 (Clough and Duncan, 1991). The extreme values for expansion and contraction are proportional to the height of the wall. The movement required to reach the maximum passive pressure is on the order of ten times the movement required to reach the active soil pressure. The movement required to reach the extreme pressures are larger for loose soils than that for dense soils

(Figure C6 and Figure C7). Table C5 highlights the required movements necessary to achieve maximum pressures.

The force-deflection design curves (Barker, Duncan, Rojiani, Ooi and Tan, 1991) shall be based on Figure C6 and Figure C7 (Clough and Duncan, 1991). The stiffness of the springs behind the abutment wall is nonlinear and depends on the type of the soil.

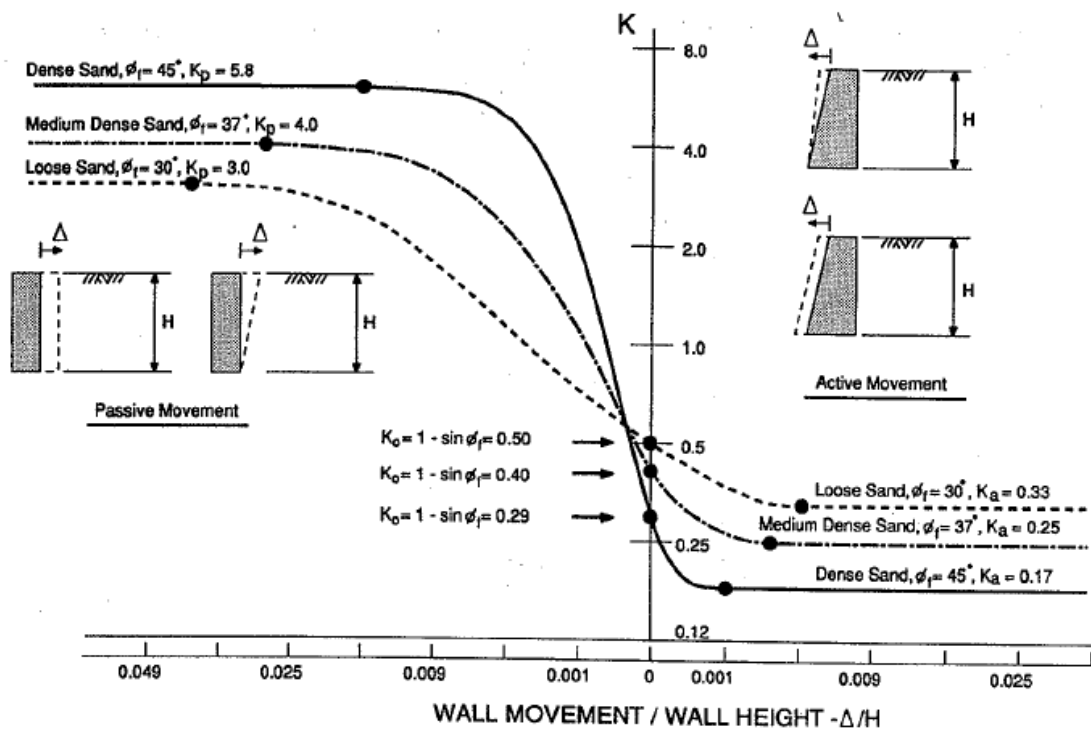


Figure C6- Relationship between wall movement and earth pressure (Clough and Duncan, 1991)

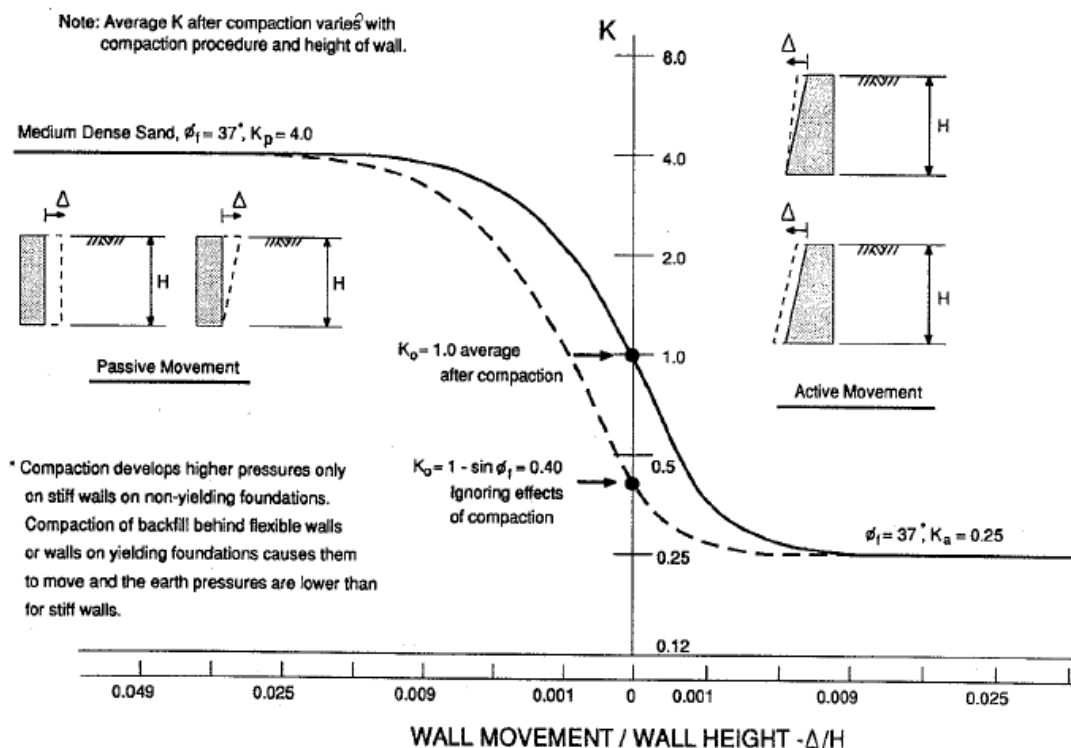


Figure C7- Relationship between wall movement and earth pressure for a wall with compacted backfill (Clough and Duncan, 1991)

Table C5- Approximate magnitudes of movements required to reach extreme soil pressure condition (Clough and Duncan, 1991)

Type of Backfill	Values of $\Delta/H^{(a)}$	
	Active	Passive
Dense Sand	0.001	0.01
Medium-Dense Sand	0.002	0.02
Loose Sand	0.004	0.04
Compacted Silt	0.002	0.02
Compacted lean clay	0.01 ^(b)	0.05 ^(b)
Compacted fat clay	0.01 ^(b)	0.05 ^(b)

(a) Δ = movement of top of the wall required to reach extreme soil pressure, by tilting or lateral translation, H = height of the wall

(b) Under stress conditions close to the minimum active or maximum passive pressures, cohesive soils creep continually. The movement shown would produce temporary passive pressures. If pressures remain constant with time, the movements shown will increase. If movement remains constant, active pressures will increase while passive pressures will decrease.

C6.2.1.3.2. Soil Load on Piles

Design of piles shall consider soil-structure interaction using p-y curves (Federal Highway Administration (FHWA) and also American Petroleum Institute (API, 1993)).

Soil-structure interaction analysis of piles can be carried out using available software (LPILE, COM624P, FB-MultiPier) utilize this approach. Further information on this topic is provided in Article 10.7 of AASHTO LRFD Bridge Design Specifications (2010).

C6.2.1.4. Thermal Loads

In order to account for the effect of temperature changes in design of jointless bridges two different effects should be considered: the effect of uniform temperature change and the effect of temperature gradient within the structure. These two effects are explained in the following subsections.

C6.2.1.4.1. Uniform Temperature Change

The calculation of uniform temperature changes should be in accordance to Article 3.12.2 of AASHTO LRFD (2010). In those specifications, two procedures are recommended: Procedure A and Procedure B. Both procedures may be used for concrete deck bridges having concrete or steel girders. For all other types of bridges, Procedure A should be employed.

C6.2.1.4.1.1. Procedure A

Table C6 presents the temperature ranges to calculate the design thermal movements. The difference between these values and the base construction temperature should be used to calculate thermal movements.

Table C6- Procedure A Temperature Changes (Table 3.12.2.1-1 of AASHTO)

Climate	Steel or Aluminum	Concrete	Wood
Moderate	0 to 120 °F	10 to 80 °F	10 to 75 °F
Cold	-30 to 120 °F	0 to 80 °F	0 to 75 °F

C6.2.1.4.1.2. Procedure B

The range of temperature change is the difference between maximum design temperature and minimum design temperature. In concrete girder bridges with concrete decks, the maximum design temperature is given in Figure C8 and the minimum design temperature is given in Figure C9. In the case of steel girder bridges, the maximum and minimum design temperatures are given Figure C10 in Figure C11 and, respectively.

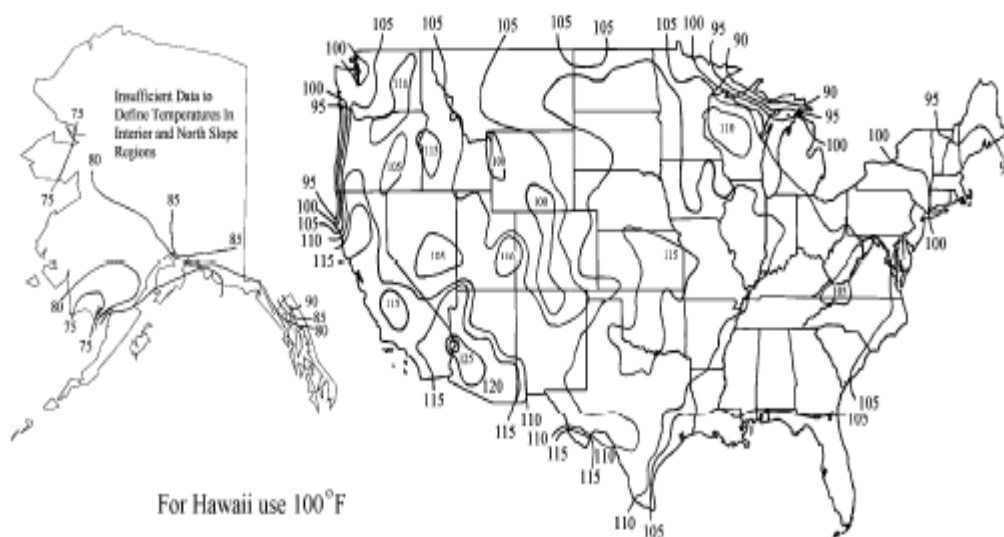


Figure C8- Maximum design temperature for concrete girder bridges. (figure 3.12.2.2-1 from AASHTO)

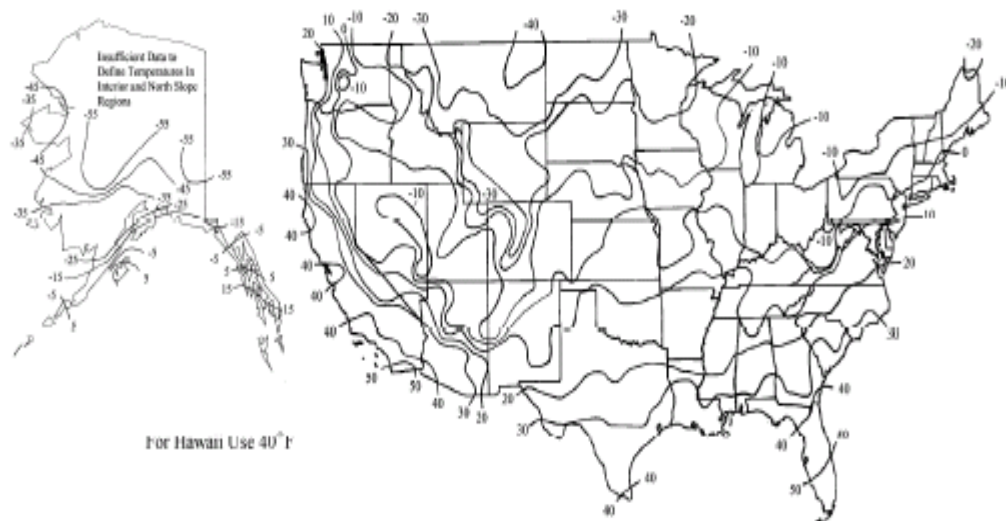


Figure C9- Minimum design temperature for concrete girder bridges. (figure 3.12.2.2-2 from AASHTO)

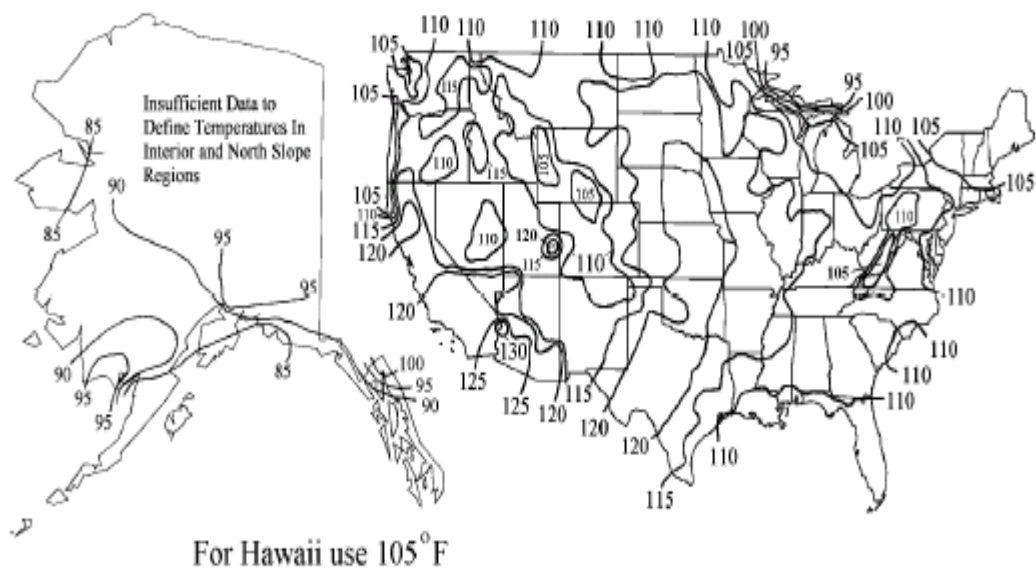


Figure C10- Maximum design temperature for steel girder bridges. (figure 3.12.2.2-3 from AASHTO)

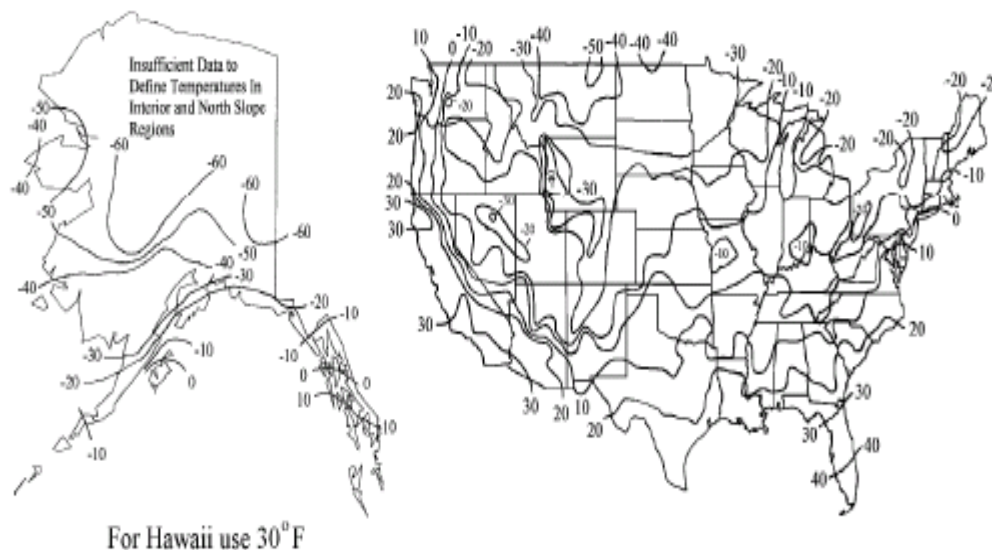


Figure C11- Minimum design temperature for steel girder bridges. (figure 3.12.2.2-4 from AASHTO)

C6.2.1.4.2. Temperature Gradient

The effect of temperature gradient may be ignored. But if the designer decides to consider the effect of temperature gradient the following provisions are recommended. To account for temperature gradient, country is divided (Chapter 3 of AASHTO LRFD) into 4 zones as illustrated in Figure C12. Positive temperature values shall be taken from AASHTO (2010). Negative temperature values shall be obtained by multiplying the values from the same table by -0.3 for plain concrete decks and by -0.2 for decks with asphalt overlay.

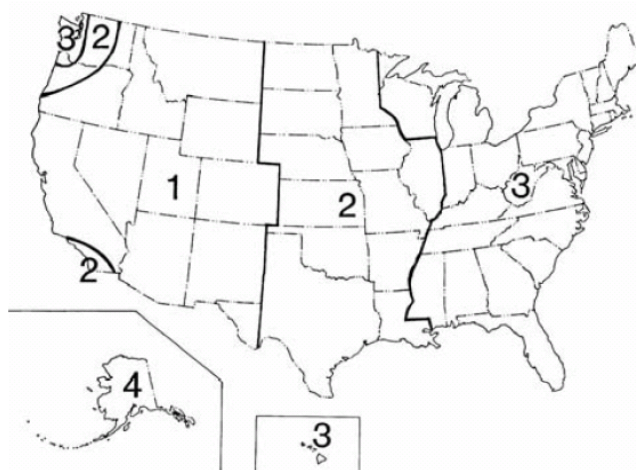


Figure C12- Solar radiation zones for the united states. (figure 3.12.3-1 from AASHTO)

Table C7- Basis for temperature gradients (table 3.12.3-1 from AASHTO)

Zone	T_1 (°F)	T_2 (°F)
1	54	14
2	46	12
3	41	11
4	38	9

The profile of the temperature in steel and concrete girder bridges may be taken as shown in Figure C13 in which t is the thickness of concrete deck. Dimension A in this figure shall be taken as:

- 12.0 in. for concrete superstructures deeper than 16 in,
- (Depth-4.0in.) for concrete superstructures shallower than 16 in,
- 12.0 in. for steel superstructures.
- This article also specifies that the value T_3 shall be taken zero, unless a specific field study is carried out to determine this value. In this case T_3 should not exceed 5°F.

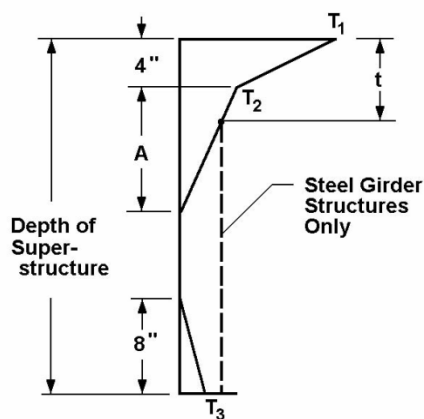


Figure C13- Positive vertical temperature gradient in concrete and steel superstructures (figure 3.12.3-2 from AASHTO)

When considering temperature gradient in the section profile, the analysis should consider axial extension, flexural deformation, and internal stresses (section 4.6.6 of AASHTO LRFD). The response of the structure to temperature gradient can be divided into three parts as follows:

- Axial Expansion: This component is due to the uniform part of the temperature gradient and can be calculated as (equation C4.6.6-1 from AASHTO):

$$T_{UG} = \frac{1}{A_c} \iint T_G dw \cdot dz \quad \text{Eq. C2}$$

Where,

T_G = temperature gradient ($\Delta^\circ\text{F}$),

T_{UG} = temperature averaged across the cross-section ($^\circ\text{F}$),

A_c = cross-section area—transformed for steel beams (in^2),

w = width of element in cross-section (in),

z = vertical distance from center of gravity of cross-section (in).

The corresponding uniform axial strain shall be taken as (equation C4.6.6-2 from AASHTO):

$$\varepsilon_u = \alpha(T_{UG} + T_U) \quad \text{Eq. C3}$$

Where,

α = coefficient of thermal expansion (in./in./°F),

T_U = uniform specified temperature (°F).

- Flexural Deformation: The consequence of temperature gradient is the development of curvature over the cross section. The rotation per unit length corresponding to this curvature may be determined as:

$$\phi = \frac{\alpha}{I_c} \iint T_G z dw \cdot dz = \frac{1}{R} \quad \text{Eq. C4}$$

Where,

I_c = inertia of cross-section—transformed for steel beams (in⁴),

R = radius of curvature (ft).

- Additional stresses because of curvature, created by thermal gradient shall be calculated as:

$$\sigma_E = E[\alpha T_G - \alpha T_{UG} - \phi z] \quad \text{Eq. C5}$$

Where,

E = modulus of elasticity (ksi).

C6.2.1.5. Creep

Concrete creep strains shall be calculated using Article 5.4.2.3.2 of AASHTO LRFD Spec. Time dependence and changes in concrete strength shall be taken into account in determining the effect of concrete creep. Creep coefficient shall be determined using equation 5.4.2.3.2-1 of AASHTO LRFD spec.

$$\Psi(t, t_i) = 1.9k_s k_{hc} k_f k_{td} t_i^{-0.118} \quad \text{Eq. C6}$$

In which,

$$k_s = 1.45 - 0.13 \frac{V}{S} \quad \text{Eq. C7}$$

$$k_{hc} = 1.56 - 0.008H \quad \text{Eq. C8}$$

$$k_f = \frac{5}{1 + f'_{ci}} \quad \text{Eq. C9}$$

$$k_{td} = \left(\frac{t}{61 - 4f'_{ci} + t} \right) \quad \text{Eq. C10}$$

Where,

$H =$ relative humidity (%). In the absence of better information, H may be taken from Figure C14,

$k_s =$ factor for the effect of the volume-to-surface ratio of the component,

$k_f =$ factor for the effect of concrete strength,

$k_{hc} =$ humidity factor for creep,

$k_{td} =$ time development factor,

t = maturity of concrete (day), defined as age of concrete between time of loading for creep calculations, or end of curing for shrinkage calculations, and time being considered for analysis of creep or shrinkage effects,

t_i = age of concrete at time of load application (day),

V/S = volume-to-surface ratio (in.),

f'_{ci} = specified compressive strength of concrete at time of pre-stressing for pre-tensioned members and at time of initial loading for non-prestressed members. If concrete age at time of initial loading is unknown at design time, f'_{ci} may be taken as 0.80

f'_c (ksi).

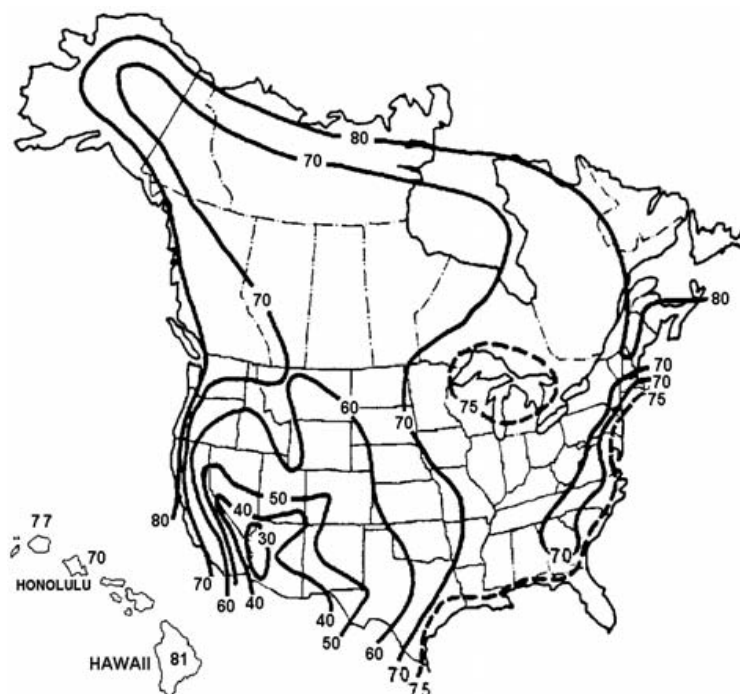


Figure C14- Annual average ambient relative humidity in percent. (figure 5.4.2.3.3-1 from AASHTO)

C6.2.1.6. Shrinkage

Concrete shrinkage should be calculated in accordance with the provisions of Article 5.4.2.3.3 in AASHTO LRFD where appropriate. For concrete elements, shrinkage strain ϵ_{sh} shall be calculated as (equation 5.4.2.3.3-1 from AASHTO)

$$\epsilon_{sh} = k_s k_{hs} k_f k_{td} 0.48 \times 10^{-3} \quad \text{Eq. C11}$$

In which,

$$k_{hs} = (2.00 - 0.014H) \quad \text{Eq. C12}$$

Where,

k_{hs} = Humidity factor for Shrinkage.

This article states that if the concrete is exposed to drying before 5 days of curing have elapsed, the shrinkage as determined in Eq. 11 should be increased by 20 percent.

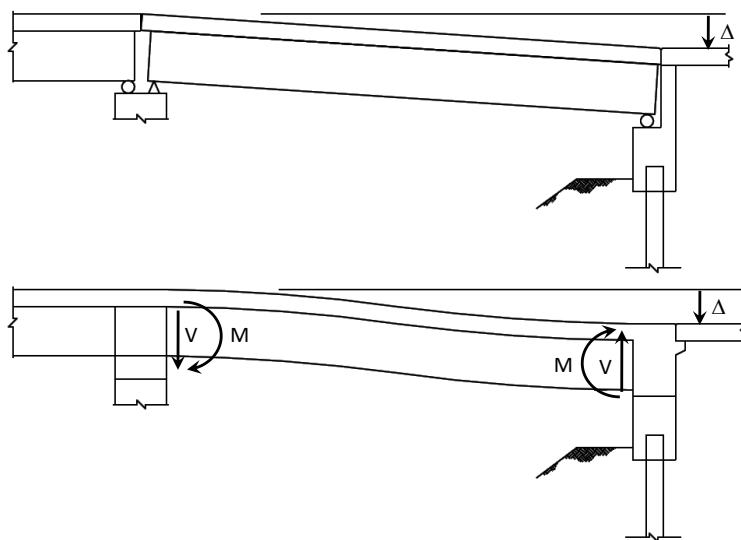
C6.2.1.7. Settlement

Settlement is not a deterrent to the use of jointless bridges if sufficiently accounted for in the design of the effected components. AASHTO provided guidance on estimating settlement for structures in Article 10.7.2.3.

It must be recognized that bridges with simply spans and simple abutment bearings are able to accommodate the shifting and the associated rotation of the end spans with flexibility of the bearings. With continuous jointless superstructures and integral abutments, vertical or longitudinal movement of the foundation will introduce additional stresses in the superstructure, deck, or both. Also with semi-integral abutments, vertical movement of the foundation will introduce additional stresses in the superstructure, deck,

or both. Figure C15 demonstrates this concept with an exaggerated illustration showing a settlement, Δ . Where traditional bearings are used, the superstructure is free to rotate to accommodate the movement. Contrastingly, when the superstructure is integral with the substructure, the superstructure is not permitted to rotate or shift and thus forces are introduced from the fixed end displacement.

One of two strategies can be used to reduce or eliminate the effect of settlement on integral abutments. One option is to evaluate the anticipated settlement and account for the resulting forces in the design. The second option would be to determine the maximum permissible displacement allowable by design and take measurements to insure that that settlement limit is not exceeded. There are various strategies for reducing or minimizing settlement of foundations.



(Not to Scale)

Figure C15- Illustration comparing of settlement effects on the superstructure

C6.2.1.8. *Wind*

Wind Load need to be considered in accordance with AASHTO Article 3.8. As with braking and centrifugal forces, longitudinal and transverse forces resulting from wind

loads also should take into consideration the considerable stiffness of the integral abutments (see Section C6.2.1.2).

C6.2.1.9. Other Loads

All other AASHTO loads such as collision forces and water and ice loads need to be applied to jointless structures in the same manner as other structures. As with all designs, it is the engineers responsibility to appropriately determine and apply the necessary load conditions appropriate for each jointless bridge's unique situation.

C6.2.2. Load Combinations and Limit States

This chapter will provide summary of available information in AASHTO and those to be developed under R19A as related to load combinations and limit states to be considered. This chapter will also provide explanations and discussions for many parameters included in the load combinations associated with sub-structure.

C6.2.2.1. Load Combinations

C6.2.2.1.1. Load combinations are prescribed per AASHTO procedures.

C6.2.2.1.2. Loads and Load Designations

The following loads shall be considered for jointless bridges:

DC = dead load of structural components and nonstructural attachments,

DW = dead load of wearing surfaces and utilities,

EH = horizontal earth pressure load,

LL = vehicular live load,

WS = wind load on structure,

WL = wind on live load,

TU = uniform temperature,

CR = creep,

SH = shrinkage,

TG = temperature gradient,

SE = settlement.

C6.2.2.1.3. Load Factors and Combinations

Table C8 - lists all load combinations required in the design of jointless bridges based on AASHTO LRFD.

Table C8 - Load combinations and load factors (from table 3.4.1-1 in AASHTO LRFD)

Load Combination Limit State	DC DW EH	LL	WS	WL	TU CR SH	TG	SE
Strength I	γ_p	1.75	-	-	0.50/1.20	γ_{TG}	γ_{SE}
Strength II	γ_p	1.35	-	-	0.50/1.20	γ_{TG}	γ_{SE}
Strength III	γ_p	-	1.40	-	0.50/1.20	γ_{TG}	γ_{SE}
Strength IV	γ_p	-	-	-	0.50/1.20	-	-
Strength V	γ_p	1.35	0.40	1.00	0.50/1.20	γ_{TG}	γ_{SE}
Service I	1.00	1.00	0.30	1.00	1.00/1.20	γ_{TG}	γ_{SE}
Service II	1.00	1.30	-	-	1.00/1.20	-	-
Service III	1.00	0.80	-	-	1.00/1.20	γ_{TG}	γ_{SE}
Service IV	1.00	-	0.70	-	1.00/1.20	-	1.00

Table C9- Load factors for permanent loads, γ_p (from table 3.4.1-2 in AASHTO LRFD)

Type of Load and Foundation Type	Load Factor	
	Maximum	Minimum
DC: Component and Attachments	1.25	0.90
DC: Strength IV only	1.50	0.90
DW: Wearing Surface and Utilities	1.50	0.65

Type of Load and Foundation Type	Load Factor	
	Maximum	Minimum
EH: Horizontal Earth Pressure		
Active	1.50	0.90
At-Rest	1.35	0.90

AASHTO specifies that the load factor for temperature gradient, γ_{TG} , should be considered on a project-specific basis or may be taken as:

- 0 at the strength limit states,
- 1.0 at the service limit states where live load is not considered,
- 0.50 at the service limit state when live load is considered,

Since effects of γ_{TG} are typically self-limiting and do not significantly affect strength or ductility at strength limit states for the types of bridge girders typically used in jointless bridges, γ_{TG} can commonly be taken as 0.

Similarly, the load factor for settlement, γ_{SE} , should be considered on a project-specific information or may be taken as 1.0. Load combinations which include settlement should also be applied without settlement.

C6.2.3. Bridge Movement

Three methods are provided for calculation of bridge maximum end displacements. The first one is applicable to straight bridges and the second addresses transverse movement of skewed bridges and the third one is a general method for curved bridges.

C6.2.3.1. Displacement of Straight Bridges (Non-Skew)

Bridges expand and contract because of temperature changes and time-dependent volume changes associated with concrete creep and shrinkage. In jointless bridges, it is

important to estimate the maximum expansion and contraction at each end of a bridge to determine the longitudinal displacement expected for the abutment piles. It is also important to predict the movement at each pier and the joint width needed between the approach slab and the pavement. Another important movement is the maximum total thermal movement at each end resulting from the total effective temperature range. The starting point to determine the maximum passive pressure should conservatively be at the maximum contraction (Oesterle, et al. 2005). The maximum passive pressure is related to the end movement, with re-expansion for the full effective temperature range.

Calculation of the length change for a prestressed concrete bridge can be accomplished through use of typical design values for the coefficient of thermal expansion combined with creep and shrinkage strains. However, the overall variability of these factors adds uncertainty to the calculated end movements. Although a coefficient of thermal expansion for concrete is typically assumed to be 5.5 to 6.0 millionths/°F, it is known that this value can range from approximately 3.0 to 7.0 millionths/°F (Kosmatka and Panarese, 1988). Also, the variability of creep, shrinkage, and modulus of elasticity of concrete is known to be significant (Bazant and Panula, 1980). In addition, resistance to length change from abutments and piers, combined with the variability of the restraint (primarily caused by the variability of the soil), leads to unequal movement at each end of a bridge (even in theoretically symmetrical bridges) and uncertainty as to the magnitude of the movement at each end. Finally, the effective setting temperature of the bridge and the age of concrete girders at completion of the superstructure are typically unknown, making the relative magnitude of expansion and contraction and the starting point for temperature, creep, and shrinkage calculations uncertain.

To investigate the effects of the variability of the parameters and to provide guidance in formulating recommendations for design calculations, Monte Carlo studies were carried out for calculation of bridge movements to generate a large number of computer analyses using the statistical variation of material parameters affecting the movement (Oesterle, 2005, Oesterle and Volz, 2005). Within each analysis, values for the coefficient of thermal expansion, temperature at construction, creep and shrinkage parameters of concrete, modulus of elasticity of concrete, and soil stiffness were selected based on statistical distributions of the values of these parameters. The variations in calculated bridge end abutment movements are then used to determine a 98 percent confidence interval for the maximum calculated movements. These maximum values were used to determine magnification factors, referred to as Γ factors, for modification of calculated values to account for uncertainty in the various parameters affecting results.

Procedures are presented in the following sections for determining the maximum end movements of jointless bridges including use of these Γ factors. In these calculations, it is assumed that the bridge has unknown construction timing and that no specific data on material properties are available.

C6.2.3.1.1. Prestressed Concrete Bridges

- Determine the average construction temperature using Section C6.2.1.4.1.
- Determine the maximum and minimum effective bridge temperatures based on the recommendations of Section C6.2.1.4.1.2.
- Assume the following parameters for concrete:

Table C10- Concrete parameters (Oesterle, Tabatabai, Lawson, Refai, Volz and Scanlon, 2005)

	Coefficient of Expansion	Modulus of Elasticity
Value (English)	$6.0 \times 10^{-6}/\text{oF}$	$57000\sqrt{f'_c}$ (psi)
Value (Metric)	$10.8 \times 10^{-6}/\text{oC}$	$4700\sqrt{f'_c}$ (MPa)

- Determine point of zero movement of fixity point of the bridge based on the stiffness of the piers and the abutments. Use section C6.2.1.3.1 provisions (Clough and Duncan, 1991) to estimate the backfill passive pressure and p-y method to evaluate the nonlinear behavior of the soil surrounding the piles. It should be noted that for symmetric bridges, fixity point of the bridge will be in the middle of the bridge.
- Use the following equations to calculate the strain values in the bridge:

$$\varepsilon_{th} = \alpha \Delta T \quad \text{Eq. C13}$$

$$\varepsilon_{sh} = \varepsilon_{sh,girder} + \frac{\varepsilon_{sh,deck} - \varepsilon_{sh,girder}}{1 + \frac{(EA)_{girder}}{(EA)_{deck}}} \quad \text{Eq. C14}$$

$$\varepsilon_{cr} = \varepsilon_{cr,girder} \left[\frac{1}{1 + \frac{(EA)_{girder}}{(EA)_{deck}}} \right] \quad \text{Eq. C15}$$

$$\Delta\lambda = \Gamma \varepsilon_{total} \lambda \quad \text{Eq. C16}$$

Where,

ε_{th} = thermal strain,

ε_{sh} = shrinkage strain,

ε_{cr} = creep strain,

α = coefficient of thermal expansion,

$E =$ modulus of elasticity,

$A =$ cross section area,

$\lambda =$ length from the point of fixity to the end of the bridge. Note that for unsymmetrical bridge two different λ are involved,

$\Gamma =$ magnification factor to account for uncertainty listed in Table C11,

$\varepsilon_{total} = \varepsilon_{th} - \varepsilon_{sh} - \varepsilon_{cr}$ For expansion,

$\varepsilon_{total} = -\varepsilon_{th} - \varepsilon_{sh} - \varepsilon_{cr}$ For contraction,

$\Delta\lambda =$ maximum end movement.

- For maximum expansion, which occurs shortly after construction, use the temperature difference between the maximum effective bridge temperature and the mean construction temperature for the location of the bridge from Technical Report No. 65 (1979). For creep and shrinkage calculations, assume the girders are 90 days old. Based on Monte-Carlo simulation Γ should be 1.6 to account for uncertainties with 98 percent confidence that the movement will be less than the calculated value.
- For maximum contraction which occurs after several years of service use the temperature difference between the minimum effective bridge temperature and the mean construction temperature. For creep and shrinkage, assume ultimate values with the girder to be 10 days old at the time of casting the deck. Based on Monte-Carlo simulation Γ should be 1.35 to account for uncertainties with 98 percent confidence that the movement will be less than the calculated value.

- For maximum thermal re-expansion from a starting point of full contraction, use the full effective bridge temperature range without any creep and shrinkage movements. Based on Monte-Carlo simulation Γ should be 1.2 to account for uncertainties.
- It should be noted that Γ values in the first two columns of Table C11 for maximum expansion and maximum contraction are relatively large and possibly over conservative because they are affected by the relatively large uncertainty of the construction or “setting” temperature. Further studies to include a more deterministic method to incorporate the construction temperature for a given bridge may reduce these magnification factors for a more efficient design approach.

Table C11- Summary of recommended magnification factors

	Maximum Expansion	Maximum Contraction	Maximum Thermal Re-Expansion
Prestressed Concrete Bridges	$\Gamma = 1.6$ Creep+shrinkage+thermal	$\Gamma = 1.35$ creep+shrinkage+thermal	$\Gamma = 1.2$ thermal
Reinforced Concrete Bridges	$\Gamma = 1.6$ shrinkage+thermal	$\Gamma = 1.4$ shrinkage+thermal	$\Gamma = 1.2$ thermal
Composite Steel Bridges	$\Gamma = 1.7$ shrinkage+thermal	$\Gamma = 1.5$ shrinkage+thermal	$\Gamma = 1.2$ thermal

C6.2.3.1.2. Reinforced Concrete Bridges

Same procedure as that used for prestressed concrete bridges shall be used to calculate bridge end movements. Shortening caused by creep is not a factor. Magnification factors for different cases are listed in Table C11.

C6.2.3.1.3. Composite Steel Bridges

Same procedure as that used for prestressed concrete bridges shall be used to calculate bridge end movements, except that the extreme effective bridge temperatures should be calculated using the recommendations of Section C6.2.1.4.

Other parameters needed are provided in Table C12.

Table C12- Recommended steel parameters (Oesterle, Tabatabai, Lawson, Refai, Volz and Scanlon, 2005)

	Coefficient of Expansion	Modulus of Elasticity
Value (English)	$6.5 \times 10^{-6}/^{\circ}\text{F}$	2.9×10^7 (psi)
Value (Metric)	$11.7 \times 10^{-6}/^{\circ}\text{C}$	2.0×10^5 (MPa)

The effective coefficient of thermal expansion for steel composite bridges can be estimated as (Emanuel and Hulsey, 1977)

$$\alpha_e = \frac{(\alpha EA)_{girder} + (\alpha EA)_{deck}}{(EA)_{girder} + (EA)_{deck}} \quad \text{Eq. C17}$$

Magnification factors for different cases are listed in Table C11.

C6.2.3.2. Displacement of Skewed Bridges

C6.2.3.2.1. Background

A skewed bridge is a bridge with the longitudinal axis at an angle other than 90° with the piers and abutments. The skew angle, θ , is shown in Figure C16. With skewed integral abutment bridges, the soil passive pressure developed in response to thermal elongation has a component in the transverse direction as illustrated in Figure C16. Within certain limits of the skew angle, soil friction on the abutment will resist the transverse component of passive pressure. However, if the soil friction is insufficient, then, depending on the transverse stiffness of the abutment, either significant transverse forces or significant transverse movements could be generated.

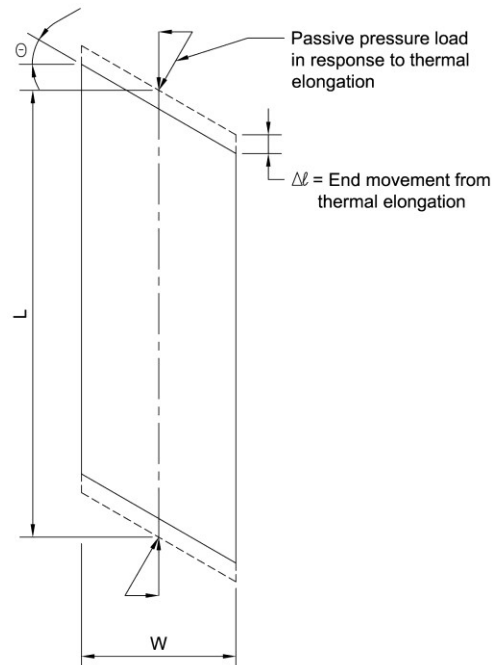


Figure C16- Components of abutment soil passive pressure response to thermal elongation in skewed integral abutment bridges.

Figure C17 shows a two-span bridge with a skew angle of 45° (Nicholson, Barr, Cooke, Hickman, Jones and Taylor, 1997). This bridge was constructed in 1969 with semi-integral abutments. The semi-integral construction included an integral end diaphragm that moves with the superstructure that slides longitudinally on and is guided transversely by relatively stiff abutments.



Figure C17- Two-span semi-integral abutment bridge with an overall length of 89 m, width of 11.6 m, and a skew angle of 45° (Nicholson, Barr, Cooke, Hickman, Jones and Taylor, 1997).

Figure C18 show cracking in the abutment wall near an acute corner of the superstructure, presumably caused by transverse forces related to soil pressures.

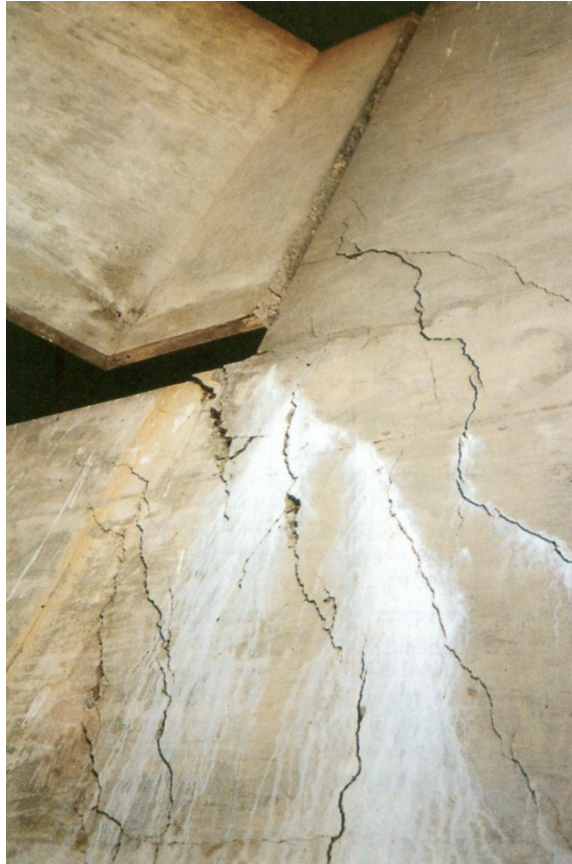


Figure C18- Cracking in the abutment wall near an acute corner of the superstructure for the bridge shown in Figure C17 (Nicholson, Barr, Cooke, Hickman, Jones and Taylor, 1997).

Figure C19 shows distress in an asphalt overlay at the skewed end of an approach slab because of the transverse movement (Tabatabai, Oesterle and Lawson, 2005). Figure C20 shows a closer view of the barrier wall joint at the end of the approach slab. The expansion joint in the barrier wall was made perpendicular to the longitudinal direction and therefore could not accommodate the transverse movement.

C6.2.3.2.2. Design Recommendations for Transverse Response of Skewed Bridges

Because of potential problems and uncertainty related to the response of skewed integral abutments, many State DOTs limit the skew angle. A typical limit for maximum

skew angle for integral abutment bridges used by many States is 30° . However, maximum skew angle limits in various States range from 0° to no limit (Chandra, 1995).



Figure C19- Asphalt overlay distress (west end) (Tabatabai, Oesterle and Lawson, 2005).



Figure C20- Barrier distress at west abutment (Tabatabai, Oesterle and Lawson, 2005).

The following guidelines, based on studies were carried out in the FHWA Jointless Bridge Project (Oesterle and Lotfi, 2005), are recommended for:

6. Maximum skew angle for limiting transverse effect due to abutment soil friction.
7. A relationship to estimate the magnitude of forces required to restrain transverse movement in integral abutment bridges with large skew angles.
8. A relationship to estimate expected transverse movement for a typical integral stub abutment with no special design features to restrain this movement.

These recommendations are based on analyses considering equilibrium and compatibility equations for end abutment forces for various skew angles and bridge length-to-width ratios for the case of a typical stub abutment.

C6.2.3.2.2.1. Skew Angle Limit for Limiting Transverse Effects

Figure C21 shows the passive soil pressure response, P_p , due to thermal expansion and soil/abutment interface friction, F_{af} , assuming no rotation of the superstructure. The

bridge superstructure can essentially be held in rotational equilibrium until the skew angle exceeds the angle of interface friction. Considering that integral abutments are typically backfilled with granular material with a friction angle of 22° to 26° between the soil and concrete abutment, a skew angle of $\theta = 20^\circ$ is recommended as a skew angle limit below which special considerations for transverse forces or transverse movement are not needed.

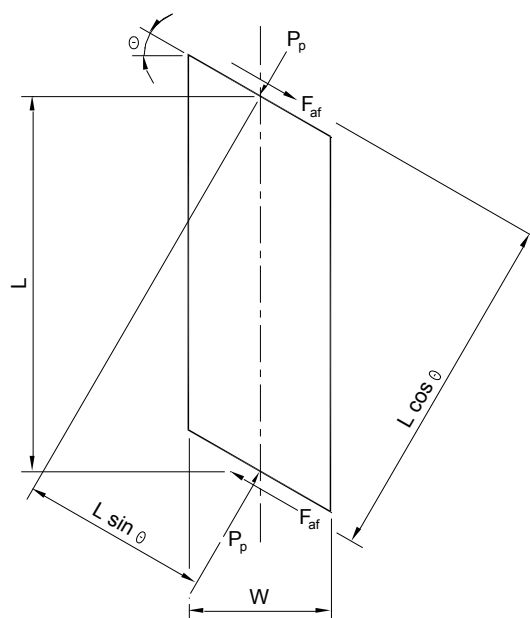


Figure C21- Soil pressure load, P_p , and soil abutment interface friction, F_{af} .

With larger skew angles, the integral abutment can either be designed to resist the transverse force generated by the soil passive pressure in an attempt to guide the abutment movement to be predominantly longitudinal or the abutment can be detailed to accommodate the transverse movement.

C6.2.3.2.2.2. Forces Required to Resist Transverse Movement

Figure C22 shows a relationship between F_a and P_p , assuming the interface friction angle, δ , to be 20° for the case of a typical stub abutment. As shown in Figure C22, the

force required to resist transverse movement is a significant portion of the soil passive pressure, P_p . It should be noted that P_p is not necessarily full passive pressure, but can be determined for the end movement using relationships calculated by Clough and Duncan (Clough and Duncan, 1991, Barker, Duncan, Rojiani, Ooi and Tan, 1991) shown in Figure C20 and Figure C22. The end movement to consider in calculating passive pressure is the end movement normal to the abutment, Δl_n .

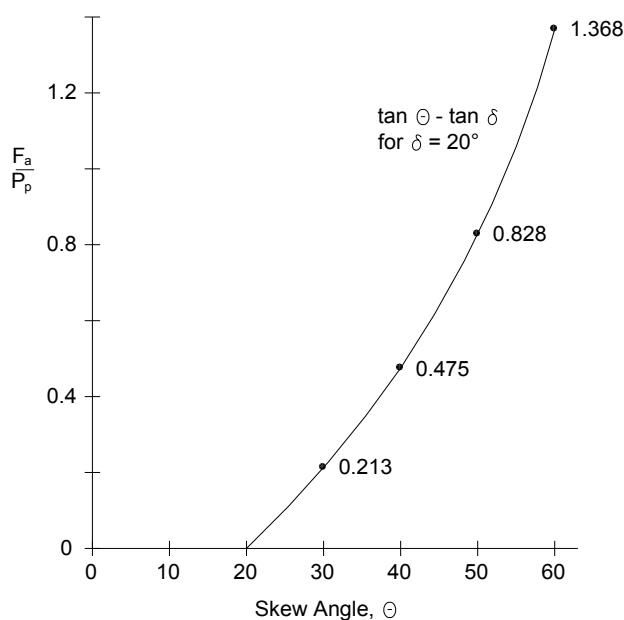


Figure C22- Relationship between force required for abutment lateral resistance, F_a , and passive pressure response, P_p , to restrain lateral movement.

As illustrated in Figure C23, this end movement is:

$$\Delta l_n = \Delta l \cos \theta \quad \text{Eq. C18}$$

Where, Δl is the maximum expected end movement for thermal re-expansion from the starting point of full contraction for the full range of effective bridge temperatures as discussed in Section C6.2.3.1. From Figure C23, it can be seen that Δl_n is reduced with

respect to Δl as the skew angle, θ , increases. This relationship helps offset the increase in

F_a/P_p with increasing θ . However, F_a will still be a sizeable portion of P_p .

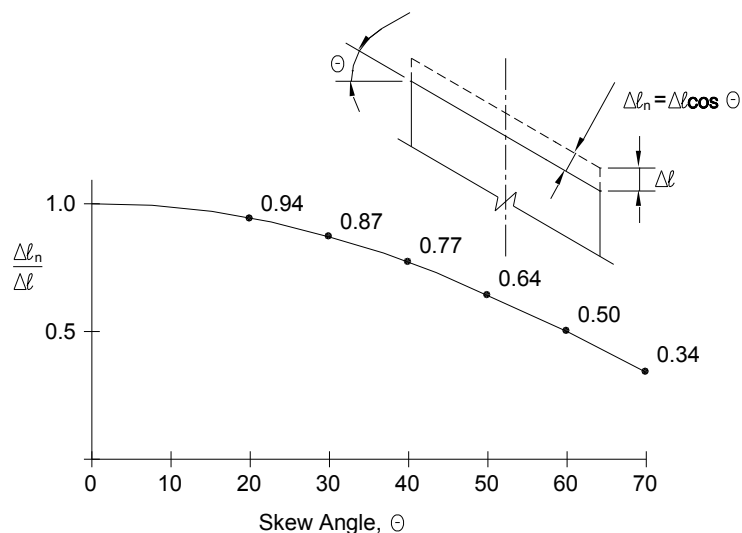


Figure C23- Relationship between end normal movement, $\Delta \ell_n$, and end thermal expansion, $\Delta \ell$.

For relatively short bridges and/or bridges in locations with small effective temperature ranges, it may be feasible to design the abutment substructure to resist F_a . It should be understood though that for whatever means used to develop F_a (battered pile and/or lateral passive soil resistance), lateral movements are required to develop the resistance, F_a . Therefore, details anticipating some transverse movement should be used. The expected movements are a function of the relative stiffnesses of response for P_p and F_a . It should also be noted that adding battered piles to an integral abutment for lateral loading will also increase the stiffness in the longitudinal direction, which induces more demand on the superstructure and connections between the girders and abutments.

C6.2.3.2.2.3. Expected Transverse Movement with Typical Integral Abutment

A relationship between skew angle and expected transverse movement was determined for a typical integral stub abutment based on equilibrium and compatibility of end abutment forces in the plane of the bridge superstructure. For this analysis, the superstructure is assumed to act as a rigid body with rotation, β , about the center of the deck (for a longitudinally symmetrical bridge). The rotation occurs to accommodate the thermal end movement, Δl . Forces considered in response to this movement include soil pressure on the abutment and wingwalls, wall-soil interface friction on the abutment, and pile forces normal to and in line with the abutment and wingwalls. Details of the forces, stiffness, and equations of compatibility and equilibrium are provided in the report on the analytical work for the FHWA jointless bridge project (Oesterle, 2005).

Results of these analyses for the ratio of transverse movement to longitudinal movement, $\Delta_{t1}/\Delta l$, for a Δl of 1 inch, are shown in Figure C24. The transverse movement, Δ_{t1} , is the transverse movement of the acute corner of the bridge deck. This is the corner that experiences the greatest transverse movement because of the skew angle.

Data in Figure C24 demonstrate the increase in the transverse movement with increasing skew angle. The data in Figure C24 also demonstrate the increase in transverse movement with decreasing L/W ratio where L and W are the length and width of the bridge respectively.

The baseline abutment used in the analyses for the data in Figure C24 is a relatively typical stub abutment (but also relatively deep, with an abutment height of 13.0 ft and with strong axis pile bending for movement normal to the abutment versus weak axis

bending for movement parallel to the abutment). Therefore, the data in Figure C24 represent a reasonably large estimate for the transverse movement of skewed abutments. Although there is significant uncertainty for actual soil and pile stiffness, the maximum expected end movement, Δl , discussed in Section C6.2.3.1 includes a multiplier to account for uncertainty. Therefore, it is suggested that the data in Figure C24 can be used by designers to determine an approximate estimate for expected transverse movement in skewed integral abutments resulting from the restraint of longitudinal thermal expansion. This transverse movement should be anticipated in the details for barrier walls, drainage structures and the ends of the approach slabs. In addition, the transverse movements can be used to estimate the transverse forces on the wingwalls resulting from passive soil load and pile and to estimate longitudinal and transverse movement for the abutment pile.

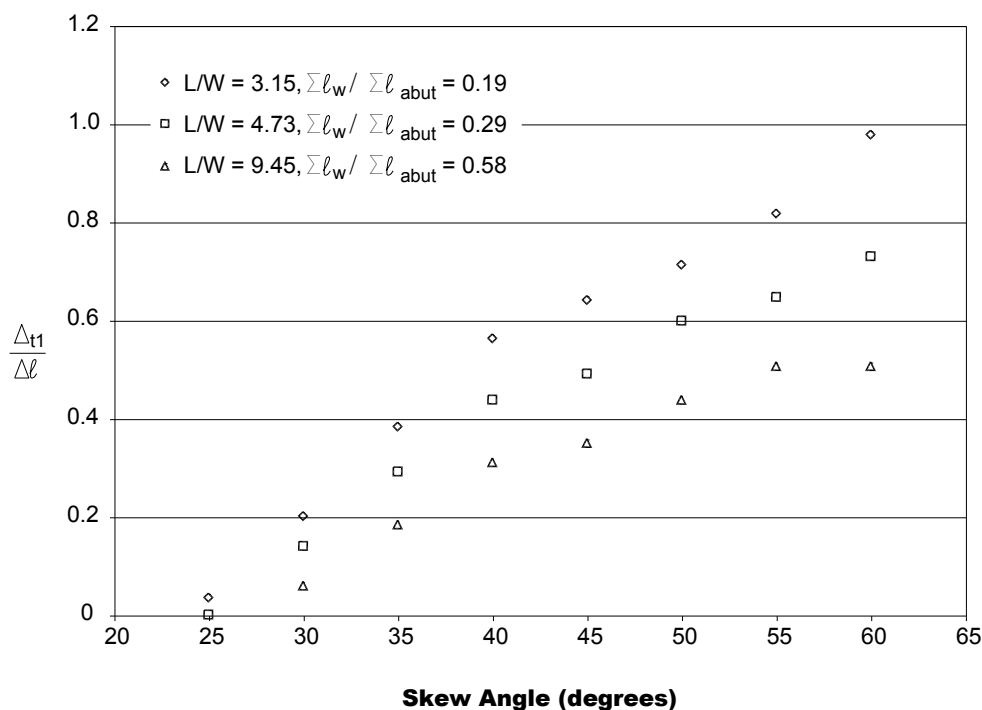


Figure C24- Relationship between transverse movement at the acute corner, Δ_{t1} , and thermal expansion, Δl , for an expansion of 1 inch with constant length bridge, $L = 415.92$ ft, and varying L/W .

Figure C25 shows the resulting total longitudinal restraint force for these analyses and demonstrates the decrease in longitudinal restraint with increasing skew angle. The relationships in Figure C25 can be used to estimate the relative decrease in restraint forces in a skewed bridge. All of the other components of movement and forces can be determined from Δ_{l1} and Δl using equations presented in the full analytical report (Oesterle, 2005). For more accurate estimates, the equations in the full report can be used to analyze specific skewed abutments.

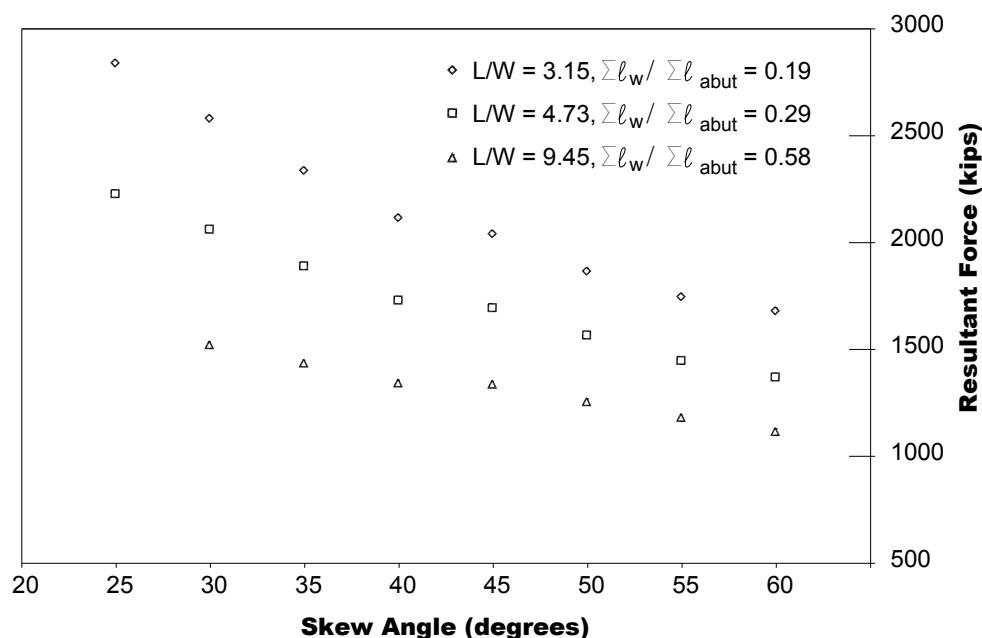


Figure C25- Relationship between resultant longitudinal restraint force and skew angle for thermal expansion, Δl , of 1 inch with constant length bridge, $L = 415.92$ ft, and varying L/W .

C6.2.3.3. Displacement of Curved Bridges

In this section, a numerical method is presented to calculate the end displacements of a curved bridge. This method is based on finite element simulation of several curved integral steel I-girder bridges (Doust and Azizinamini, 2011). There are some limitations for the application of this method. These limitations include bridge symmetry in plan,

non-skewed supports, length over width ratio larger than 3 and end span over middle span ratio close to 0.8. To calculate the end displacements of a curved bridge, the following step by step procedure should be taken.

1. Determine the point of zero movement for the bridge and therefore the length of the bridge that participates in end displacement, L_o . For symmetric bridges, it can be assumed to be equal to half of the length of bridge. Otherwise, more sophisticated methods found in the literature can be employed.
2. Determine the effective coefficient of thermal expansion using:

$$\alpha_{eq} = \frac{(EA\alpha)_{deck} + (EA\alpha)_{girder}}{(EA)_{deck} + (EA)_{girder}} \quad \text{Eq. C19}$$

3. Calculate the bridge shortening due to contraction using:

$$\Delta_{contraction} = \alpha_{eq} \cdot \Delta T \cdot L_o \quad \text{Eq. C20}$$

4. Find the modification factor for bridge shortening due to contraction using the following figure:

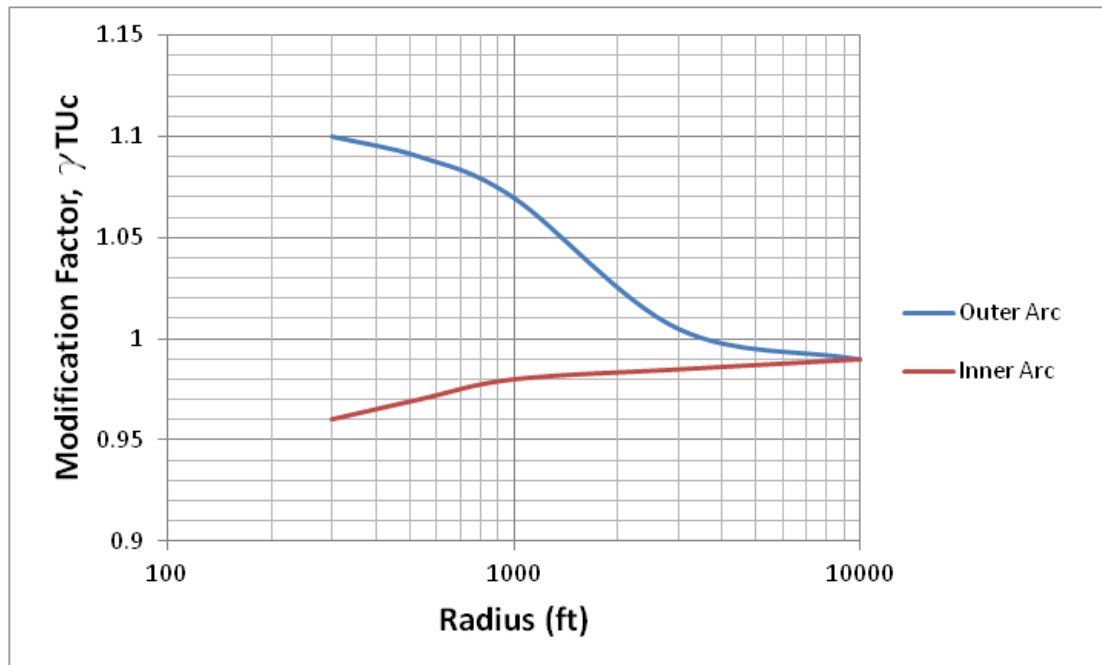


Figure C26- Modification factor for bridge contraction

5. Determine the equivalent shrinkage strain using:

$$\varepsilon_{sh,eq} = \varepsilon_{sh,girder} + \left(\varepsilon_{sh,deck} - \varepsilon_{sh,girder} \right) \frac{(EA)_{deck}}{(EA)_{deck} + (EA)_{girder}} \quad \text{Eq. C21}$$

6. Calculate the bridge shortening due to shrinkage using:

$$\Delta_{shrinkage} = \varepsilon_{sh,eq} \cdot L_o \quad \text{Eq. C22}$$

7. Find the modification factor for bridge shortening due to shrinkage using the following figure:

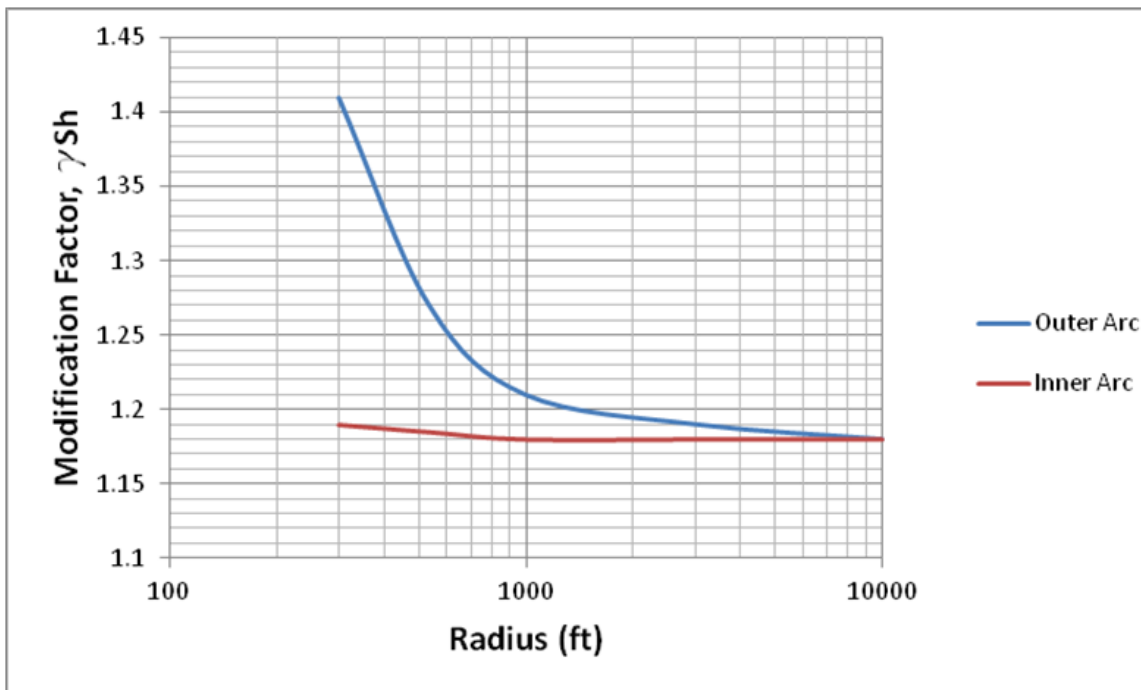


Figure C27- Modification factor for bridge shrinkage

8. Calculate the total bridge shortening using:

$$\Delta_{total} = 1.3 \left(\gamma_{Tuc} \Delta_{thermal} + \gamma_{sh} \Delta_{shrinkage} \right) \quad \text{Eq. C23}$$

9. Calculate the bridge width effect factor using the following equations. These factors are calculated for the inner and outer corners of the bridge separately.

$$k_{in} = 1 + 0.84 \frac{w}{L_c} \quad \text{Eq. C24}$$

$$k_{out} = 1 - 0.84 \frac{w}{L_c} \quad \text{Eq. C25}$$

10. Find the direction of the bridge corners displacements using:

$$\alpha_{in} = k_{in} \left[90^\circ - 11 \left(\frac{L}{R} \right) \right] \quad \text{Eq. C26}$$

$$\alpha_{out} = k_{out} \left[90^\circ - 11 \left(\frac{L}{R} \right) \right] \quad \text{Eq. C27}$$

11. Knowing the total bridge shortening found in step 8 and the direction found in step 10, solve Eq. C28 through Eq. C34 to find the new location of the bridge

corner. The corner of the bridge is assumed to be originally located at the coordinates $x_A = R_A$ and $y_A = 0$ in which R_A is the radius of the bridge at that specific corner.

$$x_{A'} = \frac{\left(-ab + \sqrt{a^2b^2 - (b^2 - R'^2)(1+a^2)}\right)}{(1+a^2)} \quad \text{Eq. C28}$$

$$y_{A'} = ax_{A'} + b \quad \text{Eq. C29}$$

Where,

$$a = -\tan \alpha \quad \text{Eq. C30}$$

$$b = R \tan \alpha \quad \text{Eq. C31}$$

$$\gamma = \tan^{-1} \left(\frac{y_{A'}}{x_{A'}} \right) \quad \text{Eq. C32}$$

$$L' = 2R'(\beta - \gamma) \quad \text{Eq. C33}$$

In which,

$$\beta = \frac{L}{2R} \quad \text{Eq. C34}$$

12. Using the new coordinates of the bridge corner $x_{A'}$ and $y_{A'}$, the components of

bridge corner displacement are found as follows:

$$\Delta_x = x_{A'} - R_A$$

$$\Delta_y = y_{A'}$$

C6.2.4. Restraint Moments

C6.2.4.1. Background

In simple-span non-composite bridges, time-dependent deformations result in little or no change in the distribution of forces and moments within the structure. However, continuous multiple-span composite bridges are statically indeterminate. As a result, inelastic deformations that occur after construction is completed will generally induce statically indeterminate forces and restraining moments in the girders.

Sources of inelastic deformation include concrete creep and shrinkage, and temperature gradients. As an example, a common type of jointless bridge construction consists of precast, prestressed girders connected with a continuous cast-in-place deck slab as illustrated in Figure C28. The girders are simply supported for dead load but may be considered continuous for live load. Continuity is established with deck steel as negative moment reinforcement over the piers. Commonly, a positive moment connection is also provided in the diaphragms.

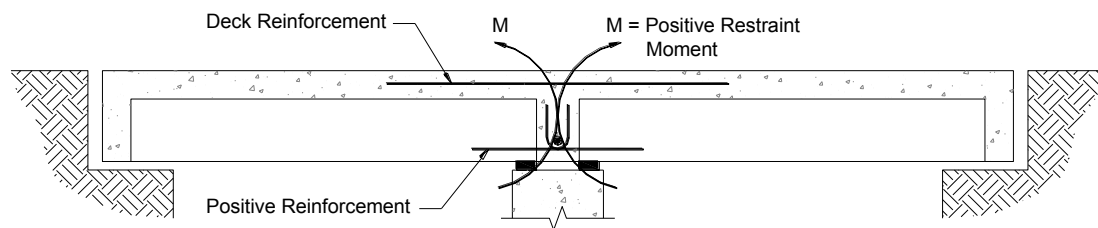


Figure C28- A typical precast prestressed bridge simply supported for dead load and made continuous for live load.

It has long been recognized that positive secondary moments develop in the connection at piers of continuous prestressed concrete bridges when the deck is cast at a relatively young girder age (Freyermuth, 1969). Creep of the girder concrete under the net effects of prestressing and self-weight will tend to produce additional upward camber

with time. The piers prevent this upward movement. When girders are made continuous at a relatively young age, it is possible that positive moments will develop at the supports over time as shown in Figure C29.

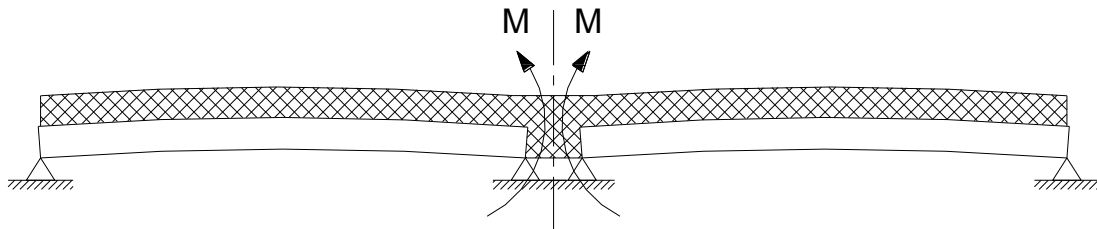


Figure C29- Restraint against upward movement, positive secondary moment.

Conversely, differential shrinkage, with the newer deck slab concrete shrinking more than the girder concrete, causes the continuous structure to bow down. Therefore, differential shrinkage has a tendency to reduce the positive moment due to creep or result in negative secondary moments at the supports.

In addition to creep and shrinkage of concrete, temperature gradients can play a major role if the girders are made continuous. Solar heating of the top deck will tend to produce upward camber adding to the positive restraint moment caused by creep. Large restraining positive moment can cause cracking in the bottom flange near the pier locations. Heat of hydration in the cast-in-place deck concrete can have a mitigating effect on the development of positive restraint moment. The cast-in-place deck may be heated to temperature that is higher than the supporting girder temperature by heat of hydration during the initial hydration when the concrete is still plastic. Contraction of the deck concrete with subsequent cooling after the concrete has hardened results in a downward deflection thereby reducing the positive restraint moment caused by creep and solar heating.

Oesterle et al. (1989, 2004, 2004) presented the results of an experimental and analytical research program, funded by NCHRP, and the Federal Highway Administration, on the behavior of continuous and jointless integral abutment prestressed concrete bridges with cast-in-place deck slab.

Results of analytical studies (Oesterle, Mehrabi, Tabatabai, Scanlon and Ligozio, 2004) showed that the age of the girder when the deck was cast was the most significant factor in determining whether positive or negative restraint moments occurred at the interior transverse joints over the piers due to the interaction of creep and shrinkage. Results of analytical and experimental research (Oesterle, Glikin and Larson, 1989, Oesterle, Mehrabi, Tabatabai, Scanlon and Ligozio, 2004, Oesterle, Mehrabi, Tabatabai, Scanlon and Ligozio, 2004) indicated that the live load continuity of the bridge may be reduced significantly with long-term and time dependent loading effects and with thermal effects.

In the experimental part of the jointless bridge research (Oesterle, Mehrabi, Tabatabai, Scanlon and Ligozio, 2004, Oesterle, Mehrabi, Tabatabai, Scanlon and Ligozio, 2004), testing of materials, bridge components, and a full scale girder indicated that:

1. Expected shrinkage of the deck concrete did not occur in the concrete in the outdoor environment of Skokie, Illinois. Thus, the effects of deck shrinkage to mitigate the effects of girder creep did not occur.
2. Heat of hydration effects in the cast-in-place deck concrete can have a mitigating effect on the development of positive restraint moment.

3. Daily temperature effects with heating and cooling of the deck with respect to the girder have a significant effect on restraint moments. Solar heating of the deck causes positive restraint moments of the same order of magnitude as the moments due to girder creep and are additive to the moments caused by creep.
4. Tests on a full scale girder that was monitored and loaded periodically with simulated live load on sunny days and on cloudy days during different seasons over an 18 month time frame, demonstrated that positive restraint moment and the resulting cracking at the transverse connection significantly reduced continuity for live-load.
 - a. Using change in beam reactions under application of live load to assess continuity, the lowest measured percentage of full live load continuity was 48% measured on a cloudy day in summer.
5. However, continuity induces restraint moments and effective continuity requires assessment considering all loads. Effective continuity in the test girder was assessed using the distribution of total reactions supporting the test girder that included effects of dead load, live-load, and restraint moments. Effective continuity is defined as 100% if the distribution of total reactions corresponds to the combination of simply supported dead load reactions plus fully continuous live load reactions. Effective continuity is 0% if the distribution of total reactions corresponds to the combination of simply supported dead load reactions and simply supported live load reactions. The measured effective continuity in two of the live load tests in the jointless bridge study was in fact negative (i.e., less than

0%). That is, the total midspan positive moment in the tested “continuous” girder was slightly higher than the anticipated positive moment if the girder was a simply supported girder for both dead and live load.

6. The positive moment due to combined creep and temperature effects in the test girder resulted in stresses in the positive moment reinforcement in the connection over the pier that reached or exceeded yield stress.

Results of this research indicated that use of a positive moment connection in the diaphragms is not beneficial in determining the net resultant midspan service level stresses under dead, live, and restraint loads. Without a positive moment connection at the supports, effects that would tend to produce a positive restraint moment (creep in the prestressed girders and solar heating of the deck) will likely cause a crack to form at the bottom of the diaphragm concrete between the ends of the girders. With application of live load that would tend to produce a negative moment at the support, the crack at the bottom of the diaphragm concrete has to close before full negative moment develops. The net effect is that some live load continuity is lost. Depending on the parameters, the loss can range from 0 to 100% of live load continuity. If effects that would tend to produce a positive restraint moment are large enough, the crack at the bottom of the diaphragm can remain open under live load and the girder acts as if it is simply supported.

If a positive moment connection is provided, a crack will still likely form at the bottom of the diaphragm concrete from effects that tend to cause positive restraint moment. The positive moment connection will decrease the crack width but a positive restraint moment will develop. The positive restraint moment superimposed on live load

negative moment will negate, at least in-part, the beneficial effects of the negative moment continuity connection over the piers (for service load stresses). Studies (Oesterle, Glikin and Larson, 1989, Oesterle, Mehrabi, Tabatabai, Scanlon and Ligozio, 2004, Oesterle, Mehrabi, Tabatabai, Scanlon and Ligozio, 2004, Mirmiran, Kulkarni, Castrodale, Miller and Hastak, 2001) have shown that the effect of the crack at the bottom of the diaphragm that would form without the positive moment connection is essentially equivalent to superposition of a positive restraint moment that would form if a positive moment connection is provided (assuming the amount of positive moment reinforced provided is not excessive).

If effects that tend to cause negative restraint moments in the connection over the supports predominate, positive moment reinforcement is not needed. Therefore, these studies indicated that there is no net benefit, in terms of service level stresses in the prestressed girder, by providing positive moment reinforcement in the transverse connections. It is understood, however, that there may be benefit, in terms of structural integrity, for providing the positive moment reinforcement.

Recently, NCHRP Project 12-53 was completed and results are included in NCHRP Report 519 (Miller, R., Mirmiran and Hastak, 2004). This project was carried out to further examine the behavior of simple-span precast/prestressed girders made continuous by connections at the transverse joints over the piers. The focus was on the effectiveness of the positive moment connection and on design criteria for this connection. Results of analytical studies (Mirmiran, Kulkarni, Castrodale, Miller and Hastak, 2001) were similar to those reported in the previous NCHRP study (Oesterle, Glikin and Larson, 1989). That is, if positive restraint moments develop, these restraint moments must be added to

the moments caused by dead and live load, and that the net positive moment at the midspan is essentially independent of the amount of positive moment reinforcement provided in the transverse connection (assuming the amount of positive moment reinforced provided is not excessive). In addition, analytical studies indicated that cracking in the transverse joint decreases live-load continuity.

NCHRP Project 12-53 also included experimental studies. Live load testing indicated that, contrary to analyses results, the continuity with application of live load was near 100% unless the positive moment crack at the connection became very large. The full scale testing result in the NCHRP 12-53 study, with essentially no live-load continuity lost due to positive moment cracking, differed from the analytical results in the NCHRP studies (Oesterle, Glikin and Larson, 1989, Mirmiran, Kulkarni, Castrodale, Miller and Hastak, 2001) and the result of full-scale testing in the jointless bridge study (Oesterle, Mehrabi, Tabatabai, Scanlon and Ligozio, 2004, Oesterle, Mehrabi, Tabatabai, Scanlon and Ligozio, 2004). However, live load continuity in the NCHRP 12-53 study was assessed using change in reactions with application of live load. It is not clear how restraint moment present in the test specimen connection was considered.

Also, a reason provided in the NCHRP Report 519 for the difference between the analytical studies and the experimental studies was that the observed positive moment cracks did not extend into the top flange until the crack was very large whereas, in the analytical model, the crack extends into the top flange as soon as it forms. In the NCHRP 12-53 experimental beams however, effects of concrete creep were simulated by applying post-tensioning near the bottom flanges after the diaphragm concrete was cast. Post-tensioning rods were dead-headed at the ends of the girders on each side of the

diaphragm and used to apply a relatively concentrated load near the bottom flanges at the end of the girders. The additional compressive strain due to the post-tensioning was intended to simulate the creep strain in the girders due to the pre-tensioned prestress and produce simulated positive moment cracks in the bottom of the diaphragm concrete. Applying the post-tensioning forces concentrated near the bottom at the ends of the girders however may have distorted the plane of the ends of the girders so that the change in crack width over girder depth did not simulate an expected positive moment crack in an actual bridge. Experimental tests in the jointless bridge study (Oesterle, Mehrabi, Tabatabai, Scanlon and Ligozio, 2004, Oesterle, Mehrabi, Tabatabai, Scanlon and Ligozio, 2004) were carried out with full scale girders with positive moment cracks in the diaphragm that were primarily the result of actual long term creep in the girders due to the original pre-tensioned prestress combined with temperature gradient caused by actual solar heating.

Several results from the NCHRP 12-53 full-scale tests though were similar to those observed in the jointless bridge study including:

1. The shrinkage strains in the deck concrete were significantly less than expected.
2. The effects of heat of hydration in the deck concrete were significant.
3. Daily thermal effects were significant.

Based on the analyses and testing, recommendations for the positive moment connection in NCHRP Report 519 included:

1. The positive moment connection should be provided and designed for the calculated moment due to dead, live and restraint moment. At least minimum

reinforcement should be provided for a moment equal to $0.6 M_{cr}$ where M_{cr} is the cracking moment of the connection. Also, the design moment should not exceed $1.2 M_{cr}$ because providing more reinforcement is not effective. If the design moment exceeds $1.2 M_{cr}$, design parameters should be changed. The easiest change to reduce the positive moment is to specify a minimum age of the girder at the time of making the continuity connection.

2. If the contract documents specify that the girders are a minimum age of 90 days when continuity is established, the restraint moment does not have to be calculated. This is based on the observation from surveys and analytical work that, if the girders are more than 90 days old when continuity is formed, it is unlikely that time-dependent positive restraint moments from concrete creep and shrinkage will form.
3. The transverse connection can be considered fully effective if, "... the calculated stress at the bottom of the continuity diaphragm for the combination of super imposed permanent loads, settlement, creep, shrinkage, 50% live load and temperature gradient, if applicable, is compressive."

Results presented in NCHRP Report 519 were used to provide extensive and comprehensive revisions and additions to AASHTO LRFD (4th edition)(2007) Article 5.14.1.4 for Bridges Composed of Simple Span Precast Girders Made Continuous. Based on Article 5.14.1.4.1, the connections between girders shall be designed for all effects that cause moments at the connections, including restraint moments from time dependent effects. (Restraint moment due to thermal gradient is not specifically mentioned in

Article 5.14.1.4.1 but should be included). However, Article 5.14.1.4 includes the following two exceptions regarding the need to design for the restraint moments:

1. Per Article 5.14.1.4.1, multispan bridges composed of precast girders with continuity diaphragms at interior supports that are designed as a series of simple spans are not required to satisfy Article 5.14.1.4.
2. Per Article 5.1.14.4.4, if contract documents require a minimum girder age of at least 90 days when continuity is established:
 - a. Positive restraint moments cause by girder creep and shrinkage and deck slab shrinkage may be taken as zero.
 - b. Computation of restraint moments shall not be required.
 - c. A positive moment connection shall be provided as specified in Article 5.1.14.4.9.

C6.2.4.2. Design Recommendations

C6.2.4.2.1. Restraint Moments in Prestressed Concrete Girders

In general, it is recommended that Article 5.14.1.4 should be followed in design of jointless bridges constructed with precast prestressed girders made continuous for live load. However, the following further considerations should be taken into account:

1. Thermal Effects - Calculated thermal gradient stress caused by the combined internal restraint and secondary continuity moments can be very high, particularly when combined with other secondary effects (Oesterle, Mehrabi, Tabatabai, Scanlon and Ligozio, 2004, Oesterle, Mehrabi, Tabatabai, Scanlon and Ligozio,

2004). NCHRP Report 519 stated that daily thermal effects were significant and mentions that they should be considered in design. However, results of analyses and example calculations included in the report to demonstrate that restraint moment is near zero if the girder age is at least 90 days when continuity is established did not include the effects of thermal gradient. Also, the commentary to Article 5.14.1.4.2 mentions temperature variation as a cause of restraint moments but Article 5.14.1.4 does not specifically address design considerations for thermal effects. It is commonly considered that thermal effects are self-limiting for strength limit states and generally can be disregarded. However, prestressed girders also have to be designed for service level stresses and thermal stresses in continuous prestressed concrete bridges need to be considered.

2. Differential Shrinkage Effects – Results of the FHWA jointless bridge project determined that expected shrinkage based on theoretical shrinkage models and on laboratory shrinkage tests did not occur in the outside environment. NCHRP Report 519 (Miller, R., Mirmiran and Hastak, 2004) included a similar observation. However, analyses and example calculations included in the NCHRP Report 519 to demonstrate that restraint moment is near zero if the girder age is at least 90 days when continuity is established did include the effects of differential shrinkage determined from a theoretical shrinkage model. It can be seen in the results of the analyses presented in the report that early negative moment due to differential shrinkage between the deck and the girder essentially offset the longer term positive moment that developed due to creep in the prestressed girder.

3. Combined Creep, Shrinkage, and Thermal Effects – The effects of creep in the prestressed girders and solar heating of the deck are additive with respect to inducing positive moment at the connection over the supports. When creep and solar heating are combined with an absence of differential shrinkage, it is not clear, even in bridges constructed with 90 day old girders, that positive moments will not be significant.
4. Potential Negative Moments – Limiting construction to use of girders with a minimum age of 90 days will increase the potential that factors that induce negative restraint moments over the supports may predominate. Increasing the potential for negative moment increases the risk of cracking in the deck over the support regions. Deck cracking over the support regions may have a more detrimental effect on long term durability of a bridge than positive moment cracking in the diaphragm.
5. Uncertainties in Determining Restraint Moments - In addition to concrete creep, shrinkage, and solar heating of the deck, a number of other effects can contribute significantly to restraint moments. These include differential settlement of supports; heat of hydration of the deck concrete during construction; variation of the coefficient of thermal expansion between the girder and the deck; and seasonal moisture changes in the concrete, causing shrinkage reversals. In addition, in jointless bridges with integral abutments, additional forces may be imparted on the positive moment connection by the restraint of the abutment to longitudinal temperature movements. All of these factors contribute to restraint forces within a continuous jointless bridge structure. In some instances, these

factors are additive, while in others, they oppose one another. The magnitudes of these effects to be considered in design and the critical combinations to be considered are uncertain. Although there are methods available to estimate restraint moments due to all these effects, the moments that actually occur may be significantly different than the estimated values.

6. Effects of Excessive Positive Moment Reinforced – In spite of all the uncertainties regarding magnitudes and combinations of restraint moments, there have not been many cases of distress related to these secondary stresses. In general, concrete cracking and reinforcement yielding will diminish the stresses caused by the secondary effects. However, an overly strong connection combined with effects of creep and thermal gradient may result in excessive positive restraint moment (ENR, 1994, AL-DOT, 1994, Telang and Mehrabi, 2003). A strong positive moment connection increases the positive moment along the span and in some cases may result in cracking in the beams. Figure C30 shows an example bridge (Telang and Mehrabi, 2003) with significant flexural cracking of this type. The flexural crack occurred at the end of the embedment of the positive moment connection bars near the ends of the prestressed girders with a large quantity of positive moment reinforcement. On the other hand, Figure C31 shows the end region of another girder in the same example bridge where cracking and spalling occurred within the diaphragm. This diaphragm cracking and spalling was associated with positive moment connection bars bent out of place during erection (because of constructability issues) for several girders in the bridge such

that the connection bars became ineffective. However, no flexural cracking occurred within the span of these girders.



Figure C30- Cracks near girder supports



Figure C31- Crack and spall at diaphragm over pier support

Because of the uncertainty associated with calculations of positive continuity moments resulting from the variability of the creep and shrinkage effects, temperature gradient, differential coefficient of expansion effects, locked-in heat of hydration effects, settlement, and cracking, calculations to determine restraint moments are complex and probable unreliable. Therefore, in order to eliminate the need to attempt to calculate

restraint moments and to simplify the design, the following recommendations for positive moment connections were developed based on the work in the NCHRP projects (Oesterle, Glikin and Larson, 1989, Mirmiran, Kulkarni, Castrodale, Miller and Hastak, 2001, Miller, R., Mirmiran and Hastak, 2004), the FHWA jointless bridge project (Oesterle, Mehrabi, Tabatabai, Scanlon and Ligozio, 2004, Oesterle, Mehrabi, Tabatabai, Scanlon and Ligozio, 2004) and on the AASHTO LRFD 4th Edition:

1. Option 1: Do not provide any positive moment connection reinforcement at the piers. This approach prevents the development of significant positive restraint moments in the pier diaphragms (and eliminates constructability issues with the overlapping reinforcement). Analyze the girders as simply supported for dead plus live loads at service levels. This is allowed by AASHTO Article 5.14.1.4.1; eliminates the requirement to calculate restraint moments (without the need to age girders prior to construction); and, as stated in the AASHTO commentary, has been used successfully by several state DOT's.
2. Option 2: If positive moment connections are used to improve structural integrity and for some crack control, as recommended in the commentary of AASHTO Article 5.14.1.4.1, it is suggested that the positive moment capacity, ϕM_n , be limited to the minimum moment of $0.6 M_{cr}$ recommended in AASHTO. Note that M_{cr} should be determined using the properties of the diaphragm concrete. If additional reinforcement is used to increase crack control, do not exceed the upper limit recommended by AASHTO of $\phi M_n = 1.2 M_{cr}$. To eliminate the need for calculation of restraint moments, analyze the girders as simply supported for dead plus live loads at service levels as allowed by AASHTO Article 5.14.1.4.1.

However, consider that positive restraint moments may likely occur. In spite of this, additional stresses in the girders due to positive restraint moment can be minimized by limiting the capacity of the connection ϕM_n so that the connection acts as a fuse to yield prior to development of detrimental stresses. Therefore, the girder service load stresses should be checked along the length of the girder under simple supported dead and live loads plus ϕM_n of the positive moment connections superimposed on the spans such that the allowable tensile stress in the bottom of the beam of $0.19 \sqrt{f'_c}$, ksi, ($6 \sqrt{f'_c}$, psi) is not exceeded. Particular attention should be given to region of termination of the positive moment steel if mild reinforcement is used for the connection.

The girder/diaphragm interface should consider details to allow relative movement between the bottom of the girder and diaphragm concrete for girders partially embedded in the diaphragm concrete. For the exterior surface of fascia girders, consider providing a sealed crack control joint at the beam-to-diaphragm interface.

Negative moment reinforcement should be provided over the supports and diaphragm concrete should be provided between the ends of the girder bottom flanges. Negative restraint moments may develop (for example, when the deck and diaphragms are cast when the concrete girders are older). However, parametric studies carried out in the FHWA jointless bridge project indicate that, with high restraint moments, cracking occurs in the deck and sufficient moment redistribution occurs to prevent the deck reinforcement from becoming overstressed. Therefore, restraint moments do not have to be calculated. Negative moment reinforcement in the deck can be designed for applied

dead and live load moments calculated based on uncracked section properties. The girder can be assumed to be simply supported for dead load and fully continuous for live and superimposed dead loads (because of the parapets, barrier walls, wear surface, etc.). Since the deck in the negative moment region is considered reinforced concrete, the negative moment connection is only designed for strength limit states.

C6.2.4.2.2. Restraint Moments in Composite Steel Bridge Beams

Temperature gradients and differential coefficients of thermal expansion in continuous composite steel beams produce both positive and negative restraint moments, while the shrinkage of deck concrete and the heat of hydration locked-in strains produce negative restraint moments. Deck slab cracking partially relieves negative restraint moments.

The parametric studies in the FHWA jointless bridge project indicate that stresses in both the concrete deck slab and steel beams are not excessive under the combination of dead and live load forces combined with positive restraint moments. Therefore, explicit calculations considering positive restraint moments are not necessary.

The analyses for effects of negative restraint moments in composite steel beams indicated that, in general, if negative moments are high, deck cracking results in redistribution and calculated stresses are not excessive. However, analyses were carried out to include the effects of a negative temperature gradient (that produces negative restraint moments) combined with dead and live load and restraint of longitudinal expansion provided by passive pressure in backfill and the lateral force in the piles of integral abutments. These analyses indicated that, under certain circumstances, calculated compressive stresses in the bottom flange of the steel beams near interior supports may

be excessive, even after allowance for redistribution of the stresses because of deck cracking. Based on the parametric studies, the combination of loads described above may become critical for larger beam spacing. Calculations indicate that, for stringer spacing equal to or greater than 7 ft for Grade A36 beams, and 9 ft for Grade A572 beams, an explicit check of the effects of the combined load effects of dead and live loads, negative temperature gradient, and restraint of longitudinal expansion may be required to check for lateral torsional buckling of the bottom flange near interior supports.

C6.2.5. Design of Pile Foundation

Pile design requires following considerations (Barker, Duncan, Rojiani, Ooi and Tan, 1991):

- Based on soil borings develop a soil profile for the site. Details of strength profiles, compressibility characteristics, stress history, and geology of the soil should be included. Further identify favorable and unfavorable zones in the subsoil.
- Estimate the loads for the strength and the serviceability limit states.
- Determine the water profiles for the site and the expected depth of scour during 100-year flood.
- Select candidate pile types and pile lengths and consider the strength and serviceability limit states. Then eliminate the unsatisfactory alternatives.
- Make a general comparison between the satisfactory candidate piles. Then design with the most cost effective ones based on the following steps below.
- Estimate the axial pile capacity considering soil and structural capacity.

- Determine the required number of piles and their spacing.
- Estimate the capacity of the pile group based on pile group interaction. If the group capacity is not sufficient, increase the number of piles or the pile spacing.
- Check the possibility of punching of the pile into any weak stratum that may be present beneath the bearing stratum.
- Determine the tolerable settlement of the pile group and estimate its settlement. If the settlement is greater than the tolerable settlement, increase the length of the piles or number of the pile spacing.
- If the pile group is subject to uplift, check its uplift capacity.
- Check the lateral capacity of the piles under combined axial load and lateral displacements determined from Section C6.2.3.
- Determine the loads on top of pile under design lateral displacements to determine design forces for interaction with the pile cap.
- Determine whether pile load tests are needed to verify the design.

Table C13- Summary of strength and serviceability limit states that must be considered in the design of pile foundations (Barker, et al. 1991)

Design Consideration	Strength Limit State	Serviceability Limit State
Structural capacity of single pile		
Bearing capacity of single pile		
Bearing capacity of pile groups		
Punching into lower weak stratum		
Settlement of pile groups		
Tensile capacity of piles during uplift		
Uplift capacity of single piles		
Structural capacity of piles under lateral loading		
Lateral movement of pile groups when subjected to lateral loads		

C6.2.5.1. Pile Orientation

C6.2.5.1.1. Straight Bridges

Abutment piles of straight bridges should be oriented so that the strong axis of the piles is perpendicular to the longitudinal direction of the bridge. This orientation results in strong-axis bending of the piles due to longitudinal movement of straight non-skew bridges and to the combination of longitudinal and transverse movements in skewed bridges.

C6.2.5.1.2. Curved Bridges

In curved bridges, the optimum orientation of the piles depends mainly on the bridge geometry. Therefore, in contrast to straight bridges, the optimum direction is not the same for all curved bridges. In this section, a method is presented to find the optimum pile orientation in a curved bridge. This method is based on finite element simulation of several curved integral steel I-girder bridges (Doust and Azizinamini, 2011). The concept employed for straight bridges is implemented to curved bridges; which is the piles should be oriented so that the strong axis of their sections be perpendicular to the direction of bridge maximum displacement. There are some limitations for the application of this method. These limitations include bridge symmetry in plan, non-skewed supports, length over width ratio larger than 3 and end span over middle span ratio close to 0.8. The following steps should be taken to find the optimal abutment pile orientation:

- Step 1- The critical load combination for design of the piles should be determined to be either expansion based or contraction based. Figure C32 may help the designer to determine the type of controlling load combination.

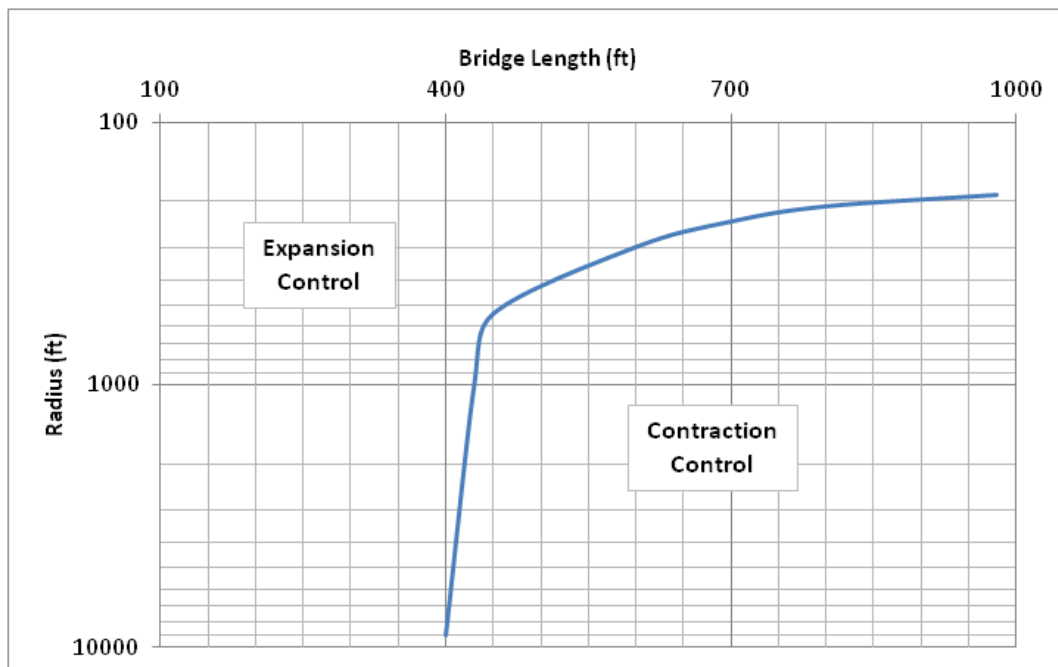


Figure C32- Controlling type of load combination

- Step 2- The direction of bridge maximum end displacement, as defined in Figure C33, should be determined using the curves presented in Figure C34.

$$\alpha = \tan^{-1} \left(\frac{U_y}{U_x} \right) \frac{180}{\pi}$$

Eq. C35

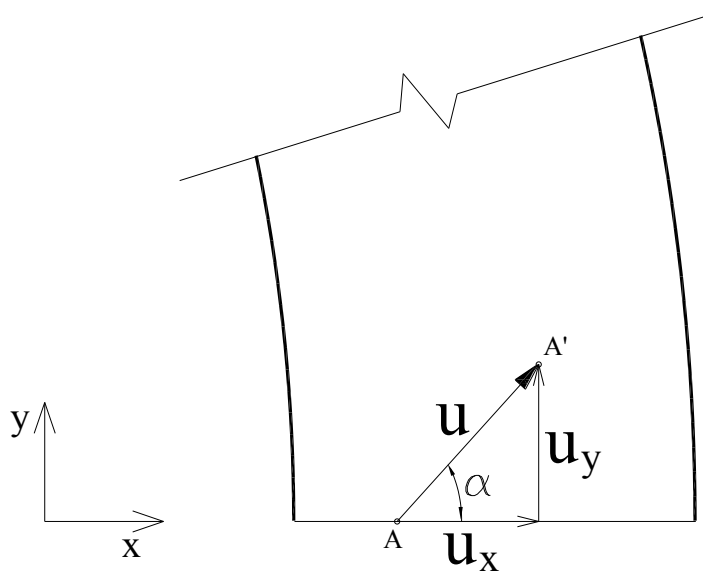


Figure C33- Direction of bridge end displacement

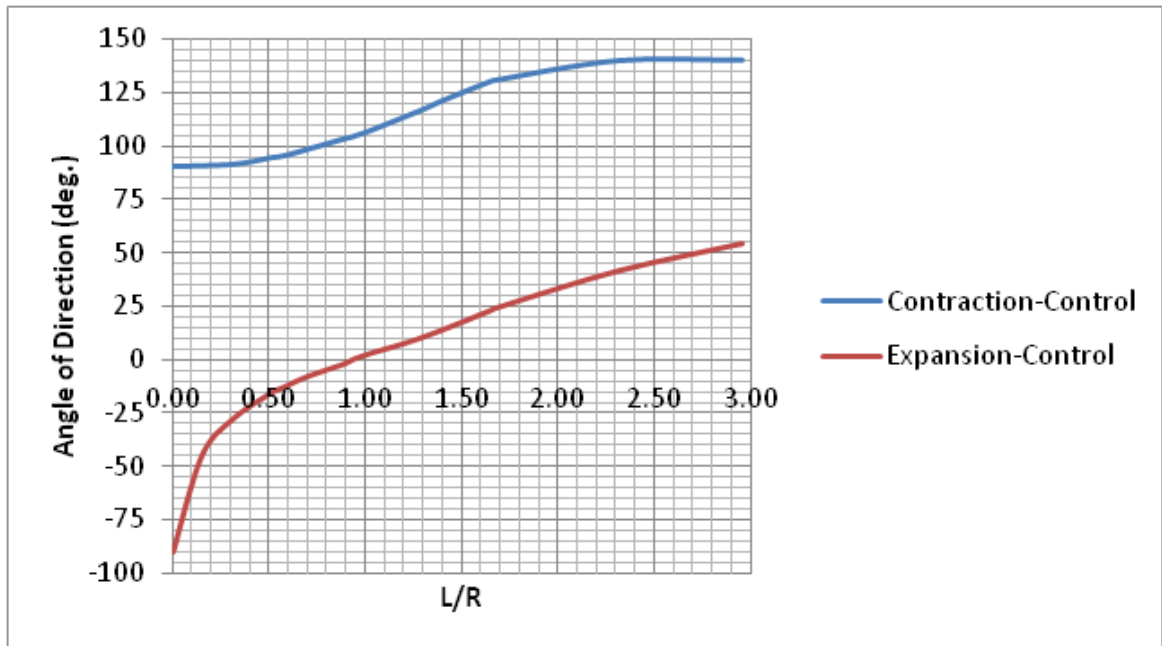


Figure C34- Angle of direction of bridge end displacement

- Step 3- Orient the strong axis of the abutment piles perpendicular to the displacement direction found in Step 2. If the type of critical load combination cannot be distinguished for a specific bridge, the bridge should be analyzed for both expansion-based and contraction-based pile orientations from Step 2 and then the optimum one should be chosen.

C6.2.5.2. Pile Design

Design of pile should consider:

- Strength
- Ductility
- Fatigue
- Stability

- Pile group interaction

Minimum penetration length required to satisfy the requirements for uplift, scour, down-drag, liquefaction, lateral loads, and seismic forces

C6.2.5.2.1. Ductility

Compactness of steel sections is important factor in their ability to accommodate large plastic deformations without local buckling (Dicleli and Albhaisi, 2004). Based on article 6.10.8.2.2 from AASHTO LRFD (AASHTO, 2010) the limiting slenderness ratio for compact flange is:

$$\lambda_{pf} = 0.38 \sqrt{\frac{E}{F_{yc}}} \quad \text{Eq. C36}$$

Since large inelastic deformations are required in piles undergoing lateral deformations, piles should satisfy the compactness requirement. The following table lists compactness of HP cross sections:

Table C14- Compactness of HP sections

Cross Section	b_f (in)	t_f (in)	$b_f / 2t_f$	$F_y = 36 \text{ ksi}$ $\lambda_{pf} = 10.8$	$F_y = 50 \text{ ksi}$ $\lambda_{pf} = 9.2$
HP 8x36	8.16	0.445	9.17	Compact	
HP 10x42	10.1	0.42	12.02		
HP 10x57	10.2	0.565	9.03	Compact	Compact
HP 12x53	12	0.435	13.79		
HP 12x63	12.1	0.515	11.75		
HP 12x74	12.2	0.61	10.00	Compact	
HP 12x84	12.3	0.685	8.98	Compact	Compact
HP 14x73	14.6	0.505	14.46		
HP 14x89	14.7	0.615	11.95		
HP 14x102	14.8	0.705	10.50	Compact	
HP 14x117	14.9	0.805	9.25	Compact	

As shown in this table, only 6 and 2 HP sections meet the compactness requirement for $F_y = 36 \text{ ksi}$ and $F_y = 50 \text{ ksi}$ respectively. The designer should select the pile cross section among the compact ones; otherwise local buckling of the flanges may happen.

C6.2.5.2.2. Fatigue

Based on the method described in Chapter 0 the following figures summarize the maximum allowable pile head displacement in soft and medium clay for 36 ksi steel pipes (Sherafati and Azizinamini, 2011a).

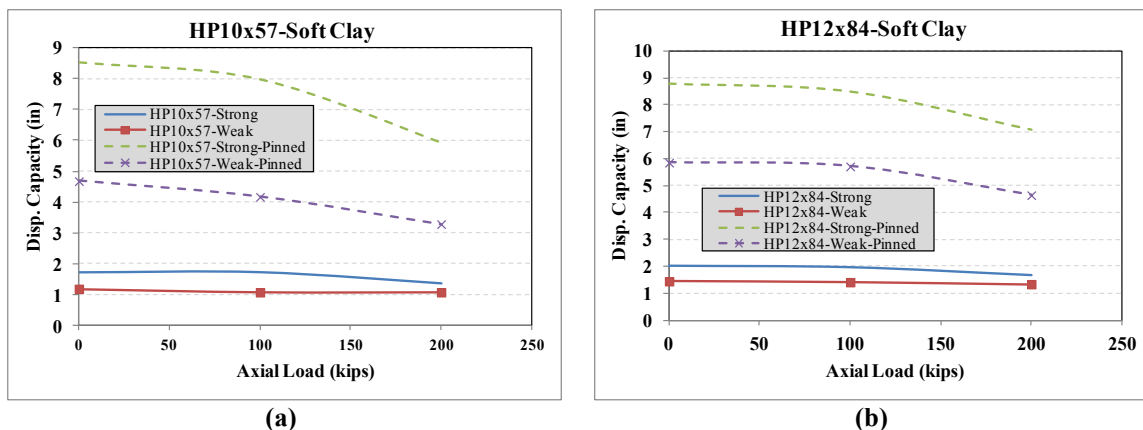


Figure C35- Displacement capacity of compact HP sections in soft clay ($c_u = 2.9$ psi) (a) HP10x57 (b) HP12x84

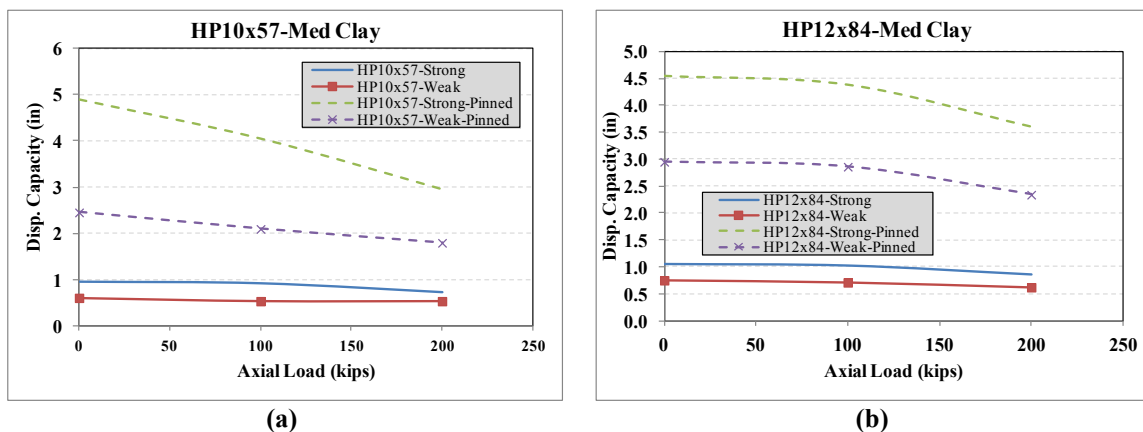


Figure C36- Displacement capacity of compact HP sections in medium clay ($c_u = 5.8$ psi) (a) HP10x57 (b) HP12x84

C6.2.5.2.2.1.1. Global Buckling of Partially Embedded Piles

Piles that extend above the ground level may buckle when subjected to axial loads, and the possibility of buckling failure may control their structural capacity.

C6.2.5.2.2.2. Soil Capacity

The bearing capacity of a pile is sum of its tip and friction resistance minus the weight of the pile.

$$Q_{ult} = Q_s + Q_t - W \quad \text{Eq. C37}$$

Where,

Q_{ult} = ultimate bearing capacity of a pile

Q_s = ultimate load carried by the pile shaft ($A_s q_s$),

Q_t = ultimate load carried by the pile tip ($A_t q_t$)

W = weight of the pile

A_s = surface area of the pile shaft

q_s = ultimate unit skin resistance of the pile

A_t = area of the pile tip

q_t = ultimate unit tip resistance of the pile.

Most of the times (except for large concrete piles in bent piers), the weight of the pile is small compared to the other terms and is usually disregarded.

C6.2.5.2.3. Pile Group Interaction

Provisions of AASHTO 10.7.2.4 shall be used when p-y method of analysis is utilized to evaluate pile group horizontal movement. The values of p should be multiplied by p-multiplier values, P_m from Table C15 to account for group effect.

Table C15- Pile P-Multipliers, P_m for multiple row shading (table 10.7.2.4-1 from AASHTO)

Pile CTC spacing (in the direction of loading)	P-Multipliers, P_m		
	Row 1	Row 2	Row 3 and higher
$3B$	0.7	0.5	0.35
$5B$	1.0	0.85	0.7

Figure C37 defines the loading direction and spacing. In jointless bridge the common practice is to use one row of piles. A group reduction factor of less than 1.0 should only be used if the pile spacing is $5B$ or less.

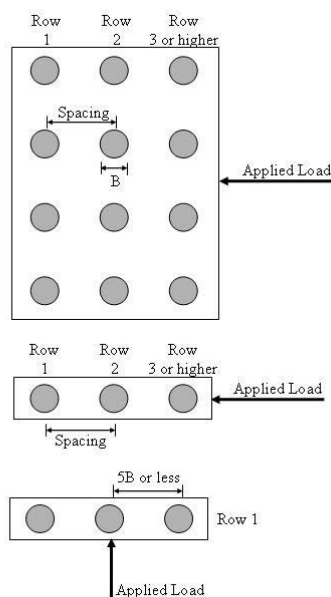


Figure C37- Definition of loading direction and spacing for group effects (figure 10.7.2.4-1 from AASHTO)

C6.2.5.2.3.1. Pile Spacing

The minimum spacing of piles shall be 3 times the pile diameter. Closer spacing in dense sand and saturated plastic soils may cause heave, damage, or misalignment of previously driven piles.

C6.2.5.2.3.2. Minimum Penetration Length

AASHTO LRFD Article 10.7.1.5 specifies the provisions for the minimum penetration length necessary to satisfy the requirements for uplift, scour, settlement, down-drag, liquefaction, lateral loads, and seismic response. This guidance is also appropriate for the design of jointless bridges and the designer should follow the provisions therein.

C6.2.5.2.3.3. Uplift

Uplift of foundation may be caused by swelling soils, frost heave, buoyancy, lateral loads, and upward lift. Piles subjected to uplift should be designed to withstand tensile stresses and pullout from the soil.

Uplift is common for a foundation design and it is well covered in AASHTO LRFD (5th edition), which provides guidance to design against uplift for both single piles and pile groups. For Strength Limit Design, single pile, single drilled shaft, and single micropile uplift are covered by Sections 10.7.3.10, 10.8.3.7.2, and 10.9.3.7, respectively. Similarly, uplift resistance by pile groups, drilled shaft groups, and micropile groups are covered by Sections 10.7.3.11, 10.8.3.7.4, and 10.9.3.8, respectively.

C6.2.5.2.3.4. Scour

Scour around the foundation is an important issue that should be considered in the design. In geotechnical analysis, it should be assumed that the soil above the scour line does not exist to provide bearing or lateral support. Three possible scour effects should be considered in design (Barker, et al. 1991):

- Aggradation and degradation which are long-term effects. Aggradation is defined as the deposit of stream bed material eroded from other portions of a stream. Degradation is the removal of stream bed material and thus lowering the bed elevation.
- General scour and contraction scour are distinguished by removal of bed material across the entire width of the stream as a result of increasing flow velocities.
- Local scour happens when bed material is removed from a small portion of the width of the stream. Bridge piers and abutments induce acceleration of the flow because of obstruction of the flow and cause vortices that wash away the bed material.

Scour is usually evaluated for a flood with a return period of 100 years (or more depending on the importance of the structure). As recommended by FHWA, the top of the pile cap should be located below the depth of contraction scour to reduce obstruction to flow and to minimize local scour. Also to increase the safety against pile failure due to scour, a few longer piles should be used rather than many short piles.

C6.2.5.2.3.5. Settlement

Settlement is not a deterrent to the use of jointless bridges if sufficiently accounted for in the design of the effected components (see Section C6.2.1.7). Minimum penetration lengths with respect to settlement calculations for the foundation are not an additional concern for jointless bridges.

C6.2.5.3. Analysis Tools

This Section provides general discussion of different analysis approaches and available tools that designers can use to analyze jointless systems.

C6.2.5.3.1. Simplified Analysis (p-y method)

The ability to estimate the response of laterally loaded piles is of great importance in the design of jointless bridges. This problem is similar to beam-on-elastic foundation problem. If the piles are deep enough, modeling soil with Winkler springs is a useful method. Basically, in this method, the soil is considered as series of independent layers in providing resistance (p) to the pile deflection (y). This resistance may be a highly nonlinear function of the deflection. The proper form of a $p-y$ relation is influenced by many factors, including:

- Variation of soil properties with depth,
- The form of pile deflection
- The state of stress and strain throughout the affected soil zone,
- The rate sequence and history of load cycles.

Technically, to perform an analysis for a given design, the complex pile-soil interaction is reduced at each depth to a simple p-y curve.

C6.2.5.3.2. Finite element Analysis

Finite element modeling can be used as a robust method to analyze a jointless bridge. There can be several different levels of finite element analysis for such a structure ranging from a simplified analysis to a refined one.

In a simplified finite element analysis, different elements including composite girders, abutment walls, piers and piles are modeled using frame elements. The modeling can be 2D or 3D; however a 3D analysis is preferred. The soil-structure interaction

should be modeled by means of springs. The springs load-deflection curve can be assumed to be linear for a simplified model. In the case of 2D models, the girder distribution factors should be calculated using AASHTO LRFD equations.

On the other hand, a refined finite element analysis is a 3D modeling of a jointless bridge. In such a model, everywhere in the bridge that the 3rd dimension of an element has a crucial structural role, the modeling should be done using the elements that can include the effect of the 3rd dimension. For example, the web and flanges of steel girders and also the concrete deck or abutment wall should be modeled using shell (or solid) elements. 3D skeletal space frame models which are not able to account for the 3D action of the deck slab or girder web/flanges are not considered refined finite element analyses. The soil-structure interaction can be modeled using nonlinear springs. In abutments, the created gap between the soil and abutment wall under specific loads like bridge contraction should be taken into account.

Based on the importance and complexity, a bridge the finite element model can be between the simplified and refined models explained in the above two paragraphs. For example, it can be composed of some shell elements and can have linear soil springs or it can consist just frame elements while having nonlinear soil springs.

C6.2.6. Design of other Foundation Types

It is recognized that other foundation types may be appropriate depending on the requirements for each individual bridge. Presented below are some additional considerations for other foundations

C6.2.6.1. Drilled Shafts

Drilled shaft should be designed considering the same design requirements as piles. Note, however, that traditional Drilled shaft diameters of 30” and larger may prove to be too stiff for longer bridge lengths. Semi-integral abutments may be designed using drilled shafts with no additional consideration.

C6.2.6.2. Spread Footings

Use of spread footing should with integral abutments is not common practice. However, spread footings may potentially be appropriate for integral or semi-integral abutments when rock is close to the surface, or even when competent soil is near the surface, particularly for single-span bridges as discussed in Section C4.5.1.

C6.2.6.3. Micro-piles

Micro-piles may be a viable option for jointless bridges. Note that micro-piles, similar to regular piling should only be used in a single row for integral abutments. Additionally, the micro-pile design must take into consideration the cyclic nature of the bending load resulting from the integral abutment configuration. Multiple rows should only be used for semi-integral abutments.

C6.2.7. Design of Pile Cap

The pile cap for the foundations of jointless bridges may require special consideration based on the selected jointless system. In particular for integral abutments, the pile cap no longer serves solely as a transfer for gravity loads. The pile cap must transfer longitudinal movements and other forces introduced by making the abutment integral.

Experience with integral abutments has demonstrated that no special exception is required for concrete cover for reinforcing bars. Similarly, spacing of reinforcing should follow existing AASHTO guidelines. Designs typically lead to increased confinement of the pile ends.

C6.2.7.1. Integral Pile Cap Design

Pile termination in integral abutments can take one of two forms. The first option is to fix the pile tip against rotation. Alternately, as recently demonstrated by the University of Nebraska, the pile tip can be fitted with an elastomer-based collar. This collar allows for limited end rotation and displacements to occur which serve to alleviate some of the stresses induced by the bending of the piles.

C6.2.7.1.1. Encased Piles (Fixed condition)

The pile cap for integral abutments must take into account and be able to develop the moment resulting from the restraint of the pile tips. Figure C38 illustrates how the shear restraint develops as a moment over the length to fixity of the pile (assuming no soil support) as the force couple develops. This force, in turn is resisted by the pile cap as shown in Figure C39. Note that the shear (V) and bending resultant (C_m) will be additive. Wasserman and Walker (1996) indicate that the depth of the stress block is:

$$a_p = 0.85 \left(\frac{l_{pe}}{2} \right) \quad \text{Eq. C38}$$

Where, l_{pe} is the pile embedment length. It is of note that it can intuitively be seen that increasing the embedment length will directly decrease the bending resultant stresses on the cap, both by increasing the moment arm and the length of a_p .

Taking M_p as the plastic moment of the pile, the force couple balance is represented by:

$$M_p = C_m D \quad \text{Eq. C39}$$

Or,

$$M_p = a_p b f_{cb2} (l_{pe} - a_p) \quad \text{Eq. C40}$$

Where,

$b =$ the either the pile section depth (weak axis bending) or flange width (strong axis bending), respective to pile orientation; or pipe diameter.

$f_{cb2} =$ the bending resultant stress

It follows then that the maximum stress on the concrete cap is the combined resultant of the bending and shear stresses (f_{cb1})

$$f_{cb1} = f_{cb2} + V/a_p b \quad \text{Eq. C41}$$

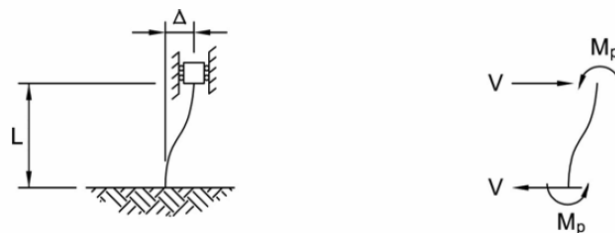


Figure C38- Moment transfer from pile to cap

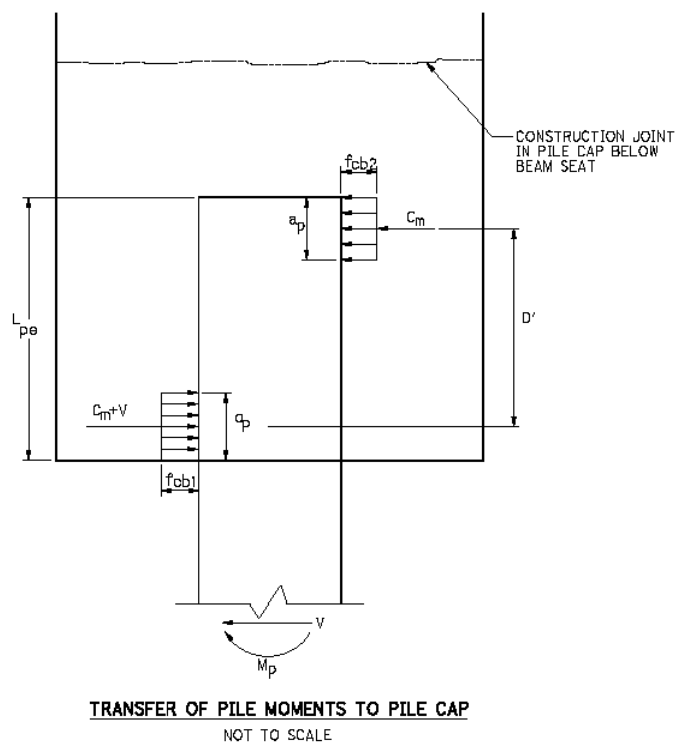


Figure C39- Moment transfer from pile to cap

C6.2.7.1.2. Pin Head Piles (Flexible condition)

By providing rotational capacity at the pile head, the stiffness of the piling system is reduced efficiently, and also the moments developed in the pile as a result of lateral movement are decreased, since the pile will deform in a single curvature shape rather than double. Since the major criterion limiting the application of jointless bridges is the capacity of the piles in lateral movement, the proposed detail can allow the application of jointless construction to longer bridge lengths (Sherafati and Azizinamini, 2011a).

C6.2.7.1.2.1. Pile Cap Detail

The proposed detail consists of elastomeric casing at the pile head. To alleviate the stress concentration due to rotation steel plates that slide on each other are considered. One of these plates is welded to the end of the pile while the other one is embedded in the concrete by shear studs (Figure C40). Note that both Figure C40 and Figure C41 show cylindrically shaped piles. This method can be adopted for H-piles as well, utilizing a pile cap to accommodate uniaxial response.

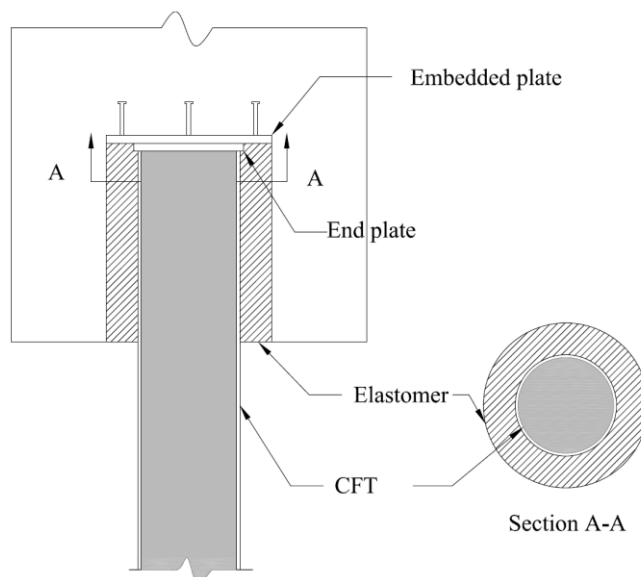


Figure C40- Proposed detail

There are certain definable advantages using this system. Compared to other details, this system will be able to provide much longer service life, and can be effectively used for jointless skewed or curved bridges. Furthermore, the main advantage of this system is that it allows construction of longer span jointless bridges. Since the lateral stiffness of the pile is reduced, smaller forces are developed in the abutment. Similarly, the transmitted forces back to the superstructure are highly reduced. With respect to construction, this system can reduce the time and labor costs during the construction, as it

can be built using prefabricated caps with circular cutout holes. This prefabricated cap can be placed on the pile heads with rubber casing around them (Figure C41).



Figure C41- Prefabricated pile cap

C6.2.7.1.2.2. Design Considerations

The soft material is intended to have very small elastic modulus to provide rotational capacity. Since the soft material for the detail experiences large strains, it should be able to carry these strains while having minute damage in cyclic loading.

Elastomeric material, regularly used as bearing for girder bridges is recommended for the detail (Sherafati and Azizinamini, 2011b). Enough thickness needs to be provided to ensure the efficiency of the detail. Based on FEM analyses, 4" thickness is recommended.

C6.2.7.2. Semi Integral Pile Cap Design

Since a semi-integral abutment is used to support traditional loads, vertical gravity loads from the superstructure and active pressure from the soil, termination of the piles does not require special consideration. That is, traditional methods set forth by AASHTO or other local agencies will continue to sufficiently perform following existing design guidelines. The only exception that may be necessary is to check that the standard pile

design can sufficiently carry the additional dead load introduced by supporting the backwall (end diaphragm), as this can be significantly larger than a traditional end diaphragm.

C6.2.7.3. *Seamless Details*

The design of cap for a seamless bridge should follow the recommendations of Section C6.2.7.1 for integral pile caps. The additional considerations for seamless bridges are primarily associated with the approach slab, or transition, portion of the bridge and are presented in Section ---.

C6.2.8. *End-Diaphragm (Backwall) Design*

In addition to being integral with the superstructure, the end diaphragm acts as a backwall for integral, and semi-integral jointless bridge abutments. As such, the end diaphragm needs to be designed to resist forces resulting from soil loads and will henceforth be referred to as the backwall. The soil loads includes the passive pressure force (in addition to live load surcharges) that is created by thermal expansion. The calculation of this passive pressure is shown in Section C6.2.1.3.

Similar to traditional back wall design, the soil pressure is resisted by the backwall. For jointless bridges, however, the superstructure elements act as supports creating “spans” of length S between the beams or girders and moments and shears along the length of the backwall are introduced as shown in Figure C42. The moment should be calculated so as to create the maximum bending effects on both the front face (positive moment) and back face (negative moment) on the backwall. The bending resulting from the pressure shown in Figure C42 is resisted by transverse reinforcing, while the shear at

the face of the superstructure elements is resisted by dowels through the elements. The dowels also provide additional continuity between the backwall and superstructure.

Experience with jointless bridge backwalls has demonstrated that no special exception is required made for concrete cover for reinforcing bars. Similarly, spacing of reinforcing should follow existing AASHTO guidelines.

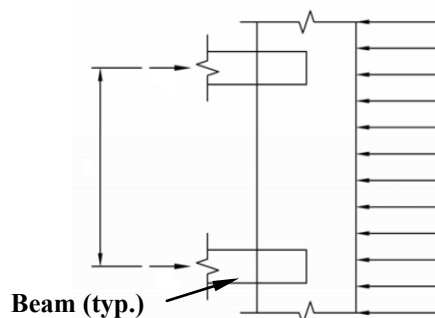
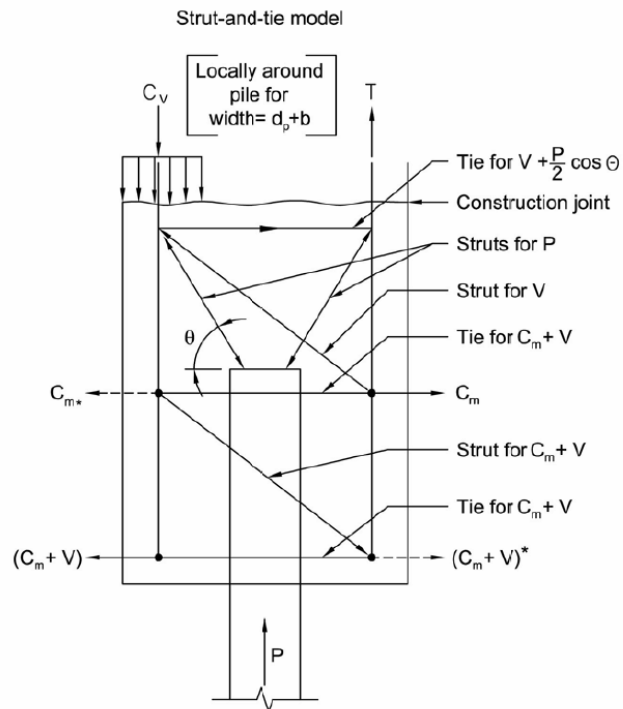


Figure C42- Lateral pressure restraint by superstructure (Oesterle, Tabatabai, Lawson, Refai, Volz and Scanlon, 2005)

There are additional considerations that are slightly differing for each jointless bridge type and those are discussed here.

C6.2.8.1. Integral

The backwall for an integral bridge abutment must be designed to adequately transfer forces across the construction joint and into the foundation cap for each direction in which the pile bends. This transfer of forces is illustrated through an example strut-and-tie model in Figure C43. In this figure, section A-A shows the local section recommended for a local region ($d_p + b$) over which the forces can be transferred and a suggested reinforcing pattern. Length d_p is the distance from the forward face of the pile cap to the face of the pile.



Strut-and-tie model for pile forces.

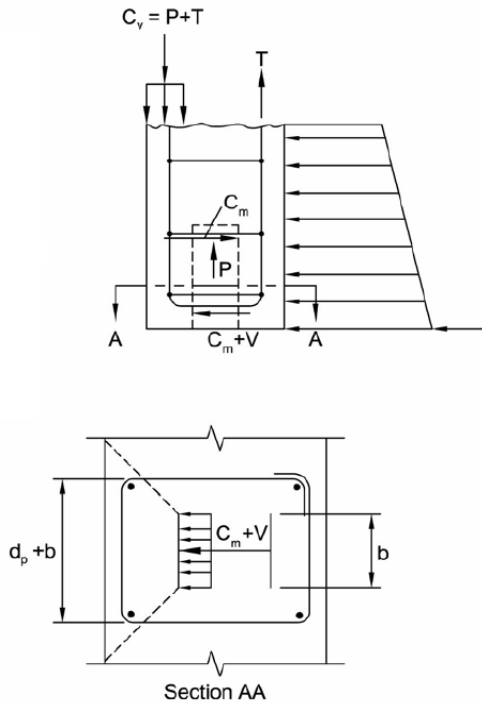


Figure C43- Lateral pressure restraint by superstructure (Oesterle, Tabatabai, Lawson, Refai, Volz and Scanlon, 2005)

C6.2.8.2. Semi-Integral

Semi integral backwalls do not require additional considerations above what is outlined in Section C6.2.8.1. The one item of note, however, is that if removable forms are not used to form the backwall over the foundation cap, the joint fill material used needs to be sufficiently stiff to support the concrete weight, yet flexible enough to not interfere with the movement permitted by the bearings. This has been successfully accomplished with expanded polystyrene filler.

C6.2.8.3. Seamless

As with the design of the foundation cap, the backwall design for a seamless bridge should follow the recommendations of Section C6.2.8.1 for integral abutments.

C6.2.9. Approach Slab Design

Jointless bridges require approach slabs for two main reasons. First, the slab needs to be positively attached to the deck and/or substructure to eliminate the joint over the abutment. Second, the slab must span the area behind the abutment where the potential for backfill settlement exists. Backfill settlement will occur and introduce voids regardless of the degree of compaction due to the thermal movements of the bridge superstructure (Schaefer and Koch, 1992)

C6.2.9.1. Integral and Semi-integral

For both Integral and semi integral abutments, the length of the approach slab is determined by the extent of the backfill. Gangarao and Thippeswamy (1996) determined that the rate of backfill settlement decreased greatly once beyond 20ft from the back face of the backwall. As it happens, this is a typical standard approach slab dimension for several State standards. The study by Schaefer and Koch (1992) demonstrated that

backfill movements are recorded within a 1.5 horizontal to 1.0 vertical line from the bottom of the abutment for integral abutments. A general recommendation for the design length of the approach slab is therefore set at a line of 2.0 horizontal to 1.0 vertical from the bottom of the abutment but with a minimum of 20ft, for both integral and semi-integral abutments as shown in Figure C44.

Additionally, experience from several States has found that the approach slab should be positively attached to the backwall by at least No. 8 reinforcing bars anchored with a hook as shown in Figure C44. The condition shown in the figure allows for a separate pour of the approach slab and design as a simple span. It is not recommended to create a moment connection between the approach slab and the deck slab. The connection should be detailed to act as a pin with tension steel transferred across the approach span in to the backwall for integral and semi-integral abutments. If a moment connection is desired, it is recommended to use a seamless deck transition for the design. (See Section C6.2.9.2)

A final consideration for the approach slab is the development of compression forces. Sufficient allowance for expansion of the superstructure must be accommodated in the sleeper slab. Otherwise, compression can be introduced into the slab resulting from closing the expansion gap and then activating the passive pressure behind the sleeper slab or contact with the adjacent roadway pavement.

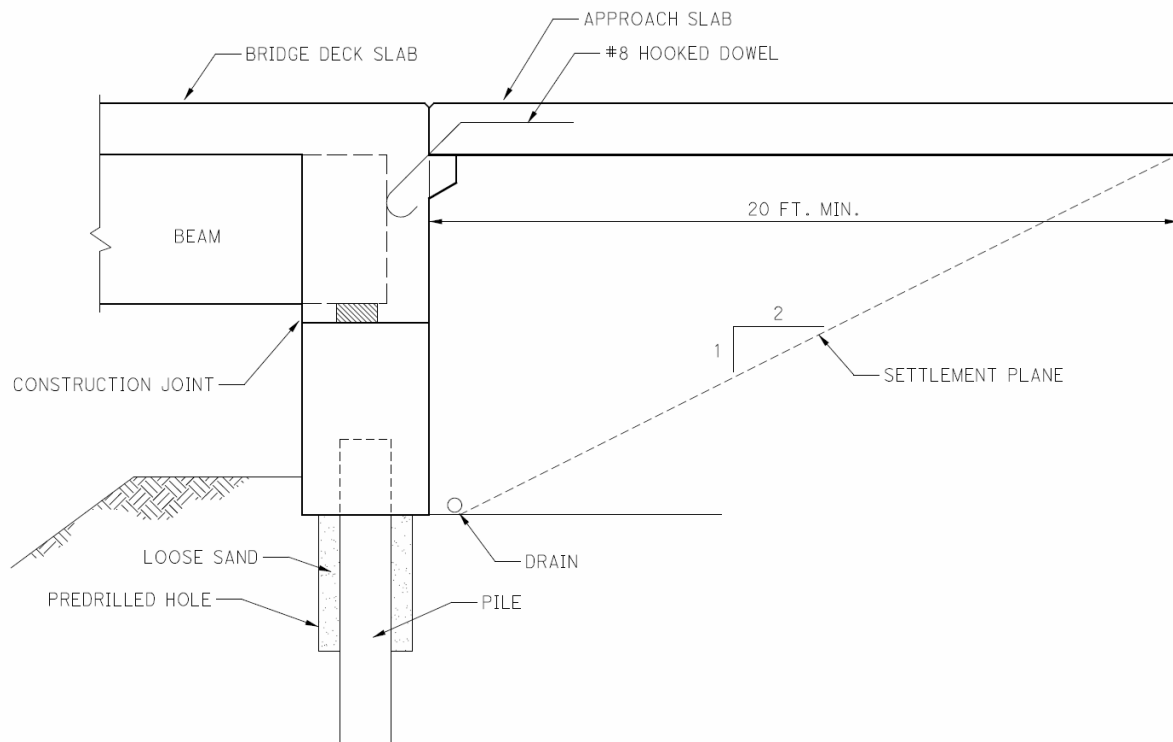


Figure C44- Determination of Approach Slab Length

C6.2.9.2. Seamless Deck Transition Zone

A transition that has been proposed introduces simplicity and ease of construction (Jung, Zollinger and Tayabji, 2007). The concept slowly transitions from a heavily reinforced region to a plain jointed condition over an extended transition length. Within a heavily reinforced region, crack spacing is quite small. As the level of reinforcement is reduced, the crack spacing increases. These cracks may be allowed to occur naturally or may be forced by saw cutting.

The system is shown in Figure C45 and Figure C46. Immediately adjacent to the bridge is a thickened and reinforced approach zone. The approach zone behaves similar to a reinforced concrete slab bridge and is intended to carry flexural forces that may arise as a result of settlement.

The design of this system is based on the design of an approach slab for an integral or semi-integral bridge. The difference is that beyond the approach zone is the transition zone. Within the transition zone, the level of reinforcement is slowly reduced and the crack spacing increased as the zone progresses further from the bridge. Jointed plain concrete pavement continues beyond a final transverse joint. The transition zone is not designed, per se, but the reinforcing step down is specified at the appropriate locations. This transition is shown in Figure C45 and Figure C46.

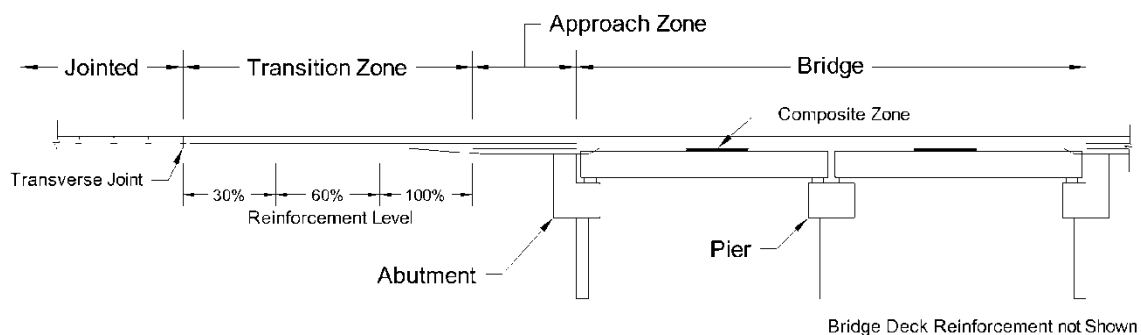


Figure C45- Seamless paving over bridge transitioning to jointed pavement

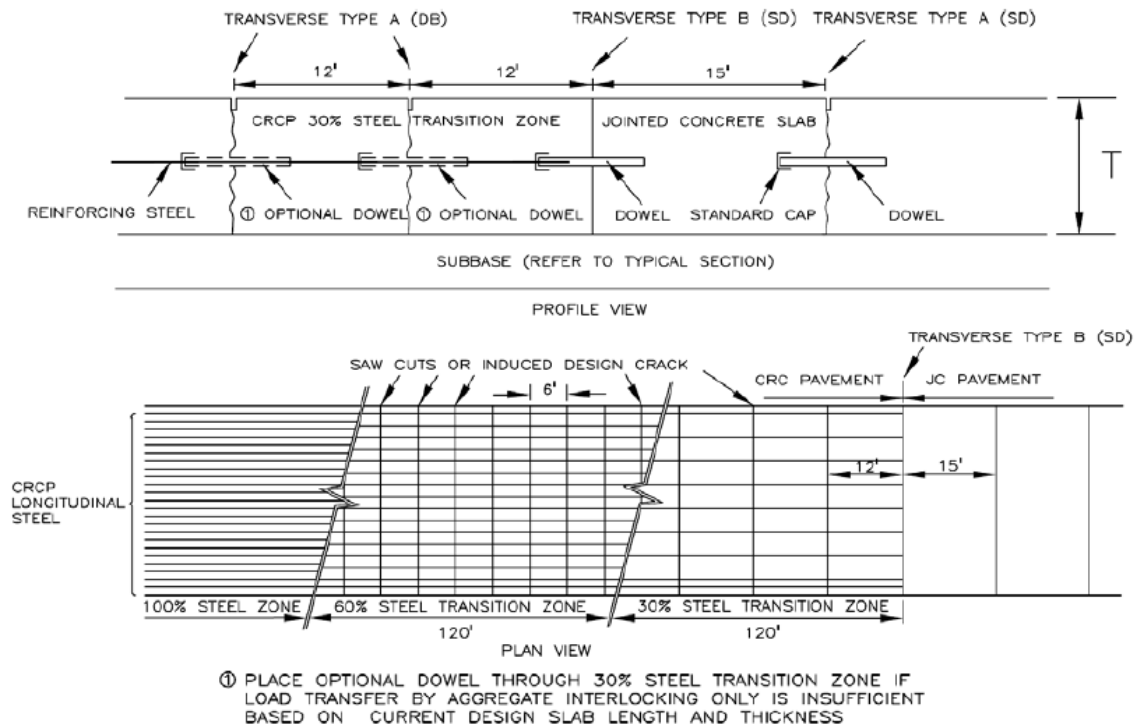


Figure C46- Continuously reinforced to jointed pavement (Jung, Zollinger and Tayabji, 2007)

C6.2.10. Design of Superstructure-Pier Connection

By the definition, the bridge decks in jointless bridges are continuous. This includes over the piers. The connection between the piers and the bridge deck could be integral, pin or expansion types, or connected with a link slab. Figure C47 shows these different configurations conceptually.

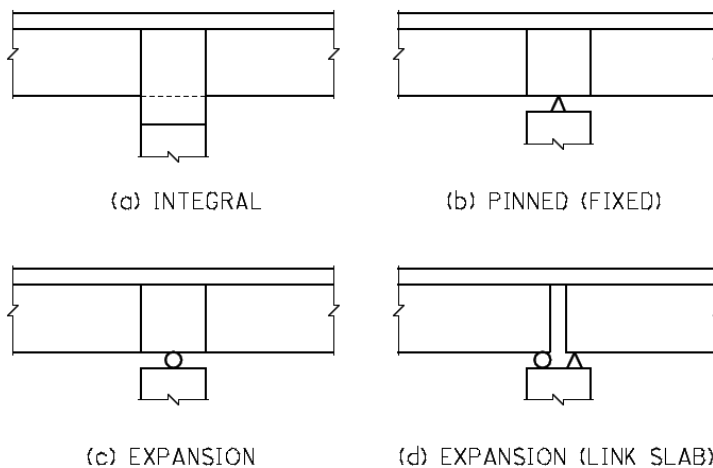


Figure C47- Integral, pinned, and expansion type bearings for jointless bridges

In integral type connections (Figure C47a), the pier and superstructure are monolithic and frame action is developed between the superstructure and substructure. The advantage of this type of connection is the elimination of any bearings. Further, the system provides higher levels of redundancy, especially in highly seismic areas. The longitudinal movement of the bridge superstructure is not affected by making the piers integral with superstructure. However, the longitudinal expansion of the deck must be considered in the design of the pier columns and foundations.

In pin type connection between pier and superstructure (Figure C47b), bearings restricting longitudinal movement are used. Rotation at the bearing is allowed. Although designated a pin type connection, typical bridge terminology where a bearing is not permitted to move longitudinally is designated a fixed joint, commonly denoted as “F” (Fixed) in traditional design plans. For this connection, the longitudinal movements between superstructure and pier are not permitted. Similar to integral type connections, the longitudinal expansion of the deck must be considered in the design of the pier.

In expansion type connection between pier and superstructure (Figure C47c), bearings are necessary and are required to accommodate both rotation and longitudinal movements. This detail uses traditional expansion or type bearings as determined by the design requirements for the bearings.

In the three connection types (a), (b), and (c) shown in Figure C47, the superstructure is made continuous over the pier. This can be accomplished in one of two ways. One option is to shift the location of the superstructure splice location so that the splices are made at or near the dead load inflection points for the continuous bridge. The other method is to use a continuity splice over the pier. This second option, where the splice is

placed over the piers itself, is commonly referred to as simple-for-dead-load, continuous-for-live-load. This is constructed as shown conceptually in Figure C48 for an integral pier. The beams are placed as simply supported over the pier. The beams are either spliced mechanically or additional reinforcing is provided for the diaphragm. Finally, a closure pour is made.

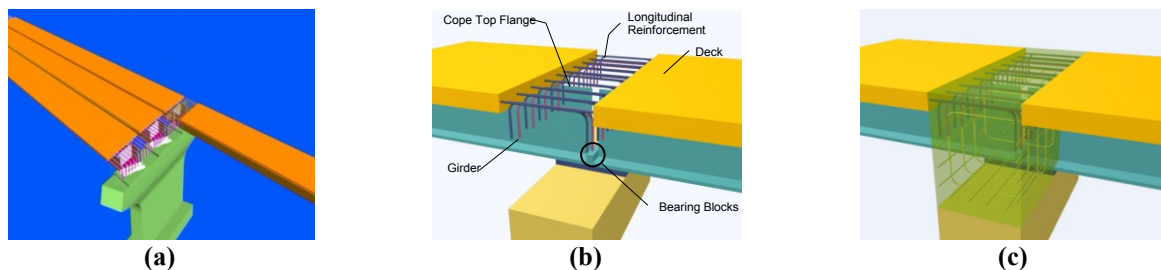


Figure C48- Simple for dead and continuous for live pier detail after the placing of girders (b), and after the closure pour (c)....

The last construction option is the expansion condition using a link slab (Figure C47d). A linkage slab is used where the beams are not positively connected, as is the case with the other types (a), (b), and (c) as shown in Figure C47. For this condition, the superstructure is designed and constructed with traditional bearing considerations.

The design considerations for each of these types of pier cap connections are provided in the following sections.

C6.2.10.1. Integral Pier Cap

When making the superstructure truly integral with the pier cap it must be recognized that both positive and negative moments will be introduced to the cap from live loads. As such, sufficient strength needs to be provided through the deck, integral diaphragm, and pier cap. This type of connection eliminates the need for bearings at the piers and can increase clearance, but introduce more complex forces in the superstructure and the piers (see Figure C49).



Figure C49- Integral cap as completed

The total longitudinal movement expected at the top of the integral piers is accommodated by the longitudinal deflection movement of the foundation and the pier (see Section C6.2.11 for more information). When designing the integral cap, the connection between the beams, continuity diaphragm, pier cap, and pier column must be sufficient to transfer the moments developed resulting from this deflection. Resolution of these forces should be computed by an analytical method or structural model with the capacity to properly capture the behavior of the whole bridge system.

C6.2.10.2. Fixed (pinned) and Expansion Pier Caps

Similar to the Integral cap, the superstructure is made continuous over the pier for both fixed (pinned) and expansion pier caps. The difference being that it is not made integral with the pier caps. The connection between the superstructure and the pier is treated with traditional bearings.

Various details are used over the interior supports of multi-span bridges to eliminate joints. One of the concepts implemented by a number of owner agencies for concrete bridges has been the use of simple spans for dead load made continuous for live load

(Freyermuth, 1969, Oesterle, Glikin and Larson, 1989) The girders are simply-supported for dead load, but continuity is achieved with deck steel as negative moment reinforcement over the piers. Also, the girders are made integral with the interior pier diaphragms and commonly positive moment reinforcement is included as shown in Figure C50.

Badie et al. (2001) discussed the alternate use of an interior steel pier diaphragm with prestressed girders to speed the construction and achieve better overall design economy. The concept of a simple span made continuous also has been applied to eliminate interior joints and improve the construction speed and design economy for short- and medium-span steel girder bridges (Azizinamini, et al. 2008). The concept of a simple span for dead load and continuous for live load for steel bridges has many advantages, among them completely eliminating joints and accelerating construction.

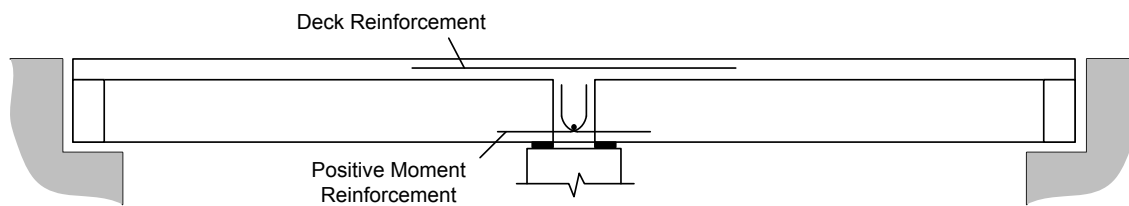


Figure C50- Precast, prestressed girders connected with live load continuity

As discussed in Section C6.2.4, attention must be paid to the effects of providing positive moment restraint at the diaphragms. Some simple-made continuous prestressed concrete girder bridges have experienced severe cracking in the girders near the interior diaphragms. One example that has been studied extensively was on the Francis Case Memorial Bridge spanning the Washington Channel of the Potomac River in the District of Columbia (Telang and Mehrabi, 2003). The prime cause of this distress was the restraint of upward camber of the prestressed girders under the influence of prestressing

and temperature gradient. According to Telang and Mehrabi (2003), “By providing a large amount of positive moment reinforcement at the diaphragms, designers inadvertently make the diaphragm area stronger than the adjacent girder sections, thereby forcing the cracking to occur in far more critical but weaker areas of the girder span.” The article states, “In closing, it is important to note that this seemingly simple transformation of simple-span prestressed girders to continuous spans should be attempted with caution, and significant attention must be paid during analysis and design to include loading conditions that can cause counterintuitive behavior such as secondary positive moments at the piers. Most importantly, positive moment reinforcement should be designed and detailed such that any cracking, if it occurs, should be limited to the relatively less critical diaphragm region of this type of structural system.” Further discussion of this problem and solutions to avoid it have been published by Oesterle et al. (2004) and Arockiasamy and Sivakumar (2005) and are discussed in Section C6.2.4.

C6.2.10.3. Link Slab Expansion Pier Cap

Link slab is a type of detail that is used in conjunction with existing or new bridges having girders that act as simple beams for both dead and live loads. In this type of deck detail, the slab spans continuously over the length between the adjacent girders while the adjacent girders are kept as simple-spans. The length of the deck connecting the two adjacent simple-span girders is called the link slab (Caner and Zia, 1998). Link slabs generally require less deck reinforcement, but have more girder positive moment demands than simple-made-continuous designs. It is believed that Caner and Zia (1998) are the first to develop the link slab idea. Limited analysis and laboratory experiments were carried out and design recommendations are provided (Caner and Zia, 1998). The

use of this promising detail has been very limited due to field observed cracking. In fact, link slabs are not common in the snow belt states. A crack is invariably formed due to deck slab rotation as the bridge is loaded with live loads.

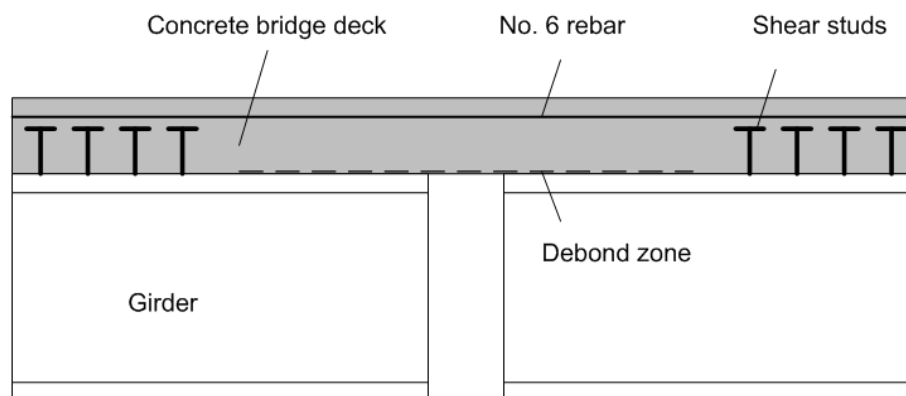


Figure C51- Conceptual detail for link slab

Research on the link slab indicated that it offered negligible rotational end restraint to the bridge girders and that the link slab can be analyzed as a beam subjected to the same end rotations as the adjacent girders. The researchers found that under service-load conditions, the link slab would crack primarily due to bending. In addition, the authors found that prior programs developed by Gatal (1989) and El-Safty (1994) were capable of predicting the forces, stresses and crack widths in the link slab due to thermal and creep and shrinkage effects. Caner (1996) modified the programs developed by Gatal and El-Safty to properly capture the link-slab actions. All of the solutions were based on beam theory. The reinforcing bar stresses compared reasonably well with the data measured from the experimental tests. The predicted crack widths were somewhat larger than the measured crack widths. The researchers concluded that bending and cracking under live load plus impact are the governing factors that must be considered in the design of the link slab.

Caner and Zia (1998) suggested design of the link slab using only one layer of rebar placed near the top of the deck, but suggested that two layers could be used to improve performance in bridges having horizontal restraints.

C6.2.11. Design of Integral Piers

As mentioned in the design of integral pier caps, the total longitudinal movement expected at the top of the integral piers is accommodated by two modes of deformation: longitudinal movement via rotation of the foundation system; flexural deflection of the pier. Pier deflection can be both elastic and inelastic in response.

C6.2.11.1. Foundation Rotation

For spread footings, Zederbaum (1969) provides an equation to estimate the rotational stiffness of the soil or rock responding to an applied moment:

$$K_{\theta} = \frac{3E_s I_f}{b} \quad \text{Eq. C42}$$

Where,

K_{θ} = rotational stiffness of the foundation

b = one-third of the spread footing width

E_s = compression modulus of the soil or rock

I_f = the moment of inertia of the footing base

For pile supported and drilled shaft supported foundations, the rotational stiffness is estimated from the elastic stiffness of the pile or shaft group. Rotation of the foundation can be attributed to the elastic shortening and elongation of the piles or shafts for multiple

rows. Note that the elongation and shortening in the pile groups add additional up uplift and downward forces, respectively, that must be accounted for in the foundation design. For a single row of piles or drilled shafts, the rotational stiffness is based on the cantilever response of the single row. The length of the cantilever is based on the soil-structure interaction at the foundation and can be based on the assumed or calculated point of fixity for the pile or shaft.

C6.2.11.2. Pier Displacement

The differential between the pier displacement at the integral cap and the rotation of the foundation is accommodated by the modulus of the pier column. The resulting design moment can be estimated by the following. First, calculate the expected movement of the superstructure at the pier cap as outlined in Section C6.2.3 . Alternately, this can be sufficiently approximated by determining the point of zero movement on the bridge and multiplying the end displacement by the ratio of the distance from the fixed point to the pier to the distance from fixity to the end support. Second, assume that 30 percent of the expected lateral deflection is accommodated by the foundation rotation. 30 percent is based on a parametric study that demonstrated foundation rotation can vary from 30 to 80 percent with an average close to 45 percent. Third, calculate the anticipated bending moment with the equation:

$$M = \frac{6EI_e \Delta b}{H^2} \quad \text{Eq. C43}$$

Where,

$E =$ concrete modulus

$I_e =$ effective section modulus (ACI 318-08 Eq. 9-8)

$\Delta b =$ lateral deflection at pier cap

Note that I_e in ACI 318-05 Equation 9-8 is based on the design moment and thus the two equations need to be solved simultaneously or iteratively. For fixed (pinned) continuous piers, divide Eq. C43 by a factor of 2 (fixed end moment for a fixed-guided beam is one half that of a fixed-fixed beam).

C6.2.12. Design of Wing Walls

The design of wing walls depends on their orientation relative to the abutment stem, their method of support, and the abutment skew. There are various possible configurations for wingwalls, but the traditional configurations include the U-shaped, straight, or flared. The latter being some degree of angle between the other two.

Oesterle et al. (2005) indicates that the U-shape configuration is preferable for wingwalls in that this configuration inherently reduces the passive pressure introduced by the longitudinal movement of the abutment end diaphragms. Additionally, they note that the U-shape configuration conveniently contains the soil behind the abutment and decreases bulging of the embankment soil.

Use of both straight and flared walls leads to the development of passive pressure on the wing walls as the jointless abutment moves. Oesterle et al. (2005) note that this pressure can be expected to decrease as the distance from the abutment increases, but that the degradation cannot be effectively predicted. Thus, the wingwalls need to be designed for the same passive pressure as that of the abutment end diaphragm across the length.

For integral and seamless bridges, additional considerations for wingwalls include the loading effect they have on the bridge structure. When cantilevered from the

abutment stem, the weight of the wingwalls will create additional torsion and/or bending along the length of the abutment. These forces are resisted by a counteracting negative moment at the end of the external beam or girder.

If wingwalls for integral abutments are placed on supports, such as piles or spread foundation, the support must be able to accommodate the movements of the jointless bridge as well. For this condition, Oesterle et al. (2005) note that the shear and moment developed in the wingwall foundation must be transferred through the wingwall structure to the abutment and superstructure. They also note that U-shaped wingwalls on piles create significant resistance to abutment rotation which creates partial fixity for beam end moments on the exterior beams or girders. These additional moments need to be included in the design of the connections of the exterior beams to the integral abutment.

C7. Details

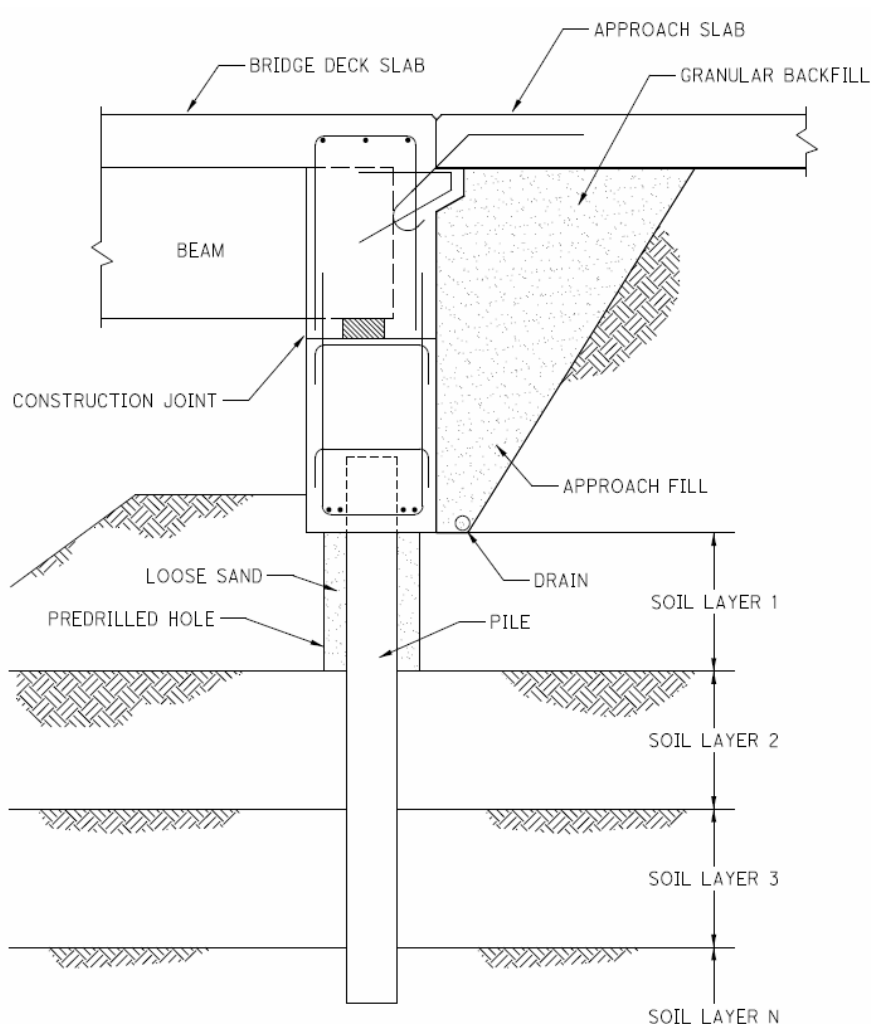
The introduction of different mechanisms for transferring force to the foundations requires that additional details be considered when designing for jointless bridges. The following chapter presents particular details associated with each jointless bridge type. In this section, the term backwall will be used to describe the end diaphragm that resists soil loads.

C7.1. General Abutment Details for Jointless Bridges

Various details that have been used in the past with success by various states are presented along with general concepts. The figures presented represent recent research efforts and the accumulated experience of several States that have used jointless bridge technology.

C7.1.1. Integral Abutments

Figure C52 shows the overall concept for an integral bridge abutment. Shown in the figure is the typical layout with the beam, end diaphragm (backwall) and pile cap all integral. It is not necessary in all cases, but the beam shown in this figure is sitting on a temporary pedestal to achieve proper alignment before being cast integral with the rest of the abutment. Alternately, the cap can be stepped to accommodate elevations prior to pouring the backwall. For proper alignment and to allow for rotations that occur when placing the beam, at a minimum a small elastomeric pad should be placed at the girder bearing even though each beam will eventually be cast composite with the abutment. Note that the need to design the pads and for what capacity they need be designed has not been thoroughly studied. Accepted as a temporary condition, the pads need not be designed to meet the criteria for rotational capacity. The maximum rotation of the pad is realized during placement of the beam. A reasonable assumption is to design the pad to accommodate only non-composite bearing pressure.



INTEGRAL ABUTMENT ON PILE ARRANGEMENT

NOT TO SCALE

Figure C52- General integral abutment concept

Drainage is also important to avoid ice expansion and removal of backfill from washout. A drain pipe needs to be placed at the appropriate location to properly remove any water that might otherwise accumulate behind the backwall.

Within the end diaphragm, additional details on successful detailing strategies that have been used are presented in Figure C53. Note that an H-pile foundation is shown in the figure; however, each of the foundation types noted in the section strategy table in Section C5 can be interchanged. The minimum embedment length of 2 ft. should be

maintained for H-piles, prestressed piles, and CFT piles. Also shown in the figure is an approximate cap height of 5 ft., which is typical of the cold weather regions where the 5 ft. dimension allows for embedment below the frost depth and to be 2 ft. below the finished grade and the bottom of the beam. A depth of 3 ft. to 3.5 ft. is more common where frost depth need not be considered. Another alternate two what is shown in the figure is to use threaded inserts instead of the through holes. Threaded inserts are preferred by some precast concrete companies do to the ease of securing them in the forms.

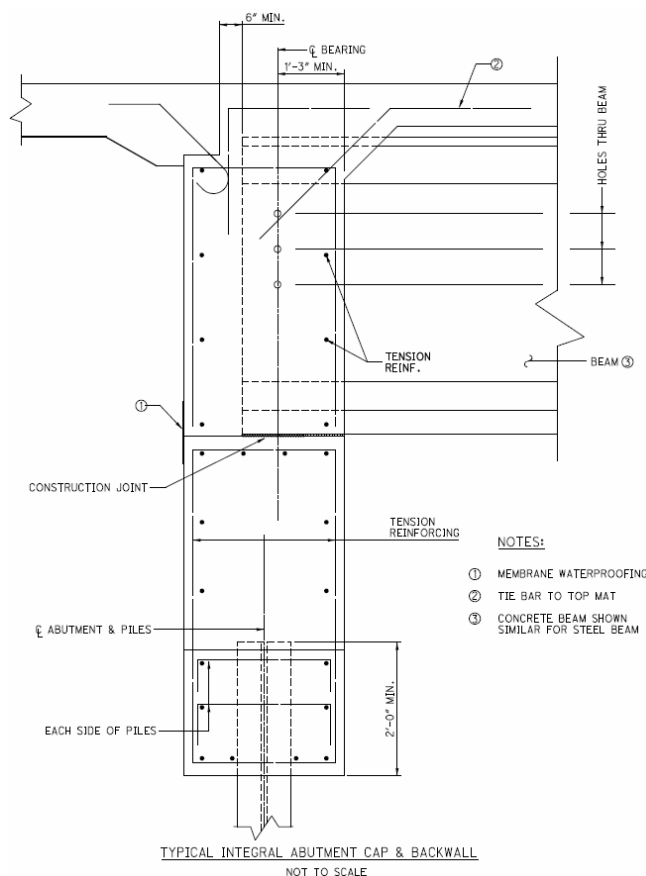
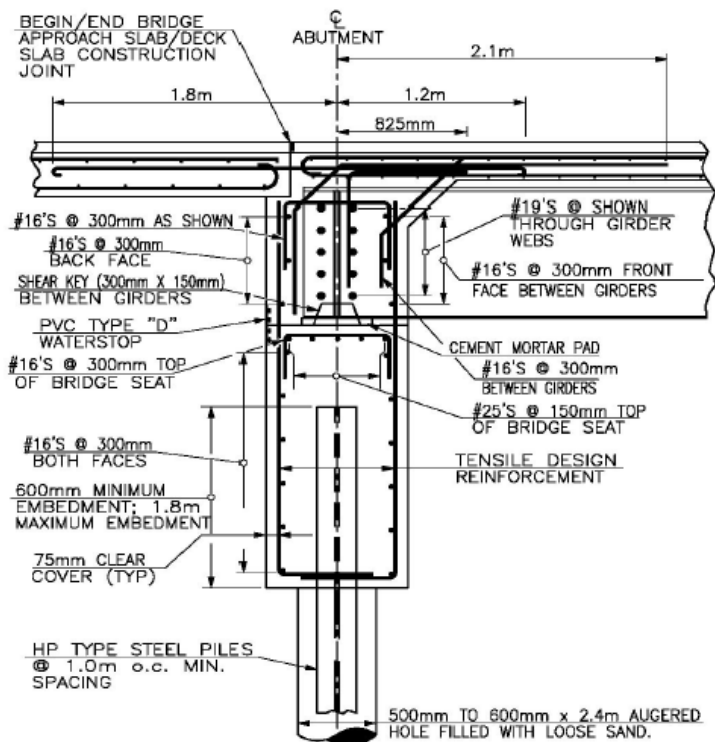


Figure C53- Integral abutment details

Figure C54 is an adaptation from an Ohio Department of Transportation standard drawing showing a prestressed concrete beam. Now a standard detail for most prestressed girders, holes are provided through the beam for reinforcing. This reinforcing

more typical of DOT design standards in that the reinforcing is made continuous across the construction joint. Additionally, when comparing the details in Figure C53 and Figure C55, although both details have had repeated success, there are two obvious differences in how they approach the detailing. First, Figure C53 shows a bent hook bar connecting the approach slab, whereas Figure C55 shows that continuity is maintained by a straight bar connecting the approach slab to the deck. Second, the Figure C53 detail utilizes a shear key, while the Figure C55 detail relies solely on the continuity of the reinforcing across the construction joint. Each detail has demonstrated success in application and the designer should consider which option may be more appropriate for each bridge's unique situation.

For more information on backwall detailing see Section C7.2.



TYPICAL INTEGRAL ABUTMENT SECTION W/STEEL SUPERSTRUCTURE

DETAIL 4.6.2.2.a

N.T.S.

Figure C55- Integral abutment details (NYSDOT)

C7.1.2. Semi-Integral Abutments

Figure C56 shows the overall concept for a semi-integral bridge abutment. Shown in the figure is the typical layout with the beam and end diaphragm (backwall) cast integral.

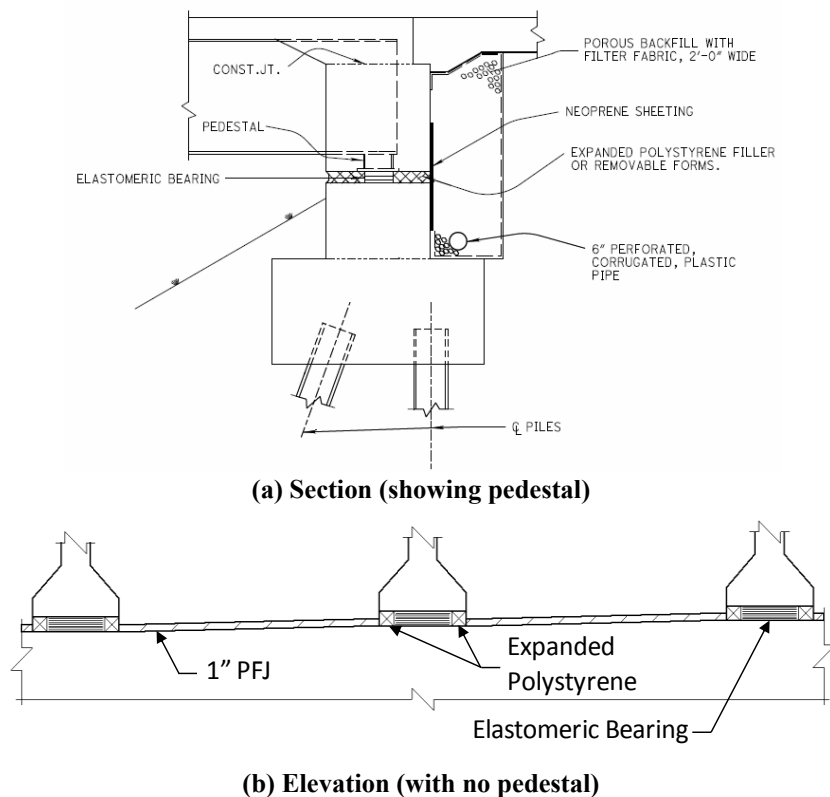


Figure C56- General semi-integral abutment concept

Drainage and porous backfill are necessary for the same reasons as for integral abutments, formation of ice and integrity of the backfill. For semi-integral abutments, two bearing strategies have been used with success. First, the pile cap may be cast level and the superstructure superelevation can be accommodated through the use of bearing pedestals. The second method is to step the pile cap pour. In this case, the polystyrene filler must be used on both the top of the cap and on the sides of the step to allow for movement. Due to the nature of the superstructure movement it is recommended that the first case with pedestals be used for locations of high skew (larger than 20°) and bridges on a curve. If it is desired to inspect the bearings during the life of the bridge, removable filler material can be placed in front of the bearings.

Figure C57 shows the successful detailing strategies that have been used in various States. The foundation shown is for a drilled shaft, but other foundation types are equally

applicable. Similar to integral abutments, dowel holes are placed through the beam or girder. Unlike, integral abutments, bearings are used to accommodate movement between the superstructure and the foundation. Efforts must be made to seal the gap between the cap and backwall yet still accommodate movement. This has traditionally been accomplished with preformed filler surrounding the bearing area and a layer of waterproofing applied to the rear face of the seam prior to placing the backfill. For more information on backwall detailing see Section C7.2.

Other than the backwall and treatment of the bearing area, detailing for the rest of a semi-integral abutment is the same as traditional design.

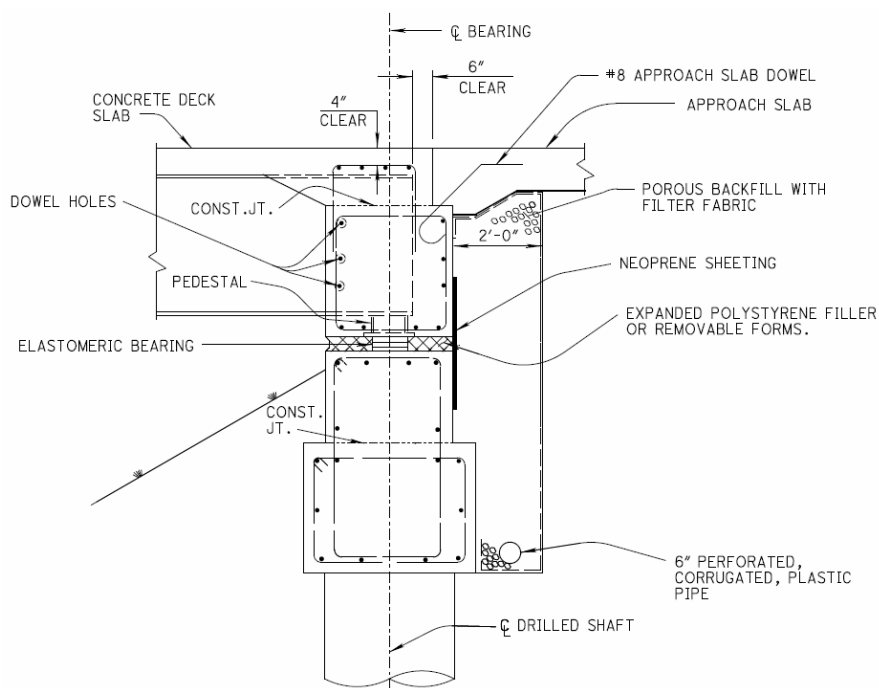


Figure C57- Semi-integral details

Figure C58, similar to Figure C57, shows an alternate detail that is used where the diaphragm is extended and a lip is dropped down over the pile cap. This detail replaces the neoprene sheeting that provided the barrier between the porous backfill and the

expanded polystyrene filler surrounding the bearings. Preformed elastomeric material is placed between the extended diaphragm and the abutment stem.

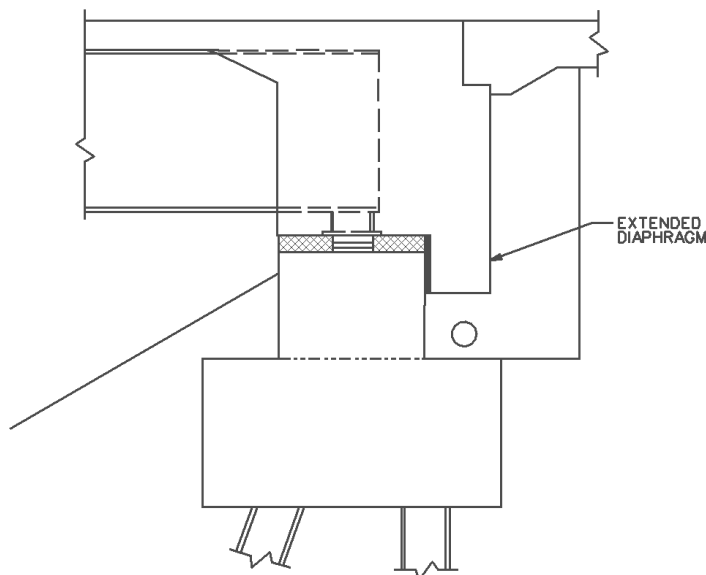


Figure C58- Semi-integral details with extended diaphragm
C7.1.3. Seamless Abutments

Details recommendations for the transition zone are not well established and thus no standard details are available for reference. However, the recommendations for the abutment cap and backwall are the same as those presented in Section C7.1.1.

C7.2. Pile Cap and Backwall

In addition to the details presented in Section C7.1, because of the concentrated beam reactions, Oesterle et al. (2005) recommend that vertical reinforcement for the moment from the soil load be distributed with 75% of the bars within 25% of the beam spacing on either side of the beam. Furthermore, for crack control, they recommend the center-to-center spacing of the flexural reinforcement not exceed (in inches):

$$s \leq \frac{540}{f_s} - 2.5c_c \text{ or}$$

$$s \leq 12 \left(\frac{36}{f_s} \right)$$

Eq. C44

Where,

c_c = clear cover from the nearest surface in tension

f_s = calculated stress (ksi) at service load, or alternately as $0.60F_y$

This limitation is taken from ACI 318-05, section 10.6.4 rules for the distribution of flexural reinforcing to control cracking in one-way slabs. Further commentary on this requirement can be found there.

C7.3. Sleeper Slab

A sleeper slab is appropriate for any integral or semi-integral bridges and is placed at the roadway end of the approach slab. The intent of the slab is to provide a relatively solid foundation for the far end of the approach slab and to provide a location for limited expansion and contraction. Although no formal design is suggested, a typical suggested detail has been provided by Wasserman (1996).

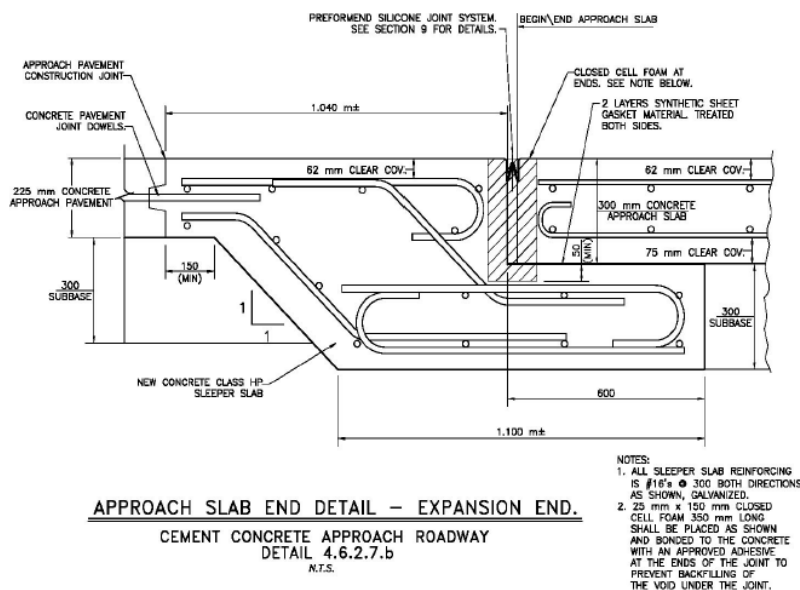


Figure C60- Sleeper slab with concrete pavement approach (NYSDOT)

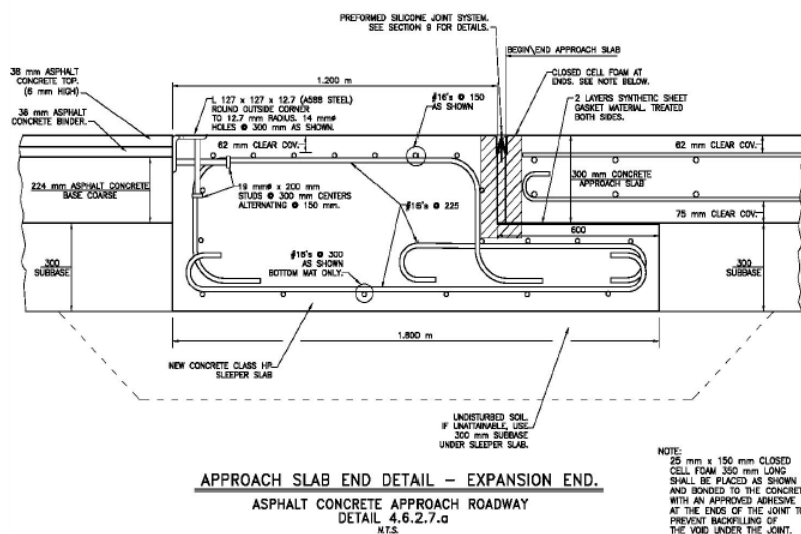


Figure C61- Sleeper slab with asphalt pavement approach (NYSDOT)

The location of the sleeper slab should be placed so that the entirety of the slab is outside the failure plane as discussed in Section C6.2.9.1.

C7.4. Details for Skewed and Curved Bridge

Transverse movements of integral abutments associated with large skews or horizontal curves should be anticipated by the details for barrier walls, drainage

structures and the ends of the approach slabs. In addition, the foundation and pier structure stiffness will likely be significant for movement parallel to the pier cap. Therefore, it is recommended that the connection between the bottoms of the girders and diaphragms and the pier caps be flexible in this direction. This approach, however, may not be appropriate for seismic design. In this case, design of the diaphragms should consider the interior pier restraint of the rigid body rotations that result from passive abutment restraint of longitudinal thermal expansion.

C8. Construction

C8.1. Construction Stability

Due to concerns about the repetitive bending stresses on the pile, it is recommended that no seam (weld) be placed at the top 30ft. of the pile. This will ensure proper ductility and eliminate the possibility of having a poor fatigue detail near the region of higher bending response. Additionally, this will better ensure proper alignment of the pile at the cap.

The order of construction is also important to insure the stability of each item during construction as well as the overall global stability of the bridge. See Section C8.4 for more information.

C8.2. Utilities

Non-flexible utilities should not be permitted to pass through integral and semi-integral abutments. Multiple DOTs report experience having problems with the flexibility of the integral cap creating issues with the rigid utilities. Only utilities that are

able to sufficiently flex with the movement of the integral abutment should be permitted, but it is preferable to locate all utilities adjacent to the bridge structure.

C8.3. Cracking Control

Vertical cracks have often been found at the bottom of diaphragms between precast beams over the piers, in the positive moment connection region for the external (fascia) girders. On the interior girders encased in the diaphragm, spalling of the diaphragm has been observed near the bottom flange. This spalling resulted from slipping of the bottom flange outward (away from the diaphragm) from the end rotation of the girder associated with creep and thermal changes. These vertical cracks in the diaphragm and end rotation of the girders serve to relieve tensile stresses due to creep, shrinkage, and thermal movement and are not detrimental to the integrity of the structure. Attempts to control this cracking through over-reinforcing may result in cracks in less desirable locations.

Horizontal cracks and efflorescence have been found on the forward face of integral abutments at the construction joint on top of the pile cap. This can be alleviated by placing adequate sealing from water behind the stem across the construction joint.

Settlement of the approach slab is common. This can cause cracking and further damage to the barrier rail. Rails that are attached to both the deck and approach slab should be jointed to accommodate the differential settlement.

C8.4. Construction Sequencing

Guidelines for concrete bridge deck materials and construction to control transverse cracking in concrete bridge decks is presented in NCHRP Report 380 (Krauss, 1996). Among the issues that affect deck cracking are weather, time of placement, curing,

vibration, finishing, loads, and placement sequencing. Certain current practices are presented here for jointless bridges.

For jointless bridges the construction sequence should generally follow:

1. Complete any embankment prior to pile driving and allow for consolidation (if required)
2. Place piling and fill pre-drill holes (if used)
3. Construct abutments and wing walls to elevation of bearing seat
4. (Semi-integral) Set elastomeric bearings; or (Integral) set beam pads allowing for rotation from beam and deck DL
5. Set beams
6. Cast the deck slab and the integral backwall. The ends of the slab should be poured last in order to minimize locked-in stresses at the supports.
7. Place drainage and backfill behind the abutments after the deck has achieved the appropriate strength. It is important that the backfill be placed simultaneously behind each abutment so as to not inadvertently shift the bridge in the potentially unsupported direction.
8. Cast the approach slab. Ideally, the approach slab should be cast with the bridge in the thermally contracted position (i.e. early morning). This avoids putting the slab into tension until the concrete has gained sufficient strength

It should be emphasized that placement of the backfill is even more important to be conducted simultaneously for semi-integral abutments. The reason for this emphasis is semi-integral bridges is that the superstructure is sitting on flexible bearings, rather than being positively attached to the abutment and is more likely to move do to the pressure from the compacting procedures.

C8.5. Fill Compaction

Construction can follow normal compaction procedures as specified by the owner state except as noted in the construction sequencing. Fill compaction has been modified and adjusted using several variables, including the use of specialized material. General experience has indicated that properly compacted normal fill material is sufficient for jointless bridge construction. More important is proper drainage behind the backwall.

C9. Maintenance and Repair

C9.1. Problems with Jointless Construction

Although adoption of integral-type bridges will eliminate some of more troublesome problems associated with jointed bridges and yield significantly more durable structures, they will not eliminate endemic highway construction problems that are somewhat related to accelerated construction, all-weather construction, marginal construction supervision, etc.

Transverse and diagonal deck slab cracks, stage construction issues, lateral rotation of superstructure, erosion of embankments, marginal quality of structure movement systems, and other problems have appeared to trouble design, construction, and maintenance engineers. Except for early age deck slab cracking these problems are

generally the result of failure of bridge engineers to anticipate and apply typical design and construction provisions to achieve trouble-free construction and more durable structures.

C9.1.1. Deck Cracking

Diagonal deck slab cracks located at acute corners of integral-type bridges are occasionally reported. When constructing integral-type bridges, stationary abutments and moving superstructures must be joined together by cast-in-place continuity connections. Consequently, these fresh connections could be stressed and cracked if a substantial temperature drop were to occur during initial concrete setting, or if concrete placement sequences were not suitably controlled. To address this problem, the following placement procedures should be used:

- Placing continuity connections at sunrise
- Placing deck slab and continuity connections at sunrise
- Placing continuity connections after deck slab placement
- Using crack sealers
- Using one or more of the above.

C9.1.2. Lateral rotation of semi-integral bridges

One of the primary aspects of semi-integral bridges that must be considered and effectively resolved is the design of guide bearings for the superstructure of skewed bridges. Unfortunately, many of the retention devices currently being used are not fully functional, because friction and binding of retention devices and, consequently the long term stability of abutments, especially those not supported by rigid foundations, have not

been effectively provided for. However, it appears inevitable that this aspect of semi-integral bridge concept will be improved when bearing manufacturers and other bridge design engineers unite their talent to design and manufacture more functional structure movement system for these applications.

C9.1.3. Approach Slabs

Ohio experienced slab distress shortly after it adapted the integral concept to continuous steel beam bridges in the early 1960s. Where these bridges were constructed adjacent to compressible asphalt concrete approach pavements, approach slab seats at the ends of bridge superstructure were found to be fractured, approach slabs had settled, and the vertical discontinuity in the roadway surface at the approach slab/superstructure interface was hindering movement of vehicular traffic.

C9.1.4. Drainage

Washout has been noted on several existing structures where drainage was not properly designed or not properly maintained, including some where the piles became exposed. It is imperative that proper drainage material including filter fabric and perforated piping be placed behind the abutment. The preferred alternative is to direct water away from the bridge approach, but it is acknowledged that this can be difficult to accomplish.

Additionally, with semi-integral abutments, improper drainage can lead to washout of one side of the bridge and not the other. This leads to an unbalanced soil pressure during thermal expansion and can lead to additional maintenance issues at the bearing locations.

Drainage can also affect settlement of the sleeper slab and create settlement of the approach slab. It is recommended that runoff be intercepted or diverted so as not to reach the end of the approach slab.

In regions that experience freezing temperatures, proper drainage is also important to minimize the potential for frozen soil behind the abutment. The magnitude of the potential restraining force is unknown for frozen soil, but it will be minimized with proper drainage (Briaud, James and Hoffman, 1997).

C9.1.5. Cycle-control Joints

Probably, the most significant unresolved problem with integral and semi-integral bridges is the availability of cost-effective functional and durable cycle-control joints, the moveable transverse joints used between approach slabs of integral-type bridges and approach pavements. For the shortest bridges, the usual pavement movement joints composed of preformed fillers are currently being used. For the longest bridges, finger-plate joints with easily maintainable curb inlets and drainage troughs have been successfully employed. However, for intermediate-length bridges, development of suitable cycle-control joint is still in the evolutionary stages.

C9.2. Deck Replacement

Figure C62 shows what can happen when the proper procedures are not followed for deck replacement or deck rehabilitation procedures. It should be anticipated that large compressive forces are acting on the whole structure as a result of soil pressure on the abutments. In order to insure the global stability of the structure, one of two procedures must be followed. The first procedure is to use proper construction sequencing as follows:

1. Remove the approach slab
2. Remove backfill to the bottom of the stem for integral or to the bottom of the end diaphragm for semi-integral abutments. Excavation should be done simultaneously behind both backwalls.
3. Remove the deck
4. Replace the deck according to the guidance provided in Section C8.4.

This procedure should always be used for whole deck replacement.

The second option is to calculate the stress applied by the passive pressure of the abutment backwalls. This force can then be applied to the superstructure with portions of the deck removed to check the stability of the system and each structural item that might be affected by the removal of the deck. This includes checking both local and global buckling stability. It is recommended that this only be used for partial width deck repair.



Figure C62- Improper deck removal

C9.3. Bearing Replacement for Semi-Integral

An additional factor to consider when detailing semi-integral jointless bridges is that, should bearing repair or replacement be required, it can be difficult to accomplish. That

is, provisions should be made to jack the entire backwall. This will require removal of the approach slab and the backfill. Consideration should be given to examining and/or replacing the abutment bearings at the time of deck replacement since the approach and backfill must be removed for this procedure as well.

C10. Retrofits

A large percentage of existing bridges are simple span bridges that rely on expansion joints to accommodate longitudinal movements. This fact is due to complexity of analysis of continuous structures, as well as construction difficulties. Most of deficient bridges include these jointed structures which need upgrade and repair. Retrofitting existing jointed bridges to jointless ones is highly recommended in this case.

The following considerations are required in integral conversion (Leathers, 1990)

1. The existing structural elements should be able to properly function without the expansion joint.
2. Movement calculation should be based on AASHTO LRFD.
3. Continuity can be achieved by making the deck continuous, or by making the girders continuous.
4. All obsolete and/or deteriorated bearings should be replaced with elastomeric bearing devices.
5. If the abutment is unrestrained, a fixed integral condition can be developed for many of the shorter bridges. Abutments that are free to rotate are considered

unrestrained, such as a stub abutment on one row of piles or an abutment hinged at the footing.

C10.1. Details over the Pier

Two practical options that can be used with or without integral abutments are available for retrofitting existing jointed bridges into jointless bridges.

1. Provide beam continuity for live load only. In this case, the negative moment continuity is provided over the piers, with or without positive moment continuity at these locations.
2. Only provide deck slab continuity. In this option, although the deck is continuous, beams are technically, simply supported. This method involves removing some length of slab at the ends of the adjacent beams, splicing the existing reinforcement and adding new bars, and recasting that part of the deck.

C10.1.1. Retrofit with Girder Continuity

C10.1.2. Link Slab

When retrofit of an existing open joint is considered, the following approach may be used as shown in Figure C63 (Note that in this detail only the deck is made continuous):

1. Remove concrete as necessary to eliminate existing armoring
2. Add negative moment steel at the level of existing top-deck steel sufficient to resist transverse cracking
3. Reconstruct with regular concrete to original grade

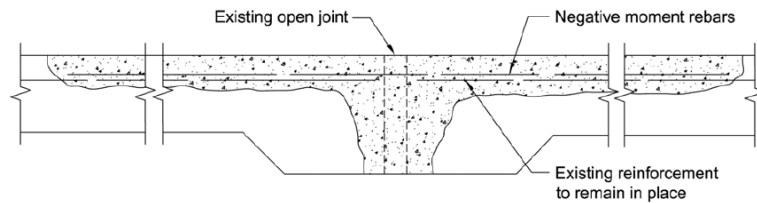


Figure C63- Integral conversion at piers (Leathers, 1990)

Since the deck slab would be exposed to longitudinal flexure due to rotation of beam ends responding to the movement of vehicular traffic, cracks will occur over the link slab. However for short and medium span bridges, the deck cracking associated with such behavior is preferred over long term consequences associated with open moveable deck joints or poorly executed joint seals.

In the design of link slab detail the followings should be considered:

1. Each span should be considered as simply supported and standard design procedures without considering the effect of link slab should be used.
2. Determine the maximum end rotations of girders as simply supported under service loads and impose the end rotations on the link slab to determine a design moment for the link slab.
3. Design the reinforcement using crack control criteria to limit the crack width at the surface of the link slab.

C10.2. Details over the Abutment

For existing stub abutments with single row of piles the following procedure shown in Figure C64 should be used (integral abutment retrofit):

1. Check the capacity of piles and pile-cap connection for the expected movement.

2. Demolish the stub abutment to the top of the piles. Cast reinforced concrete around beam ends and connect to approach slab to replace the old abutment.
3. Excavate the backfill to the bottom of the pile cap. Then provide drainage, backfill and approach slabs behind the new abutment.

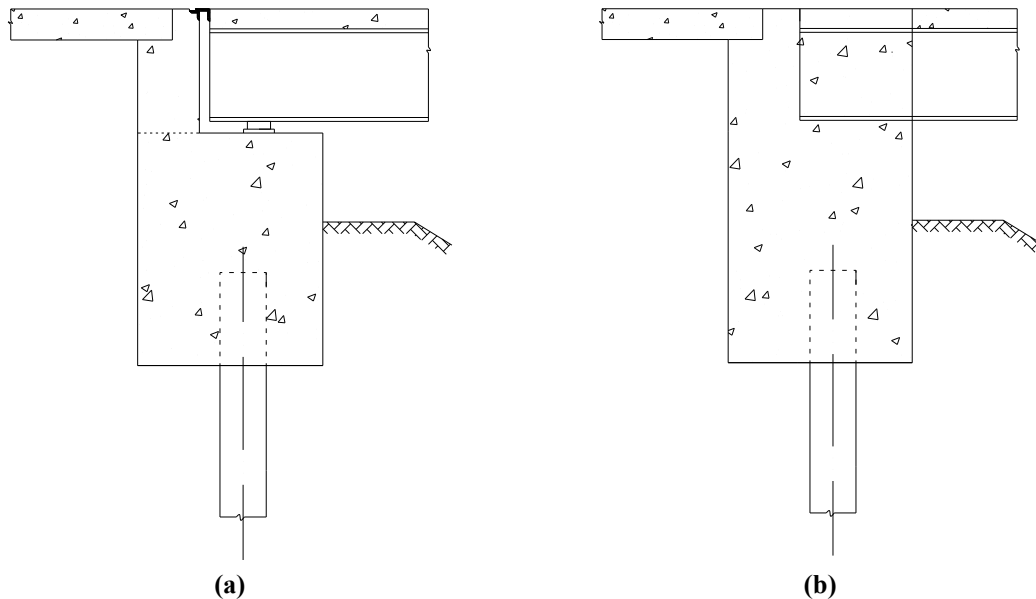


Figure C64- Conversion of a bridge with moveable deck joints at the superstructure-abutment interface with integral abutment (a) before conversion (b) after conversion

For existing stub abutments with rigid foundation or existing full height wall abutments the following procedure should be used (semi-integral abutment retrofit):

1. Remove the existing abutment to the top of the piles.
2. Provide sliding surface between the pile cap and the abutment stem which is cast integrally with the beam ends and approach slab.
3. Provide details for both horizontal and vertical sliding joints using lateral guide bearings, sheet seals, and drainage and backfill.

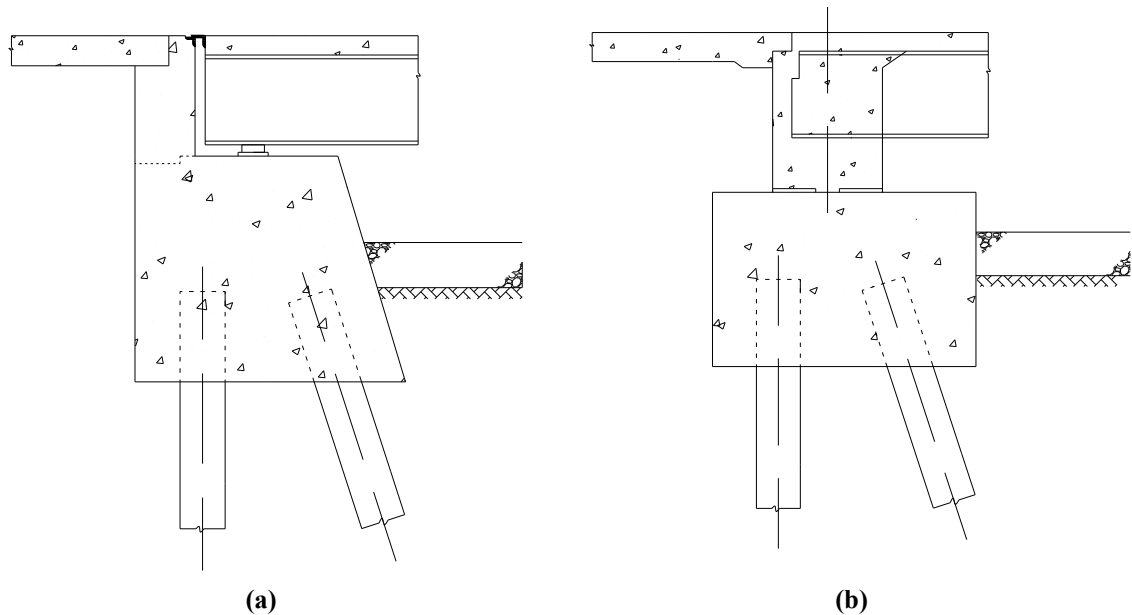


Figure C65- Conversion of a very short span bridge with moveable deck joints at the superstructure-abutment interface with integral abutment (a) before conversion (b) after conversion
C10.3. Conversion

General experience has shown that most common bridge types can be converted to jointless bridges. Jointed bridges can be converted to jointless bridges to enhance their performance with the same goal as new construction, i.e. joint elimination. Examples of candidates that have already been converted are pin-and-hanger bridges and multi-span, simple span bridges for both steel and concrete superstructures.

Several States have had success converting old pin-and-hanger expansion joints to a bolted full moment connection, thus eliminating the expansion joints. Based on the work by Connor et al. (2005), they were made continuous for live loads. The project used instrumentation and structural monitoring to verify the analysis results.

The state of New Mexico also presented several case studies (Maberry, Camp and Bowser, 2005). In one project, they converted simple span concrete girders by the use of a linkage slab. The project demonstrated that attention must be paid to the bearings. Overlooked by the retrofit assessment was the greatly increased expansion that would

transfer to the outer bearing locations. Subsequently, the resulting expansion loads were absorbed by the pile caps, which quickly deteriorated.

The key to any conversion is the ability of the bridge to withstand the new continuous loading and expansion demands introduced by the changing load path. Due to the complex nature of the converted structure, it is recommended that conversions be treated with the same level of analysis as required for a new design.